DOTTORATO DI RICERCA IN
Chemical Sciences

CICLO XXXVIII - PNRR NextGenerationEU

Design, characterization and optimization of nanostructured vectors for the delivery of DNA and siRNA

Settore Scientifico Disciplinare
CHEM08A

Dottoranda
Dott.ssa Ilaria Chiarugi

Supervisore
Prof.ssa Francesca Maestrelli

Co-supervisore
Prof.ssa Anna Rita Bilia

Co-supervisore
Prof.ssa Sandra Ristori

Coordinatore
Prof.ssa Anna Maria Papini

Overview

This thesis addressed the development of nanovectors (NVs) for the complexation and delivery of genetic material, particularly small interfering RNA (siRNA), for the treatment of inflammatory and autoimmune diseases.

The doctoral grant was provided by a PNRR project carried out within the CN3 center in Florence, under Spoke 5 “RNA and Gene Therapy.” The research was conducted in collaboration with several laboratories: the laboratory of Professor Francesca Maestrelli, the laboratory of Professor Sandra Ristori (Department of Chemistry, Sesto Fiorentino), the laboratory of Professor Francesco Ranaldi (Department of experimental and clinic biomedical sciences “Mario Serio”, Florence), and the laboratory of Professor Noemi Csaba (CIMUS, Centro Singular de Investigación en Medicina Molecular y Enfermedades Crónicas, Santiago de Compostela).

Gene therapy has demonstrated tremendous potential in recent years, reaching a milestone with the approval of the first siRNA-based lipid nanoparticle drug, Patisiran, in 2018, and the subsequent commercialization of RNA-based COVID-19 vaccines in 2020. Since then, the number of RNA and siRNA therapeutics, both approved and in clinical development, has grown exponentially, opening highly promising avenues for the treatment of diseases that currently lack effective therapies, such as cancer, chronic disorders, and autoimmune diseases. Genetic materials, such as RNA or siRNA, allow the upregulation or silencing of specific genes that are dysregulated in many of these pathologies. However, naked genetic material is highly susceptible to

degradation and unable to cross cellular barriers on its own. Consequently, research has increasingly focused on the development of vectors capable of complexing, protecting, and guiding these molecules through the human body, facilitating endosomal escape and intracellular release.

Moreover, these vectors can be chemically modified on the surface, enabling functionalization with specific molecules or ligands to achieve targeted delivery to selected receptors, organs, or tissues. Despite these advances, many NVs have shown instability, cytotoxicity, or limited efficacy, and thus the search for improved materials, lipid-based and beyond, remains an active and expanding research field.

Within this framework, the present project involved the development of two classes of nanocarriers:

- Lipid nanoparticles (LNPs)
- Modified cationic β-cyclodextrin-based NVs (β-CD NVs)

This thesis is organized into an introductory abstract followed by a general introduction, two main experimental chapters and a concluding section.

The abstract summarizes the overall objectives, methodologies, and key experimental approaches undertaken for the design, development, and characterization of NVs and intended for the delivery of genetic material.

A general introduction explores the importance of nanocarriers for gene delivery and the main types of NVs employed.

The first part of this work focused on the optimization of LNPs formulation and composition through a Design of Experiments (DoE) approach. Several cationic lipids were systematically evaluated, and the most promising LNP formulations were subsequently complexed with siRNA at an N/P ratio of 10. The resulting LNPs were characterized in terms of:

-Structural properties: investigated by Dynamic Light Scattering (DLS) and Synchrotron Small-Angle X-ray Scattering (SAXS).
-Stability: both over time and in cell culture media, assessed by DLS analysis.
- *In vitro* tests: including cytotoxicity, cellular internalization, and gene-silencing efficiency.

The obtained results demonstrated favourable physicochemical and biological properties of the optimized LNPs, confirming their potential as promising carriers for siRNA delivery.

The second part of the work focused on the design and development of NVs using three novel self-assembling cationic β-cyclodextrin derivatives. These systems were designed with the support of CarboHyde Zrt.

The three novel compounds were characterized by Differential Scanning Calorimetry (DSC) and Infrared Spectroscopy (IR) to gain deeper insight into their structural features. Dispersibility studies were then carried out in various solvents, and the critical micellar concentration (CMC) was determined in order to establish an optimal production method and concentration range for obtaining NVs with the desired physicochemical properties.

The nanocarriers were initially complexed with a plasmid DNA encoding Green Fluorescent Protein (GFP) and later with siRNA, both at an N/P ratio of 10. The empty and loaded NVs were analysed using DLS, Transmission Electron Microscopy (TEM), Cryo-Electron Microscopy (Cryo-EM), and Synchrotron SAXS. Subsequently, cellular studies were performed to evaluate cytotoxicity, internalization, transfection efficiency, and gene-silencing activity. In addition, the impact of incorporating two different cationic polymers on NVs performance was investigated.

The results obtained are highly encouraging and lay the groundwork for further optimization e.g. by surface functionalization aimed at achieving targeted delivery to specific cells or tissues.

The final chapter highlights and discusses the most significant outcomes of this research. The insights gained open promise for future applications in gene therapy and in the targeted treatment of inflammatory and autoimmune diseases.

Lists of abbreviations

NV(s): Nanovector(s)

siRNA: Small Interfering RNA

LNP(s): Lipid Nanoparticle(s)

β-CD: β-Cyclodextrins

DoE: Design of Experiment

DLS: Dynamic Light Scattering

Synchrotron SAXS: Synchrotron-based Small-Angle X-ray Scattering

DSC: Differential Scanning Calorimetry

IR: Infrared Spectroscopy

CMC: Critical Micellar Concentration

TEM: Transmission Electron Microscopy

Cryo-EM: Cryogenic Electron Microscopy

RNAi: RNA Interference

DOPE: Dioleoyl phosphatidylethanolamine

TLE: Thin Layer Evaporation

Size: Particle Size

PdI: Polydispersity Index

Z: Zeta Potential

GFP: Green Fluorescent Protein

P: Plasmid

HA: Sodium Hyaluronate

HP: Polysialic Acid

FDA: Food and Drug Administration

mRNA: Messenger RNA

ncRNAs: Non-coding RNAs

rRNA: Ribosomal RNA

tRNA: Transfer RNA

miRNA: MicroRNA

circRNA: Circular RNA

RISC: RNA-induced Silencing Complex

Ago: Argonaute Proteins

AAVs: Adeno-associated Viruses

hATTR: Hereditary Transthyretin Amyloidosis

TTR: Transthyretin

PEG2000-DMG: 1,2-dimyristoyl-rac-glycero-3-methoxypolyethylene glycol-2000

DSPC: Distearoylphosphatidylcholine

ALC-0315: ((4-hydroxybutyl)azanediyl)bis(hexane-6,1-diyl)bis(2-hexyldecanoate)

SM-102: Heptadecan-9-yl 8-[(2-hydroxyethyl)(6-oxo-6-undecyloxyhexyl)amino]octanoate

PEI: Polyethylenimine

PLL: Poly-L-lysine

Chol: Cholesterol

DOPC: 1,2-dioleoyl-sn-glycero-3-phosphocholine

DOTAP: 1,2-dioleoyl-3-trimethylammonium-propane

DC-CH: 3β-[N′,N′-dimethylaminoethane)-carbamoyl]cholesterol hydrochloride

MTAB: (11-mercaptoundecyl)-N,N,N-trimethylammonium bromide

DOPE-PEG-2000: 1,2-dioleoyl-sn-glycero-3-phosphoethanolamine-N-[amino(polyethylene glycol)-2000] ammonium salt

18:0-PEG-2000: 1,2-distearoyl-sn-glycero-3-phosphoethanolamine-N-[carbonyl-methoxy(polyethylene glycol)-2000]

PBS: Phosphate-buffered Saline

DiD: 1,1′-Dioctadecyl-3,3,3′,3′-Tetramethylindodicarbocyanine

DMEM: Dulbecco's Modified Eagle Medium

FBS: Fetal Bovine Serum

TBE: Tris–Borate–EDTA

Summary

1 General Abstract

Gene therapy represents a highly promising approach for the treatment of severe and currently untreatable diseases. It relies on the introduction of genetic material into target cells for restoring, replacing, or silencing specific genes responsible for pathological conditions [1]. Among the available strategies, RNA interference (RNAi) has emerged as a powerful post-transcriptional gene regulation mechanism mediated by siRNAs [2,3].

Despite remarkable therapeutic potential, the clinical application of siRNAs remains limited due to their instability in biological fluids, susceptibility to nuclease degradation, and poor cellular uptake. Consequently, the development of safe and efficient delivery systems is a key requirement for the successful translation of gene-based therapeutics into clinical practice [1-4].

In this work, we developed and optimized two different nanocarrier systems for gene delivery: Lipid Nanoparticles (LNPs) and β-Cyclodextrin Nanovectors (β-CD NVs).

LNPs represent one of the most advanced delivery platforms, offering efficient protection for siRNA molecules with respect to enzymatic degradation and facilitating their intracellular delivery mainly through electrostatic interactions [5-7].

In this study, LNPs were prepared using the Thin Layer Evaporation (TLE) method and characterized for particle size (size), polydispersity index (PdI), and zeta potential (Z) by Dynamic Light Scattering (DLS). The objective was to obtain NPs suitable for siRNA complexation and delivery, with size below 200 nm and PdI < 0.3 [4,6].

A Design of Experiments (DoE) approach was applied to optimize critical parameters for LNPs production, identifying optimal conditions [5,11]. Based on these optimized parameters, additional cationic lipids were incorporated, and the resulting LNPs were complexed with either negative control or GFP-targeting siRNA at an N/P (+/-) ratio of 10. N/P ratio represents the molar ratio between the nitrogen atoms in the cationic components and the phosphate groups of the siRNA backbone [12].

Complexation efficiency was verified by agarose gel electrophoresis, which identified two lead formulations (designated B and D) for further study. Both formulations exhibited good stability after seven days of storage at 4 ± 1 °C [6,13].

The biological performance of these systems was evaluated *in vitro*, assessing their stability in culture medium (with and without serum), cytotoxicity toward HeLa cells, internalization in HeLa-GFP and RAW 264.7 cells, and gene silencing efficiency in HeLa-GFP cells.

High resolution structural characterization was performed by Synchrotron Small-Angle X-ray Scattering (SAXS). Both LNP formulations displayed sizes below 200 nm with PdI ≤ 0.3, efficient siRNA complexation, high internalization efficiency in HeLa cells (> 85%), and good GFP silencing after 72 h (~50% reduction for formulation B and ~30% for formulation D). These findings highlight the promising potential of the optimized LNPs as effective carriers for siRNA delivery [6,9,14-16].

β-Cyclodextrins are cyclic oligosaccharides known for their biocompatibility, chemical versatility, and ability to self-assemble into nanostructures, making them attractive candidates for non-viral gene delivery [8-10]. In this work, three novel cationic β-CD derivatives (CD1,

CD2, and CD3), synthesized by CarboHyde Zrt, were evaluated as NVs for nucleic acid delivery.

These compounds were initially characterized by Differential Scanning Calorimetry (DSC) and Infrared Spectroscopy (IR) to investigate their structural features and degree of crystallinity or amorphousness [18]. Dispersibility studies in various solvents were then conducted to determine the critical micellar concentration (CMC) and identify the optimal formulation and concentration range for NVs production. The resulting β-CD NVs were complexed with a GFP-encoding plasmid (P) at an N/P ratio of 10, and their size, PdI, and Z were measured to assess formulation quality. Selected formulations were further modified with Sodium Hyaluronate (HA) or Polysialic Acid (HP) (10% w/w) to evaluate the impact of these polymers on safety and stability.

Comprehensive structural characterization of β-CD NVs was performed by Transmission Electron Microscopy (TEM), Cryogenic Electron Microscopy (Cryo-EM), and Synchrotron SAXS, while agarose gel electrophoresis confirmed efficient plasmid complexation. The physical stability of the NVs was monitored at 4 °C and 25 °C (± 1 °C) for up to one week and in culture medium for 24 h [8-10,14].

Cytotoxicity was assessed via MTT assays in HeLa and RAW 264.7 cell lines, while cellular uptake and transfection efficiency were quantified by flow cytometry and fluorescence microscopy.

Stable NVs were obtained for CD1 and CD2, exhibiting particle sizes below 200 nm and PdI < 0.3. Both these formulations were stable over time and in serum-supplemented medium. Internalization efficiency exceeded 85% across all tested conditions, and transfection efficiency surpassed 50%, with CD1 showing higher GFP fluorescence intensity compared to CD2-based NVs [19].

The β-CD NVs were also complexed with GFP-siRNA at an N/P ratio of 10, which led to a moderate increase in size and PdI, except for the formulation containing HA. Gene silencing efficiency in HeLa-GFP cells was comparable to that of commercial Lipofectamine for CD1 NVs (around 90%), while CD2 NVs exhibited good transfection performance. These results underscore the potential of CD1 NVs as effective, biocompatible, and versatile non-viral carriers for gene delivery applications.

1.1 Bibliography

[1] Adams D. et al. Patisiran, an RNAi Therapeutic, for Hereditary Transthyretin Amyloidosis. N Engl J Med. 2018;379(1):11–21. doi:10.1056/NEJMoa1716153.

[2] Hou X. et al. Lipid nanoparticles for mRNA delivery. Nat Rev Mater. 2021; 6:1078–1094. doi:10.1038/s41578-021-00358-0.

[3] Yonezawa S. et al. Recent Advances in siRNA Delivery Mediated by Lipid-Based Nanoparticles. Adv Drug Deliv Rev. 2020;154-155:64-78. doi: 10.1016/j.addr.2020.07.022

[4] Stetefeld J. et al. Dynamic light scattering: a practical guide and applications in biomedical sciences. Biophys Rev. 2016;8(4):409–427. doi: 10.1007/s12551-016-0218-6.

[5] Gurba-Bryśkiewicz L. et al. Quality by Design (QbD) and Design of Experiments (DOE) as a Strategy for Tuning Lipid Nanoparticle Formulations for RNA Delivery. Biomed. 2023;11(10):2752. doi: 10.3390/biomedicines11102752.

[6] Rampado R. et al. Design of experiments in the optimization of nanoparticle-based drug delivery systems. J Control Release. 2023 ;358: 398-419. doi:10.1016/j.jconrel.2023.05.001.

[7] Spinozzi F. et al. Small-angle X-ray scattering unveils internal structure of lipid nanoparticles. J Colloid Interface Sci. 2024; 662: 446-549. doi: 10.1016/j.jcis.2024.02.076.

[8] Sartori B. et al. Tailoring Lipid-Based Drug Delivery Nanosystems by Synchrotron Small Angle X-ray Scattering. Pharm. 2022;14(12):2704. doi: 10.3390/pharmaceutics14122704.

[9] Haley RM. et al. Cyclodextrins in drug delivery: applications in gene and combination therapy. Drug Deliv Transl Res. 2020;10(3):661-677. doi: 10.1007/s13346-020-00724-5.

[10] Popielarski SR. et al. Structural effects of carbohydrate-containing polycations on gene delivery. 3. Cyclodextrin type and functionalization. Bioconjug Chem. 2003 ;14(3):672-8. doi: 10.1021/bc034010b.

[11] O'Mahony AM. Click-modified cyclodextrins as nonviral vectors for neuronal siRNA delivery. ACS Chem Neurosci. 2012; 17;3(10):744-52. doi: 10.1021/cn3000372

[12] Godbey WT, et al. Poly(ethylenimine) and its role in gene delivery. J Control Release. 1999; 60: 149-160. doi: 10.1016/S0168-3659(99)00090-5.

[13] Davis ME. Cyclodextrin-based pharmaceutics: past, present and future. Nat Rev Drug Discov. 2004;3(12):1023-35. doi: 10.1038/nrd1576.

[14] Tetyczka C, et al. Comprehensive characterization of nanostructured lipid carriers using laboratory and synchrotron X-ray scattering and diffraction. J Drug Deliv Sci Technol. 2019; 139: 153-160. doi: 10.1016/j.ejpb.2019.03.017.

[15] Rodriguez-Loya J. Dynamic Light Scattering and Its Application to Control Nanoparticle Aggregation in Colloidal Systems: A Review. *Micromachines* 2024; *15*: 24. doi: 10.3390/mi15010024

[16] El Moukhtari SH. Lipid nanoparticles for siRNA delivery in cancer treatment. J Control Release. 2023;361:130-146. doi: 10.1016/j.jconrel.2023.07.054.

[17] Maurer MS, et al. Patisiran Treatment in Patients with Transthyretin Cardiac Amyloidosis. N Engl J Med. 2023;389(17):1553-1565. doi: 10.1056/NEJMoa2300757.

[18] Chiu MH. Differential scanning calorimetry: An invaluable tool for a detailed thermodynamic characterization of macromolecules and their interactions. J Pharm Bioallied Sci. 2011;3(1):39-59. doi: 10.4103/0975-7406.76463.

[19] Hoti G. Cyclodextrin-based therapeutics delivery systems: A review of current clinical trials. Curr Res Pharmacol Drug Discov. 2025;9:100232. doi: 10.1016/j.crphar.2025.100232.

2 General Introduction

2.1 Nanotechnologies and nanomedicines

Nanotechnology can be defined as the scientific discipline concerned with design, fabrication, and optimization of materials and devices operating at the nanometric scale, typically from a few to several hundred nanometers (approximately one billionth of a meter). It constitutes an inherently interdisciplinary field, bridging physics, chemistry, and biology. Within the biomedical domain, nanotechnological systems have demonstrated great potential owing to their ability to interact selectively with cells and tissues. This in turn allows achieving enhanced therapeutic efficacy while minimizing systemic side effects [1].

The conceptual foundation of nanotechnology was first articulated by physicist Richard P. Feynman in his seminal 1959 lecture *"There's Plenty of Room at the Bottom."* Feynman proposed the possibility of manipulating matter at atomic and molecular dimensions, foreseeing profound implications for science and technology. The term *nanotechnology*, however, was later introduced by Norio Taniguchi at the University of Tokyo, who referred to the engineering of materials at atomic or molecular resolution; that is, at scales below one nanometer [2-4].

Over the past few decades, nanotechnology has evolved into a strategic platform technology with extensive applications across numerous industrial and scientific sectors. In the biomedical field, research interest has markedly increased, particularly in the development of nanoparticle-based delivery systems. Among these, non-viral vectors have gained attention as safer and versatile alternatives to viral systems. Such nanocarriers have been designed for targeted drug delivery to cancer

cells and for the encapsulation of poorly soluble bioactive molecules to improve their pharmacokinetic profiles. Following the COVID-19 pandemic, considerable research efforts have also focused on nanoparticle platforms for gene therapy, demonstrating their versatility as vectors for nucleic acid delivery [1-3].

The rapid technological advances observed in recent years represent a significant milestone for modern healthcare. These developments are expected to yield major benefits in both therapeutics and diagnostics, supporting the emergence of personalized medicine. Indeed, the integration of nanotechnology into medical practice offers opportunities for patient-specific treatments with higher efficacy and reduced toxicity. Consequently, nanoparticle research is widely regarded as a frontier of biomedicine, with far-reaching implications for the future of healthcare systems [5-6].

2.2 Gene Therapy

Gene therapy represents an innovative medical approach in which genetic material, such as DNA or RNA, is introduced into a patient's cells to achieve a therapeutic effect. Over recent years, this modality has achieved considerable success and rapid advancement: indeed, more than two dozen gene therapy products have been approved for clinical use by regulatory agencies in multiple countries. [7,8]

The notion of gene therapy emerged in the 1960s and 1970s, a period characterised by foundational advances in our understanding of cellular transformation and genetically marked cell lines. With the development of recombinant-DNA techniques, cloned genes became available and were exploited in *in vitro* experiments to demonstrate that an exogenous gene

might correct genetic defects and associated disease phenotypes in cultured cells. [9-11]

According to the U.S. Food and Drug Administration (FDA), gene therapy products are defined as those “administered as nucleic acids, viruses, or genetically modified microorganisms, … that mediate their effects by transcription and/or translation of transferred genetic material and/or by integrating into the host genome. These products may be used to modify cells *in vivo* or to transfer cells *ex vivo* before administration to the recipient.” [12]

Gene therapy can be classified into two principal categories:

- germ-line gene therapy; in which the modified gene is introduced into germ cells (or early embryos) and thus can be transmitted to subsequent generations.
- somatic gene therapy: in which the therapeutic gene is delivered only to the target somatic (non-germline) cells of the patient and is not passed on to offspring. [11-12]

The transferred genetic material acts either by enabling the expression of the therapeutic gene or by inhibiting the expression of a target gene. Another useful distinction is between *in vivo* and *ex vivo* gene-therapy approaches. *In vivo* delivery involves administering the vector directly into the patient’s body, thereby circumventing the challenges associated with *ex vivo* manipulation (such as cell harvesting, culture, genetic modification, and transplantation). However, *in vivo* approaches heavily depend on the specific tissue targeted on the efficiency of local vector delivery and on the sustained expression of the gene in the target cells [13].

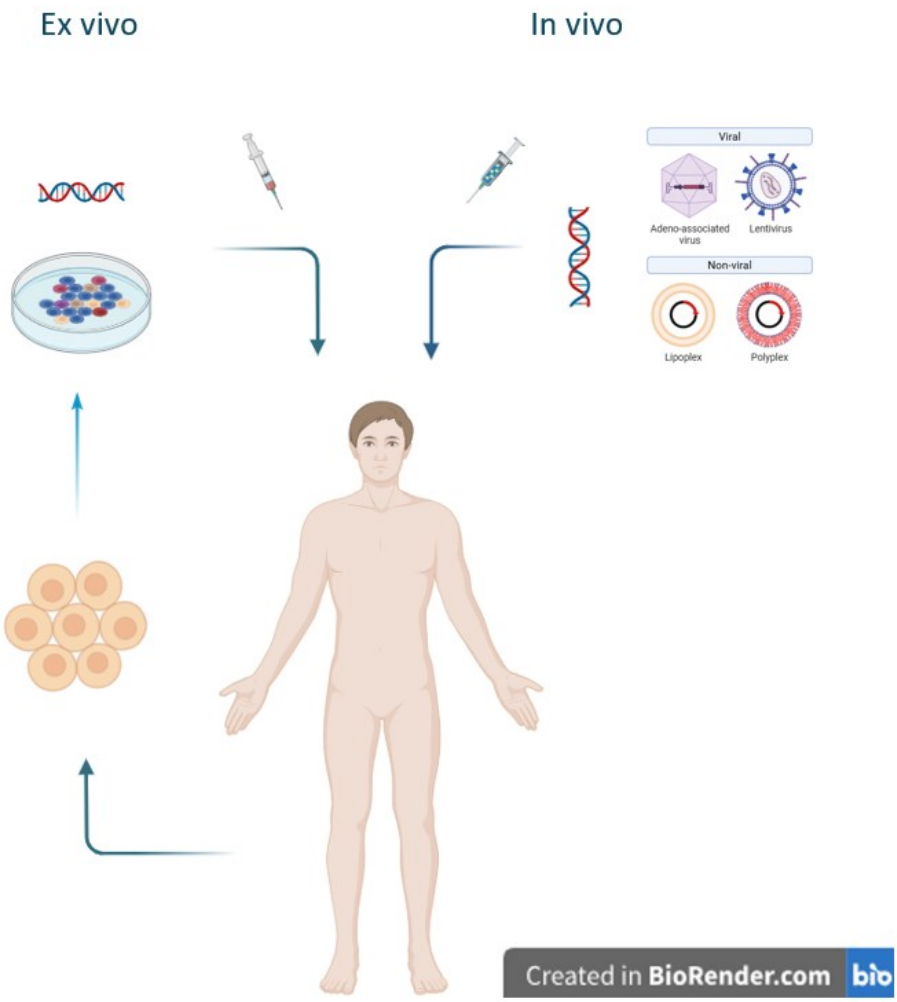

Figure 1. Ex vivo and In vivo Gene therapy approaches. Created with BioRender.com.

Despite the many advantages, gene therapy has historically raised concerns about safety and ethical issues. Nevertheless, thanks to advances in vector design, genome-editing technology and regulatory oversight, the majority of the earlier safety issues have been largely mitigated.

2.3 DNA and RNA

DNA (deoxyribonucleic acid) and RNA (ribonucleic acid) are the fundamental carriers of genetic information in all living organisms. DNA acts as the long-term repository of hereditary instructions, while RNA functions primarily as transient messenger and, in some forms, as a regulatory and catalytic molecule. In therapeutic contexts, plasmid DNA (P), a small, circular, double-stranded DNA molecule distinct from chromosomal DNA, has gained importance as a tool for delivering genetic material into cells. P can be engineered to carry therapeutic gene cassettes under suitable promoters and delivered into target cells. P vectors are widely used for gene therapy, vaccination, and protein expression, offering safety advantages since they do not integrate into the host genome and can be produced on a large scale with high purity [11, 14].

RNA was identified as a bioactive macromolecule in the early 20th century and is now recognized as the key regulator of numerous biological processes, promoting or inhibiting molecular events such as signal transduction, gene regulation at both transcriptional and post-transcriptional levels, and information storage [15-18].

RNA molecules can be broadly categorized into two main classes:

- coding RNA, primarily messenger RNA (mRNA), which serves as a template for protein synthesis.
- non-coding RNAs (ncRNAs), which include ribosomal RNA (rRNA), transfer RNA (tRNA), microRNA (miRNA), small interfering RNA (siRNA), circular RNA (circRNA), and other regulatory forms.

Among the non-coding RNAs, miRNAs and siRNAs exploit the mechanism of RNA interference (RNAi), a process by which gene expression is silenced through sequence-specific interactions with target mRNAs. In the case of siRNA, double-stranded RNA molecules of approximately 21–22 base pairs, they can be synthesized chemically or produced *in vitro* using T7 RNA polymerase. siRNAs are designed to be fully complementary to their target mRNA sequences, enabling precise gene silencing through mRNA degradation.

Once introduced into cells, siRNAs are incorporated into the RNA-induced silencing complex (RISC), a multi-protein assembly responsible for gene silencing. The antisense (guide) strand of the siRNA is selectively retained within RISC and directs the complex to the complementary mRNA. Argonaute proteins (Ago), which form the catalytic core of RISC, mediate the cleavage of the target mRNA, after which endogenous nucleases complete the degradation process [19-22].

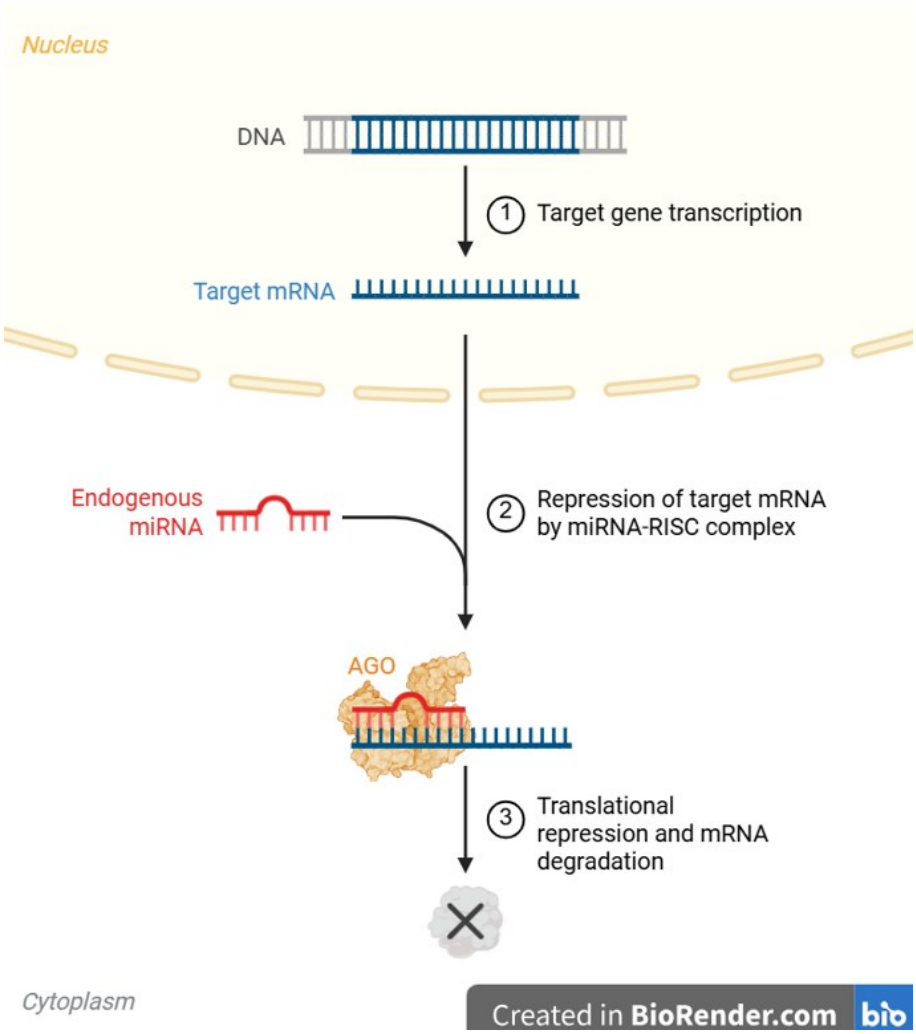

Figure 2. miRNA mechanism of action. Image from BioRender.com. © BioRender.

Despite their great potential, the therapeutic application of naked DNA, RNA, or siRNA is limited by major challenges. These include poor stability in biological fluids due to degradation by endonucleases and exonucleases, inefficient targeting to the desired site of action, and low cellular uptake arising from their hydrophilic, negatively charged, and relatively large molecular structure. Furthermore, siRNAs may exhibit off-

target effects, as even minor sequence mismatches can lead to unintended gene silencing [22-24].

To overcome these limitations, researchers have developed chemical modifications of siRNA structures (such as backbone, sugar, or base modifications) to enhance stability and specificity, as well as nano delivery systems including lipid nanoparticles (LNPs), polymeric carriers, and conjugates that improve cellular uptake and biodistribution while reducing toxicity [25-28].

2.4 Nanocarriers for Gene Therapy

Gene delivery carriers can generally be categorized into two main classes:

- viral
- non-viral

Among viral systems, the most widely employed are retroviruses, lentiviruses, adenoviruses, adeno-associated viruses (AAVs), and herpes simplex viruses. In all cases, the viral genome is rendered replication-deficient through targeted deletions or mutations, preventing autonomous propagation while maintaining its high transduction efficiency [29,30].

AAVs are single-stranded DNA viruses lacking a lipid envelope, and they have emerged as one of the leading platforms for *in vivo* gene therapy. They can be engineered to deliver therapeutic genes to specific target tissues and are predominantly used in treatments for monogenic diseases, particularly within the group of rare disorders. Adenoviral vectors, which possess double-stranded DNA genomes, are similarly non-integrating and have been employed in oncogene therapy and immunotherapy. Lentiviruses, a subclass of retroviruses, are capable of

integrating into the host genome, providing stable and long-term gene expression, a feature especially beneficial in paediatric and chronic treatments [31-34].

Despite their efficiency, viral vectors pose several limitations, including immunogenicity, cytotoxicity, and insertional mutagenesis, where integration of viral sequences can disrupt host-gene regulation. Furthermore, improvements are still needed in gene-transfer efficiency, tissue specificity, and expression duration [35]. Consequently, research has increasingly focused on the development of non-viral nanocarriers, which can offer safer and more versatile delivery platforms.

Among non-viral systems, those containing cationic lipids and cationic polymers represent the most extensively used categories [36]. Cationic lipids contain positively charged hydrophilic head groups linked to hydrophobic tails via a chemical linker. The cationic head interacts electrostatically with the phosphate backbone of nucleic acids, allowing condensation and protection of the genetic cargo [37]. LNPs have demonstrated exceptional success in the delivery of mRNA and siRNA, most notably with the FDA-approved siRNA therapeutic Onpattro® (patisiran) and the mRNA vaccine Comirnaty® (Pfizer/BioNTech) for COVID-19 [38-39].

Patisiran is used for the treatment of hereditary transthyretin amyloidosis (hATTR), a disorder caused by mutations in the transthyretin (TTR) gene. The main clinical manifestations of the disease include progressive polyneuropathy and cardiomyopathy, which can ultimately lead to death. TTR is a transport protein synthesized primarily by the liver, responsible for carrying thyroxine and retinol-binding protein–bound retinol. Mutations in the TTR gene result in the production of unstable TTR monomers that

misfold and aggregate into amyloid fibrils, which deposit in various organs and tissues, causing progressive damage.

Patisiran acts by reducing serum TTR levels and tissue amyloid deposition. The drug is administered intravenously every three weeks at a recommended dose of 0.3 mg/kg. Following intravenous infusion, PEG lipids on the surface of the LNPs are exchanged with serum proteins, particularly apolipoproteins. This interaction facilitates hepatic uptake through association with cholesterol and subsequent internalization into hepatocytes via endocytosis. Within the endosome, the acidic environment leads to protonation of the ionizable lipid DLin-MC3-DMA, promoting endosomal disruption and release of the siRNA into the cytoplasm, where it mediates TTR mRNA degradation [38].

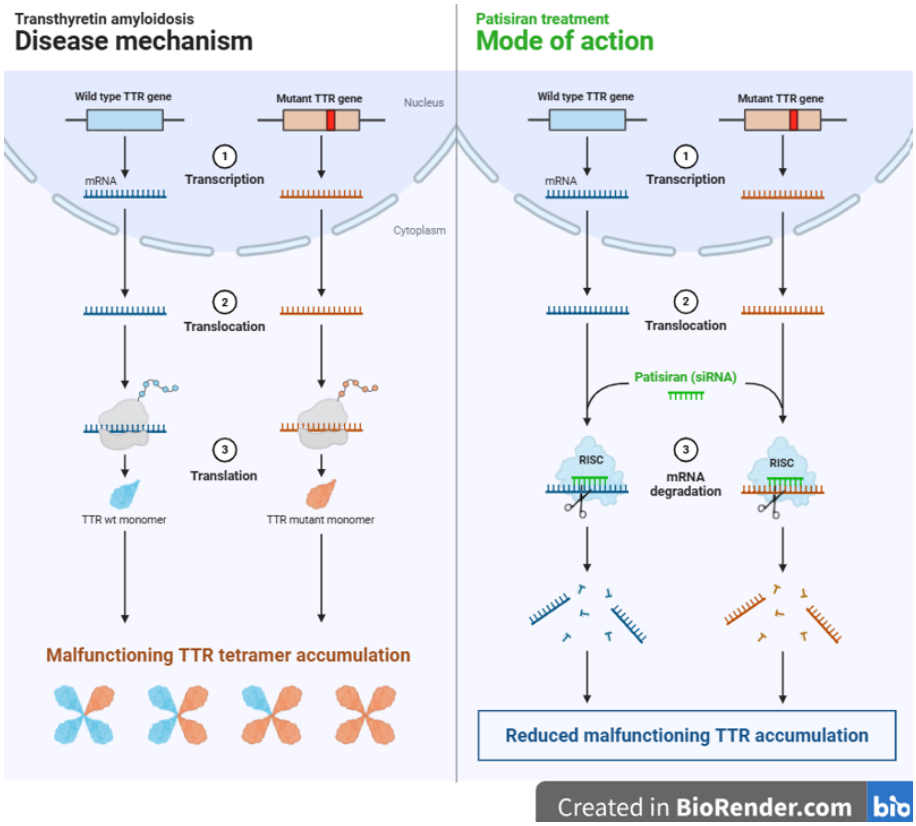

Figure 3. Transthyretin amyloidosis disease mechanism and patisiran mode of action. Image from BioRender.com. © BioRender.

Regarding mRNA-based vaccines for COVID-19, two major formulations have been developed and approved for clinical use: Comirnaty® (BNT162b2), developed by BioNTech in collaboration with Pfizer, and mRNA-1273, developed by Moderna in partnership with the National Institute of Allergy and Infectious Diseases.

These vaccines share a similar composition and formulation principle in that each consists of a lipid nanoparticle (LNP) system designed to encapsulate and protect mRNA molecules, thus ensuring its stability and efficient delivery into target cells.

The lipid components include:

- Cholesterol, which contributes to membrane fluidity and structural stability
- 1,2-dimyristoyl-rac-glycero-3-methoxypolyethylene glycol-2000 (PEG2000-DMG), a PEGylated lipid that enhances nanoparticle stability and prolongs circulation time;
- Distearoylphosphatidylcholine (DSPC), a phospholipid providing bilayer structure;
- An ionizable cationic lipid, which facilitates endosomal escape of the mRNA: ALC-0315 ((4-hydroxybutyl) azanediyl) bis(hexane-6,1-diyl) bis(2-hexyldecanoate)) is used in the Pfizer/BioNTech vaccine, while SM-102 (heptadecan-9-yl 8-[(2-hydroxyethyl)(6-oxo-6-undecyloxyhexyl)amino]octanoate) is used in the Moderna formulation.

Both vaccines contain messenger RNA encoding the SARS-CoV-2 spike protein, although there are slight molecular differences. The BNT162b2 vaccine contains nucleoside-modified mRNA, designed to enhance stability and reduce innate immune activation, whereas the mRNA-1273 vaccine includes a stabilized mRNA sequence encoding the prefusion conformation of the viral spike protein. The mRNA is encapsulated within LNPs that facilitate its delivery into target cells. Upon release into the cytoplasm, the mRNA is translated by the host's ribosomal machinery into the SARS-CoV-2 spike protein, which in turn elicits a specific immune response through both humoral and cellular pathways [39].

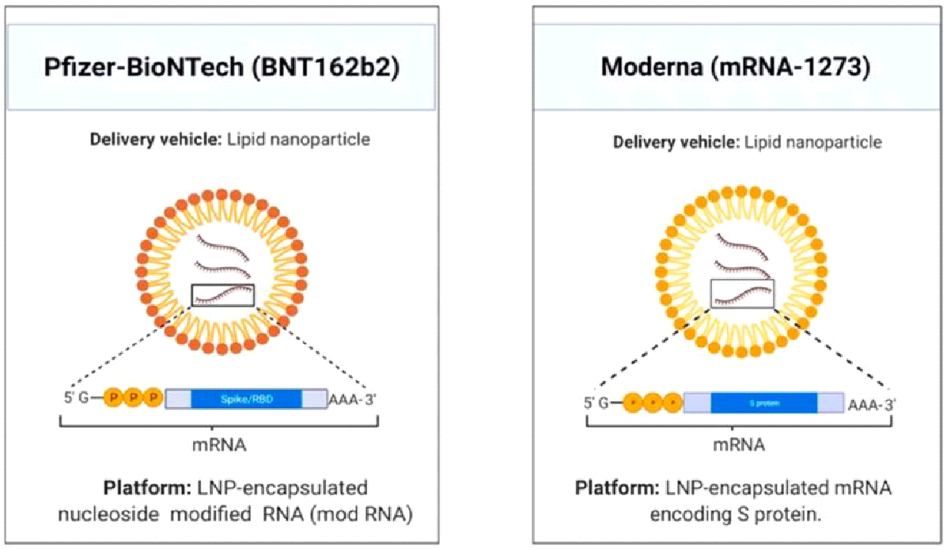

Figure 4. Comparison of delivery vehicle and platform of BNT162b2 (Pfizer-BioNTech) and mRNA-1273 (Moderna) vaccines. Image from BioRender.com. © BioRender.

Cationic polymers, such as polyethylenimine (PEI), poly-L-lysine (PLL), and dendrimers have also proven effective in gene delivery. PEI is particularly valued for its high transfection efficiency and buffering capacity, the so-called “proton sponge” effect that facilitates endosomal escape. PLL is biodegradable and suitable for systemic DNA delivery, though its high-molecular-weight forms display greater stability than low-molecular-weight analogues [40,41]. Dendrimers, with their spherical, highly branched structures, possess numerous amine groups: primary amines on the surface interact with DNA, whereas tertiary amines in the interior enhance endosomal escape [42]. Similarly, chitosan, a biocompatible and biodegradable polysaccharide derived from chitin, forms stable nanoscale complexes with DNA or siRNA and adheres

effectively to negatively charged biological membranes, improving mucosal absorption [43].

Recent work has highlighted the potential of modified cyclodextrins (CDs) as gene-delivery vehicles. β-cyclodextrin derivatives have shown to be efficient siRNA transport into hippocampal and hypothalamic neurons while maintaining cellular viability (around 80 %) and achieving significant gene-silencing efficiency up to 68 % reduction in luciferase and 40 % in GAPDH expression [44]. These results underline the versatility of nanocarrier platforms and their ability to overcome traditional barriers of nucleic-acid delivery, including stability, targeting and intracellular release.

In this PhD project we focused on the Development of LNPs and CD NVs.

2.5 Bibliography

[1] Puri S. et al. Evolution of nanomedicine formulations for targeted delivery and controlled release. Adv Drug Deliv Rev. 2023;200:114962. doi:10.1016/j.addr.2023.114962.

[2] Durgam L.K. et al. Revolutionizing healthcare: the transformative potential of nanotechnology in medicine. Front Drug Deliv. 2025; 5:1556426. doi: 10.3389/fddev.2025.1556426.

[3] Karnwal A. et al. Transforming medicine with nanobiotechnology: nanocarriers and their biomedical applications. Pharmaceutics. 2024;16(9):1114. doi:10.3390/pharmaceutics16091114.

[4] Silva G.A. Introduction to nanotechnology and its applications to medicine. Surg Neurol. 2004;61(3):216–220. doi: 10.1016/j.surneu.2003.09.036.

[5] Mirzaie M. et al. Nanotechnology in vascular medicine: a review. Int J Dev Res. 2021;11:22380 doi: 10.37118/ijdr.22680.08.2021

[6] Sahoo S.K. et al. The present and future of nanotechnology in human health care. Nanomedicine. 2007;3(1):20–31. doi: 10.1016/j.nano.2006.11.008.

[7] Tang R. Gene therapy: a double-edged sword with great powers. Mol Cell Biochem. 2020;474(1–2):73–81. doi: 10.1007/s11010-020-03834-3

[8] U.S. Food and Drug Administration. What Is Gene Therapy? Online, 2018. https://www.fda.gov/vaccines-blood-biologics/cellular-gene-therapy-products/what-gene-therapy

[9] Friedmann T. A brief history of gene therapy. Nat Genet. 1992 Oct;2(2):93–8. doi: 10.1038/ng1092-93

[10] NCATS Toolkit. Genetic therapies – Glossary: gene therapy. Online. https://toolkit.ncats.nih.gov/glossary/gene-therapy/

[11] Wirth T. et al. History of gene therapy. Gene. 2013;525(2):162–169. doi: 10.1016/j.gene.2013.03.137.

[12] U.S. Food and Drug Administration. Human Gene Therapy Products. Guidance Document, 2024. Online. https://www.fda.gov/media/156894/download

[13] Cell and Gene Therapy Domain and Regulation. American Pharmaceutical Review. 2023. Online. https://www.americanpharmaceuticalreview.com/Featured-Articles/596270-Cell-and-Gene-Therapy-Domain-and-Regulation/

[14] U.S. Food and Drug Administration. Plasmid DNA vaccines – Guidance for industry. 2020. https://www.fda.gov/media/102132/download.

[15] Sasso J.M. et al. The progress and promise of RNA medicine—An arsenal of targeted treatments. J Med Chem. 2022;65(10):6975–7015. doi: 10.1021/acs.jmedchem.2c00024.

[16] Dai X. et al. RNA: interactions drive functionalities. Mol Biol Rep. 2020;47(2):1413–1434. doi:10.1007/s11033-019-05230-7.

[17] De Weerdt S. RNA therapeutics: the long and winding road to the clinic. Nat Biotechnol. 2020; 38:122–125.

[18] Statello L. et al. Gene regulation by long non-coding RNAs and its biological functions. Nat Rev Mol Cell Biol. 2021; 22:96–118. doi: 10.1038/s41580-021-00330-4

[19] Han H. RNA interference to knock down gene expression. Methods Mol Biol. 2018; 1706:293–302. doi:10.1007/978-1-4939-7471-9_16.

[20] Hu B. et al. Therapeutic siRNA: state of the art. Signal Transduct Target Ther. 2020;5(1):1–25. doi:10.1038/s41392-020-0207-x.

[21] Kim D.H. et al. RNAi mechanisms and applications. BioTechniques. 2008;44(5):613–616. doi: 10.2144/000112792

[22] Joshua-Tor L. et al. Ancestral Roles of Small RNAs: An Ago-Centric prospective. Cold Spring Harb Perspect Biol. 2011;3(10): a003772. doi: 10.1101/cshperspect.a003772

[23] Khvorova A. et al. The chemical evolution of oligonucleotide therapies of clinical utility. Nat Biotechnol. 2017; 35:238–248. doi: 10.1038/nbt.3765

[24] Wittrup A. et al. Knocking down disease: a progress report on siRNA therapeutics. Nat Rev Genet. 2015;16(9):543–552. doi:10.1038/nrg3978.

[25] Zhou J. et al. Nanoparticle-Based Delivery of RNAi Therapeutics: Progress and Challenges. Pharm. 2013;6(1) doi: 10.3390/ph6010085.

[26] Rinoldi C. et al. Nanotechnology-assisted RNA delivery: from nucleic acid therapeutics to COVID-19 vaccines. Small Methods. 2021;5(9):210. doi:10.1002/smtd.202100402.

[27] Zhang C. et al. RNA therapeutics: updates and future potential. Sci China Life Sci. 2023 Jan;66(1):12-30. doi: 10.1007/s11427-022-2171-2.

[28] Sahin U. et al. mRNA-based therapeutics—developing a new class of drugs. Nat Rev Drug Discov. 2014;13(10):759–780. doi: 10.1038/nrd4278.

[29] Ramamoorth M. et al. Non-viral vectors in gene therapy: an overview. J Clin Diagn Res. 2015;9(1):GE01–GE06. doi: 10.7860/JCDR/2015/10443.5394.

[30] Patil S. et al. The development of functional non-viral vectors for gene delivery. Int J Mol Sci. 2019;20(21). doi: 10.3390/ijms20215491.

[31] Li C. et al. AAV-mediated gene delivery and its therapeutic applications. Nat Biomed Eng. 2024;8(4):456–472. doi: 10.1146/annurev-virology-031413-085355.

[32] Wang JH. et al. Adeno-associated virus as a delivery vector for gene therapy of human diseases. Sig Transduct Target Ther 9, 78 (2024). https://doi.org/10.1038/s41392-024-01780-w

[33] Escors D. et al. Lentiviral vectors in gene therapy: their current status and future potential. Arch Immunol Ther Exp (Warsz). 2010;58(2):107–119. doi:10.1007/s00005-010-0063-4.

[34] Li X. et al. Viral vector-based gene therapy. Int J Mol Sci. 2023;24(9) doi: 10.3390/ijms24097736.

[35] Shirley JL. Et al. Immune Responses to Viral Gene Therapy Vectors. Mol Ther. 2020 Mar 4;28(3):709-722. doi: 10.1016/j.ymthe.2020.01.001.

[36] Zu H. et al. Non-viral vectors in gene therapy: recent development, challenges, and prospects. AAPS J. 2021;23(4):78. 10.1208/s12248-021-00608-7.

[37] Eygeris Y. et al. Chemistry of lipid nanoparticles for RNA delivery. Acc Chem Res. 2022;55(1):2–12. doi: 10.1021/acs.accounts.1c00544.

[38] S. M. Hoy, “Patisiran: First Global Approval,” Drugs, vol. 78, no. 15, pp. 1625–1631, Oct. 2018, doi: 10.1007/s40265-018-0983-6.

[39] Hou X. et al. Lipid nanoparticles for mRNA delivery. Nat Rev Mater. 2021;6(12):1078–1094.

[40] Qin Y. et al. Delivery of nucleic acids using nanomaterials. Mol Biomed. 2023; 4:48. doi: 10.1186/s43556-023-00160-0.

[41] Khan M. Polymers as efficient non-viral gene delivery vectors: the role of the chemical and physical architecture of macromolecules. Polymers (Basel). 2024;16(18):2629. doi:10.3390/polym16182629.

[42] Gorzkiewicz M. et al. Poly(lysine) dendrimers form complexes with siRNA and provide its efficient uptake by myeloid cells: model studies for therapeutic nucleic acid delivery. Int J Mol Sci. 2020;21(9):3138. doi:10.3390/ijms21093138.

[43] Karayianni M. et al. Chitosan-based nanoparticles for nucleic acid delivery: technological aspects, applications, and future perspectives. Pharm. 2023;15(7) doi: 10.3390/pharmaceutics15071849
[44] O'Mahony A.M. et al. O'Driscoll C.M. Click-modified cyclodextrins as nonviral vectors for neuronal siRNA delivery. ACS Chem Neurosci. 2012;3(10):744–752 doi: 10.1021/cn3000372

3 Formulation and Evaluation of Lipid Nanoparticles for Enhanced siRNA Delivery and Gene Silencing Efficiency

3.1 Introduction

LNPs represent an advanced generation of lipid-based delivery systems that evolved from the original liposome concept developed in the 1960s. Alec C. Bangham and colleagues were the first to demonstrate that phospholipids dispersed in aqueous environments spontaneously self-assemble into bilayer vesicles, forming what were termed liposomes. These structures mimic biological membranes and were soon recognized as potential carriers for biologically active molecules, including drugs and nucleic acids [1;2].

Over subsequent decades, liposomal technology was refined through advances in lipid chemistry, colloidal stability, and controlled release, leading to the emergence of lipid nanoparticles as more complex and efficient delivery platforms [3;4].

In particular, LNPs have emerged as one of the most effective delivery platforms for nucleic acids, offering protection from enzymatic degradation and facilitating cellular internalization and endosomal escape [5-8]. The inclusion of cationic or ionizable lipids within these systems enables strong electrostatic interactions with negatively charged siRNA molecules, which is essential for efficient complexation and intracellular release [9;10].

In the earliest stages of lipid-based nucleic acid delivery system development, permanently charged cationic lipids were frequently incorporated into formulations to promote efficient complexation with

negatively charged nucleic acids. The presence of a permanent positive charge ensures strong electrostatic interactions with siRNA or other nucleic acids, facilitating their condensation, encapsulation, and protection from enzymatic degradation. In addition, permanently charged lipids were initially expected to enhance cellular uptake by promoting interactions with the negatively charged cellular membrane. However, these lipids may also lead to increased cytotoxicity and undesired interactions with serum proteins due to their persistent surface charge under physiological conditions. To overcome these limitations, more recent LNP formulations often employ ionizable lipids, which remain largely neutral at physiological pH but become protonated in acidic environments, enabling efficient nucleic acid complexation and endosomal escape while reducing systemic toxicity [11].

Optimized LNPs formulations generally incorporate a combination of:

- Cationic/Ionizable lipid, which becomes positively charged in acidic conditions, allowing complexation with negatively charged RNA.
- Helper phospholipid, supporting bilayer formation and membrane fusion.
- Cholesterol, which stabilizes the structure.
- PEG-modified lipid, to improve colloidal stability and circulation half-life [8-12].

These components, collectively, confer desirable physicochemical characteristics, such as appropriate size, PdI and Z, along with high biocompatibility and minimal immunogenicity [13;14].

Several preparative advancements have been fundamental in enabling the clinical translation of siRNA-loaded LNPs, exemplified by Patisiran, the first FDA-approved siRNA therapeutic for the treatment of hereditary transthyretin amyloidosis [15-17].

Other milestones for LNPs in gene delivery were the authorization of mRNA–LNP vaccines for COVID-19 in 2020–2021, namely BNT162b2 (Pfizer-BioNTech) and mRNA-1273 (Moderna), which demonstrated global-scale [18].

Although some relevant challenges remain to be addressed regarding LNPs, particularly in terms of safety, large-scale manufacturing, and regulatory compliance, these systems continue to represent the most advanced and promising formulations for nucleic acid and gene delivery applications [19-21].

The present study focuses on the formulation and optimization of LNPs for enhanced siRNA delivery. In the present work, both permanently charged and ionizable cationic lipids were evaluated in order to assess their contribution to the physicochemical properties, stability, and biological performance of the developed LNP formulations.

LNPs were prepared via TLE method and characterized for their physicochemical properties, using DLS [22;26;27]. A DoE strategy, based on a full factorial design performed with MODDEGo software (version 12.01), was applied to define key formulation parameters and identify optimal lipid compositions [23-28]. DoE aimed to evaluate: the effect of sonication cycles on size and PdI, the influence of increasing DOPE concentration, given its role in affecting the spontaneous curvature of LNPs and the possibility of eliminating the extrusion step, which results in a significant sample loss (30–40%).

Using the parameters defined by the DoE, additional cationic lipids were incorporated to produce LNPs and were then complexed, initially with a siRNA Negative control and then with GFP-targeting siRNA at an N/P (+/–) ratio of 10.

The complexation efficiency was evaluated by agarose gel electrophoresis, leading to selection of the two most promising formulations (B and D) for further investigation. DLS analysis and stability at 4°C (±1°C) after 1,4 and 7 days were performed.

Biological evaluation included stability in cells medium (with and without FBS) after 24h, cytotoxicity assays in HeLa cells after 24h, performed with both empty and siRNA-loaded LNPs, internalization test in HeLa GFP and RAW 264.7 cells after 24h, and silencing efficiency in HeLa GFP cells,

after 48 and 72h. To gain further insight into LNP structure, selected formulations were analyzed by SAXS, providing complementary information on internal architecture and stability [29].

3.2 Materials and Methods

3.2.1 Materials

All the lipids; Cholesterol (Chol), 1,2-dioleoyl-sn-glycero-3-phosphoethanolamine (DOPE), 1,2-dioleoyl-sn-glycero-3-phosphocholine (DOPC), 1,2-dioleoyl-3-trimethylammonium-propane (DOTAP), 3β-[N′,N′-dimethylaminoethane)-carbamoyl]cholesterol hydrochloride (DC-CH), (11-mercaptoundecyl)-N,N,N-trimethylammonium bromide (MTAB), ((4-hydroxybutyl)azanediyl)bis(hexane-6,1-diyl)bis(2-hexyldecanoate) (ALC-0315), 1,2-dioleoyl-sn-glycero-3-phosphoethanolamine-N-[amino(polyethylene glycol)-2000] ammonium salt(DOPE-PEG-2000), 1,2-distearoyl-sn-glycero-3-phosphoethanolamine-N-[carbonyl-methoxy(polyethylene glycol)-2000] (18:0 PEG 2000) were purchased from Merck (Darmstadt, Germany).

HeLa cells, HeLa GFP cells and RAW 264.7 cells were obtained from the American Type Culture Collection (ATCC, Manassas, VA, USA). GFP-targeting siRNA was purchased from Biospring (Frankfurt, Germany). SiRNA negative control, 1,1′-Dioctadecyl-3,3,3′,3′-Tetramethylindodicarbocyanine (DiD), RNase-free water, Lipofectamine, and Opti-MEM were purchased from Thermo Fisher Scientific (Waltham,USA). Chloroform ($CHCl_3$), and phosphate-buffered saline (PBS) were purchased from Merck (Darmstadt, Germany). Dulbecco's Modified Eagle Medium (DMEM), fetal bovine serum (FBS), Tris–Borate EDTA buffer (TBE) and trypsin were obtained from VWR (Pennsylvania, USA).

3.2.2 LNPs Production and siRNA complexation

LNPs were obtained under sterile conditions in a laminar flow hood. Lipid stock solutions in chloroform were prepared, stored at −20 °C, and mixed in defined ratios. After solvent evaporation under nitrogen and further drying in a vacuum oven (30 °C, −70/−80 cm Hg, 1 h), the lipid film was hydrated with 3 mL of H2O RNase-free. Samples were vortexed, stored overnight at 4 °C, and subjected to five freeze–thaw cycles (liquid nitrogen/40–50 °C water bath), followed by 3–5 probe sonication cycles (1 min, 50% amplitude, 1 s pulse). The final suspensions were diluted with 3 mL of RNase-free water. The extrusion step initially included in the protocol was omitted based on the DoE results [30].

siRNA complexation was performed after LNP formation. The aqueous siRNA solution was added to preformed LNPs at an N/P ratio of 10 and gently stirred for 1 hour at 300 rpm to allow electrostatic complexation. This approach was intentionally adopted to prevent potential mechanical or shear stress that could occur if RNA were present during nanoparticle preparation.

3.2.3 Dynamic Light Scattering (DLS) and Electrophoretic Light Scattering (ELS)

Size and PdI of LNPs were determined by DLS, while Z was measured by ELS, using a Zetasizer Pro Red Label instrument (Malvern Instruments, Malvern, UK). Measurements were performed on both empty LNPs and siRNA-loaded LNPs, as well as to assess their stability at 4°C (±1°C) and in cell culture medium. For size and PdI analysis, disposable polystyrene cuvettes (12 × 12 × 45 mm; minimum volume: 40 µL) were used, with 100 µL of each sample directly loaded into the cuvette. Z

measurements were carried out using capillary cells (minimum volume: 0.7 mL); in this case, 100 µL of LNPs suspension was diluted with RNase-free water to a final volume of 700 µL. In both cases, the cuvette or capillary cell was placed into the instrument sample holder for analysis. All measurements were carried out in triplicate at a constant temperature of 25 °C with a detection angle of 173°.

3.2.4 Design of experiment (DoE)

Two full factorial designs (one for formulation A and one for formulation B) with three factors at two levels were carried out using MODDE Go software (version 12.01, Umetrics). The design consisted of 11 experiments in total, including 8 factorial points and 3 center points. One qualitative factor was included, namely the application of the extrusion step, together with two quantitative factors at two levels with evaluation of the intermediate level:

- DOPE percentage (10–60%).
- number of sonication cycles (1–5).

The evaluated responses were:

- size of LNPs (target range: 90–150 nm);
- PDI (target: 0–0.3).

Formulations were prepared according to the procedure described in section 3.2.2 Partial least squares (PLS) regression was applied to the experimental data, and statistical analysis was performed by analysis of variance (ANOVA) to confirm model significance and validity for all responses.

3.2.5 Complexation Efficiency

Complexation efficiency was assessed by horizontal agarose gel electrophoresis. A 2% (w/v) agarose gel was prepared in a 1× TBE buffer, poured into a casting tray, and allowed to solidify at room temperature. The gel was then placed in a horizontal electrophoresis chamber filled with 1× TBE buffer. For each sample, 20 µL were loaded per well after mixing with 2 µL SYBR™ Gold nucleic acid stain and 1 µL loading buffer (Thermo Fisher Scientific, Waltham, MA, USA). Free siRNA was run as a control.

To evaluate siRNA release, LNP samples were incubated with triton 10 mg/mL at a 10-fold excess for 1 h at 37 °C under shaking (420 rpm, Titramax 1000 with Inkubator 1000, Heidolph Instruments, Schwabach, Germany). All preparations were performed in Eppendorf tubes. Gels were imaged using a GelDoc XR+ system (Bio-Rad, Hercules, CA, USA). A simple estimate of the siRNA complexation percentages was obtained analysing the gel images by means of dedicated ImageJ macros [31].

3.2.6 Synchrotron-SAXS

SAXS measurements on solutions of nanoparticles, both empty and complexed with the siRNA, were performed at the ID02 beamline of the European Synchrotron Radiation Facility (ESRF-Grenoble, France) using a flow-through capillary with 2 mm diameter and maintaining the temperature at 37°C to reproduce physiological conditions. The scattering vector q covered a range of 0.11 to 9.70 nm-1 with a sample-detector distance of 0.8 m. The wavelength and energy of the incoming beam were 0.995 Å and 12.46 keV, respectively. The 2D SAXS patterns were circularly averaged and normalised to the absolute scale to obtain merged

1D patterns from the different configurations, followed by background subtraction. These resulting 1D curves were fitted using SASView 6.0 package.

Formulations with different cationic lipid content (5%, 10%, and 20%) were prepared to evaluate whether and how the cationic component affects nanoparticle morphology. Samples were prepared to achieve a final total lipid concentration of 10 mg/mL to ensure enough scattering intensity. To obtain complexed systems, 116 µL of siRNA solution (MISSION siRNA Universal Negative Control #1, Merck, Italy) at concentration 4.77×10^{-7} M were mixed with 5 µL of lipid nanoparticles and then incubated at room temperature for 15 minutes to allow equilibration. The resulting N/P ratios are reported in Table 1.

Table 1. N/P ratio of LNPs tested.

LNPs	DC-CH_5	DC-CH_10	DC-CH_20	MaBr_5	MaBr_10	MaBr_20
N/P (+/-)	2.0	4.0	8.0	3.3	6.6	13.2

3.2.7 Stability assessment

The stability of LNPs with siRNA was assessed under two conditions: storage at 4 °C and incubation in cell culture medium. For storage stability NV–pGFP formulations were stored at 4 °C (±1 °C) and analyzed after 1, 4, and 7 days using DLS, as described in Section 3.2.3.

Stability in cell culture medium was evaluated at time points 0, 2, 4, and 24 hours.For each time point, 10 µL of NV dispersion was mixed with 90 µL of either non-supplemented DMEM or DMEM supplemented with 10% FBS. Samples were analyzed by DLS with the attenuator set to 7, using

10 runs per measurement. All experiments were performed in triplicate, and results are reported as mean ± standard deviation (SD).

3.2.8 *In vitro* toxicity, Internalization and silencing efficacy

The Hela, HeLa GFP and RAW 264.7 cells lines were grown in with 10 mL DMEM supplemented with 200 mM L-Glutamine and 10% (v/v) FBS medium, in a humidified incubator (MEMMERT INE 400, Memmert, Germany) with 5% CO_2 / 95% atmospheric air at 37°C. Cells used for comparative experiments were maintained in cell culture dishes 10 mm and used between passages 5 and 25.

The cytotoxicity of empty and siRNA loaded LNPs was evaluated using the MTT assay with HeLa Cells. The assay was performed on standard 96-well tissue-culture–treated plates, with concentrations ranging from 31 to 500 µg/mL for empty NVs, and from 15.5 to 125 µg/mL for pGFP - loaded NVs. Cells were seeded in 96-well plates at fixed densities of 1 × 105 cells/mL. Cells were cultured for 24 h in standard culture medium. After this initial incubation, the medium was replaced with 160 µL of fresh medium and 40 µL of the NVs solution diluted in Opti-MEM. The cells were then incubated with NVs for an additional 24 h at 37 °C in a humidified 5% CO_2 atmosphere [32].

After incubation, the medium was removed and replaced with an MTT salt solution diluted in DMEM to a final concentration of approximately 1 mM. Plates were incubated for 1–2 h at 37 °C to allow for formazan crystal formation.

Following incubation, the MTT-containing medium was carefully removed and formazan crystals were solubilized. The absorbance was measured at 570 nm using a microplate reader Infinite M200PRO (Tecan,

Männedorf, Switzerland). Background absorbance at 630 nm was subtracted from the 570 nm readings to obtain normalized absorbance values representing cell viability.

Cell viability was expressed relative to untreated controls.

Internalization of DiD-labeled LNPs (DiD concentration5 µL/mL) was evaluated in HeLa-GFP and RAW 264.7 cells (1 × 10^5 cells/mL). Cells were seeded in 24-well plates and incubated for 24 h under standard conditions (37 °C, 5% CO_2) before exposure to LNPs diluted in Opti-MEM (50 µL) and complete DMEM (450 µL) for 24 h. The samples were analysed by flow cytometry.

Gene silencing was evaluated in HeLa-GFP cells at 48 and 72 h post-treatment. Cells were seeded in 24-well plates (1 × 10^5 cells/mL) and incubated for 24 h, then exposed to 50 µL of nanoparticle formulations diluted in Opti-MEM plus 450 µL complete DMEM. Cells were then incubated for 48 h and 72h before preparation for flow cytometry analysis. All experiments were performed in triplicate, and results are reported as mean ± standard deviation.

3.2.9 Fluorescence microscopy

Fluorescence images were acquired for transfection efficiency (24- and 48-h) post-treatment using an inverted fluorescence microscope Olympus IX73 (Olympus Corporation, Tokyo, Japan). The microscope was equipped with a digital camera and a filter set appropriate for the fluorophore used (CY3 for internalization and FITC for transfection respectively).

Images were captured using a 20× objective lens. Exposure time, gain, and contrast were adjusted to avoid saturation and maintain comparability

between samples. Image acquisition was performed using the CellSens Standard software (Olympus Corporation, Tokyo, Japan). No image manipulations that could affect data interpretation were applied.

3.2.10 Flow cytometry

Flow cytometry was performed for Internalization test (24 h) and silencing efficiency (24, 48 and 72h) using a CytoFLEX flow cytometer (Beckman Coulter, Brea, CA, USA), collecting 10,000 cells/sample. Data were analyzed using CytExpert software (Beckman Coulter, Brea, CA, USA).
At the designated time points, the medium was removed, and cells were washed with 300 µL of PBS. Then, 120 µL of trypsin was added to each well and cells were incubated for 3 min at 37 °C to allow detachment. Subsequently, 380 µL of complete culture medium was added to neutralize the trypsin, and the cell suspension was transferred to 2 mL Eppendorf tubes.
Samples were centrifuged for 5 min at 1000 rpm using an Eppendorf 5425 R centrifuge (Eppendorf, Hamburg, Germany). The supernatant was discarded, and the cell pellet was resuspended in 400 µL of PBS supplemented with 10% FBS. The samples were kept on ice until analysis. All experiments were performed in triplicate, and results are reported as mean ± standard deviation. For samples including a control group, statistical significance relative to the control was assessed by calculating P values using GraphPad Prism software 2023 (GraphPad Software, San Diego, CA, USA).

3.3 Results and discussion

3.3.1 Production and Optimization of empty LNPs

3.3.1.1 Preliminary tests

Preliminary tests were conducted to define the physicochemical parameters required for siRNA complexation. Target values were set at <200 nm for size and <0.3 for PdI. LNPs were prepared at a constant total lipid concentration of 1.66 mg/mL for all the formulations.

The initial formulations included the use of the ionizable lipid DLin-MC3-DMA together with a small percentage of a cationic lipid. Four formulations were initially selected (as reported in Table 2) [33]. LNPs were prepared as described in Section 3.2.2, but without extrusion (only by 3 cycles of sonication). A citrate buffer at pH 4 was used as the rehydration solution, due to the presence of the ionizable lipid.

Table 2. LNPs composition of formulation 1-4.

Formulation	Chol	DC-CH	DOTAP	DOPE	DOPC	DLin-MC3-DMA lipid	DMGPEG-2000
1	43	2	/	5	15	25	10
2	23	2	/	5	30	30	10
3	45	/	1	5	15	24	10
4	25	/	1	5	30	29	10

The samples were analyzed by DLS, and the corresponding data are shown in Table 3.

Table 3. DLS Analysis of LNPs 1-4.

Formulation	Size (nm)	PdI	Z (mV)
1	400 ± 137	0.5	+ 23 ± 8
2	194 ± 31	0.3	+14 ± 6
3	815 ± 54	0.5	+21 ± 6
4	160 ± 10	0.4	+40 ± 3

The size values obtained were not optimal for any of the formulations; however, formulations 2 and 4, which contained a lower amount of chol, showed smaller particle sizes and improved PdI values. Consequently, formulations 2 and 4 were reproduced, this time including extrusion after sonication. The resulting LNPs were characterized by DLS analysis (table 4).

Table 4. DLS analyses of formulation 2 and 4 extruded.

Formulation	Size (nm)	PdI	Z (mV)
2 e	161 ± 13	0.2	+ 30 ± 2
4 e	150 ± 11	0.3	+26 ± 3

It was observed that extrusion caused a slight reduction in size and a significant improvement in size uniformity. Based on these results, new LNPs were prepared by increasing the DOPE concentration (from 5% to 20%) and decreasing the concentration of the ionizable lipid, in order to investigate the effect of this modification on the spontaneous curvature.

The compositions of these formulations are reported in Table 5 and DLS data in table 6.

Table 5. LNPs composition of formulation 5-6.

Formulation	Chol	DC-CH	DOTAP	DOPE	DOPC	DLin-MC3-DMA lipid	DMGPEG-2000
5	23	2	/	20	30	15	10
6	25	/	1	20	30	14	10

Table 6. DLS analyses formulation 5-6 with and without extrusion.

Formulation	Size (nm)	PdI	Z (mV)
5	213 ± 20	0.4	+ 18 ± 2
5 e	135 ± 6	0.2	+4 ± 1
6	217 ± 14	0.4	+18 ± 3
6 e	148 ± 15	0.3	+4 ± 1

A slight decrease in size was observed after extrusion (compared to the previous formulation), along with a decrease in zeta potential. Overall, the zeta potential values were not very consistent. This may be attributed to the presence of salts in the hydration solution, which could screen the surface charge, as well as to the effect of DMG-PEG 2000.

Due to the limited availability of the ionizable lipid and with the aim of optimizing the formulation, new samples were prepared without the ionizable lipid, while doubling the amount of cationic lipids and increasing the percentages of DOPC and DOPE to 35% (Table 7 and 8).

Table 7. LNPs composition of formulation 7-8.

Formulation	Chol	DC-CH	DOTAP	DOPE	DOPC	DMG PEG-2000
7	20	4	/	35	35	6
8	22	/	2	35	35	6

Table 8. DLS analyses of formulation 7-8 with and without extrusion.

Formulation	Size (nm)	PdI
7	162 ± 8	0.3
7 e	120 ±12	0.2
8	165 ± 14	0.3
8 e	134 ± 17	0.4

We obtained zeta potential values close to zero, most likely due to the presence of salt in the formulation and the charge-shielding effect of PEG. To address this, the concentrations of the cationic lipids DOTAP and Dc-ch were increased up to 20%. Moreover, DMG-PEG-2000 was replaced with PE 18:0-PEG-2000, a PEG-lipid conjugate with a longer hydrophobic chain capable of integrating more effectively into the LNPs structure. The increase in cationic lipid content was balanced by a reduction in cholesterol concentration, thereby maintaining a constant total lipid content. The compositions of the resulting formulations and DLS data are reported below (table 9-10).

Table 9. LNPs composition of formulation 9-10

Formulation	Chol	DC-CH	DOTAP	DOPE	DOPC	PE 18:0-PEG2000
9	4	20	/	35	35	6
10	9	/	15	35	35	6

Table 10. DLS dat of formulation 9-10 with and without extrusion.

Formulation	Size (nm)	PdI
9	190 ± 11	0.3
9 e	121 ±13	0.2
10	198 ± 16	0.3
10 e	160 ± 9	0.2

DLS analyses showed a slight increase in size and PDI, although the PDI remained within the acceptable range for extruded nanoparticles. This increase is likely due to the bulkier structure of PE 18:0-PEG-2000 compared to DMG-PEG-2000. The zeta potential values remained close to zero. At this stage, the same lipid composition was prepared in RNase-free water in order to evaluate whether higher zeta potential values could be achieved, with the aim of subsequently complexing the nanoparticles with siRNA, given the absence of the ionizable lipid.
The obtained results showed satisfactory size, PDI, and zeta potential values, as reported in Table 11.
For clarity in the following experiments, the formulations were renamed Formulation A and Formulation B (instead of 9 and 10)

Table 11.DLS analyses of LNPs A and B with and without extrusion.

Formulation	Size (nm)	PdI	Z (mV)
A	149 ± 17	0.2	+ 43 ± 9
A extruded	125 ±12	0.2	+45 ± 8
B	130 ± 14	0.3	+47± 11
B extruded	91 ± 10	0.1	+38 ± 7

3.3.2 DoE Results

The DoE aimed to evaluate:

- the effect of sonication cycles on particle size and PdI
- the influence of increasing DOPE concentration, given its role in affecting the spontaneous curvature of LNPs
- the possibility of eliminating the extrusion step, which results in a significant sample loss (30–40%)

The DoE trials are reported in Table 12 and were identical for both designs (LNPs with DC-CH and LNPs with DOTAP).

Table 12. DoE trials

N° Experiment	DOPE (%)	Sonication Cycles	Extrusion
N1	10	1	NO
N2	60	1	NO
N3	10	5	NO
N4	60	5	NO
N5	10	1	Yes
N6	60	1	Yes
N7	10	5	Yes
N8	60	5	Yes
N9	35	3	NO
N10	35	3	NO
N11	35	3	NO

DLS measurements from the DoE LNPs are reported in Table 13 (DOTAP) and Table 14 (DCCH) and the response graph from ANOVA analysis is shown in Figure 1.

Table 13. DLS analysis of DoE LNPs A (DOTAP)

Formulation	Size (nm)	PdI
N1	181	0.26
N2	363	0.55
N3	121	0.26
N4	170	0.18
N5	103	0.30
N6	136	0.20
N7	107	0.26
N8	147	0.22
N9	136	0.19
N10	132	0.18
N11	139	0.18

Table 14. DLS analysis of DoE LNPs B (DC-CH)

Formulation	Size (nm)	PdI
N1	181	0.20
N2	214	0.31
N3	99	0.19
N4	130	0.21
N5	96	0.17
N6	110	0.18
N7	127	0.30
N8	125	0.23
N9	122	0.20
N10	130	0.21
N11	124	0.21

A

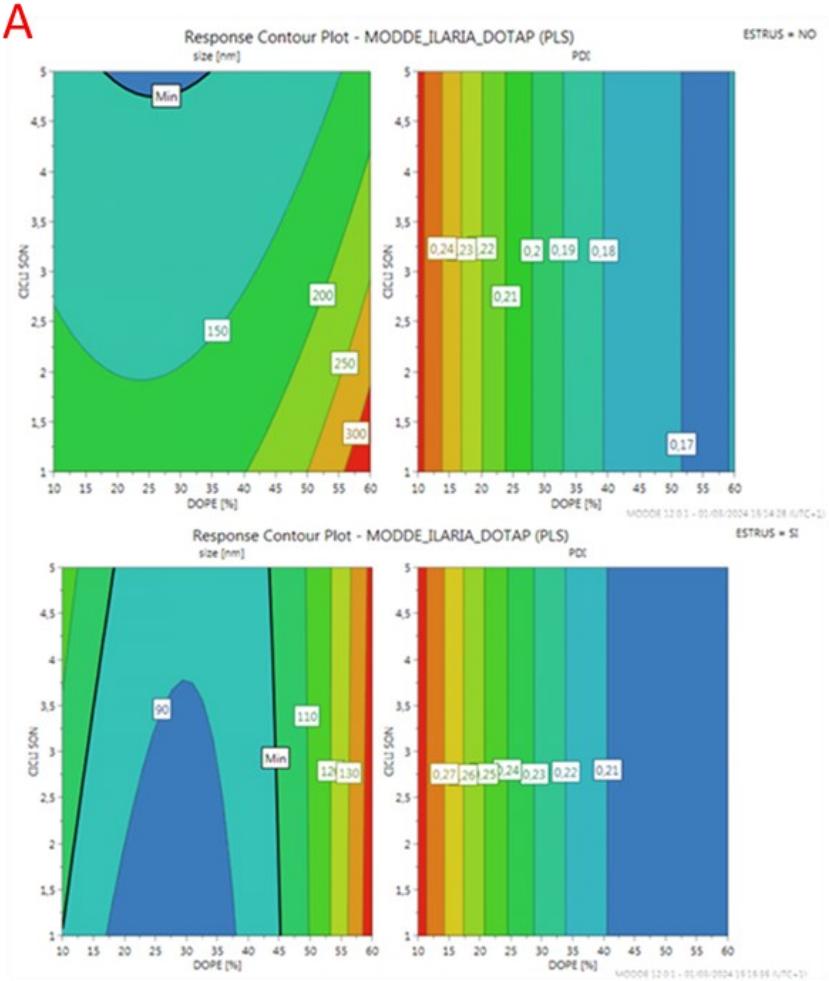
Response Contour Plot - MODDE_ILARIA_DOTAP (PLS)
ESTRUS = NO
size [nm]
PDI
Min
150
200
250
300
0,24
23
22
0,2
0,19
0,18
0,21
0,17
CICLI SON
DOPE [%]
Response Contour Plot - MODDE_ILARIA_DOTAP (PLS)
ESTRUS = SI
size [nm]
PDI
90
110
Min
120
130
0,27
26
25
24
0,23
0,22
0,21
CICLI SON
DOPE [%]

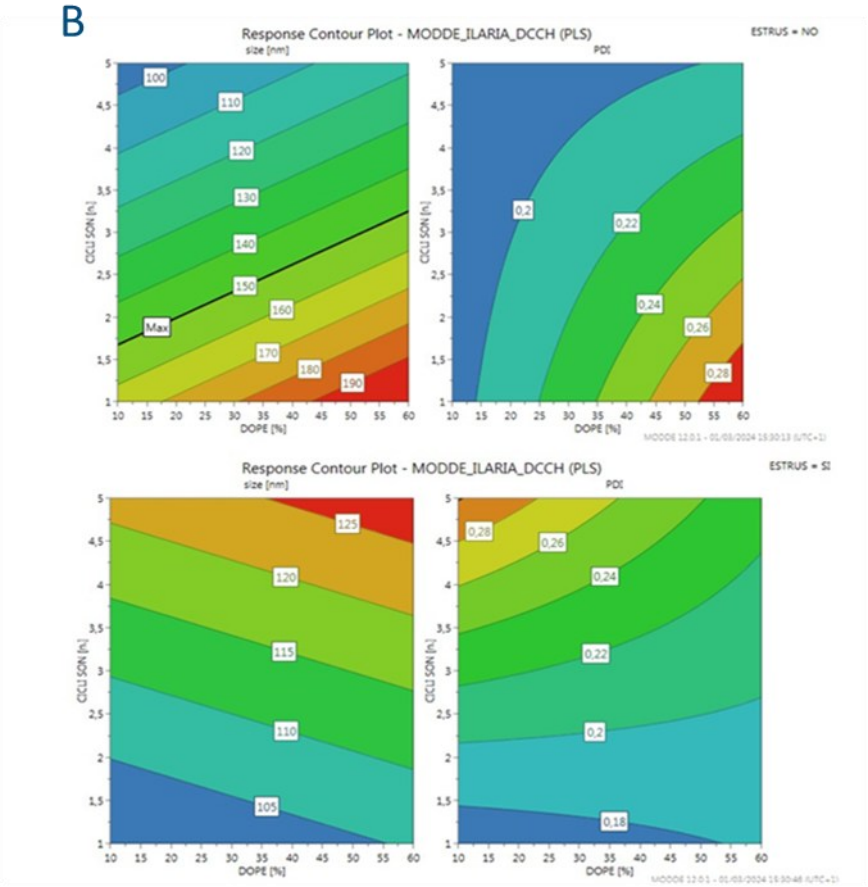

Figure 1. DoE response graph from ANOVA analysis. LNPs with DOTAP (A), and with DC-CH (B)

The DoE results were consistent across both formulations. At the highest DOPE level, both size and PdI values increased, whereas at the lowest DOPE level, the LNPs exhibited reduced dimensions but were very difficult to extrude, resulting in low yields. The number of sonication cycles also influenced LNPs size and PdI. The desired range of size and PdI for the LNPs was achieved with 35% DOPE and 4 sonication cycles, eliminating the extrusion step.

3.3.3 Effect of cationic lipid

Formulations A and B were therefore reproduced using the parameters selected through the DoE optimization. The corresponding lipid compositions are reported in Table 15, while the physicochemical characterization results obtained by DLS analysis are presented in Table 16.

Table 15. LNPs composition of formulation A-B.

Formulation	Chol	DC-CH	DOTAP	DOPE	DOPC	PE 18:0-PEG2000
A	4	20	/	35	35	6
B	9	/	15	35	35	6

Table 16.DLS analysis of LNPs with Dope-PEG 2000

Formulation	Size (nm)	PdI	Z (mV)
A	130 ± 5	0.2	+ 40 ± 6
B	128 ± 18	0.2	+ 42 ± 4

Using the same production parameters, the cationic lipid was further substituted with either the ionizable lipid ALC-0315 23-24 to generate formulation C, or with the cationic lipid MTAB, yielding formulation D [34-36]. Formulations were prepared with varying cationic lipid content (10–20%), with 20% providing the most favorable results in terms of size, PdI and Z. Lipid composition of formulation C and D is specified in table 17. DLS results are reported in Table 18.

Table 17. LNPs composition of formulation C-D

Formulation	Chol	ALC-0315	MTAB	DOPE	DOPC	PE 18:0-PEG2000
C	**4**	**20**	**/**	**35**	**35**	**6**
D	**4**	**/**	**20**	**35**	**35**	**6**

Table 18. DLS analysis of LNPs with ALC-0315 (C) and MTAB (D).

Formulation	Size (nm)	PdI	Z (mV)
C	178 ± 15	0.2	+ 33 ± 12
D	118 ± 13	0.3	+ 31 ± 5

A slight increase in size and PDI was observed for formulation C, whereas formulation D maintains similar size; however, both remained within an acceptable range.

The role of PEG was also investigated by preparing formulations in its absence; however, these exhibited markedly increased size (<300 nm) and PdI. They were therefore excluded from further analysis.

Formulations A-B-C-D were complexed with siRNA in N/P=10 and characterized.

3.3.4 SiRNA loaded LNPs

3.3.4.1 Complexation efficacy

The complexation efficiency of the lipid formulations was assessed as described in Section 3.2.5. Representative images of formulations B and D are shown in Figure 2-3, demonstrating complete siRNA complexation. Formulation B and D demonstrated complete siRNA complexation, while formulations A and C exhibited partial siRNA release, indicating incomplete complex formation. Due to these findings, *in vitro* studies were carried out on LNPs B and D.

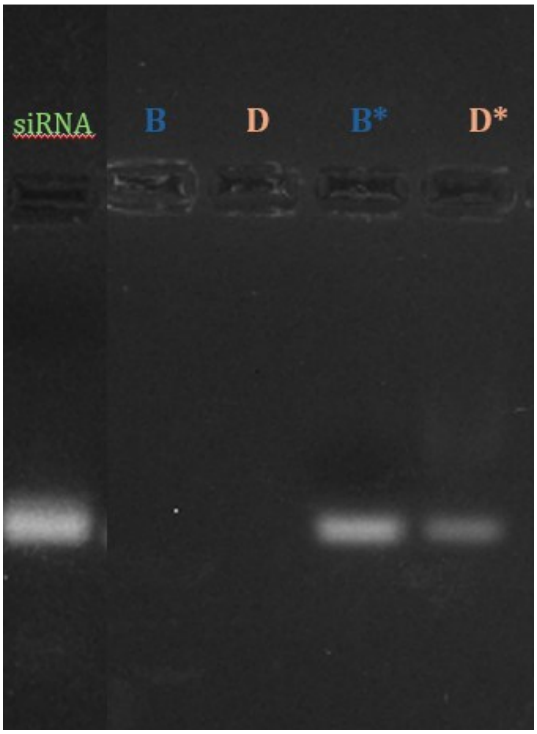

Figure 2. Agarose gel Images obtained after horizontal electrophoresis of LNPs with siRNA. SiRNA is shown in green, LNPs B in blue and LNPs D in Orange. Samples containing Triton are marked with an asterisk.

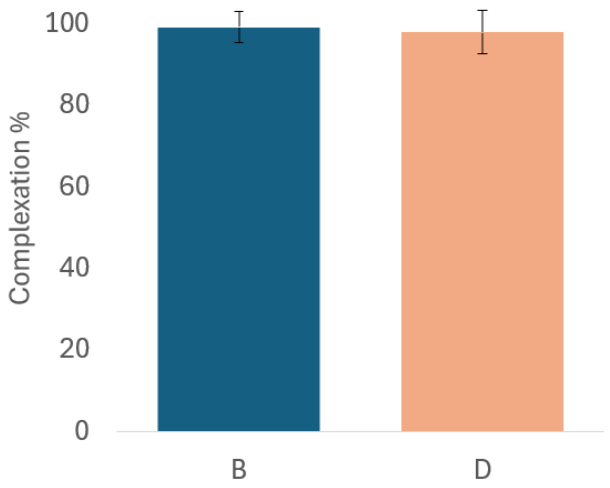

Figure 3. Complexation % of formulation B and D. n=3 mean ± S.D.

3.3.4.2 LNPs Characterization

LNPs B and D were complexed with siRNA GFP and characterized in terms of size, PdI and Z (Table 19).

Table 19. DLS analysis of LNPs B and D with siRNA-GFP

Formulation	Size (nm)	PdI	Z (mV)
C	138 ± 14	0.2	+35 ± 3
D	145 ± 23	0.3	+22 ± 6

Both formulations exhibited comparable sizes and low PdI values (<0.3). A reduction in zeta potential was observed relative to the empty LNPs, likely reflecting electrostatic interactions with the nucleic acid cargo.

LNPs loaded with siRNA stability were evaluated at 4°C (±1 °C) over 7 days. DLS analyses are reported in figure 4, demonstrating good stability of both formulations tested.

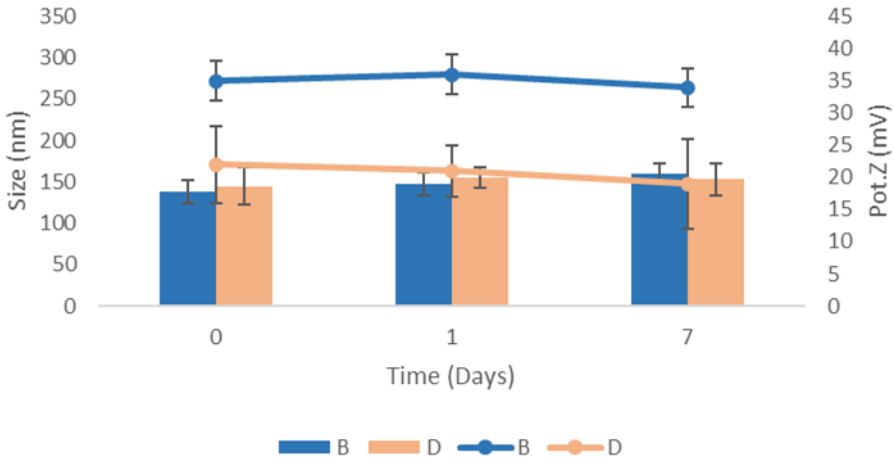

Figure 4. Stability of LNPs B and D with siRNA after 0, 1 and 7 days at 4°C (±1°C). LNPs B (Blue) LNPs D (orange).n=3 mean ± S.D.

siRNA loaded LNPs were also analyzed in culture medium for 24 h at 37°C (±1 °C), with or without supplementation.

As reported in figure 5, LNPs remained stable in all media. In FBS-containing medium (5A), an initial increase in size and Kcps was observed at time 0, followed by stabilization, confirming nanoparticle integrity. In medium without supplementation (5B), size increased slightly but remained around 200 nm after 24 h, with Kcps largely stable, indicating no significant aggregation. Overall, both formulations exhibited good stability under all tested conditions.

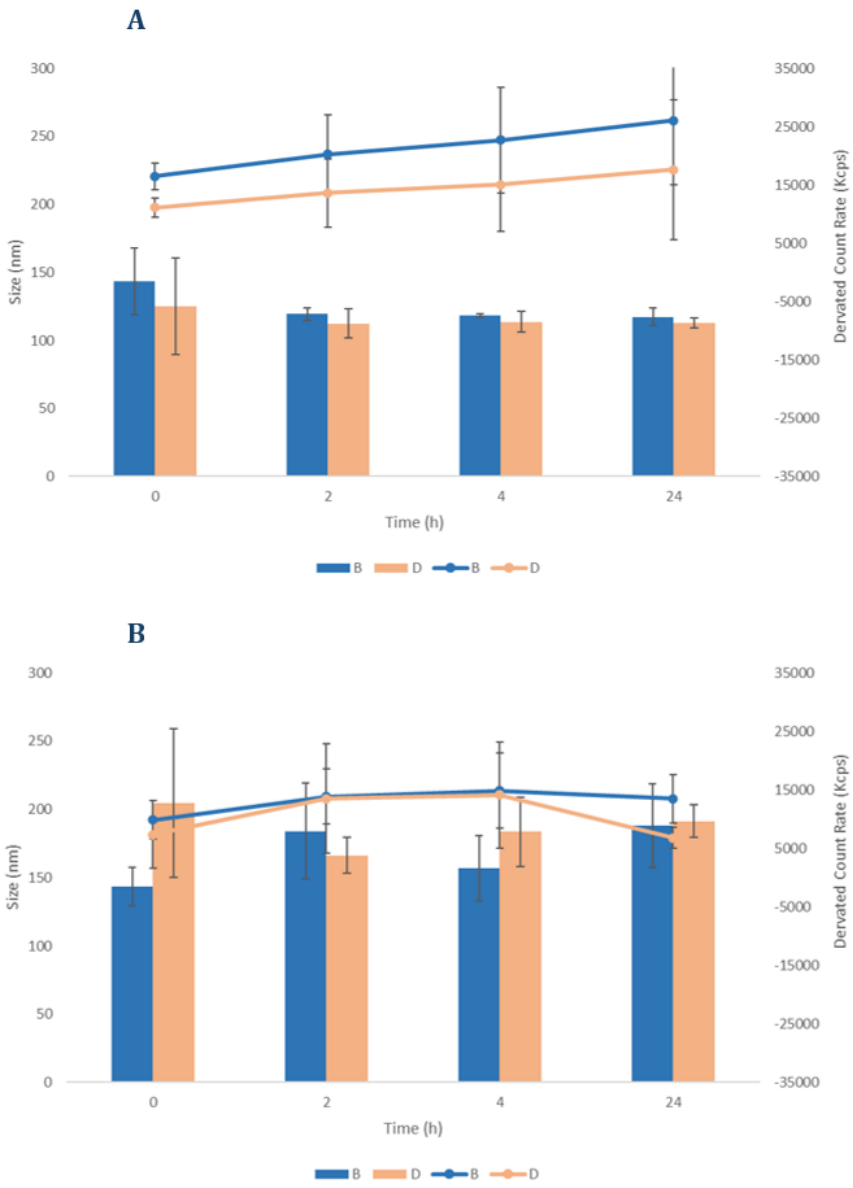

Figure 5. Stability of LNPs with siRNA In DMEM with FBS (A) and without FBS (B). LNPs B (Blue) LNPs D (Orange). $n=3$ mean ± S.D.

3.3.4.3 SAXs analysis

Figure 6 shows the experimental scattering curves of empty lipid nanoparticles.

The SAXS diagrams of Dcch-based systems displayed similar trends, characterised by an intensity upturn at low q-values and a large bump in the intermediate q-region of 0.25-2.5 nm^{-1}, which resembled a left-skewed Gaussian and was followed by damped oscillations, indicating that the empty nanovectors (Figures 6 a, b, c) were rather monodisperse and contained in prevalence unilamellar vesicles. The observed profiles are in agreement with the shape assumed by closed bilayers in dilute solution when charged lipids are part of the mixture used to build up the nano-assemblies and these charged components are homogeneously distributed in the lipid layers [37].

When MaBr was added to the lipid components (Figures 6d, e, f), the main features of the empty nanoparticles were retained in the SAXS profile, even if small but detectable variations could be observed [38]. Specifically, MaBr containing systems, were characterized by the emergence of three oscillations superimposed to the central bump in the q-region 0.4 - 1.5 nm^{-1}, which were attributed to the contribution of quasi-Bragg peaks, i.e. to partial stacking or, possibly, to the onset of partially organized domains in the bilayer [39,40].

This evidence was attributed to the dimerization tendency of the unconventional cationic lipid MaBr which can drive the formation of localized multilayer domains, as it is also reported in the literature. Indeed, MaBr, due to its unique chain and terminal sulfur atom possesses a molecular packing parameter markedly different from that of double-

chained lipids and can assume a wedge conformation, thus driving fluctuation in the local curvature of the lipid assemblies [41-45].

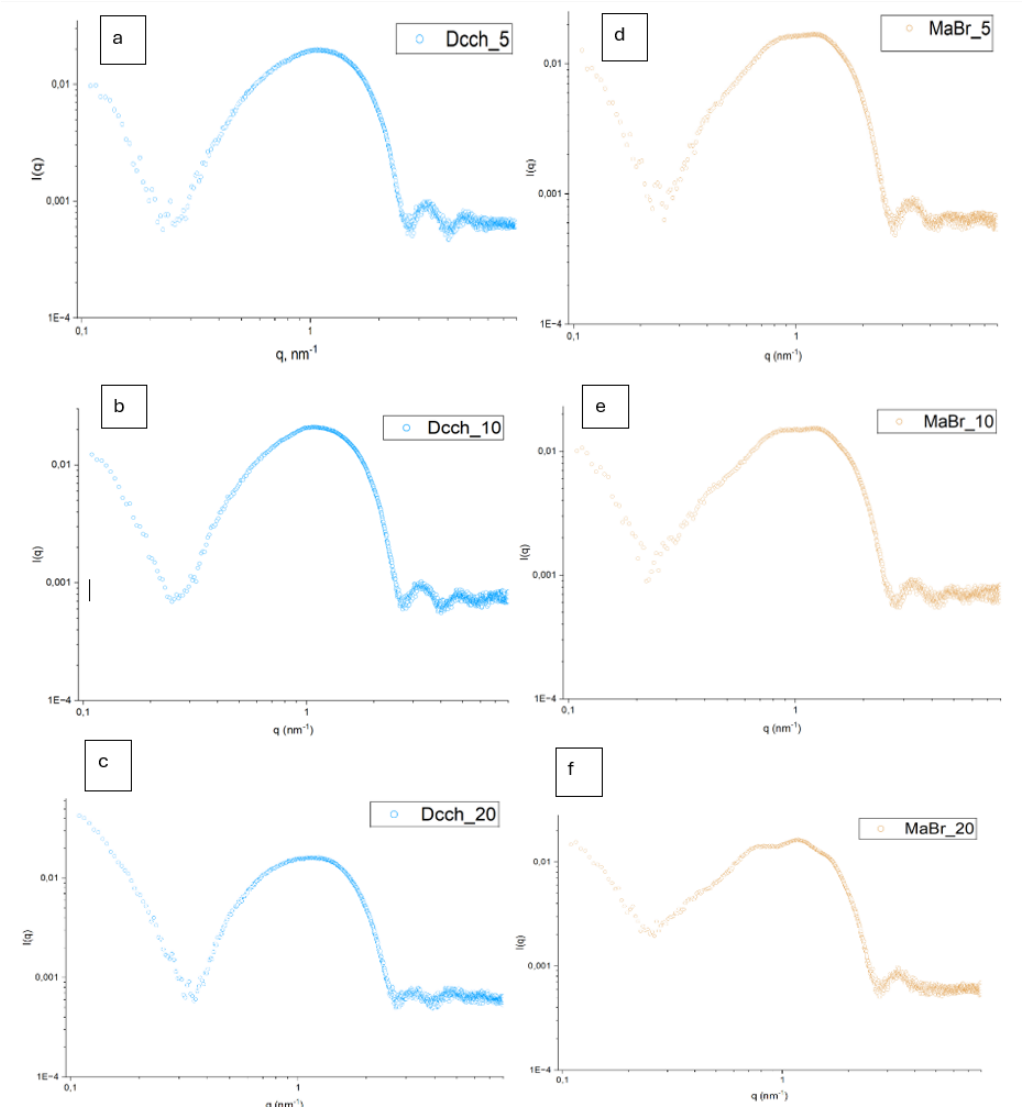

Figure 6. SAXS intensity diagrams of empty lipid nanoparticles: Dcch_5 (a.), Dcch_10 (b.), Dcch_20 (c.); and of the same aggregates complexed with the cationic component MaBr at the N/P ratios reported in Table 1: MaBr_5, (d.), MaBr_10 (e.), and MaBr_20 (f.)

Consistently with the above interpretation, the empty lipid nanoparticle SAXS diagrams were fitted using the model “lamellar_hg” of SASView (Figure 8). Only for the sample MaBr_20, which showed a more complex

morphology, we used a combination of the two models “lamellar_hg” and “lamellar_hg_stack_caille” (Figure 8f). The main parameters used for fitting are reported in Table 20 and Table 21.

Upon siRNA complexation, the SAXS diagrams underwent pronounced changes with respect to the corresponding empty systems (figure 7). The intensity patterns of siRNA-LNPs complexes could be described as featureless decays in the low and intermediate q-regions, with only one, or none at all, oscillations at q values larger than ~3 nm^{-1}. Accordingly, the SAXS profiles of all the complexed lipid nanoparticles were modelled using the “spherical_sld” model of SASView (Figure 9), with best fit values reported in table 22.

The observed behavior was likely due to the formation of coacervates lacking a defined internal organization, joint to increased polydispersity in shape, and indicated loss of local ordering among the assembly components. However, it should be noted that this effect was mainly local and did not compromise the overall stability of the siRNA-LNPs systems. In fact, these lipoplexes could be characterized and applied in biomedical essays without manipulation difficulty, as described in section 3.2.6.

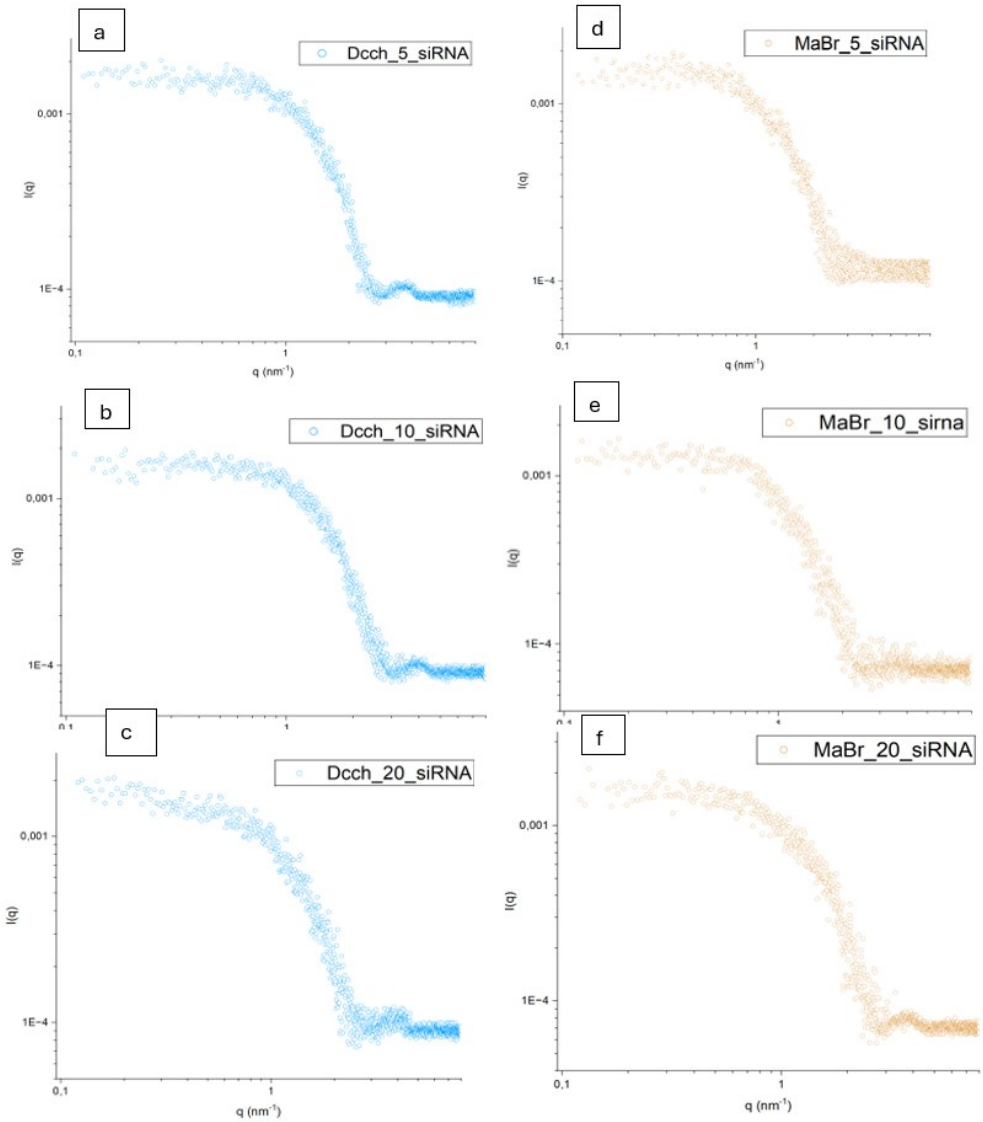

Figure 7. SAXS intensity diagrams of complexed lipid nanoparticles: Dcch_5 (a.), Dcch_10 (b.), Dcch_20 (c.); and of the same aggregates complexed with the cationic component MaBr at the N/P ratios reported in Table X: MaBr_5 (d.), MaBr_10 (e.), and MaBr_20 (f.)

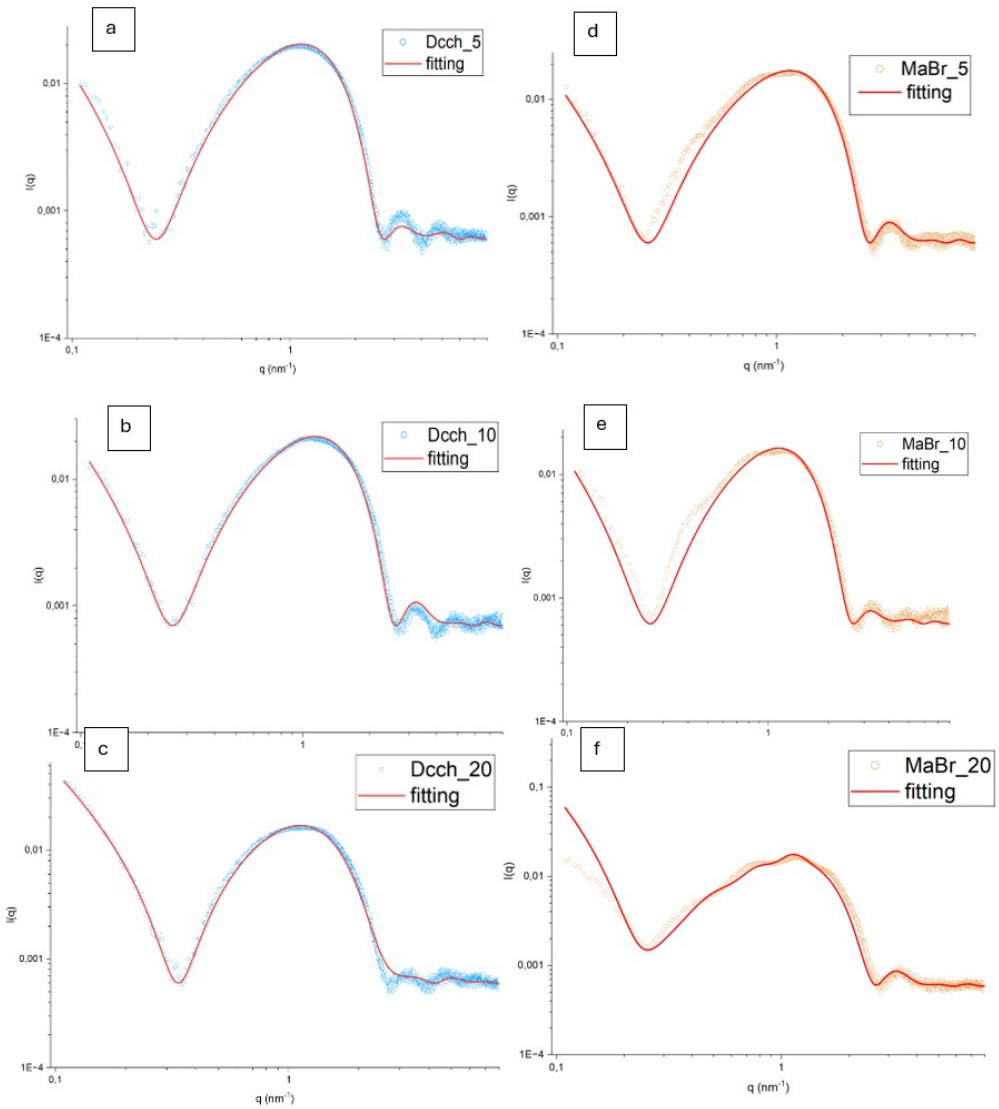

Figure 8. SAXS curves and relative fitting of the empty lipid nanoparticles (a.)Dcch_5, (b.) Dcch_10, (c.) Dcch_20, (d.) MaBr_5, (e.) MaBr_10, and (f.) MaBr_20.

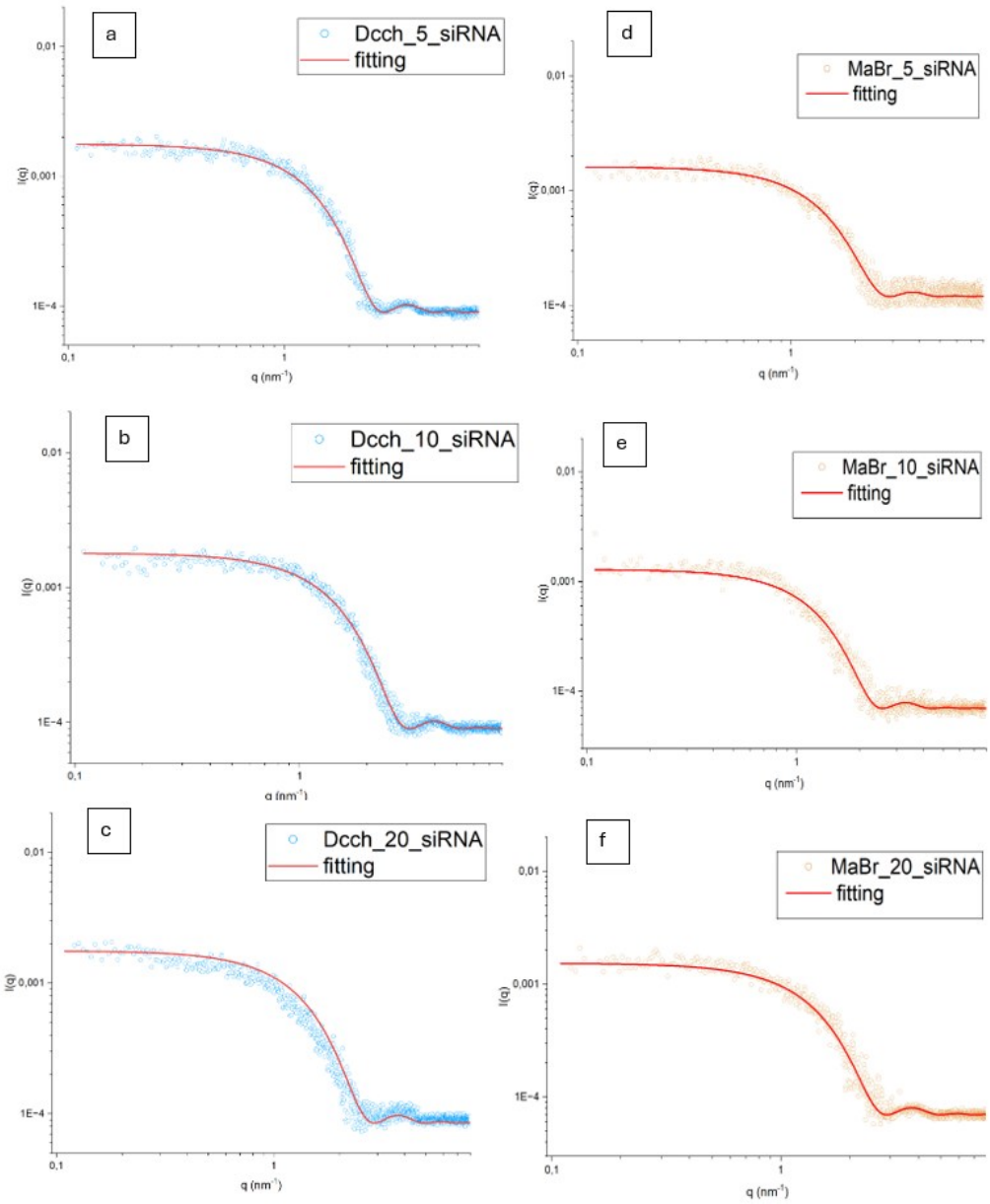

Figure 9. SAXS curves and relative fitting of the complexed lipid nanoparticles (a.) Dcch_5, (b.) Dcch_10, (c.) Dcch_20, (d.) MaBr_5, (e.) MaBr_10, and (f.) MaBr_20.

Table 20. Fitting parameters used for the fitting of the main features of the SAXS curve of the empty lipid nanoparticles.

"Lamellar_hg" Parameters	Dcch_5	Dcch_10	Dcch_20	MaBr_5	MaBr_10	MaBr_20
Length_tail (Å)	11	11	8	11	11	11
Length_head (Å)	16	14	21	14	15	14
Sld (10^{-6}/Å^2)	11.0	10.7	10.9	11.8	11.3	10.8
Sld_head (10^{-6}/Å^2)	8.2	8.2	8.7	7.3	7.9	8.2
Sld_solvent(10^{-6}/Å^2)	9.4	9.4	9.4	9.4	9.4	9.4

Table 21. Fitting parameter used for the fitting of the extra terms for the sample MaBr_20.

"Lamellar_hg_stack Caille" Parameters	MaBr_20
Length_tail (Å)	22 (PdI 0.2)
Length_head (Å)	20 (PdI 0.1)
Nlayers	4
d_spacing (Å)	51 (PdI 0.05)
Caille_parameter	0.01
Sld (10^{-6}/Å^2)	8.5
Sld_head (10^{-6}/Å^2)	11
Sld_solvent (10^{-6}/Å^2)	9.4

Table 22. Fitting parameters used for the fitting of the main features of the SAXS curve of the complexed lipid nanoparticles.

"Spherical_sld" Parameters	Dcch_ 5_na	Dcch_ 10_na	Dcch_ 20_na	MaBr_ 5_na	MaBr_ 10_na	MaBr_ 20_na
sld_solvent (10^{-6}/Å^2)	9.4	9.4	9.4	9.4	9.4	9.4
n_steps	1.0	1.0	1.0	1.0	1.0	1.0
n_shells	1.0	1.0	1.0	1.0	1.0	1.0
sld_1 (10^{-6}/Å^2)	18.6	18.0	18.0	17.8	18.0	18.0
thickness_1 (Å)	15.0	14.0	15.0	15.0	17.0	15.0
interface_1 (Å)	1.0	1.0	1.0	1.0	1.0	1.0
shape_1	erf(|nu|*z)	erf(|nu|*z)	erf(|nu|*z)	erf(|nu|*z)	erf(|nu|*z)	erf(|nu|*z)
nu1	2.5	2.5	2.5	2.5	2.5	2.5

3.3.5 *In vitro* studies

3.3.5.1 MTT Assays

Cell viability was assessed in HeLa cells after 24 hours of exposure, results are reported in figure 10.

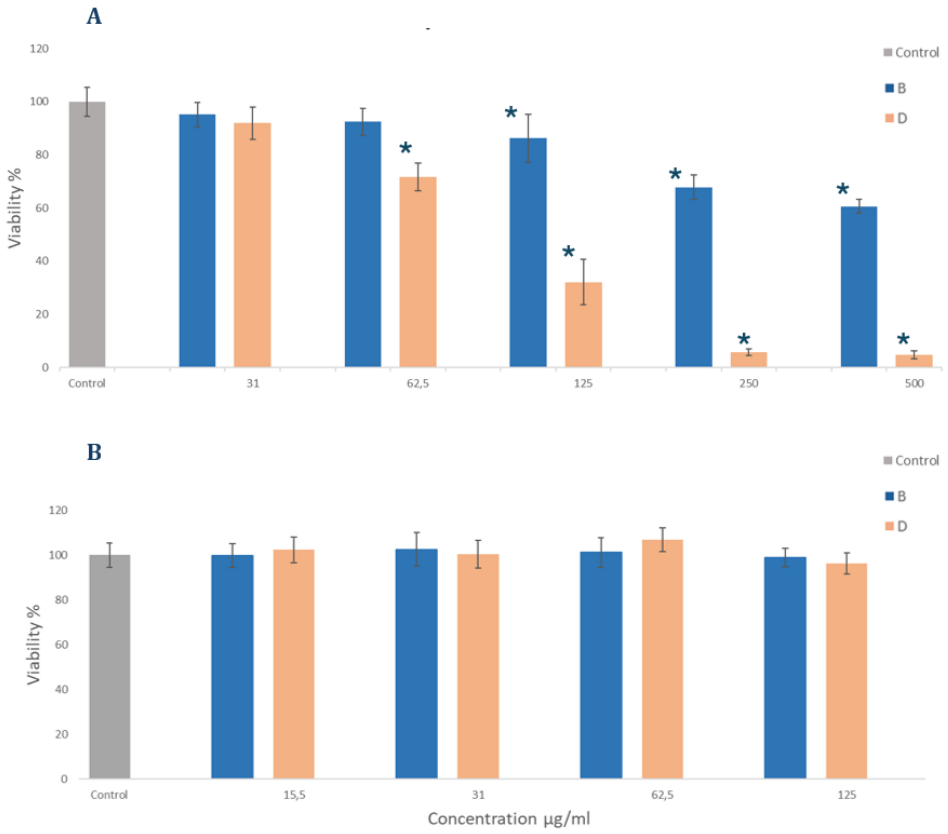

Figure 10. Cells Viability after 24h in HeLa Cells. Empty LNPs (A) and LNPs with siRNA (B). Control (Grey), LNPs B (Blue), LNPs D (Orange). n=3 mean ± S.D. Statistical significance was assessed using a t-test to calculate the P value (indicated with an asterisk).

For empty LNPs (10A), five concentrations ranging from 500 µg/mL to 31 µg/mL were tested. The highest non-toxic concentrations were identified as 62.5 µg/mL for formulation B and 31 µg/mL for formulation D.

Based on these results, LNPs loaded with siRNA were tested at lower concentrations (ranging from 125 µg/mL to 15.5 µg/mL). Notably, siRNA-loaded LNPs (10B) exhibited improved safety profiles, likely due to the reduced Z resulting from electrostatic interactions between the LNPs and the siRNA. Overall, none of the tested formulations showed significant differences compared with the control, indicating that all formulations can be considered safe under the tested conditions.

3.3.5.2 Internalization Test

We evaluated the cellular uptake of formulations B and D after 24 hours, following the method described in Section 3.2.8, using HeLa-GFP cells. LNPs were tested at three different concentrations. In HeLa-GFP cells, internalization exceeded 85% for all formulations and concentrations, as indicated by flow cytometry (Figure 11), with uptake levels comparable to those observed for DiD alone.

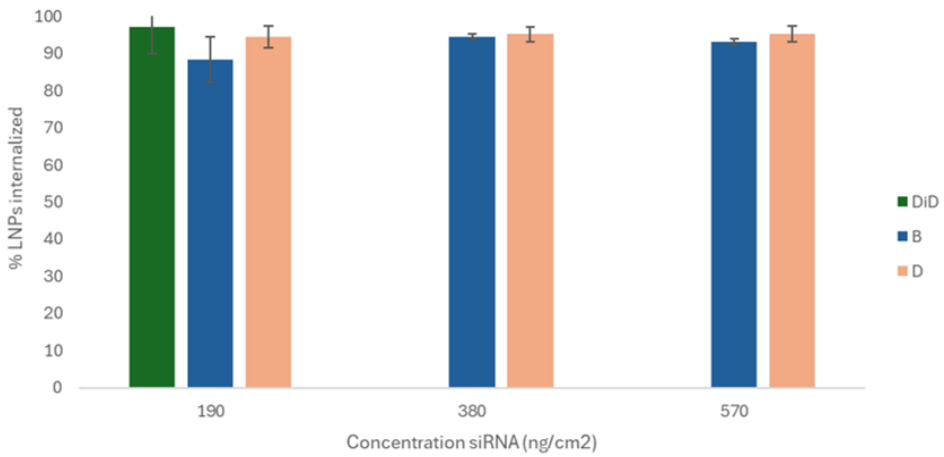

Figure 11. Cytofluorimetric Data Obtained after 24h of internalization of LNPs + siRNAin Hela-GFP Cells. Free DiD (green), LNPs B (Blue) LNPs D (Orange). n=3 mean ± S.D. Statistical significance was assessed using a t-test to calculate the P value (indicated with an asterisk).

Quantification of DiD fluorescence intensity in the LNPs (Figure 12) revealed higher signals compared to DiD alone, particularly for formulation B, suggesting enhanced cellular internalization.

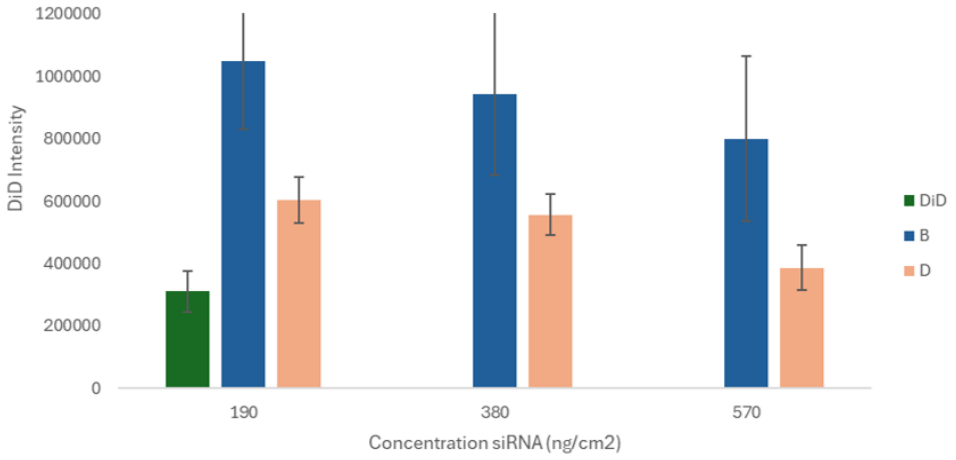

Figure 12. DiD Intensity after 24h of internalization of LNPs + siRNA in Hela-GFP Cells. Free DiD (green), LNPS B (Blue) LNPs D (Orange). n=3 mean ± S.D.

Representative fluorescence microscopy images are shown in Figure 13, further confirming the higher DiD fluorescence intensity in formulation B compared to formulation D.

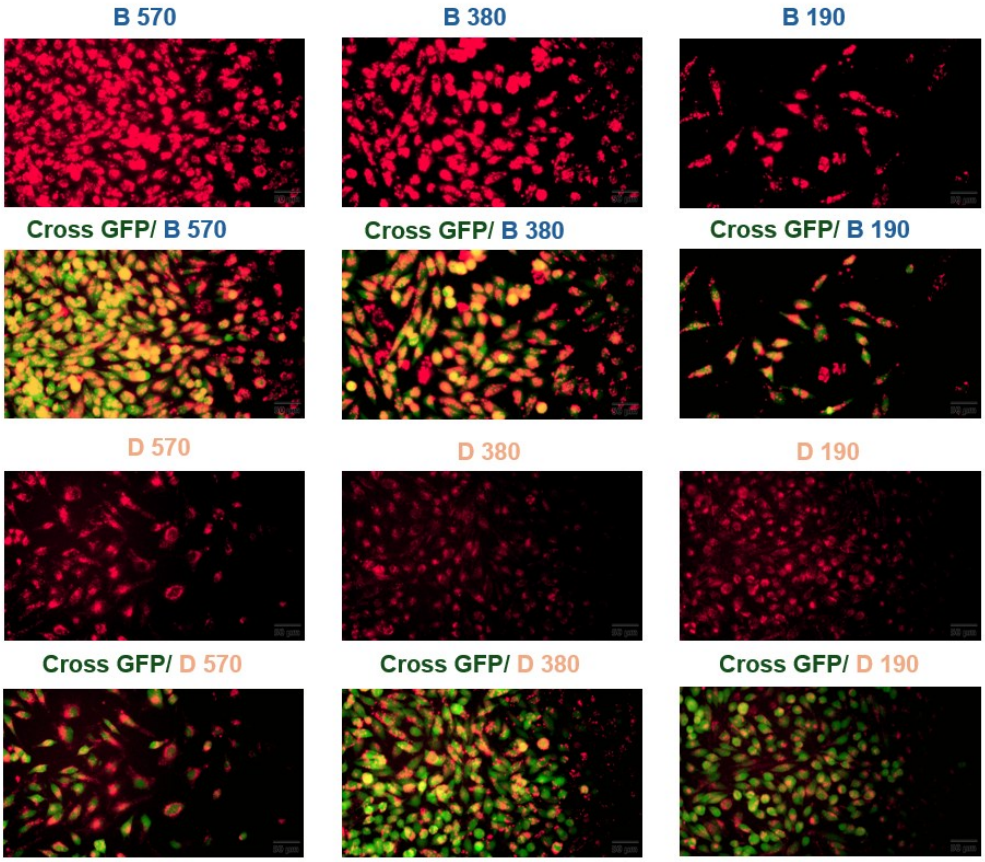

Figure 13. Microscopy Images of LNPs B and D internalized after 24h in HeLa-GFP cells.

Cellular Uptake was also verified for RAW 264.7 cells; these were included to explore potential applications in immune response modulation. In RAW cells, a similar trend was observed with internalization above 85% across all concentrations, but with DiD fluorescence intensity markedly lower than that of HeLa-GFP cells. Data are reported in supplementary materials (S1-S2-S3).

3.3.5.3 Silencing Efficiency

Silencing efficacy was evaluated in HeLa-GFP cells using siRNA concentrations of 380 and 190 ng/cm², as these conditions resulted in the lowest cytotoxicity and the highest transfection efficiency. Cytofluorimetric analyses performed after 48 h and 72 h are shown in Figure 14. As observed, the silencing effect increased over time, with higher efficacy recorded after 72 h. Both formulations B and D achieved lower percentages of silenced cells compared with the gold standard, Lipofectamine [46-48], yet the results remained promising, approximately 55% for formulation B and 35% for formulation D. Interestingly, the lower siRNA concentration (190 ng/cm²) yielded the most effective silencing.

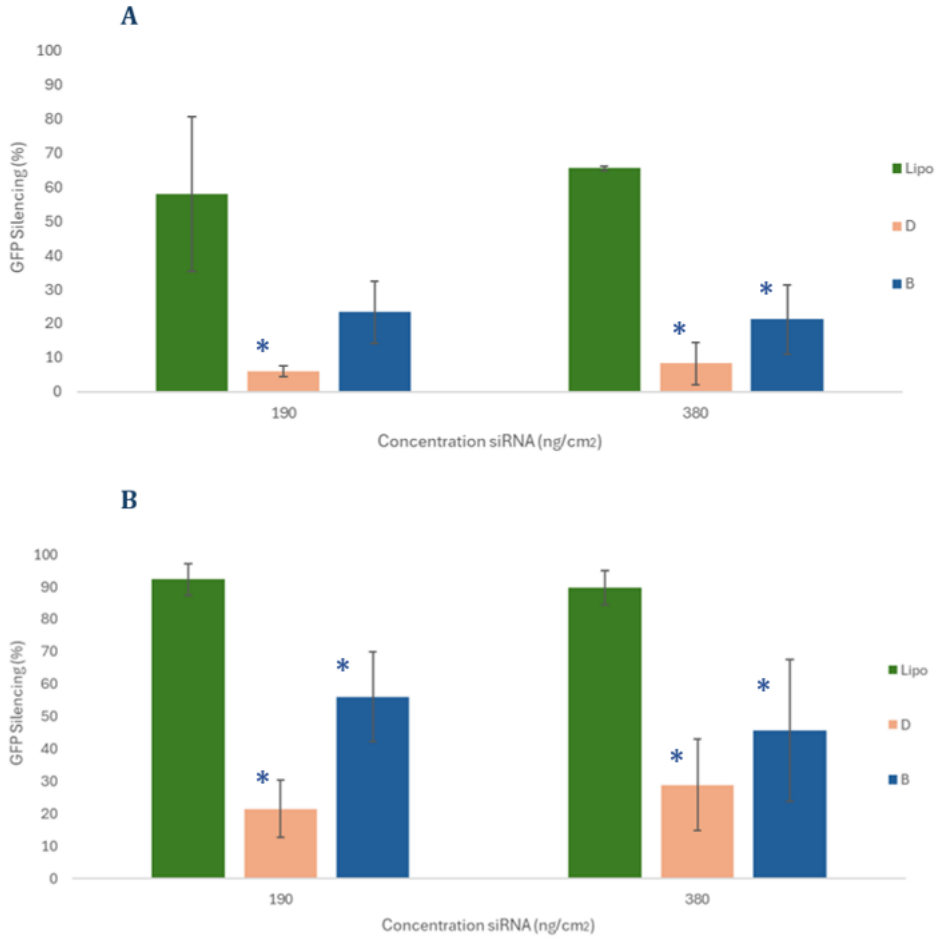

Figure 14. Cytofluorimetric Data of Silencing Efficiency of LNPs with siRNA on HeLa GFP cells after 48h (A) and 72h (B) . Lipofectamine (Green), LNPs B (blue), LNPs D (Orange). n=3 mean ± S.D. Statistical significance was assessed using a t-test to calculate the P value (indicated with an asterisk).

Figure 15 reports the GFP fluorescence intensity data after 48 h (A) and 72 h (B). In this case, formulation D produced lower fluorescence values than Lipofectamine, indicating a stronger silencing effect, while formulation B showed comparable results to Lipofectamine.

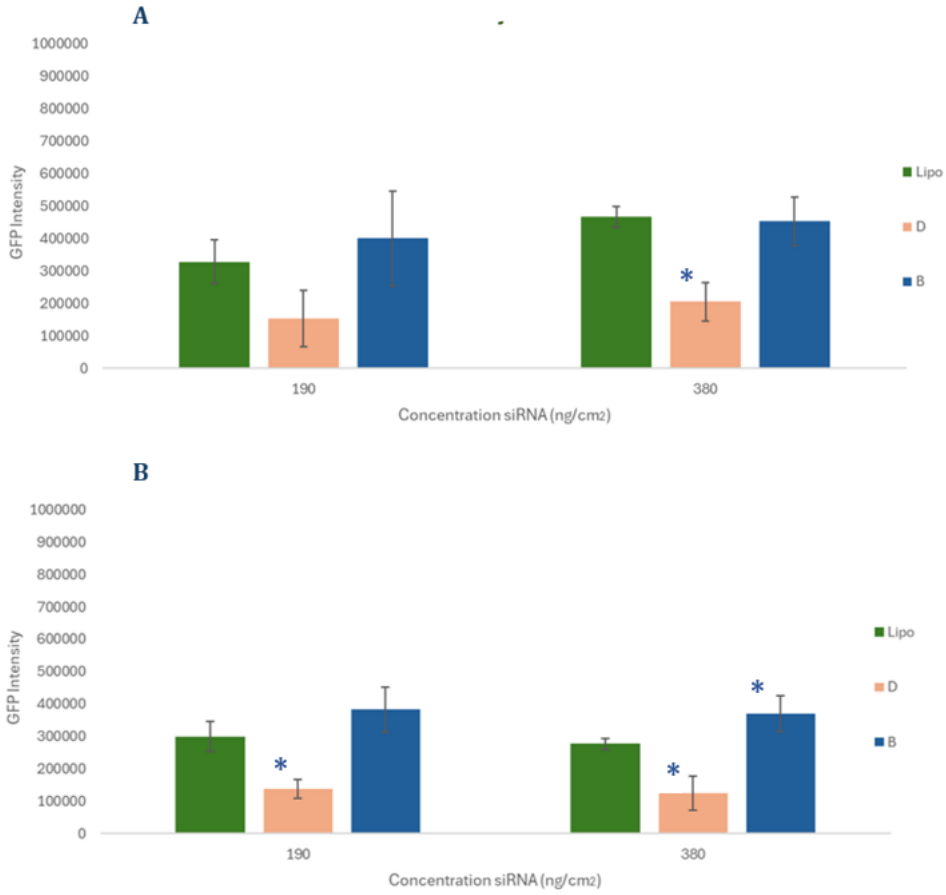

Figure 15. Cytofluorimetric Data of GFP Fluorescence intensity of LNPs with siRNA on HeLa cells after 48h (A) and 72h (B). Lipofectamine (green), LNPs B (blue), LNPS D (Orange). n=3 mean ± S.D. Statistical significance was assessed using a t-test to calculate the P value (indicated with an asterisk).

3.4 Conclusions and future prospectives

We optimized the production of LNPs using a Design of Experiments (DoE) approach, which enabled the systematic tuning of key parameters to obtain NPs with favorable physicochemical properties, including optimal size and polydispersity (size < 200 nm, PDI < 0.3). Several cationic lipids were evaluated, leading to the selection of two formulations, B and D, containing DC-CH and MTAB, respectively. Both formulations showed enhanced siRNA encapsulation efficiency while maintaining excellent size and PDI values.

These LNPs remained stable for up to one week at 4 °C and in cell culture medium, both in the presence and absence of FBS. Formulations B and D exhibited no cytotoxicity at the doses used for internalization and gene-silencing experiments, and demonstrated high uptake efficiency in HeLa-GFP and RAW 264.7 cells (>85%). Internalization in HeLa cells was particularly promising, with notably high DiD fluorescence intensity.

Gene silencing in HeLa cells was lower than that achieved with Lipofectamine (used as a reference), but remained high for formulation B (~55%) and satisfactory for formulation D (~30%) after 72 h. In contrast, when considering fluorescence intensity, formulation D produced the strongest silencing effect, surpassing even that of Lipofectamine. The optimal siRNA concentration was identified as 190 ng/cm².

Overall, both formulations appear highly promising for siRNA delivery. Future work will focus on further optimization of the LNPs and their evaluation in additional cell lines, followed by the use of nucleic acids encoding disease-relevant genes in appropriate cellular models and *in vivo* studies, to fully assess their targeted therapeutic potential.

3.5 Bibliography

[1] Bangham A.D. et al. Diffusion of univalent ions across the lamellae of swollen phospholipids. J Mol Biol. 1965;13(1):238–252. doi:10.1016/S0022-2836(65)80093-6.

[2] Gregoriadis G. Liposome technology in drug delivery:how it all happened. Pharm. 2016- 24;8(2):19. doi: 10.3390/pharmaceutics8020019.

[3] Rosenblum D. et al. Progress and challenges towards targeted delivery of cancer therapeutics. Nat Commun. 2018;9-1410 doi:10.1038/s41467-018-03705-y

[4] Hou X. et al. Lipid nanoparticles for mRNA delivery. Nat Rev Mater. 2021;6(12):1078–1094. doi:10.1038/s41578-021-00358-0.

[5] Khurana A. et al. Role of nanotechnology behind the success of mRNA vaccines for COVID-19. Nano Tod. 2021;38:101142. doi:10.1016/j.nantod.2021.101142.

[6] Kiaie S.H. et al. Recent advances in mRNA-LNP therapeutics: immunological and pharmacological aspects. J Nanobiotechnology. 2022;20(1):276. doi:10.1186/s12951-022-01478-7.

[7] Wilson B., Geetha K.M. Lipid nanoparticles in the development of mRNA vaccines for COVID-19. J Drug Deliv Sci Technol. 2022;74:103553. doi:10.1016/j.jddst.2022.103553.

[8] Haque M.A. et al. Comprehensive analysis of lipid nanoparticle formulation and characterization for siRNA delivery. Int J. Pharm.X.. 2024;10:8:100283. doi: 10.1016/j.ijpx.2024.100283.

[9] Malburet C. et al. Size and charge characterization of lipid nanoparticles for mRNA vaccines. Anal Chem. 2022;94:4677–4685. doi:10.1021/acs.analchem.1c04778.

[10] Guimarães P.P.G. et al. *In vivo* bone marrow microenvironment siRNA delivery using lipid–polymer nanoparticles for multiple myeloma therapy. Proc Natl Acad Sci U S A. 2023;120(13):e2215711120. doi:10.1073/pnas.2215711120.

[11] Lu et al. Current landscape of mRNA technologies and delivery systems for new modality therapeutics. J Biomed Sci. 2024; 10;31(1):89. doi: 10.1186/s12929-024-01080-z.

[12] Hassett K.J. et al. Optimization of lipid nanoparticles for mRNA vaccines. Mol Ther Nucleic Acids. 2021;15:1–11. doi:10.1016/j.omtn.2021.08.013.

[13] Schoenmaker L. et al. mRNA-lipid nanoparticle COVID-19 vaccines: structure and stability. Int J Pharm. 2021;601:120586. doi:10.1016/j.ijpharm.2021.120586.

[14] Wang et al. Delivery of siRNA therapeutics: barriers and carriers. AAPS J. 2010;12(4):492-503. doi: 10.1208/s12248-010-9210-4.
[15] Adams D. et al. Patisiran, an RNAi therapeutic, for hereditary transthyretin amyloidosis. N Engl J Med. 2018;379(1):11–21. doi:10.1056/NEJMoa1716153.
[16] Akinc A. et al. The Onpattro story and the clinical translation of nanomedicines containing nucleic acid-based drugs. Nat Nanotechnol. 2019;14(12):1084–1087. doi:10.1038/s41565-019-0591-y.
[17] Hoy S.M. Patisiran: first global approval. Drugs. 2018;78(15):1625–1631. doi:10.1007/s40265-018-0983-6.
[18] Cao L. Key clinical frontiers of mRNA-loaded lipid nanoparticles in cancer vaccines. Int J Nanomedicine. 2025;20:14935-14953. doi:10.2147/IJN.S565558
[19] Friedrich M., Aigner A. Therapeutic siRNA: state-of-the-art and future perspectives. BioDrugs. 2022;36(5):549–571. doi:10.1007/s40259-022-00549-3.
[20] Hadj Hassine I. COVID-19 vaccines and variants of concern: a review. Rev Med Virol. 2022;32(4):e2313. doi:10.1002/rmv.2313.
[21] Subhan A.M. et al.. Advances with Lipid-Based Nanosystems for siRNA Delivery to Breast Cancers. Pharmaceuticals (Basel). 2023; 6;16(7):970. doi: 10.3390/ph16070970.
[22] Schober G.B. et al. A careful look at lipid nanoparticle characterization: analysis of benchmark formulations for encapsulation of RNA cargo size gradient. Sci Rep. 2024;14:2403. doi:10.1038/s41598-024-52685-1
[23] Mennini N. et al. Response surface methodology in the optimization of chitosan–Ca pectinate bead formulations. Eur J Pharm Sci. 2008;35(4):318–325. doi:10.1016/j.ejps.2008.07.011.
[24] Furlanetto S. et al. Study of formulation variables influencing the drug release rate from matrix tablets by experimental design. Eur J Pharm Biopharm. 2006;62(1):77–84. doi:10.1016/j.ejpb.2005.07.001.
[25] Terada K. et al. Characterization of lipid nanoparticles containing ionizable cationic lipids using a design-of-experiments approach. Lang.2021;37;3:1120–1128. doi:10.1021/acs.langmuir.0c03039
[26] Khare P. et al. Development of lipidoid nanoparticles for siRNA delivery to neural cells. AAPS J. 2021;24(1):8. doi:10.1208/s12248-021-00653-2.
[27] Bressy C. et al. Inhibition of c-Rel expression in myeloid and lymphoid cells with distearoyl-phosphatidylserine liposomal nanoparticles encapsulating therapeutic siRNA. PLoS One. 2022;17(12):e0276905. doi:10.1371/journal.pone.0276905.

[28] Cassayre M. et al. Optimization of solid lipid nanoparticle formulation using a design of experiments approach. Nanomaterials. 2025;15(13):1034. doi:10.3390/nano15131034.
[29] Spinozzi F. et al. Small-angle X-ray scattering unveils the internal structure of lipid nanoparticles. J Colloid Interface Sci. 2024; 15;662:446-459. doi: 10.1016/j.jcis.2024.02.076
[30] Szoka F., Papahadjopoulos D. Procedure for preparation of liposomes with large internal aqueous space and high capture by reverse-phase evaporation. Proc Natl Acad Sci U S A. 1978;75:4194–4198. doi:10.1073/pnas.75.9.4194.
[31] Schindelin J. et al. Fiji: an open-source platform for biological-image analysis. Nat Methods. 2012;9:676–682. doi:10.1038/nmeth.2019.
[32] Valverde-Fraga L. et al. Design and *in vitro* assessment of chitosan nanocapsules for the pulmonary delivery of rifabutin. Eur J Pharm Sci. 2023;187:106484. doi:10.1016/j.ejps.2023.106484.
[33] Ferraresso F. et al. Comparison of DLin-MC3-DMA and ALC-0315 for siRNA delivery: ALC-0315 achieves more potent knockdown in hepatocytes and HSCs. Mol Pharm. 2022;19(11). doi:10.1021/acs.molpharmaceut.2c00033.
[34] Song Z. et al. ALC-0315 lipid-based mRNA LNP induces stronger humoral and cellular immunity compared to MC3.2025; 3;22(2):859-870. doi: 10.1021/acs.molpharmaceut.4c00995.
[35] Kashapov R. et al. Nanocarriers for Biomedicine: From Lipid Formulations to Inorganic and Hybrid Nanoparticles. Int J Mol Sci. 2021; 30;22(13):7055. doi: 10.3390/ijms22137055.
[36] Montefusco-Pereira C. V. Coupling quaternary ammonium surfactants to the surface of liposomes improves both antibacterial efficacy and host cell biocompatibility. Eur J Pharm Biopharm. 2020;149:12-20. doi: 10.1016/j.ejpb.2020.01.013.
[37] Brzustowicz, M.R et al. X-ray scattering from unilamellar lipid vesicles. J. Appl. Cryst. 2005, 38: 126-131. https://doi.org/10.1107/S0021889804029206
[38] Aburai K et al. Location of cholesterol in liposomes by using small-angle X-ray scattering (SAXS) data and the generalized indirect Fourier transformation (GIFT) method. J Oleo Sci. 2013;62(11):913-8. doi: 10.5650/jos.62.913.
[39] Konarev P.V. et al. Restoring structural parameters of lipid mixtures from small-angle X-ray scattering data. J Appl Crystallogr. 2021 Feb 1;54(Pt 1):169-179. doi: 10.1107/S1600576720015368.

[40] Pabst G. et al. Structural analysis of weakly ordered membrane stacks. J. Appl. Cryst. 2003,36: 1378-1388. https://doi.org/10.1107/S0021889803017527
[41] Komorowski K. et al. Vesicle Adhesion and Fusion Studied by Small-Angle X-Ray Scattering. Biophys J. 2018 Apr 24;114(8):1908-1920. doi: 10.1016/j.bpj.2018.02.040.
[42] Pietralik Z. et al. SAXS Study of Influence of Gemini Surfactant, 1,1'-(1,4-butanediyl)bis 3-cyclododecyloxymethylimidazolium di-chloride, on the Fully Hydrated DMPC. Acta Physica Polonica A. 2010, 117(2), 311–314. https://doi.org/10.12693/aphyspola.117.311
[43] Pabst G. et al. "Applications of neutron and X-ray scattering to the study of biologically relevant model membranes" Chem. Phys. Lipids, 163 (2010) 460
[44] E. Di Cola et al. "Small Angle X-ray and Neutron Scattering: Powerful Tools for Studying the Structure of Drug-Loaded Liposomes, Pharmaceutics, 8 (2016) 10
[45] Pabst G. et al. Liposomes, Lipid Bilayers and Model Membranes: From Basic Research to Applications", CR Press,2014.
[46] Bramato R. et al. Comparison of DNA-transfection efficiency in HeLa cells using K4 Transfection System and Lipofectamine 3000. 2019.
[47] Bulkescher R. et al. Solid-phase reverse transfection for intracellular delivery of functionally active proteins. Genome Res. 2017;27:1752–1758. doi:10.1101/gr.215103.116.
[48] Shi B. et al. An improved method for increasing the efficiency of gene transfection and transduction.Int J Physiol Pathophysiol Pharmacol. 2018; 20;10(2):95-104.

3.6 Supplementary materials

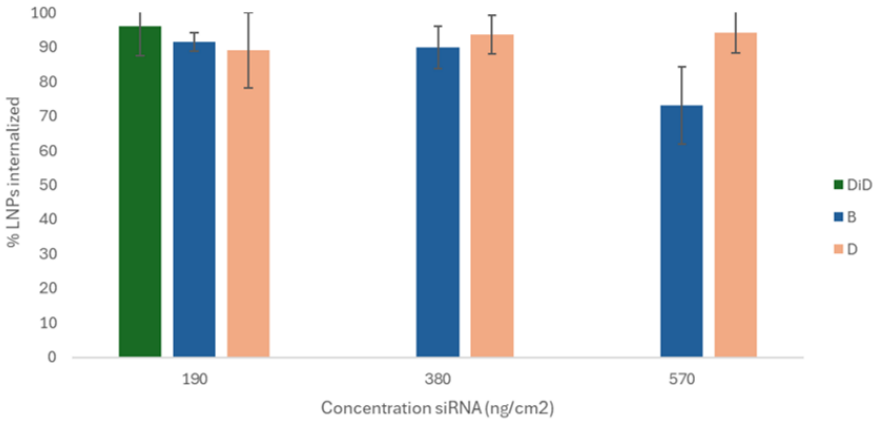

S1.Cytofluorimetric Data Obtained after 24h of internalization of LNPs + siRNAin RAW 264.7 Cells. Free DiD (green), LNPs B (Blue) LNPs D (Orange). n=3 mean ± S.D.

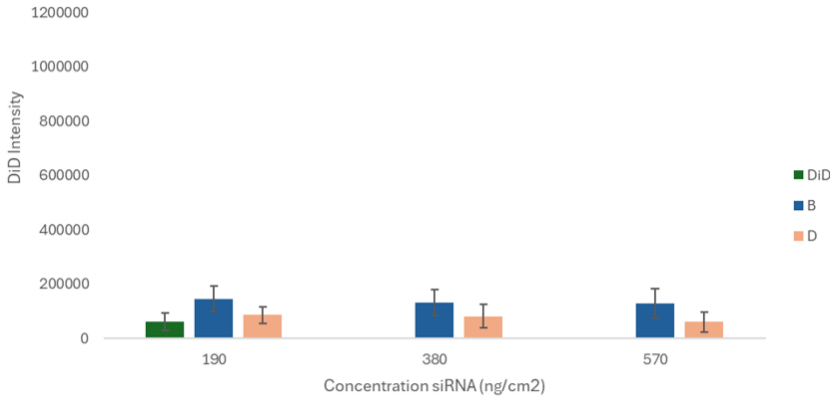

S2.DiD Intensity after 24h of internalization of LNPs + siRNA in RAW 264.7 Cells. Free DiD (green), LNPS B (Blue) LNPs D (Orange). n=3 mean ± S.D.

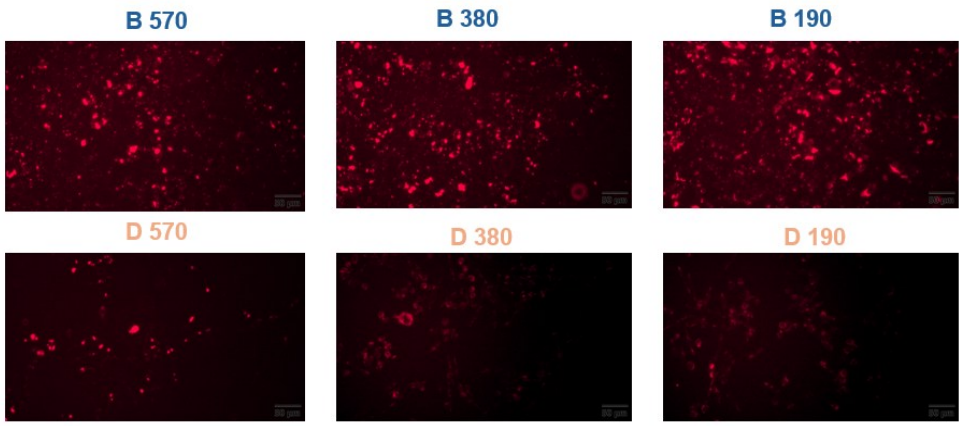

S3.Microscopy Images of LNPs B and D internalized after 24h in RAW 264.7 cells.

4 Modified cationic Beta-Cyclodextrins as Potential Nanovectors for Gene Delivery

4.1 Introduction

Cyclodextrins (CDs) have found extensive use in pharmaceutical applications due to their ability to improve the solubility of poorly soluble drugs in water, as well as to improve bioavailability, and other key properties [1].

The potential of CDs as delivery platforms for genetic materials was first systematically explored about 15 years ago, when Chaturvedi et al. reviewed their use for siRNA delivery [2]. More recently, Mousazadeh et al. (2021) highlighted the promise of cyclodextrins as effective non-viral siRNA delivery systems for cancer gene therapy [3], suggesting that specific chemical modifications can significantly enhance both transfection efficiency and biosafety. Furthermore, Ge et al. (2023) emphasized the dual diagnostic and therapeutic capabilities of CD-based systems, demonstrating how functionalized CDs can act not only as siRNA carriers but also as multifunctional platforms for imaging, controlled release, and targeted cancer therapy; bridging the gap between nanomedicine and theranostic [4]. Collectively, these studies underscore the versatility of CD architectures as robust and adaptable frameworks for next-generation gene delivery technologies.

CDs are natural cyclic oligosaccharides derived from starch, characterized by a toroidal structure with hydrophilic rims (primary and secondary hydroxyl groups) and a hydrophobic inner cavity. Owing to the abundance of reactive hydroxyl groups, CDs can be readily functionalized to introduce positive charges or other tailored functionalities [5]. Such

chemical versatility has enabled the synthesis of a wide range of CD derivatives, including cationic, amphiphilic, and PEGylated compounds. Electrostatic interactions between nucleic acids and cationic CDs promote the spontaneous formation of nanoscale self-assembled structures. Haley et al. (2020) provided a comprehensive overview of CDs as modular carriers in drug and gene delivery systems [6], highlighting their capacity to complex and protect DNA or RNA, reduce immunogenicity, and facilitate interactions with cellular membranes. Their analysis also emphasized the potential of CDs as multifunctional nanoplatforms capable of co-delivering chemotherapeutics, RNAi agents, and peptides for personalized medicine applications.

Recent developments have expanded the understanding of self-assembling and targeted CD-based systems for siRNA delivery. CD NVs have gained increasing attention due to their biocompatibility, ability to form stable complexes with siRNA, and high potential for targeted functionalization. Moreover, the combination of CDs with cationic polymers has been reported to enhance cellular uptake and endosomal escape [6], indicating that modification of the native CD structure is strongly recommended to improve internalization and delivery performance. For instance, amphiphilic cationic CDs have successfully mediated siRNA delivery and gene silencing *in vitro* and *in vivo*. Although no CD NP-based siRNA therapeutic has yet reached market approval, these nanocarriers represent a dynamic and promising area of preclinical research, with potential applications spanning oncology, neurology, and inflammatory diseases. Among the most notable examples is CALAA-01, a self-assembling CD nanoparticle formulation functionalized with transferrin for tumor targeting, developed by Calando Pharmaceuticals.

CALAA-01 was one of the first CD-based nanomedicines to enter clinical evaluation, demonstrating the translational potential of CD-derived delivery systems for targeted gene therapy [7].

In recent years, the exploration of cationic modified CDs for gene delivery has gained attention yielding promising results across different experimental models [8-13]. Nevertheless, further research is required to elucidate their mechanisms of cellular uptake, endosomal escape, and gene release, in order to optimize their therapeutic performance. Among the various CD families, β-cyclodextrins (β-CDs) have emerged as particularly suited systems for the design of NVs, provided that appropriate chemical modifications are introduced to enhance their physicochemical stability, nucleic acid complexation, and transfection efficiency [14-16].

Biocompatible anionic polymers, such as sodium hyaluronate (HA) and polysialic acid (HP) can be added to NVs to improve colloidal stability by sterical hindrance and decrease potential cytotoxicity by reducing the surface charge. Moreover, HA and HP are known to enhance cellular interactions and biocompatibility [17-20].

In this study, we investigated three novel cationic β-CDs (Figure 1), designed with and synthesized by CarboHyde Zrt, with the aim of assessing their suitability as gene delivery vectors. These will be hereinafter referred to as CD1, CD2, and CD3, respectively. All the CD derivatives share a common β-CD ring functionalized with a lipophilic alkyl chain of variable length and one or more ionizable amino groups. The presence of protonatable amino functionalities is crucial for establishing electrostatic interactions with the negatively charged genetic material, thereby facilitating complex formation, while also contributing to the self-

assembly of nanoparticles [21]. The hydrophobic alkyl chains, differing in length among the derivatives, play an essential role in modulating interactions with cellular membranes and biological environments, and can also serve as anchoring sites for further ligand conjugation or receptor-specific targeting [22]. Moreover, the presence of sulfur-containing groups may enhance biological interactions, promoting more efficient intracellular trafficking and release [23].

Specifically, CD1 has a single amino group and an octyl (C8) lipophilic chain; CD2 contains two amino groups and a longer C16 chain; while CD3 possesses one amino group coupled with a C16 hydrophobic chain. These structural variations can influence the efficiency of nucleic acid complexation and the subsequent intracellular release of the genetic payload.

As a first step, since these CDs are newly developed, we conducted Differential Scanning Calorimetry (DSC) and with X-ray powder diffraction (XRPD) to obtain more information about their structure. Then, dispersibility and preformulation studies to identify the best method and optimal concentration to obtain the NVs with suitable characteristics for gene delivery. Size, PdI and Z were evaluated with DLS and ELS.

In order to assess their potential for gene delivery the β-CDs NVs were complexed with a Plasmid (P) encoding for the Green Fluorescent Protein (GFP) at an N/P (+/-) ratio of 10.

Among the various genetic payloads investigated, P converting GFP are commonly employed as reporter systems to evaluate the transfection efficiency and intracellular trafficking of nanocarriers [24-26]. GFP P serves as valuable model systems in preclinical studies of gene delivery,

as their expression allows for rapid visualization and quantification of successful gene transfer, thereby facilitating the optimization of vector design and delivery conditions [27]. Moreover, GFP-based constructs have been used not only as research tools but also as surrogate therapeutic models for assessing the performance of plasmid-based gene therapy platforms [28].

In addition to these initial formulations, we also tested vectors by incorporating HA or HP into the β-CDs, specifically, at 10% w/w. The rationale behind this choice is that the Z of the NVs is relatively high, which may raise concerns about their safety profile. These formulations were complexed with the P at the same N/P ratio.

The vectors were further characterized by using transmission electron microscopy (TEM, Cryo-EM) and synchrotron-SAXS to assess their structure at high resolution.

Stability studies were conducted at 25 and 4°C (± 1°C) after 1, 4, and 7 days, as well as in cell culture medium (with and without supplementation) for up to 24 hours.

The plasmid-CD complexation was confirmed by Horizontal Electrophoresis on Agarose Gel.

To evaluate the potential biological impact of these NVs, cell viability was assessed in HeLa and RAW cells using the MTT assay after 24 h of incubation. Cellular uptake was first investigated in both cell lines after 24 h, followed by the evaluation of transfection efficiency in HeLa cells at 24 and 48 h. Flow cytometry was employed to quantify transfection efficiency, while fluorescence microscopy was used to visualize intracellular localization and expression patterns.

The NVs were further complexed with GFP-siRNA at an N/P ratio of 10 and characterized by DLS to determine size and PdI. The complexation efficiency was analysed by agarose gel electrophoresis, confirming the successful binding of siRNA to the NVs. The gene-silencing performance of the GFP-siRNA NV complexes was subsequently evaluated in HeLa-GFP cells after 48 and 72 h, providing insights into their transfection capability and RNAi efficiency.

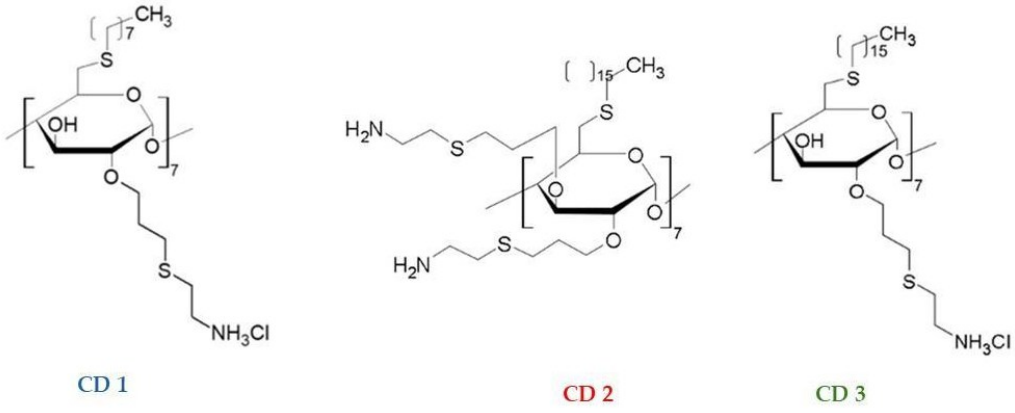

Figure 1. Modified cationic β-CDs structures

4.2 Materials and Methods

4.2.1 Materials

Modified β-CDs (CD1, CD2, CD3) were designed and synthesized by Carbohyde Zrt. (Budapest, Hungary). Hyaluronic Acid (HA, sodium hyaluronate, 40 kDa) was purchased from LifeCore Biomedical (Minnesota, USA), Polysialic Acid (HP, 30 kDa) was obtained from the Serum Institute of India (Maharashtra, India). Plasmid-GFP (P) was kindly provided by the Biomaterials & Drug Delivery (BIDD) group from the University of Santiago de Compostela. HeLa cells, HeLa GFP cells and RAW 264.7 cells were obtained from the American Type Culture Collection (ATCC, Manassas, VA, USA). GFP-targeting siRNA was purchased from Biospring (Frankfurt, Germany). RNase-free water, Syb Lipofectamine, and Opti-MEM were purchased from Thermo Fisher Scientific (USA). Ethanol (EtOH), chloroform ($CHCl_3$), dimethyl sulfoxide (DMSO), HEPES buffer (10 mM, pH 6), and phosphate-buffered saline (PBS) were purchased from Merck (Darmstadt, Germany). Dulbecco's Modified Eagle Medium (DMEM), fetal bovine serum (FBS), and trypsin were obtained from VWR (Pennsylvania, USA). DiD (1,1′-Dioctadecyl-3,3,3′,3′-Tetramethylindodicarbocyanine, Perchlorate) (Invitrogen™, Thermo Fisher Scientific, Waltham, MA, USA).

4.2.2 Differential Scanning Calorimetry (DSC)

Differential scanning calorimetry (DSC) analyses were performed using a DSC1 Star System (Mettler Toledo). The measurements were conducted over a temperature range from 25 to 125 °C, under a static air atmosphere, with a heating rate of 10 °C/min. Sample masses were accurately determined using an XS105 dual range balance (Mettler Toledo) [29-32].

4.2.3 X-ray powder diffraction (XRPD)

The sample was mechanically ground using a mortar and pestle to ensure a random orientation of the crystalline grains with respect to the incident X-ray beam. X-ray powder diffraction (XRPD) patterns of CD1, CD2, and CD3 were recorded at the Interdepartmental Center for Structural Crystallography (CRIST), University of Florence. Data were collected using the XRDynamic 500 automated multipurpose X-ray powder diffractometer (shown in Figure 30), operated under the following experimental conditions: time scan = 6 minutes, current = 39 mA, voltage = 40 kV.

4.2.4 Preformulation studies

Several tests were performed to evaluate the dispersion behaviour and their ability to form NVs of the three cyclodextrins (CD1, CD2, and CD3) using various preparation methods, solvents, and concentrations. NVs formation was assessed in RNase-free water, EtOH, $CHCl_3$, DMSO, HEPES buffer (10 mM, pH 6), and PBS, under different agitation conditions and heating up to 75 °C.

All three CDs were found to be soluble in chloroform at room temperature, forming stable solutions for 2–3 days. In RNAse Free water, the CDs solubilized after 15 minutes of agitation at 50 °C followed by 30 minutes mixing at 37°C, with the solutions remaining stable for approximately 12 hours for CD2 and 1-2 hours for CD1 and CD3. CD1 and CD3 dissolved in ethanol after heating at 50 °C for 10 minutes; however, they undergo to precipitation upon returning to room temperature. CD2 could be dispersed in ethanol, DMSO, HEPES, and water after agitation at 50 °C for 10 to 40 minutes, but precipitation occurred upon cooling in all solvents.

Based on these findings, the optimal conditions for solubilizing the CDs were identified as follows: for CD1, either dissolution in chloroform or dispersion in water under agitation at ~50 °C for 40 minutes; for CD2, dispersion in water under the same conditions was selected as the preferred method.

4.2.5 NVs Preparation

NVs were prepared and loaded with P using two methods for CD1 (in chloroform and RNAse free water) and one method for CD2 (in RNAse free water). This choice was driven by the variation in physicochemical features observed between the two CD derivatives: CD2 is stable when dispersed in aqueous medium, whereas CD1 tends to re-precipitate within a short time if it is not promptly complexed with genetic material. For this reason, it appeared relevant to investigate whether these distinct formulation strategies could influence the properties and performance of the resulting NVs. CD derivatives are amphiphilic and exhibit self-assembling behaviour in aqueous environments. Upon dispersion, the molecules initially exist as monomers, which progressively aggregate until reaching the critical micellar concentration (CMC), where nanosized vesicular structures are formed. To identify the optimal formulation conditions, different CD concentrations were tested, and the resulting assemblies were characterized at DLS. A CD concentration of 2 mg/mL was selected as it yielded NVs with the desired size distribution and PdI [33-35].

Optimal nanostructures could be obtained only for CD1 and CD2. In contrast, CD3 did not produce nanosystems with acceptable size that consistently exceeded 700 nm under all tested conditions.

CD1 – Method A (chloroform-based):

- Dissolution: CD1 was dissolved in chloroform at a concentration of 2 mg/mL.
- Evaporation: The chloroform solution was evaporated under a gentle nitrogen stream.
- Rehydration: The resulting film was rehydrated with RNAse Free water under magnetic stirring at 300 rpm for 5 minutes.
- Sonication: The dispersion was sonicated using the following parameters: Amplitude: 10%, Pulse: 1 second on / 1 second off, Time: 10 seconds, Repetition: 3 cycles.
- Complexation: The plasmid solution was added at an N/P ratio of 10 and stirred for 1 hour at 300 rpm.

CD1 – Method B (aqueous-based) and CD2:

- Dissolution: CD1 or CD2 were dissolved in RNAse free water at a concentration of 2 mg/mL at 50 °C under magnetic stirring at 450 rpm for 15 minutes, and then at 37°C for 30 minutes.

- Complexation: The P (or siRNA) solution, in RNAse free water, was added at an N/P ratio of 10 and stirred for 1 hour at 300 rpm.

When HA/HP were included, they were added at 10% w/w relative to the CD. Three approaches were tested: addition before, after, or simultaneously with the P. Although no significant differences in particle size were observed among the three approaches, the best complexation efficiency was achieved when HA/HP were added simultaneously with P, followed by stirring.

4.2.6 Dynamic Light Scattering (DLS) and Electrophoretic Light Scattering (ELS)

DLS and ELS analyses were carried out with all empty and P loaded CD NVs, as well as with or out the addition of HA or HP. Size and PdI were measured using DLS, while zeta potential (Z) was determined using ELS. All measurements were performed using a Zetasizer Pro Red Label (Malvern Instruments, Malvern, UK). The instrument was equipped with 10 mW He-Ne laser operating at 632.8 nm, an avalanche photodiode detector, a digital correlator, and a temperature controller set at 25 °C, using water dispersant viscosity was used for the analyses. Time correlation functions were analyzed using the software Zetasizer, version 7.02, provided by Malvern. For size and PdI measurements, polystyrene cuvettes (12 × 12 × 45 mm; minimum volume: 40 µL) were used, and 100 µL of the prepared solution was directly loaded into the cuvette. Z measurements were performed using capillary cells with a minimum volume of 0.7 mL; for this, 10 µL of the NVs solution was diluted to a final volume of 700 µL with RNase free water.

In both cases, the cuvette or capillary cell was placed into the instrument sample holder for analysis. All measurements were carried out in triplicate at a constant temperature of 25 °C with a detection angle of 173°.

4.2.7 Transmission Electron Microscopy (TEM) Analyses

TEM analyses were performed on CD NVs empty, complexed with P, and CD combined with HA or HP and P. 10 µL of the sample was mixed with 10 µL of 2% phosphotungstic acid. Then, 1 µL of this solution was placed on the bright copper-colored area of the round grid and left until dry. After that, washing with water, the grid was left to dry in a desiccator chamber

for at least 24 h and then the analysis was performed. The images were obtained using the FESEM Ultra Plus, (ZEISS, Jena, Germany) at the CACTUS facility, University of Santiago de Compostela [36].

4.2.8 Cryo-Electron Microscopy Analyses (Cryo-EM)

Cryo-EM was performed on CD1 and CD2 NVs with P using a JEOL JEM-1230 microscope (JEOL Ltd., Tokyo, Japan) at the CIC biogune (Bilbao, Spain). Samples were prepared on carbon-coated grids and vitrified by rapid freezing prior to imaging [37].

4.2.9 Synchrotron-SAXS

SAXS measurements of NVs, both empty and complexed with P, were performed at the ID02 beamline of the European Synchrotron Radiation Facility (ESRF-Grenoble, France). The wavelength and energy of the incoming beam were 0.995 Å and 12.46 keV, respectively. The sample holder was a flow- through capillary with 2 mm diameter, maintained at 37°C to reproduce the physiological cellular condition. The scattering vector q covered a range of 0.11 to 9.70 nm^{-1} with sample-detector distance of 0.8 m. The 2D SAXS patterns were first circularly averaged and normalized to the absolute scale to obtain 1D patterns from the different configurations merged, then the contribution of the solvent filled capillary (background) was subtracted. The resulting SAXS curves were fitted using the SasView 6.0.0 package [38].

4.2.10 Stability assessment

The stability of NVs complexed with P was assessed under two conditions: storage at 25°C and 4°C and incubation in cell culture medium.

For storage stability NV–P formulations were stored at 25°C and 4 °C (±1 °C) and analyzed after 1, 4, and 7 days using DLS, as described in Section 4.2.2

For stability in cell culture medium, NV–P stability was also evaluated at 0, 2, 4, and 24 h after dilution in cell culture medium. For each time point, 10 µL of NV dispersion was mixed with 90 µL of either non-supplemented DMEM or DMEM supplemented with 10% FBS. Samples were analyzed by DLS with the attenuator set to 7, using 10 runs per measurement, and each condition measured in triplicate.

4.2.11 Complexation efficacy-Agarose Gel

The complexation efficiency was evaluated using horizontal agarose gel electrophoresis (AGE). A 2% (w/v) agarose gel was prepared by dissolving agarose powder in 100 mL of 1× TBA buffer. The suspension was heated in a microwave oven at 800 W until the agarose was fully dissolved, then poured into a gel casting tray with an appropriate comb and rest for 1 hour at room temperature.

Once solidified, the gel was placed in a horizontal electrophoresis chamber and submerged in a 1× TBE buffer. For each sample, a total of 20 µL was loaded into each well. Each sample were mixed with 2 µL of SYBR™ Gold nucleic acid stain (Thermo Fisher Scientific, Waltham, MA, USA) and 1 µL of loading buffer (Thermo Fisher Scientific, Waltham, MA,

USA). Free P was loaded as a reference control to assess the extent of complexation.

To evaluate plasmid release from the NVs, samples were incubated with heparin at a 25-fold excess (w/w) relative to the CD content. The mixtures were incubated for 3 hours at 37 °C under shaking at 420 rpm using a Titramax 1000 orbital shaker integrated with an Inkubator 1000 temperature-controlled incubator (Heidolph Instruments, Schwabach, Germany)). All samples were prepared and incubated in Eppendorf tubes prior to electrophoresis. Gels were imaged using a GelDoc XR+ system (Bio-Rad, Hercules, CA, USA) [39]. A simple estimate of the siRNA complexation percentages was obtained analysing the gel images by means of dedicated ImageJ macros [40].

4.2.12 *In vitro* toxicity, transfection and silencing efficiency

The Hela cells lines were grown in with 10 mL DMEM supplemented with 200 mM L-Glutamine and 10% (v/v) FBS medium, in a humidified incubator (MEMMERT INE 400, Memmert, Germany) with 5% CO2/95% atmospheric air at 37°C. Cells used for comparative experiments were maintained in cell culture dishes 10 mm and used between passages 10 and 20.

The cytotoxicity of empty and P-loaded NVs was evaluated using the MTT assay with HeLa Cells. The assay was performed on standard 96-well tissue-culture–treated plates, with concentrations ranging from 31 to 500 µg/mL for empty NVs, and from 15.5 to 125 µg/mL for P-loaded NVs. Cells were seeded in 96-well plates at fixed densities of 1×10^5 cells/mL. Cells were cultured for 24 h in standard culture medium. After this initial incubation, the medium was replaced with 160 µL of fresh medium and

40 µL of the NVs solution diluted in Opti-MEM. The cells were then incubated with NVs for an additional 24 h at 37 °C in a humidified 5% CO_2 atmosphere [41].

After incubation, the medium was removed and replaced with an MTT salt solution diluted in DMEM to a final concentration of approximately 1 mM. Plates were incubated for 1h at 37 °C to allow for formazan crystal formation.

Following incubation, the MTT-containing medium was carefully removed and formazane crystals were solubilized. The absorbance was measured at 570 nm using a microplate reader Infinite M200PRO (Tecan, Männedorf, Switzerland). Background absorbance at 630 nm was subtracted from the 570 nm readings to obtain normalized absorbance values representing cell viability.

Internalization studies were performed in HeLa and RAW cells and evaluated after 24 h. The lipophilic fluorescent dye DiD was used for NVs labeling, incorporating during the formulation at a final concentration of 5 µL/mL. Excess dye was removed by dialysis after 1 h.

HeLa cells were seeded in 24-well plates at a density of 1×10^5 cells/mL, and RAW cells at 5×10^5 cells/mL and incubated for 24 h under standard culture conditions (37°C, 5% CO_2). Following incubation, the culture medium was replaced with 50 µL of the NVs formulation diluted in Opti-MEM, followed by 450 µL of complete DMEM. Cells were further incubated for 24 h prior to sample preparation for flow cytometry analysis [42;43].

To confirm that nanoparticle uptake resulted from active internalization rather than surface binding, RAW cells were also incubated with DiD-labeled nanoparticles for 4 h at 4 °C.

Transfection and silencing assays were performed in HeLa and HeLa-GFP cells, respectively. For HeLa cells, evaluations were carried out at 24 and 48 hours post-treatment, while for HeLa-GFP cells, they were performed at 48 and 72 hours post-treatment [44;45]. Cells were seeded in 24-well plates at a density of 1×10^5 cells/mL and incubated for 24 h under standard culture conditions (37 °C, 5% CO_2). Following incubation, the culture medium was removed, and 50 µL of the formulation diluted in Opti-MEM was added to each well, followed by 450 µL of complete DMEM. Cells were then incubated for 24 or 48 h (transfection assay) and for 24, 48, or 72 h (silencing assay) before preparation for flow cytometry analysis. For the silencing assay, the culture medium was replaced after 48 h of incubation.

4.2.13 Fluorescence Microscopy

Fluorescence images were acquired for Transfection efficiency (24 and 48 h) post-treatment using an inverted fluorescence microscope Olympus IX73 (Olympus Corporation, Tokyo, Japan). The microscope was equipped with a digital camera and a filter set appropriate for the fluorophore used (CY3 for internalization and FITC for Transfection) [46].

Images were captured using a 20× objective lens. Exposure time, gain, and contrast were adjusted to avoid saturation and maintain comparability between samples. Image acquisition was performed using the CellSens Standard software (Olympus Corporation, Tokyo, Japan). No image manipulations that could affect data interpretation were applied.

4.2.14 Flow cytometry

Flow cytometry was performed for Transfection efficiency (24 and 48 h) and Silencing efficiency (24, 48 and 72h) using a CytoFLEX flow cytometer (Beckman Coulter, Brea, CA, USA), collecting 10,000 cells per sample. Data were analyzed using CytExpert software (Beckman Coulter, Brea, CA, USA) [47].

At the designated time points, the medium was removed, and cells were washed with 300 µL of PBS. Then, 120 µL of trypsin was added to each well and cells were incubated for 3 minutes at 37 °C to allow detachment. Subsequently, 380 µL of complete culture medium was added to neutralize the trypsin, and the cell suspension was transferred to 2 mL Eppendorf tubes.

Samples were centrifuged for 5 minutes at 1000 rpm using an Eppendorf 5425 R centrifuge (Eppendorf, Hamburg, Germany). The supernatant was discarded, and the cell pellet was resuspended in 400 µL of PBS supplemented with 10% FBS. The samples were kept on ice until analysis.

4.3 Results

4.3.1 Solid-State Characterization

The three CDs were characterized in the solid state, with the aim of obtaining more detailed information, as these are newly synthesized compounds.

4.3.1.1 DSC

Figure 2 shows the DSC curves of CD1, CD2, and CD3. No thermal events were observed for CD1 within the investigated temperature range. For CD2, an endothermic peak is observed at low temperature (54.45 °C), which can be attributed to crystalline melting. The partial crystallinity is confirmed by the diffraction pattern. Similarly, CD3 exhibits an endothermic melting peak at 50.39 °C.

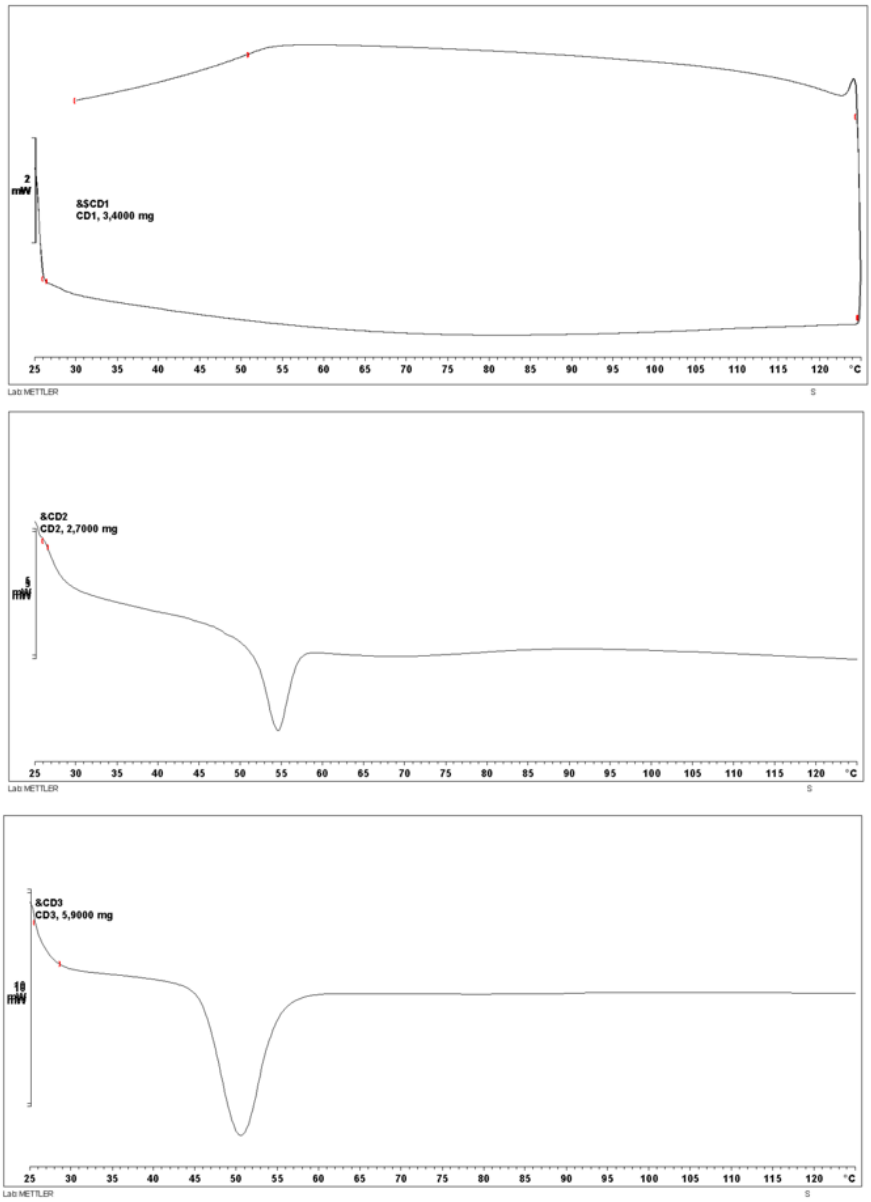

Figure 2. DCS analyses of CD1, CD2 and CD3.

4.3.1.2 XRPD

Figure 3 shows the X-ray diffraction patterns of CD1, CD2, and CD3.

CD1 can be classified as an amorphous substance, as it does not exhibit any characteristic X-ray diffraction pattern. In contrast, CD2 appears to be partially crystalline, although it lacks a well-defined ordered structure. This observation is also supported by the DSC results (Figure 2).

Similarly to CD2, CD3 can also be considered a partially crystalline material.

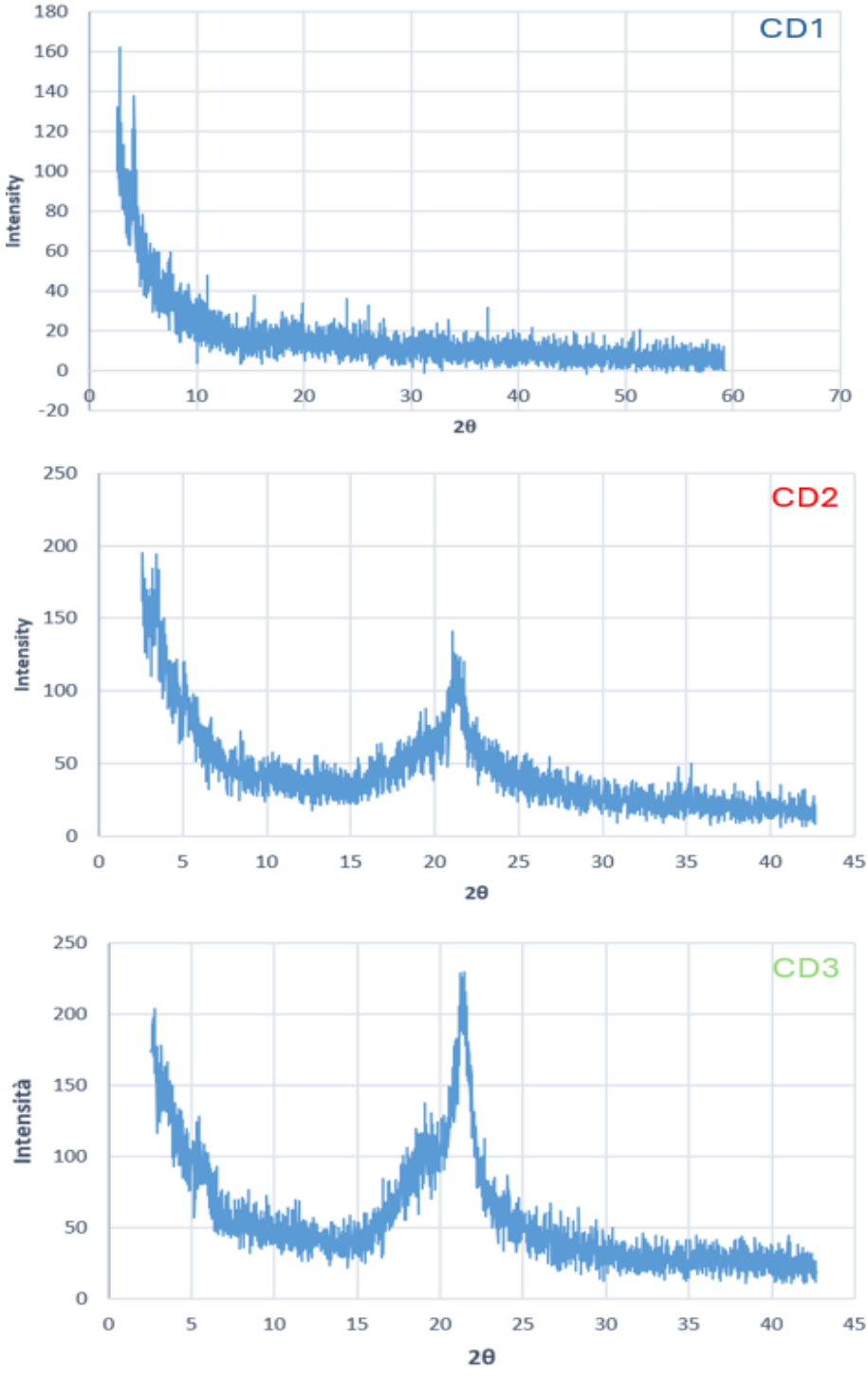

Figure 3. XRPD of CD1, CD2 and CD3

4.3.2 NVs Characterization

The obtained NVs were structurally characterized using DLS, ELS, and TEM. Acceptable size and PDI values (size <200 nm and PDI <0.3) were obtained only for CD1 and CD2; therefore, only the results related to these NVs are reported below. Additionally, the structure and interaction with P were investigated through synchrotron-SAXS.

4.3.2.1 DLS and ELS Analyses

Table 1 reports the Size, PdI, and Z values of the NVs before and after complexation with P, for both CD1 and CD2. A reduction in PdI was observed following complexation. Z remained relatively high, which prompted the introduction of an anionic polymer into the formulation, as described in Section 2.5.

Table 1. DLS and ELS analyses of CD-NVs before and after complexation with P. $n=3$ $mean \pm S.D.$

Formulation	Size (nm)	PdI	Z (mV)
CD1(A)	231 ± 13	0.2	+41 ± 3
CD1(A)+P	178 ± 19	0.2	+39 ± 2
CD1 (B)	128 ± 63	0.4	+38 ± 6
CD1(B)+P	163 ± 23	0.2	+44 ± 2
CD2	54 ± 12	0.5	+41 ± 3
CD2+P	158 ± 18	0.3	+38 ± 4

4.3.2.2 TEM

Figure 4 shows TEM images of the CDs after complexation with P. Size values obtained by DLS measurements are confirmed, and the NVs exhibit an irregular shape.

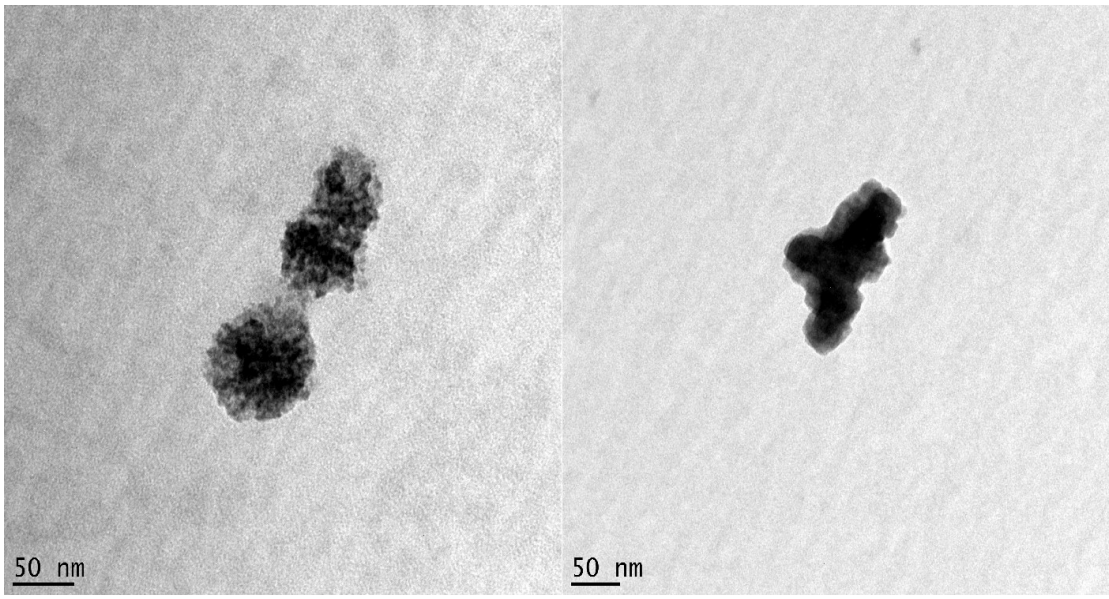

Figure 4. Tem Images of CD1+P (A) and CD2+P (B).

4.3.2.3 Cryo-EM

Cryo-em images (figure 5) of CD+P Nvs shows an irregular structure of these polyplexes, as reported also for TEM images.

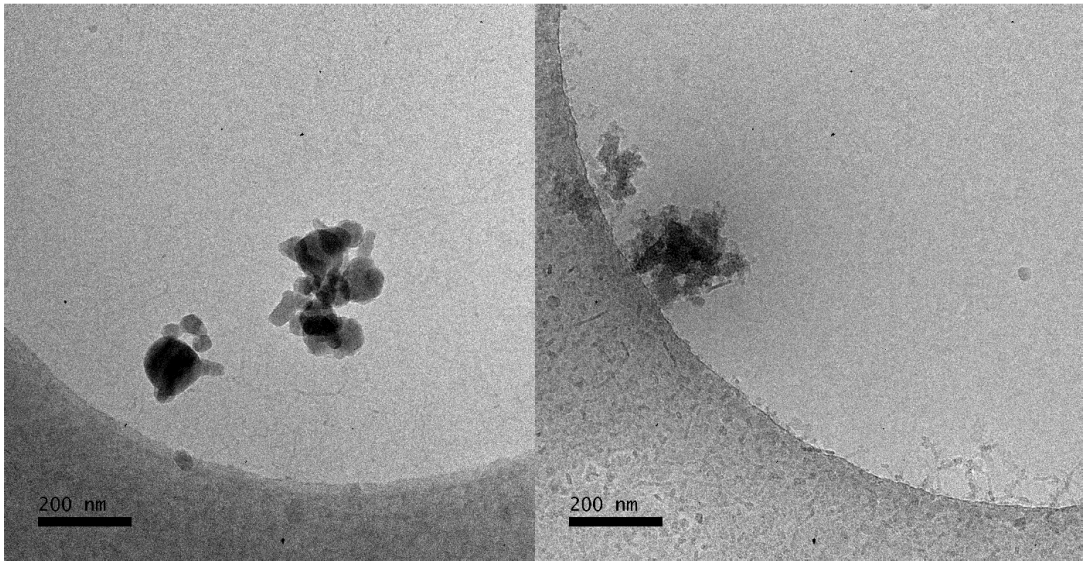

Figure 5. Cryo-em Images of CD1+P (A) and CD2+P (B).

4.3.2.4 Syncrotron SAXs

Figure 6 shows the experimental curve of the empty NVs tested.

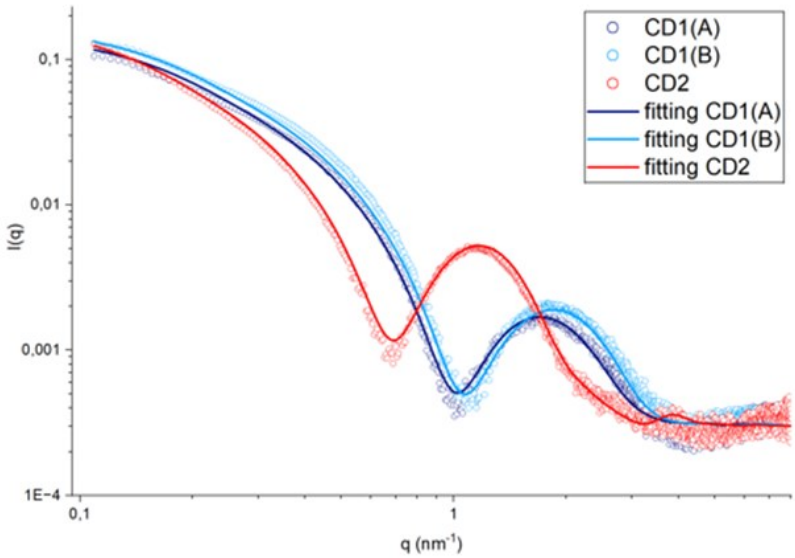

Figure 6. SAXS diagrams of empty CD NVs.

These were precisely fitted using the "core-shell bicelle elliptical belt rough" model of Sasview, as shown in the figure 7, suggesting that CD-based NVs were elongated elliptical objects.

In particular, the x_core parameter of the model, which defines ellipticity, i.e. the axial ratio of the bicelle. took values between 0.1 and 0.2, indicating elongated objects (see table 2). It is to be noted that the bicelle model was adopted as a data-driven strategy after observing that standard shapes (i.e spheres, cylinders,rotation ellipsoid and disks) were not able to give satisfactory agreement with the experimental SAXS profiles and considering that it is reasonable to assume the formation of flat aggregate when the present cyclodextrin molecules self-assembly in solution. A similar shape has been described for other modified β-

cyclodextrins which tend to assume an ellipsoid configuration when forming aggregate in water media [48;49].

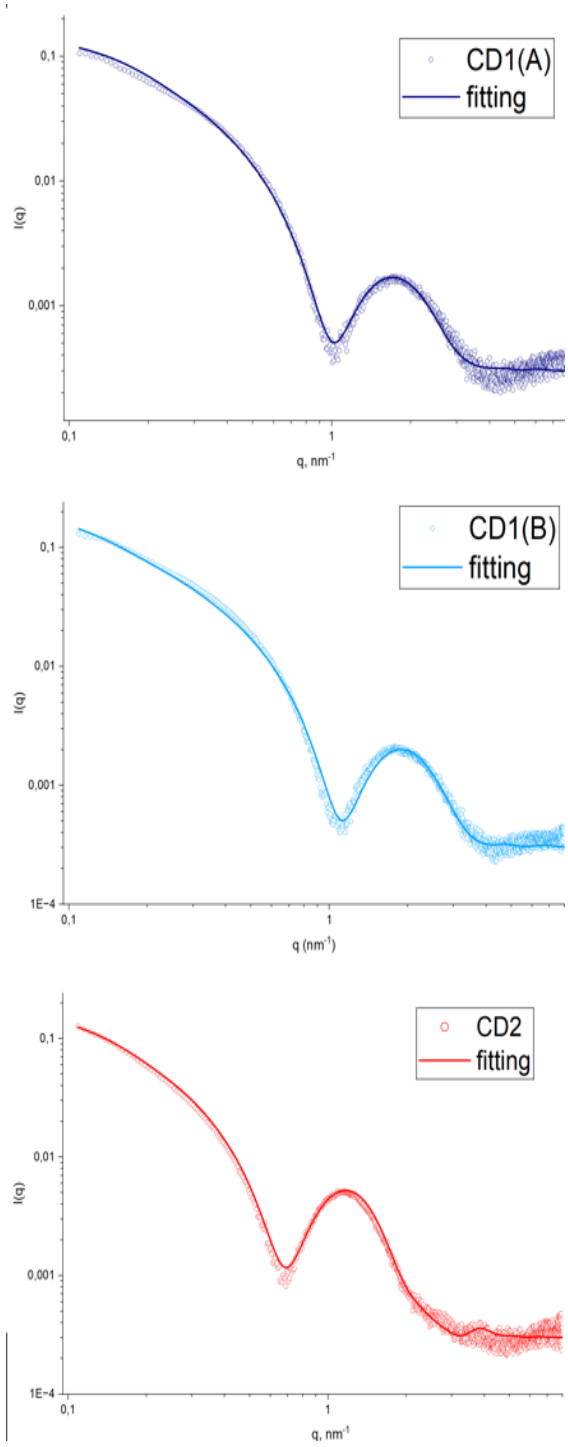

Figure 7. Experimental curve and relative fitting of (a.) CD1(A), (b.) CD1(B) and (c.) CD2

The SAXS diagrams of CD1(A) and CD1(B) display the same pattern despite the different preparation methods, whereas CD2 exhibits distinct features in the q range between 0.5 and 2 nm-1. In particular, the minimum of the SAXS curves for CD1(A) and CD1(B) is shifted toward higher q values in comparison to the CD2 experimental diagram, indicating the presence of objects with smaller dimensions (the obtained radius was 1.8 and 1.5 nm, respectively).

Table.2 Fitting model parameters used for the empty NVs (model: core shell bicelle elliptical belt rough of SASView 4.2 package).

"core_shell_bicelle_ elliptical_belt_rough" Parameters	***CD1(A)***	***CD1(B)***	***CD2***
Background (cm^{-1})	*0.0003*	*0.0003*	*0.0003*
Radius (nm)	*15.0*	*15.0*	*18.0*
X_core	*0.17*	*0.17*	*0.12*
thick_rim (nm)	*1.8*	*1.9*	*2.1*
thick_face (nm)	*1.7*	*1.5*	*2.6*
Length (nm)	*1.3*	*1.3*	*2.3*
sld_core (10^{-6}/Å)	*16*	*15.5*	*18.1*
sld_face (10^{-6}/Å)	*1.0*	*1.0*	*1.0*
sld_rim (10^{-6}/Å)	*1.0*	*2.7*	*1.0*
sld_solvent (10^{-6}/Å)	*9.4*	*9.4*	*9.4*
Polidispersity (Radius)	*0.02*	*0.02*	*0.02*

Figure 8 show the SAXS curves of the systems after complexation with P.

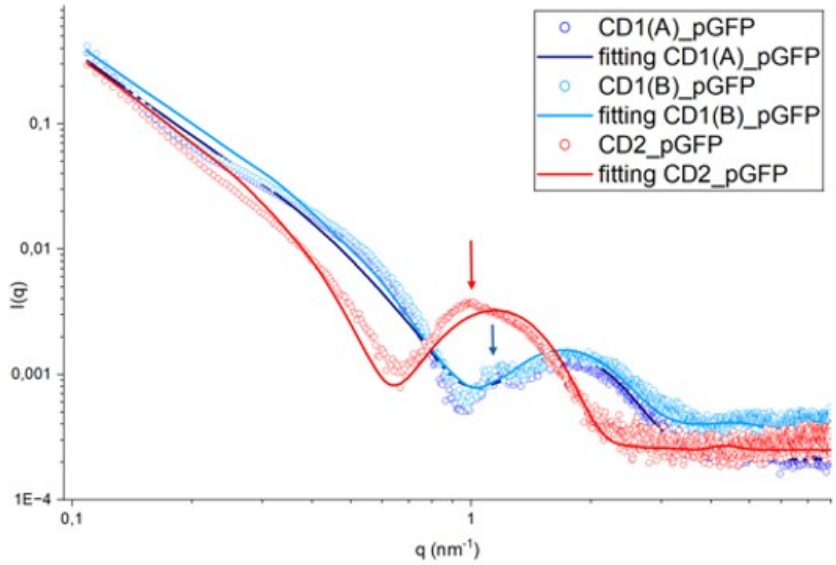

Figure 8. SAXS diagrams of the colloidal CD NVs complexed with P.

The main characteristics of the SAXS diagrams of complexed CDs were fitted using the same model as for their unloaded counterparts, showing that the structure of flattened objects was substantially retained after interaction with the plasmid (Figure 8 and table 3).

For the CD1 complexes, a small increase in thickness and radius was observed while the x-core parameter and eccentricity remain unchanged. On the other hand, the scattering profile of NVs with CD2 showed increased asymmetry, which was fitted with larger eccentricity of the NVs, while the position of the minima and peaks (with respect to q) remained unchanged.

It is worth noting that a secondary peak positioned around 1 nm^{-1} emerged in the SAXS diagrams of complexed CDs (see the arrows in figure 8). Following the interpretation given by Safinya and coworkers who report

the same small peak in multilamellar liposomes with DNA sandwiched between cationic bilayers [51], we attributed this feature to the Plasmid correlation. Therefore, in the CD-P system the DNA strands were intercalated among layers of CD NVs. Furthermore, as in the case of cationic liposomes, the presence of a peak indicates marked spatial periodicity arising from the electrostatic interactions that make up the polyplex (figure 9, table 3).

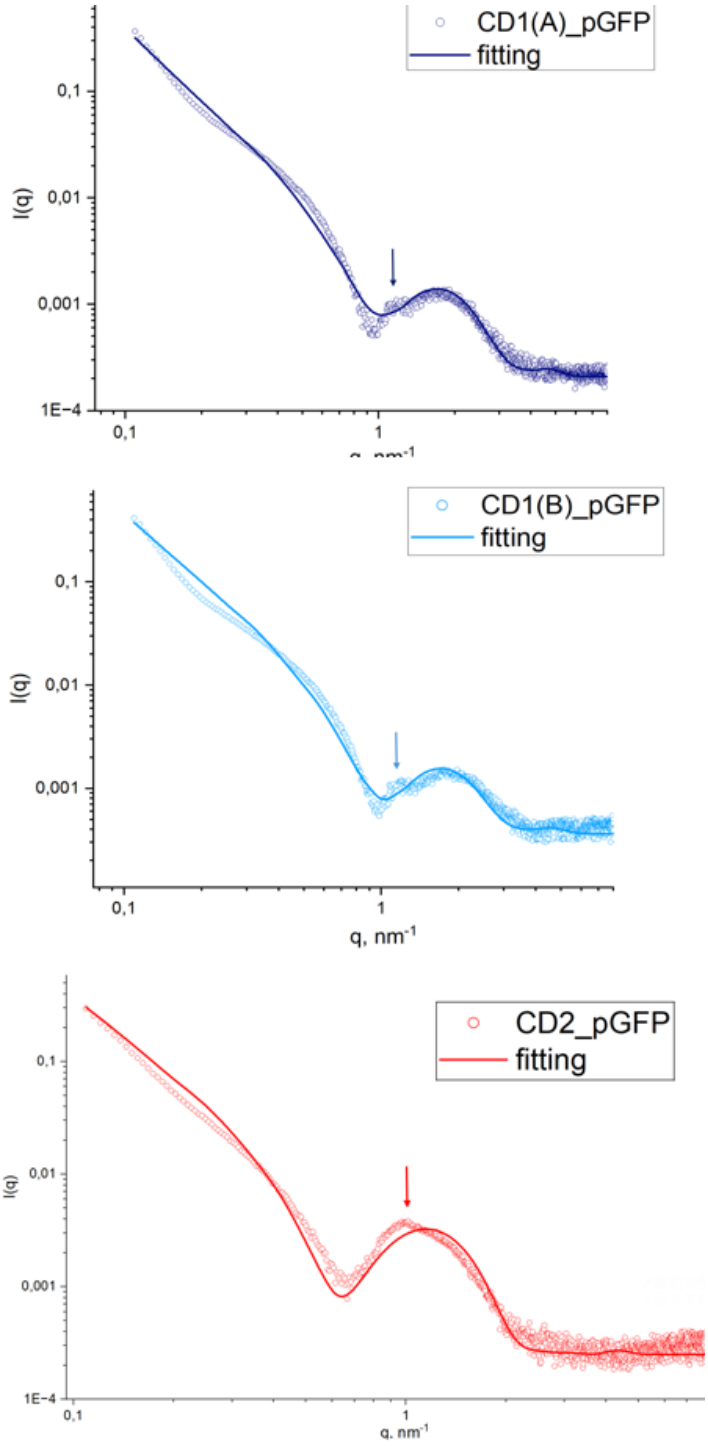

Figure 9. Experimental curve and relative fitting of (a.) CD1(A)+P, (b.) CD1(B)+P and (c.) CD2+P

Table 3. Fitting parameters used for the NVs complexed with the nucleic acid using the model core shell bicelle elliptical belt rough of SASView.

"core_shell_bicelle_ elliptical_belt_rough" Parameters	*CD1(A)+P*	*CD1(B)+P*	*CD2+P*
Background (cm^{-1})	*0.0003*	*0.0004*	*0.0003*
Radius (nm)	*80.0*	*78.0*	*18.0*
X_core	*0.2*	*0.2*	*0.48*
thick_rim (nm)	*18.0*	*22.0*	*4.0*

"core_shell_bicelle_ elliptical_belt_rough" Parameters	***CD1(A)+P***	***CD1(B)+P***	***CD2+P***
Background (cm^{-1})	*0.0003*	*0.0004*	*0.0003*
Radius (nm)	*80.0*	*78.0*	*18.0*
X_core	*0.2*	*0.2*	*0.48*
thick_rim (nm)	*18.0*	*22.0*	*4.0*

The CD NVs are made by elongated objects whose shape and size undergo minor changes upon loading the P, while their overall organization is more markedly affected, in that the DNA rods are intercalated among CDs layers and exhibit an additional correlation due to electrostatic interactions.

4.3.3 NVs Stability

4.3.3.1 Stability at 4 and 25 °C

Figure 10 shows the graph illustrating the variation in size and Z for CD/P NVs stored at 25 °C (A) and at 4°C (B) after 1, 4, and 7 days. A slight increase in size and a decrease in Z was observed over time; however, the formulations remained stable throughout the observation period.

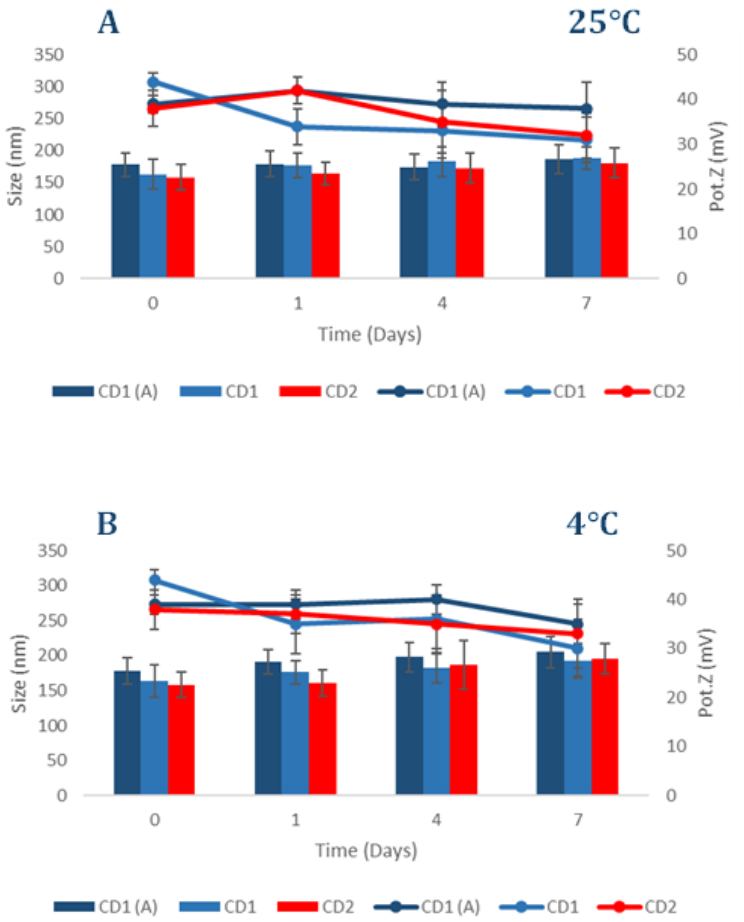

Figure 10. Stability of CD NVs with P at 25°C (A) and 4°C (B). CD1(A) (blue), CD1(B) (sky blue) and CD2 (Red).n=3 mean ± S.D.

4.3.3.2 Stability in cells medium

The stability of NVs with P was evaluated in cell culture medium (DMEM), both with and without FBS supplementation. Figure 11 shows the evolution of particle size and Kpcs over time.

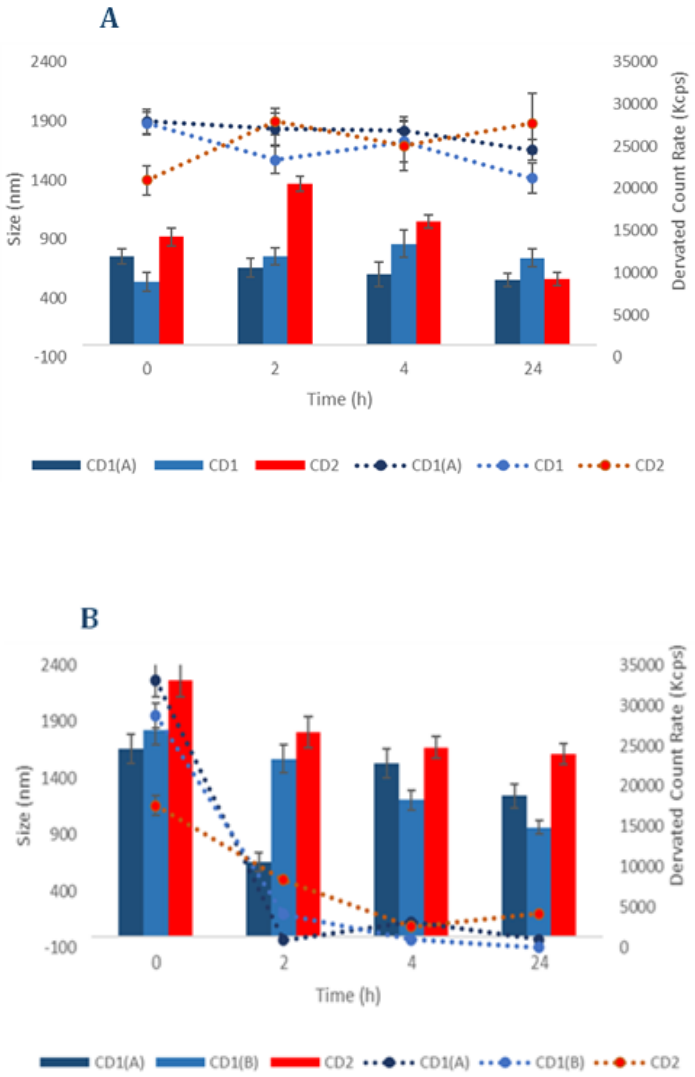

Figure 11. Stability of CD NVs with P In DMEM with FBS (A) and without FBS (B). CD1(A) (blue), CD1(B) (sky blue) and CD2 (Red). $n=3$ *mean* $\pm$ *S.D.*

In the absence of FBS, the NVs exhibited a tendency to aggregate, as evidenced by the increase in size and decrease of Kpcs values. While, in DMEM supplemented with FBS, the NVs showed an initial size increase followed by stabilization over time. Since cells are routinely cultured in DMEM supplemented with FBS and considering that this environment does not perfectly mimic physiological conditions, we consider it appropriate to proceed with further cellular studies under these supplemented conditions.

4.3.4 Complexation efficacy

Figure 12 shows the agarose gel images obtained after electrophoresis, performed as described in Section 4.2.11. Free P migrated out of the loading well, as did the NVS formulated with heparin. In contrast, the CD+P complexes did not display any bands corresponding to free plasmid, confirming the complete complexation of the plasmid with CDs at the tested ratio (>90%) (as reported in figure 13).

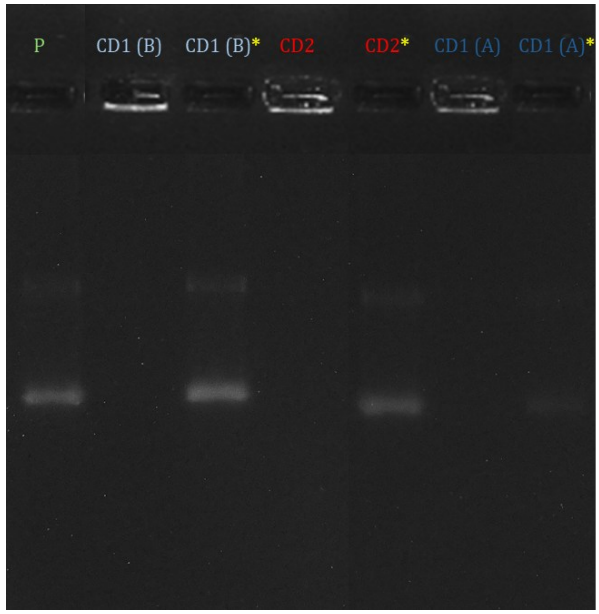

Figure 12.Agarose gel Images obtained after horizontal electrophoresis of CD NVs with P. Free plasmid is shown in green, CD1(B) in light blue, CD2 in red, and CD1(A) in blue. Samples containing heparin are marked with a yellow asterisk.

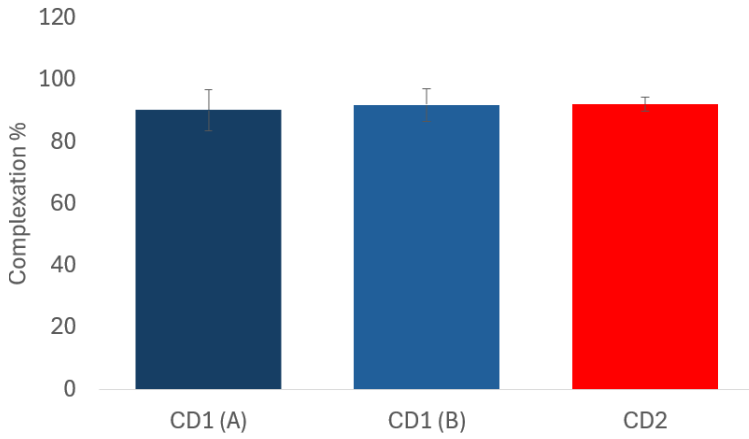

Figure 13. Complexation % CD1(A) in blue CD1(B) in light blue, CD2 in red. n=3 mean ± S.D.

4.3.5 MTT test

MTT assays were performed on HeLa and RAW 264.7 cell lines to evaluate the cytotoxicity of the tested nanocarriers. As a first step, blank CD NVs were tested to screen for non-toxic concentration ranges. The results of this preliminary assessment are shown in Figure 14. For HeLa cells, the concentration of 31 µg/mL showed no significant difference compared to the control, while for RAW cells the threshold was 62.5 µg/mL, indicating that these concentrations can be considered safe.

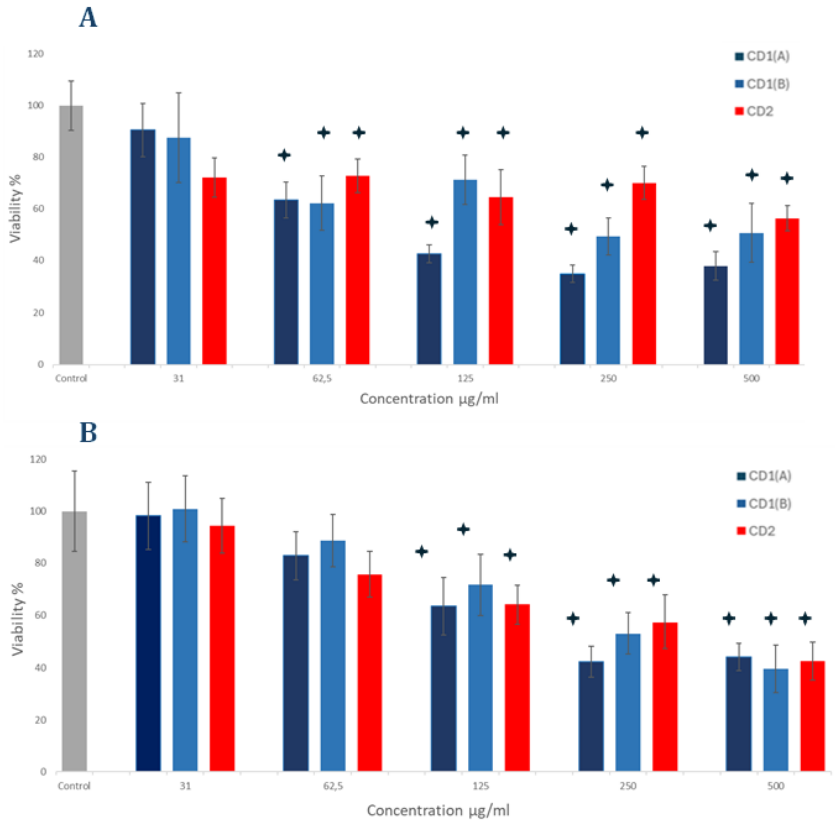

Figure 14.MTT Assays of CDs NVs on HeLa cells (A) and RAW cells (B). CD1(A) (Blue) CD1(B) (light Blue) CD2 (Red). n=3 mean ± S.D. Statistical significance was assessed using a t-test to calculate the P value (indicated with an asterisk).

Based on these results, we reduced the concentration of the tested complexes, and cell viability was subsequently evaluated after treatment with CD NVs with P, as shown in Figure 15. No significant cytotoxic effects were observed in either HeLa or RAW cells at the tested concentrations, except for CD1(A), which exhibited cytotoxicity at 125 μg/mL, defining 62.5 μg/mL as the safe dose. The data indicate an increased “safe” concentration range for CD+P complexes compared to blank NVs. This effect is likely attributable to the reduction in surface potential following plasmid complexation, which may decrease interactions with the cell membrane and thereby reduce cytotoxicity. Furthermore, RAW cells displayed greater tolerance to the NVs compared to HeLa cells, suggesting cell line–specific sensitivity.

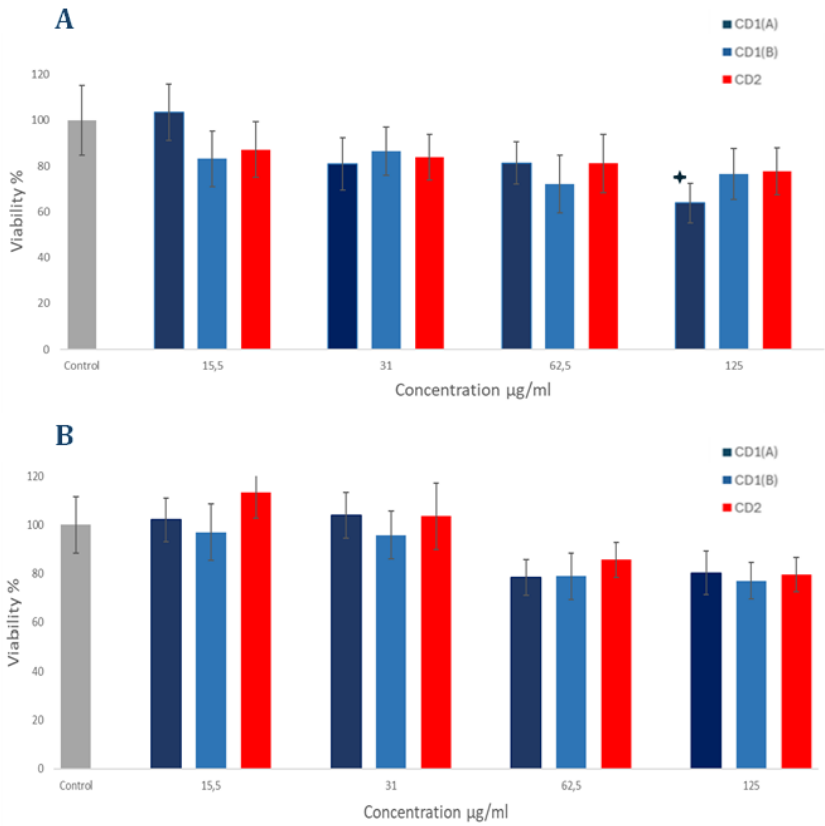

Figure 15. MTT Assays (24h) of CDs NVs+P on HeLa cells (A) and RAW cells (B). CD1(A) (Blue) CD1(B) (light Blue) CD2 (Red). n=3 mean ± S.D. Statistical significance was assessed using a t-test to calculate the P value (indicated with an asterisk).

Given the comparable results of the two CD1 production methods (A and B) in terms of size, PdI, and Z, and the demonstrated stability of both formulations, subsequent studies were focused on CD1(B) and CD2. CD1(B) was selected due to slightly improved complexation with P and a higher cell-safe dose, while CD1(A) was excluded.

4.3.6 Internalization studies

We evaluated the cellular uptake of the NVs after 24h, following the method described in paragraph 4.2.13, using HeLa and RAW cells. Both

CD1(B) and CD2 were tested at two different concentrations, and internalization exceeded 85% for all formulations and concentrations, as shown by flow cytometry data in Figure 16. These uptake levels were comparable to those observed for DiD alone.

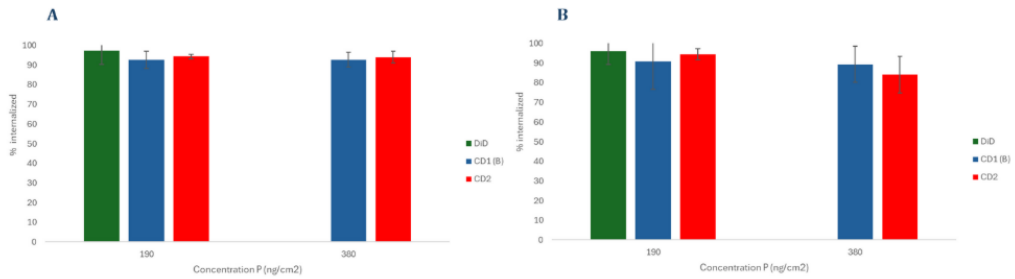

Figure 16.Citofluorimetric Data Obtained after 24h of internalization of CD NVs+P in Hela (A) and RAW (B) Cells. Free DiD (green), CD1(B) (light Blue) CD2 (Red).n=3 mean ± S.D.

We also quantified the fluorescence intensity of DiD and the CD NVs with P, reported in Figure 17, which revealed higher fluorescence for the CD NVs, indicating an enhanced capacity for cellular internalization. Additionally, the fluorescence intensity of DiD was higher in HeLa cells compared to RAW cells.

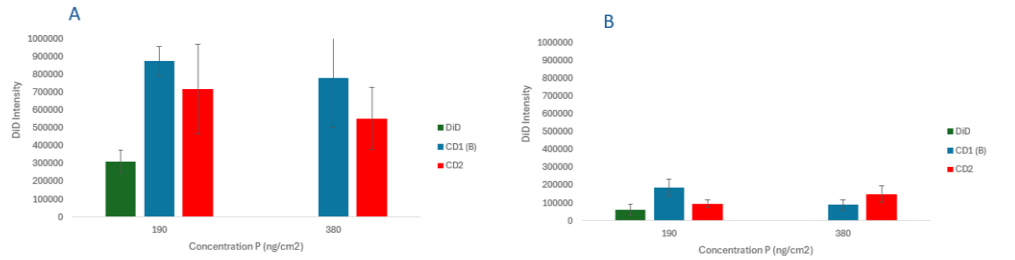

Figure 17.DiD Intensity after 24h of internalization of CD NVs+P in Hela (A) and RAW (B) Cells. Free DiD (green), CD1(B) (light Blue) CD2 (Red).n=3 mean ± S.D.

Representative fluorescence microscopy images are presented in Figure 18. Overall, these results confirm that the NVs are efficiently taken up by the cells.

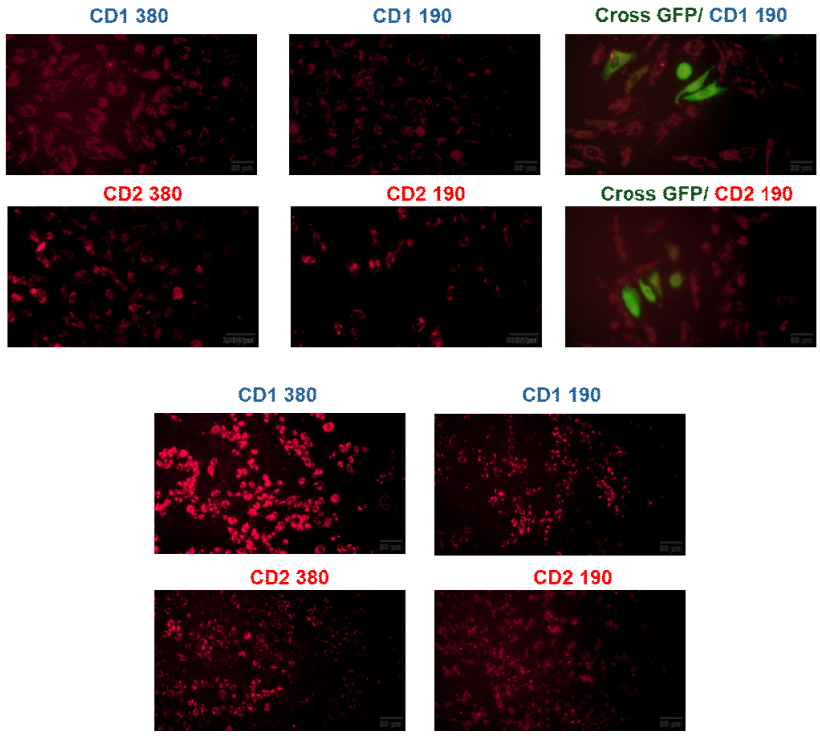

Figure 18.Microscopy Images of CD NVS+P internalized after 24h in HeLa (A) and RAW (B) cells.

4.3.7 Addition of Anionic Polymers

The DLS analysis of CD NVs with P and HA/HP are reported in Table 4. A decrease in PdI was observed for the HA-containing formulation, while both HA and HP led to a reduction in Z potential compared to normal CD NVs.

Table 4.DLS and ELS analyses of CD-NVs (P) with HA and HP.n=3 mean ± S.D.

Formulation	Size (nm)	PdI	Z (mV)
CD1+HA	195 ± 11	0.2	+28 ± 3
CD1+HA+P	166 ± 18	0.2	+31 ± 3
CD2+HA	160 ± 13	0.2	+30 ± 3
CD2+HA+P	155 ± 18	0.2	+30 ± 3
CD1+HP	188±16	0.3	+31±4
CD1+HP+P	180±13	0.3	+29±5
CD2+HP	172± 15	0.3	+23±6
CD2+HP+P	164±22	0.3	+20±5

The stability of the modified NVs at 4 °Cover 1, 4, and 7 days is shown in Figure 19, demonstrating comparable behaviour to the unmodified NVs.

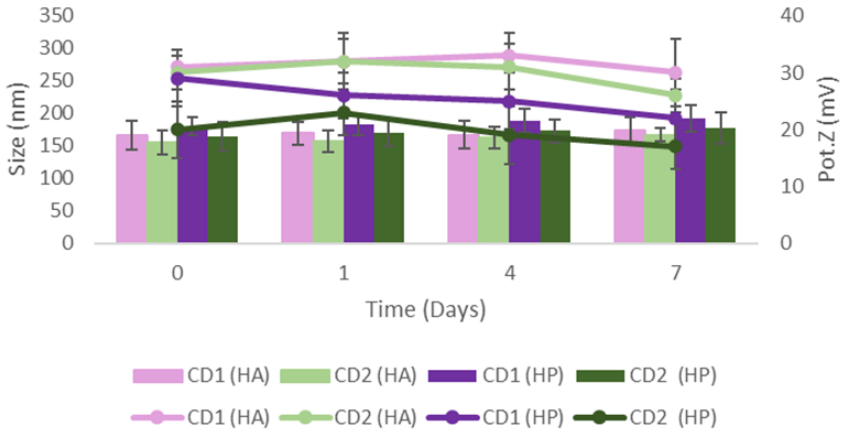

Figure 19. Stability of CD NVs at 4°C. CD1 (HA) (pink), CD1 (HP) (violet), CD2 (HA) (Light green), CD2 (HP) (Dark Green). n=3 mean ± S.D.

The encapsulation efficiency was good for all tested formulations (>90%), as shown in Figure 20-21.

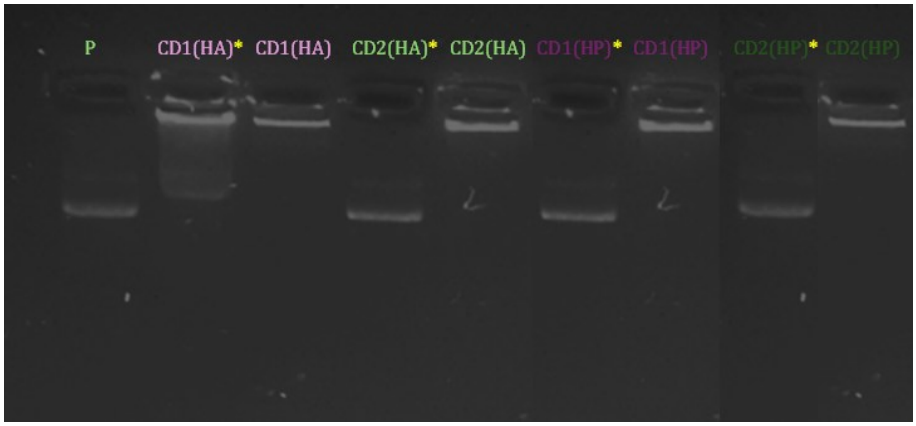

Figure 20. Agarose gel Images of CD NVs (HA/HP) with P. Free plasmid is shown in green, CD1(HA) in pink, CD1(HP) in violet, CD2(HA) in light green and CD2(HP) in dark green. Samples containing heparin are marked with a yellow asterisk.

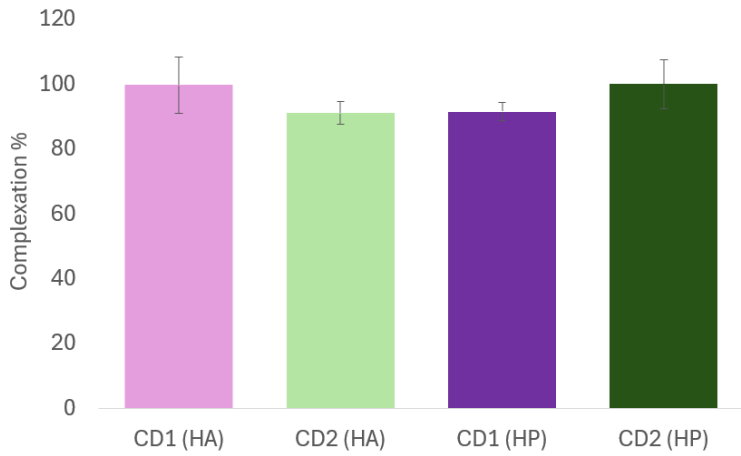

Figure 21. Complexation % CD1(HA) in pink, CD1(HP) in violet, CD2(HA) in light green and CD2(HP) in dark green. n=3 mean ± S.D.

Cell viability was evaluated in HeLa cells by MTT assay after 24 h (Figure 22). Contrary to expectations, the incorporation of HA did not reduce cytotoxicity. While the profile of HP-containing formulations remained comparable to that of unmodified NVs, the safe dose was lowered to 31 µg/mL for CD1(HA) and to 62.5 µg/mL for CD2(HA). A possible explanation, consistent with previous studies, is that although HA is generally regarded as biocompatible, its inclusion may alter NP uptake mechanisms or extracellular stability, leading to increased intracellular accumulation or aggregation. In addition, HA–NP interactions could elicit distinct cellular responses depending on receptor expression patterns.

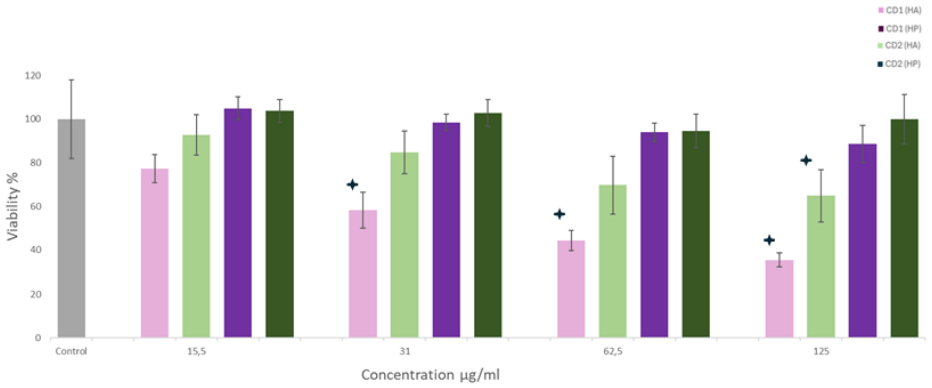

Figure 22. MTT Assays (24h) of CDs NVs+P (HA/HP) on HeLa cells. CD1 (HA) (pink), CD1 (HP) (violet), CD2 (HA) (Light green), CD2 (HP) (Dark Green). n=3 mean ± S.D. Statistical significance was assessed using a t-test to calculate the P value (indicated with an asterisk).

Despite these observations, the non-toxic concentration ranges identified remain within those typically applied in transfection experiments, supporting the feasibility of employing these formulations in subsequent studies.

4.3.8 Transfection efficiency

The experiments were carried out as described in Section 4.2.12. Transfection efficiency was evaluated in HeLa cells after 24 and 48 h for NVs formulated with CD1, CD2, and with the addition of HA or HP. Flow cytometry results obtained at 24 and 48 h are shown in Figure 23.

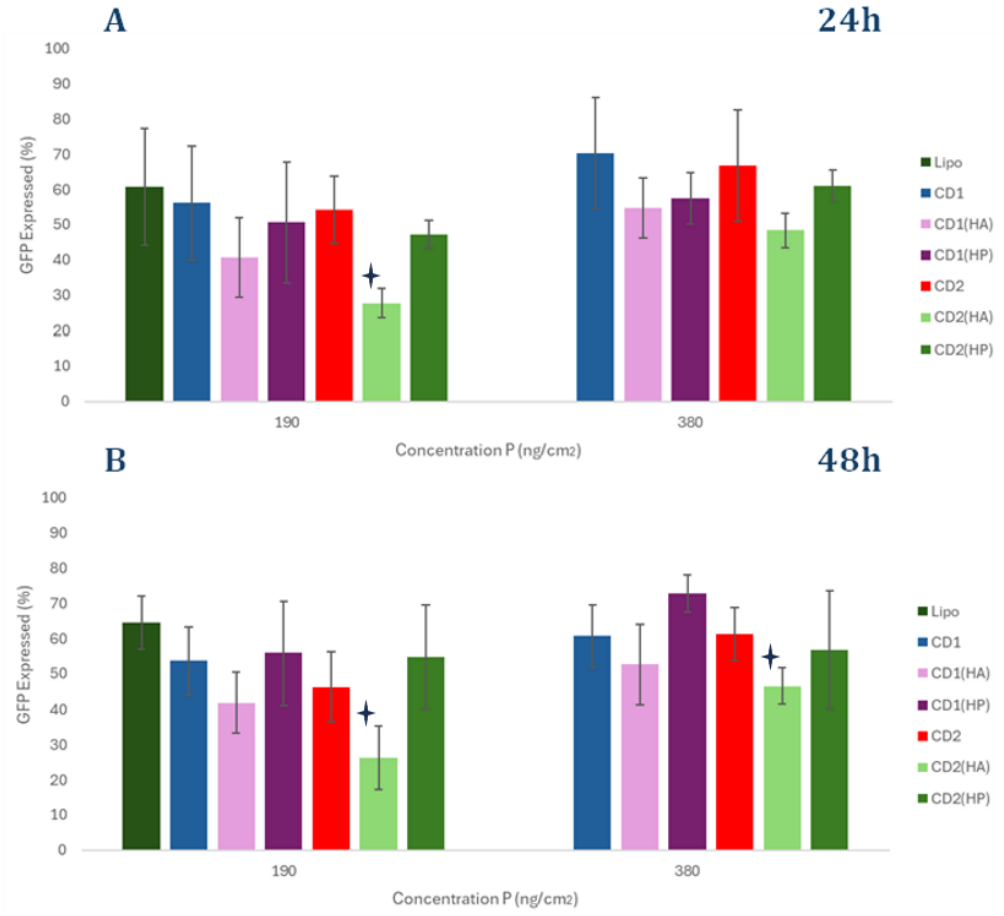

Figure 23.Cytofluorimetric Data of Transfection Efficiency of NVs+P (HA/HP) on HeLa cells after 24h (A) and 48h (B) . Lipofectamine (Green), CD1(B) (light blue), CD2 (Red), CD1 (HA) (pink), CD1 (HP) (violet), CD2 (HA) (Light green), CD2 (HP) (Dark Green).n=3 mean ± S.D. Statistical significance was assessed using a t-test to calculate the P value (indicated with an asterisk).

A substantial level of transfection was already achieved at 24 h, and by 48 h, transfection increased slightly, with reduced variability as indicated by smaller error bars. Among the two P concentrations tested (190, and 380 ng/cm^2), both achieved similarly high transfection levels, with no substantial differences between them. Therefore, 190 ng/cm^2 can be considered the optimal dose, as it provides comparable transfection

efficiency while using a lower amount of material, thereby representing a safer option. Also higher and lower plasmid (P) doses were tested. Lower doses resulted in reduced transfection efficiency, whereas higher doses increased cytotoxicity without providing a significant improvement in transfection efficiency. After 24 h, efficiency was relatively high for all tested formulations; in particular, all CD1-based formulations achieved transfection levels above 50%, comparable to those obtained with Lipofectamine, which was used as the reference gold standard [51-53]. After 48h we obtain similar results.

In Figure 24, the GFP fluorescence intensity is reported after 24 and 48 hours. As expected, Lipofectamine resulted in the highest GFP signal; however, samples treated with CD1 and CD1 (HA) NVs also displayed strong fluorescence, followed by CD2. After 48 hours, a slight decrease in GFP intensity was observed for Lipofectamine, while a more pronounced reduction was detected in CD formulations. NVs functionalized with HP and CD2(HA) showed lower fluorescence intensity compared to their non-modified counterparts. Overall, CD1 formulations exhibited the highest transfection efficiency. The relatively high variability observed among samples in this dataset can be attributed to the intrinsic biological heterogeneity of transfection experiments.

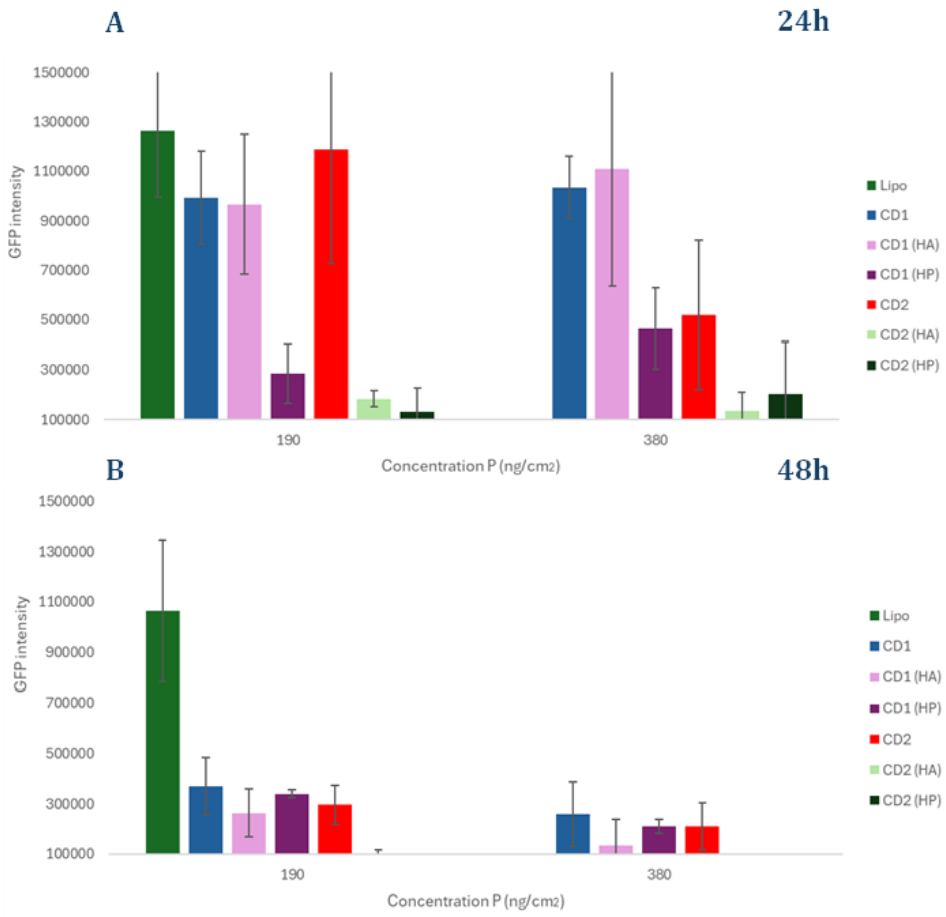

Figure 24.Citofluorimetric Data of GFP Fluorescence intensity of NVs+P (HA/HP) on HeLa cells after 24h (A) and 48h (B) . Lipofectamine (green), CD1(B) (light blue), CD2 (Red), CD1 (HA) (pink), CD1 (HP) (violet), CD2 (HA) (Light green), CD2 (HP) (Dark Green).n=3 mean ± S.D.

In Figure 25, the transfection images acquired by fluorescence microscopy are reported. Consistent with the quantitative data, these images confirm that transfection is higher in cells treated with CD1-based nanoparticles compared to those treated with CD2. Cell analyses were also performed using the Cell Discoverer 7 automated imaging system (Zeiss, Germany) to monitor and verify transfection efficiency and gene

silencing efficacy. Time-lapse videos were acquired at different time points to assess dynamic cellular responses.

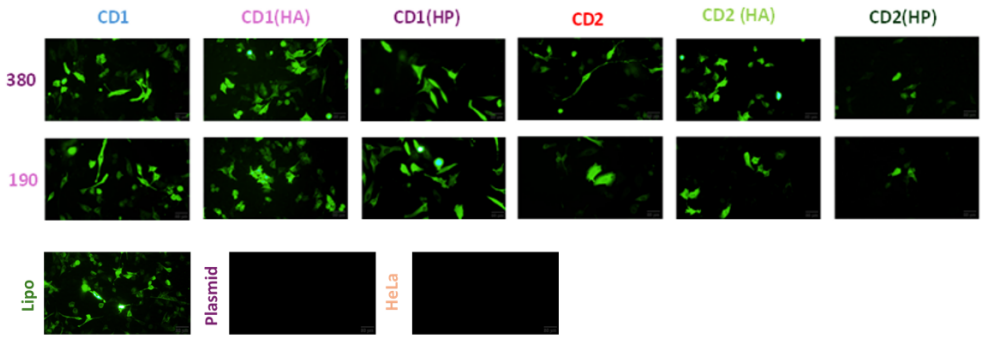

Figure 25.Fluorescence Microscopy Images of HeLa Cells after 48h of transfection.

4.3.9 siRNA Complexation

NVs of CD1 and CD2, with or without HA/HP, were additionally complexed with GFP siRNA at an N/P ratio of 10, following the methodology outlined in Section 4.2.5. Due to the high cost of siRNA, only preliminary experiments were conducted. The data obtained from these studies are presented below.

4.3.9.1 Characterization

DLS and ELS data, reported in table 5, showed an increase in size and PdI for all the formulations, except for the ones containing HA, that showed size around 150-180 nm and PdI= 0.3.

Table 5.DLS and ELS analyses of CD-NVs with siRNA (N/P=10). n=3 mean ± S.D.

Formulation	Size (nm)	PdI	Z (mV)
CD1	255 ± 45	0.5	+ 33 ± 5
CD2	156± 38	0.4	+25 ± 8
CD1 (HA)	187 ± 24	0.3	+25 ± 5
CD2 (HA)	158 ± 20	0.3	+23 ± 6
CD1 (HP)	230 ± 65	0.4	+25 ± 8
CD2 (HP)	178 ± 48	0.4	+26 ± 6

4.3.9.2 Complexation efficacy

Complexation efficacy was good for all the formulation (> 90%) as showed in figure 26-27.

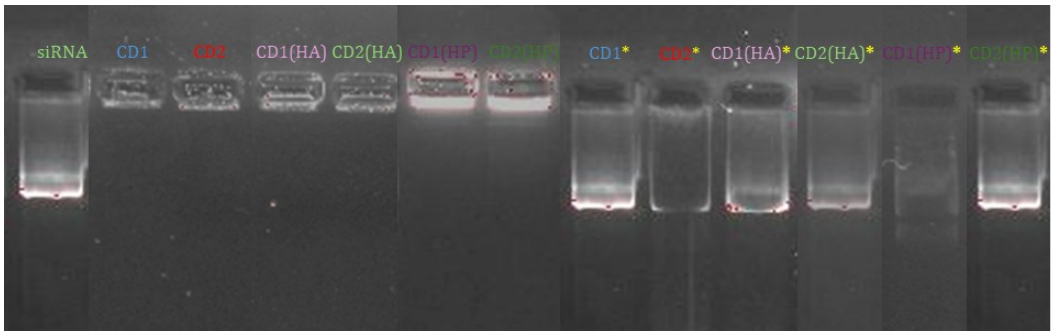

Figure 26. Agarose gel Images of CD NVs (HA/HP) with siRNA. Free siRNA (green), CD1 (light blue), CD2 (red), CD1(HA) (pink), CD1(HP) (violet), CD2(HA) (light green), CD2(HP) (dark green). Samples containing heparin are marked with a yellow asterisk.

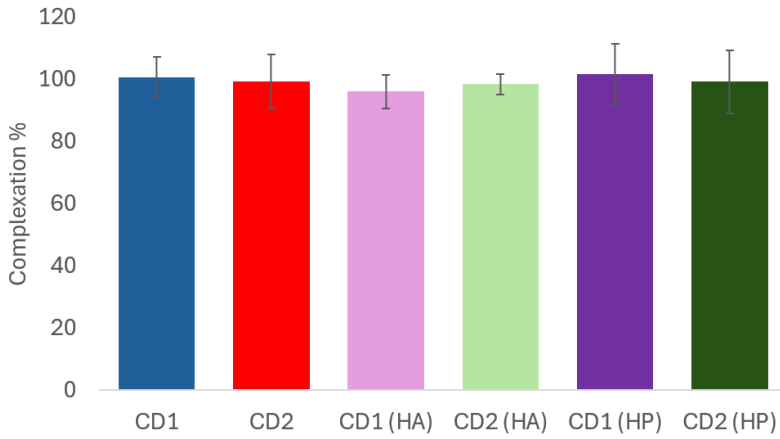

Figure 27. Complexation % CD1 (light blue), CD2 (red), CD1(HA) (pink), CD1(HP) (violet), CD2(HA) (light green), CD2(HP) (dark green). n=3 mean ± S.D.

4.3.9.3 Silencing efficiency

The silencing efficiency of all NVs was evaluated in HeLa GFP-expressing cells and quantified by flow cytometry after 24, 48, and 72 hours. GFP-targeting siRNA required a longer time compared with plasmid DNA to achieve gene silencing. After 24 hours, all formulations, including Lipofectamine, exhibited less than 15% silencing activity. Flow cytometry data at 48 and 72 hours are shown in Figure 28. A clear increase in silencing efficiency was observed at 48 hours, with maximal effects detected at 72 hours. At this time point, all samples achieved more than 50% silencing. In particular, formulations containing CD1 (with or without HA/HP) reached approximately 90% silencing, comparable to Lipofectamine. No significant differences were observed between the two tested doses, further confirming that siRNA concentration at 190 ng/cm^2 represents the most effective candidate.

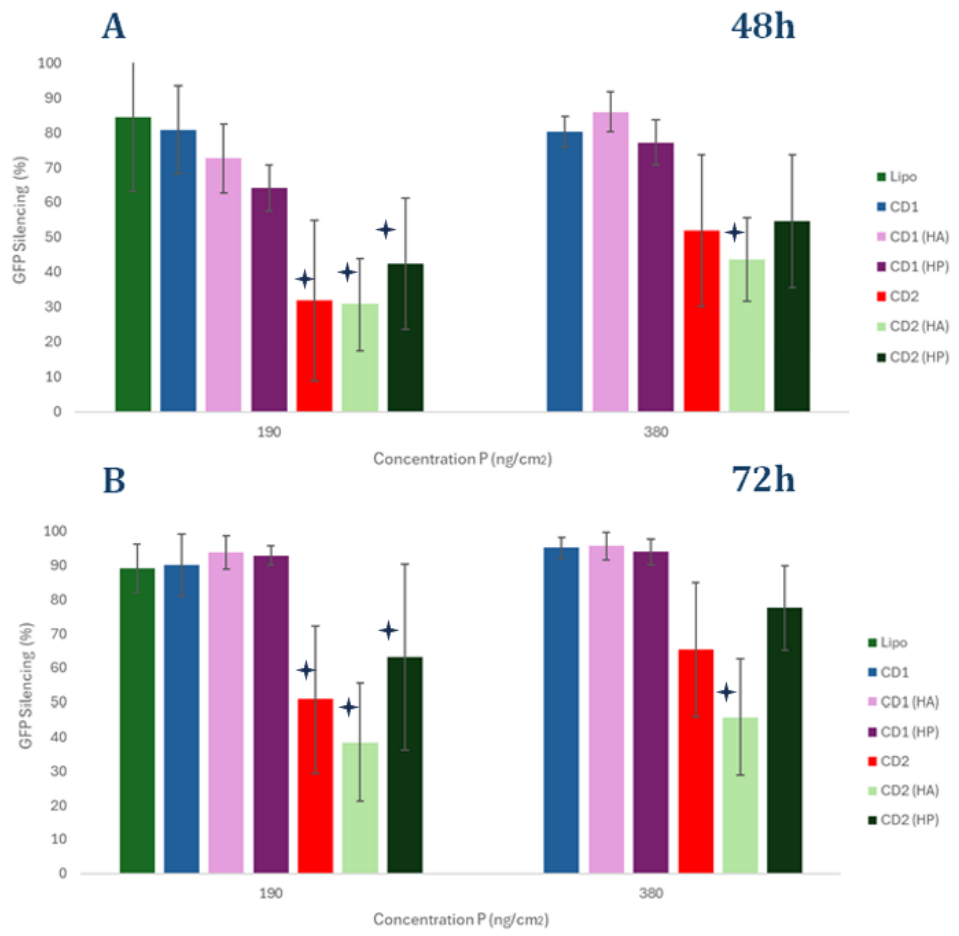

Figure 28. Citofluorimetric Data of Silencing Efficiency of NVs with siRNA (HA/HP) on HeLa GFP cells after 48h (A) and 72h (B). Lipofectamine (Green), CD1(B) (light blue), CD2 (Red), CD1 (HA) (pink), CD1 (HP) (violet), CD2 (HA) (Light green), CD2 (HP) (Dark Green).n=3 mean ± S.D. Statistical significance was assessed using a t-test to calculate the P value (indicated with an asterisk).

Figure 29 reports the GFP fluorescence intensity data, which further confirm that CD1-based nanoparticles achieve higher silencing efficiency compared with CD2-containing formulations. The GFP intensity of CD1 nanoparticles was comparable to that obtained with Lipofectamine. The

lowest fluorescence levels were detected at 72 hours, highlighting the maximal silencing efficacy at this time point.

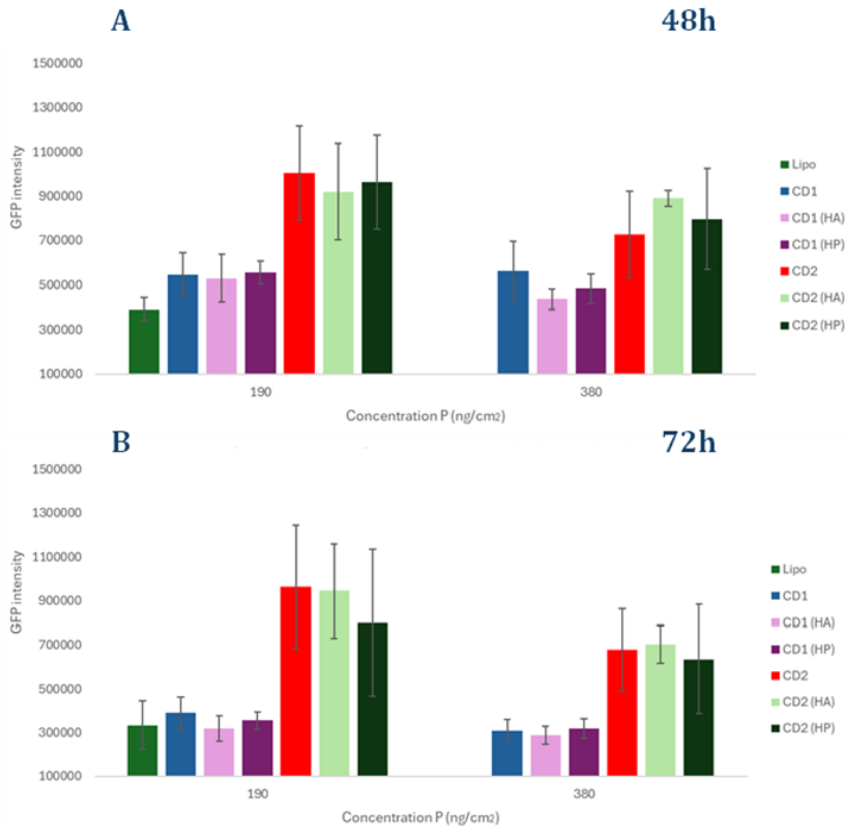

Figure 29. Citofluorimetric Data of GFP Fluorescence intensity of NVs with siRNA (HA/HP) on HeLa cells after 48h (A) and 72h (B). Lipofectamine (green), CD1(B) (light blue), CD2 (Red), CD1 (HA) (pink), CD1 (HP) (violet), CD2 (HA) (Light green), CD2 (HP) (Dark Green).n=3 mean ± S.D.

4.4 Conclusions

We obtained favorable aggregation properties forming NVs for two of the three cationic modified β-CDs tested (CD1 and CD2) upon complexation with P. Although these complexes displayed somewhat irregular morphology, Z potential, TEM imaging and SAXS analyses indicated that the genetic material was successfully encapsulated within the NVs. The architecture of the developed NVs, emerging from in depth physico-chemical investigation, can be described as follows: small ellipsoids of 1.5-2 nm are joined together in clusters with 10-50 nm mean size, which are in turn super-assembled to form the scattering objects with 150-200 nm diameter, as revealed by DLS. *In vitro* tests showed that CD1 NVs achieved a transfection efficiency of approximately 55%, outperforming CD2 NVs. The incorporation of anionic polymers HA and HP did not induce substantial changes, aside from a reduction in Z, and the modified NVs exhibited behavior comparable to their unmodified counterparts. NVs complexed with siRNA demonstrated promising performance, particularly CD1 NVs, which produced greater gene silencing than CD2 NVs, achieving knockdown efficiencies above 90%, comparable to those obtained with Lipofectamine. Notably, NVs containing HA showed improved size and PdI. The differences observed between CD1 and CD2 NVs may be attributable to their distinct structural features. CD1 contains a shorter lipophilic chain (C8) compared with CD2 (C16) and carries only one protonable amine group, whereas CD2 possesses two protonable amine groups. These variations are likely to influence their interactions with cellular membranes and their behavior during endosomal trafficking. In particular, the combination of a shorter hydrophobic tail and a single amine group in CD1 may facilitate a more efficient membrane interaction and promote endosomal uptake or escape. Overall, these vectors still

require further optimization and evaluation using nucleic acid encoding disease-relevant genes, both in appropriate cellular models and *in vivo*, to fully assess their targeted therapeutic potential. Conversely, the presence of sulfur-containing lipid chains offers a robust platform for ligand conjugation, providing a versatile strategy for future NV functionalization.

4.5 Bibliography

[1] Haley RM et al. Cyclodextrins in drug delivery: applications in gene and combination therapy. Drug Deliv Transl Res. 2020;10(3):661–677. doi:10.1007/s13346-020-00724-5.

[2] Chaturvedi K et al. Cyclodextrin-based siRNA delivery nanocarriers: a state-of-the-art review. Expert Opin Drug Deliv. 2011;8:1455–1468. doi:10.1517/17425247.2011.610790.

[3] Mousazadeh H et al. Cyclodextrin-based natural nanostructured carbohydrate polymers as effective non-viral siRNA delivery systems for cancer gene therapy. J Control Release. 2021;330:1046–1070. doi:10.1016/j.jconrel.2020.11.011.

[4] Qu G et al. Cyclodextrins as non-viral vectors in cancer theranostics: a review. Int J Biol Macromol.2025;313:143697. doi:10.1016/j.ijbiomac.2025.143697.

[5] Fitzgerald KA et al. A novel, anisamide-targeted cyclodextrin nanoformulation for siRNA delivery to prostate cancer cells expressing the sigma-1 receptor. Int J Pharm. 2016;499:131–145. doi:10.1016/j.ijpharm.2015.12.055.

[6] Nazli A et al. Cationic cyclodextrin-based carriers for drug and nucleic acid delivery. Pharmaceutics. 2025;17:81. doi:10.3390/pharmaceutics17010081.

[7] Zuckerman JE et al. Correlating animal and human phase Ia/Ib clinical data with CALAA-01, a targeted, polymer-based nanoparticle containing siRNA. Proc Natl Acad Sci U S A. 2014;111(31):11449–11454. doi:10.1073/pnas.1411393111.

[8] Varan G et al. Amphiphilic cyclodextrin nanoparticles. Int J Pharm. 2017;531(2):457–469. doi:10.1016/j.ijpharm.2017.06.010.

[9] Malhotra M et al. Cyclodextrin–siRNA conjugates as versatile gene silencing agents. Eur J Pharm Sci.2018;114:30–37. doi:10.1016/j.ejps.2017.11.024.

[10] Ceborska M Folate-appended cyclodextrins for drug, DNA, and siRNA delivery. Eur J Pharm Biopharm.2017;120:133–145. doi:10.1016/j.ejpb.2017.09.005.

[11] Mendonça MCP et al. Modified cyclodextrin-based nanoparticles mediated delivery of siRNA for huntingtin gene silencing across an *in vitro* BBB model. Eur J Pharm Biopharm. 2021;169:309–318. doi:10.1016/j.ejpb.2021.11.003.

[12] Li F et al. Delivery of miR-34a-5p by folic acid-modified β-cyclodextrin-grafted polyethylenimine copolymer nanocarriers to resist KSHV. ACS Appl Nano Mater. 2023;6(10):10826–10836. doi:10.1021/acsanm.3c02162;

[13] Chiarugi I et al. Non-viral nanovectors based on cyclodextrins for siRNA delivery: an update to current technologies. Preprint. 2025. doi:10.20944/preprints202511.1747.v1.
[14] Godinho BMDC et al. Self-assembling modified β-cyclodextrin nanoparticles as neuronal siRNA delivery vectors: focus on Huntington's disease. Mol Pharm. 2013;10(2):640–649. doi:10.1021/mp3003946.
[15] Singh RP et al. Self-assembled cationic β-cyclodextrin nanostructures for siRNA delivery. Mol Pharm.2019;16(3):1358–1366. doi:10.1021/acs.molpharmaceut.8b01307.
[16] Liu C-H et al. Tetraethylenepentamine-coated β-cyclodextrin nanoparticles for dual DNA and siRNA delivery. Pharmaceutics. 2022;14(5):921. doi:10.3390/pharmaceutics14050921.
[17] Negut I et al. Hyaluronic acid nanoparticles. In: Biopolymeric Nanomaterials: Fundamentals and Applications.Elsevier; 2021. p.155–171. doi:10.1016/B978-0-12-824364-0.00015-0.
[18] Matalqah S et al. Hyaluronic acid in nanopharmaceuticals: an overview. Curr Issues Mol Biol.2024;46(9):10444–10461. doi:10.3390/cimb46090621.
[19] Raval H et al. Exploring the potentials of hyaluronic acid-coated polymeric nanoparticles in enhanced cancer treatment by precision drug delivery, tackling drug resistance, and reshaping the tumour microenvironment. Curr Med Chem. 2025;32(20):3960–3999. doi:10.2174/0109298673302510240328050115.
[20] Krishnan A et al. Comprehensive ocular and systemic safety evaluation of polysialic acid-decorated immune modulating therapeutic nanoparticles (PolySia-NVs) to support entry into first-in-human clinical trials. Pharmaceuticals. 2024;17(4):481. doi:10.3390/ph17040481.
[21] Gadade D.D., Pekamwar S.S. Cyclodextrin-based nanoparticles for drug delivery and theranostics. Adv Pharm Bull. 2020;10(2):166–183. doi:10.34172/apb.2020.022.
[22] Liu J. et al. Cyclodextrins-based delivery systems for macro biomolecules. Eur J Med Chem. 2021;212:113105. doi:10.1016/j.ejmech.2020.113105.
[23] Neupane D. et al. A pH-sensitive thiolated β-cyclodextrin-modified nanoporous gold for controlled release of doxorubicin. J Drug Deliv Sci Technol. 2020;60:101985. doi:10.1016/j.jddst.2020.101985.
[24] Luo D et al. Synthetic DNA delivery systems. Nat Biotechnol. 2000;18(1):33–37. doi:10.1038/71889.

[25] Davis ME Non-viral gene delivery systems. Curr Opin Biotechnol. 2002;13(2):128–131. doi:10.1016/S0958-1669(02)00294-X.
[26] Niidome T et al. Gene therapy progress and prospects: nonviral vectors. Gene Ther. 2002;9(24):1647–1652. doi:10.1038/sj.gt.3301923.
[27] Elouahabi A et al. Formation and intracellular trafficking of lipoplexes and polyplexes. Mol Ther. 2005;11(3):336–347. doi:10.1016/j.ymthe.2004.12.006.
[28] Lomunova M.A., Gershovich P.M. Gene therapy for cystic fibrosis: recent advances and future prospects. Acta Naturae. 2023;15(2):20–31. doi:10.32607/actanaturae.11708
[29] Craig DQM et al. Differential scanning calorimetry and scanning thermal microscopy of pharmaceutical materials. Int J Pharm. 2002;243(1–2):71–82. doi:10.1016/S0378-5173(02)00239-9.
[30] Bunjes H, Unruh T. Characterization of lipid nanoparticles by differential scanning calorimetry, X-ray and neutron scattering. Adv Drug Deliv Rev. 2007;59(6):379–402. doi:10.1016/j.addr.2007.04.013.
[31] Mura P. et al. Cyclodextrin complexation as a fruitful strategy for improving the performance of nebivolol delivery from solid lipid nanoparticles. Int J Pharm. 2025;668:124972. doi:10.1016/j.ijpharm.2024.124972.
[32] Fiani S. et al. Curcumin's niosomes coated with chitosan for the treatment of osteoarthritis: effect of cyclodextrin complexation. Int J Pharm. 2025;682:125933. doi:10.1016/j.ijpharm.2025.125933.
[33] Trotta F. et al. Cyclodextrin-based nanosponges as drug carriers. Beilstein J Org Chem. 2012;8:2091–2099. doi:10.3762/bjoc.8.235.
[34] Auzély-Velty R. et al. *Micellization of hydrophobically modified cyclodextrins. 1. Micellar structure.* Langmuir. 2000;16(8):3727–3734. doi:10.1021/la991361z.
[35] Augis L. et al. Development of nanoparticles based on amphiphilic cyclodextrins for the delivery of active substances. Int J Pharm. 2024;651:123723. doi:10.1016/j.ijpharm.2023.123723.
[36] Dobnik D. et al. Accurate quantification and characterization of adeno-associated viral vectors. Front Microbiol. 2019;10:1570. doi:10.3389/fmicb.2019.01570.
[37] Gurunathan S. et al. Review of the isolation, characterization, biological function, and multifarious therapeutic approaches of exosomes. Cells. 2019;8(4):307. doi:10.3390/cells8040307.
[38] Doucet M. et al. SasView version 6.0.0. 2024. doi:10.5281/zenodo.11395968.

[39] Maiorano G. et al. Hybrid polyelectrolyte nanocomplexes for non-viral gene delivery with favorable efficacy and safety profile. Pharmaceutics. 2022;14:1310. doi:10.3390/pharmaceutics14071310.
[40] Schindelin J. et al. Fiji: an open-source platform for biological-image analysis. Nat Methods. 2012;9:676–682. doi:10.1038/nmeth.2019.
[41] Valverde-Fraga L. et al. Design and *in vitro* assessment of chitosan nanocapsules for the pulmonary delivery of rifabutin. Eur J Pharm Sci. 2023;187:106484. doi:10.1016/j.ejps.2023.106484.
[42] Li F. et al. Multifunctional nanoplatforms as cascade-responsive drug-delivery carriers for effective synergistic chemo-photodynamic cancer treatment. J Nanobiotechnology. 2021;19(1):140. doi:10.1186/s12951-021-00876-7.
[43] Oieni J et al. Nano-ghosts: novel biomimetic nano-vesicles for the delivery of antisense oligonucleotides. J Control Release. 2021;333:28–40. doi:10.1016/j.jconrel.2021.03.018.
[44] Tu Y et al. Photothermal/GSH-dual-responsive organic quantum dots enabling traceable DNA delivery. Int J Biol Macromol. 2025;328(Pt 2):147542. doi:10.1016/j.ijbiomac.2025.147542.
[45] Chen Z et al. A biocompatible glycogen-based nanoparticle coating with lipid bilayer for intracellular delivery of survivin siRNA to HeLa cells. J Drug Deliv Sci Technol. 2024;92:105371. doi:10.1016/j.jddst.2024.105371.
[46] Woo Y et al. Fluorescent imaging for cancer therapy and cancer gene therapy. Mol Ther Oncolytics. 2021;23:231–238. doi:10.1016/j.omto.2021.06.007.
[47] Lazarski CA et al. Review of flow cytometry as a tool for cell and gene therapy. Cytotherapy. 2024;26(2):103–112. doi:10.1016/j.jcyt.2023.10.005.
[48] Zerkoune L et al. Nano-assemblies of modified cyclodextrins and their complexes with guest molecules: incorporation in nanostructured membranes and amphiphile nanoarchitectonics design. Nanomaterials. 2014;4(3):741–765. doi:10.3390/nano4030741.
[49] Vaskan IS et al. Arrangement and dynamics of individual cyclodextrins on the surface of core–shell micelles. Physical Chemistry Chemical Physics. 2025;27(35):18444–18453. doi:10.1039/D5CP00627A.

[50] Rädler JO et al. Structure of DNA–cationic liposome complexes: DNA intercalation in multilamellar membranes in distinct interhelical packing regimes. Science. 1997;275(5301):810–814. doi:10.1126/science.275.5301.810.
[51] Bramato R et al. Comparison of DNA-transfection efficiency in HeLa cells using K4 Transfection System and Lipofectamine 3000. Biontex. 2019. Available from: Biontex website.
[52] Bulkescher R. et al. Solid-phase reverse transfection for intracellular delivery of functionally active proteins. Genome Res. 2017;27(10):1752–1758. doi:10.1101/gr.215103.116.
[53] Shi B et al. An improved method for increasing the efficiency of gene transfection and viral transduction. Sci Rep. 2018;8(1):1291.

5 Concluding remarks

In this thesis, we systematically optimized lipid- and cyclodextrin-based nanovectors for siRNA delivery, achieving significant progress in their design, characterization, and functional evaluation.

Using the DoE approach, we fine-tuned key parameters for LNPs, obtaining formulations with favourable physicochemical properties, including optimal size (<200 nm) and polydispersity index (PDI <0.3).

The screening of several cationic lipids led to the selection of two promising formulations, B and D, containing DC-CH and MTAB, respectively, both showing high siRNA encapsulation efficiency while maintaining excellent size and PdI values. These LNPs remained stable for up to one week at 4 °C and in cell culture medium, with or without FBS, and exhibited no cytotoxicity at doses used for internalization and gene-silencing studies. Cellular uptake was efficient in both HeLa-GFP and RAW 264.7 cells (>85%), with particularly strong internalization in HeLa cells. Gene silencing in HeLa cells reached ~55% for formulation B and ~30% for formulation D after 72 h, while fluorescence-based assays highlighted formulation D as achieving the most potent knockdown, even surpassing the Lipofectamine reference. The optimal siRNA dose was identified as 190 ng/cm².

Similarly, favourable aggregation properties were observed for NVs formed by two of the three cationic modified β-cyclodextrins tested (CD1 and CD2). Despite somewhat irregular morphology, Z, TEM, and SAXS analyses confirmed successful encapsulation of genetic material. The NV architecture was characterized as small ellipsoids (1.5–2 nm) clustering into 10–50 nm assemblies, which further super-assembled into 150–200 nm scattering objects, as indicated by DLS.

Both LNP formulations achieved optimal internalization efficiency, reaching approximately 85–90% in HeLa and RAW 264.7 cells. For cyclodextrin-based NVs loaded with P, CD1 NVs exhibited superior transfection efficiency (~55%) compared to CD2, and siRNA-loaded CD1 NVs achieved knockdown efficiencies above 90%, comparable to Lipofectamine. The incorporation of anionic polymers (HA and HP) into CD NVs complexed with P or siRNA did not significantly alter NV performance in terms of transfection and gene silencing efficiency. However, HA-containing NVs loaded with siRNA exhibited a reduced size and PDI.

Differences in performance between CD1 and CD2 NVs likely arise from structural variations: CD1 possesses a shorter lipophilic chain (C8) and a single protonable amine, whereas CD2 contains a longer chain (C16) and two amine groups, affecting membrane interaction, cellular uptake, and endosomal processing. Additionally, the presence of sulphur-containing lipid chains in some NVs provides a robust platform for ligand conjugation, enabling future functionalization strategies.

Overall, both LNPs and NVs developed in the studies carried out in the present thesis demonstrate strong potential as siRNA delivery systems. Future work will focus on further optimization, evaluation in diverse cellular models, and application to nucleic acids encoding disease-relevant genes *in vitro* and *in vivo*, to fully assess their therapeutic potential and enable targeted gene modulation.

6 Acknowledgements

Desidero innanzitutto ringraziare la Professoressa Maestrelli per avermi dato l'opportunità di intraprendere questo percorso e per avermi sostenuto con fiducia in tutte le iniziative affrontate durante questi anni.
Ringrazio la Professoressa Bilia per esserci stata nei momenti di maggiore necessità e per il prezioso aiuto nella stesura e pubblicazione degli articoli scientifici.
Un sincero ringraziamento va alla Professoressa Ristori per il supporto fornito nello sviluppo del progetto e per l'elaborazione di tutti i dati SAXS, fondamentali per questo lavoro.
Grazie anche a Giulia e alla Dottoressa Falsini per il supporto e l'aiuto nello svolgimento del lavoro.
Un agradecimiento especial a Noemi Csaba y al CIMUS de Santiago de Compostela, que me permitieron vivir una experiencia maravillosa, capaz de enriquecerme profundamente tanto a nivel profesional como personal.
Un abrazo a mis compañeros de laboratorio — Lorena, Rocío, Raquel, Sara, Febby, Niccolò, Kike y Sara — y a todos los técnicos del CIMUS. Os quiero mucho.
Un abbraccio e un ringraziamento speciale anche a Francesco, Paola e Alessio del Cubo di Firenze, che mi hanno sostenuto e accompagnato con affetto lungo questo percorso.
Un forte grazie alle professoresse del Gruppo Mura e alle mie compagne di avventure in laboratorio — Alice, Camilla e Silvia — che hanno contribuito a rendere questa esperienza indimenticabile. Ringrazio inoltre tutte le mie tesiste e i ragazzi e le ragazze incontrati durante questi anni in laboratorio, con cui ho condiviso momenti di crescita, confronto e collaborazione.

Questo percorso mi ha fatto crescere profondamente sotto molti punti di vista e mi ha permesso di realizzare uno dei miei sogni più grandi: fare ricerca. Grazie a questo progetto mi sono avvicinata a un mondo, quello del gene delivery e delle cellule, inizialmente lontano dalla mia formazione e dalle mie esperienze precedenti, ma che è riuscito ad appassionarmi profondamente. Nonostante le difficoltà e i momenti complessi, porterò con me il ricordo di un'esperienza intensa e preziosa, che ha ampiamente ripagato tutti i sacrifici richiesti.

Non posso non ringraziare i miei amici, che da tanti anni mi conoscono, mi sostengono e continuano a esserci sempre.

Uno dei grazie più grandi e speciali va a Fili, che fin dall'inizio di questo percorso mi ha sostenuto con fiducia, spesso più di quanta ne avessi io stessa, restando al mio fianco passo dopo passo. Ti amo.

Infine, il ringraziamento più profondo va alla mia famiglia, che fin da sempre mi ha insegnato a camminare con le mie gambe e a scegliere la strada che sento davvero mia, rimanendo però costantemente accanto a me, pronta a sostenermi e a fare il tifo in ogni momento. Sapere che, qualunque cosa accada, loro ci sono e ci saranno sempre è la mia più grande certezza.

Questo è stato un percorso scelto per mettermi alla prova, per cercare risposte e per tornare a casa con un bagaglio nuovo, pieno di esperienze e ricordi. Grazie a tutti coloro che hanno fatto parte di questo viaggio — come comparse o come protagonisti — e a chi mi ha permesso di iniziarlo e mi ha accompagnato lungo il cammino.

GRAZIE.

P.S. Un ultimo grazie va a Nonna Maria, che non ha ancora capito bene cosa sia un dottorato, a cosa serva e cosa io abbia fatto in questi anni…

e che avrebbe preferito vedermi restare in farmacia con il camice da “dottoressa” … ma che, nonostante tutto, mi guarda con gli occhi pieni d’amore e mi dice sempre: “Se sei contenta te, amore, va bene tutto.”
Ti voglio bene.

pharmaceutics

MDPI

Review

Non-Viral Nanovectors Based on Cyclodextrins for siRNA Delivery: An Update to Current Technologies

Ilaria Chiarugi, Francesca Maestrelli *, Giulia Piomboni, Sandra Ristori and Anna Rita Bilia

Department of Chemistry "Ugo Schiff" (DICUS), University of Florence, Via Ugo Schiff 6, 50019 Florence, FI, Italy; ilaria.chiarugi@unifi.it (I.C.); giulia.piomboni@edu.unifi.it (G.P.); sandra.ristori@unifi.it (S.R.); ar.bilia@unifi.it (A.R.B.)

* Correspondence: francesca.maestrelli@unifi.it

Abstract

Gene delivery/administration and, in particular, small interfering RNA (siRNA) delivery represent a therapeutic challenge, though very effective carriers have yet to be identified. Cyclodextrins (CDs) are cyclic oligosaccharides with unique host–guest inclusion capabilities, widely recognized in the pharmaceutical field for their ability to enhance drug solubility and bioavailability. Their excellent biocompatibility and chemical versatility make them powerful building blocks for the design of supramolecular nanovectors (NVs). Thanks to their facility of functionalization, CDs are highly versatile and have found numerous applications across various fields. In this context, CD-based NVs are currently explored as non-viral agents to transport and release siRNA. Recent studies suggest that self-assembled NVs based on CDs can improve the transfection and safety of siRNA delivery. This review provides a comprehensive overview of the most recent advances in the design of NVs based on CDs and their use for siRNA delivery, discussing the role played by structural differences and chemical functionalization in the context of encapsulation and release.

Keywords: cyclodextrins; modified-CD; siRNA; gene delivery; nanovectors

1. Introduction

Gene therapy is a promising medical approach to achieving the accurate and personalized cure for diverse severe pathologies. The discovery of RNA interference (RNAi) by Fire and Mello in 1998 laid the bases for a new gene therapy approach, recognized with the Nobel Prize in Physiology or Medicine in 2006 [1]. RNAi is a post-transcriptional gene silencing RNA, which acts against endogenous parasitic and exogenous pathogenic nucleic acids, with consequent regulation of the expression of protein-coding genes. RNAi is mediated by short non-coding (approximately 22 nucleotides) RNA, the small interfering RNA (siRNA), and the microRNA (miRNA). From the perspective of therapeutic development, siRNA is very interesting due to its specificity, which minimizes off-target effects, and since 2001, synthetic siRNAs have been developed, providing the foundation for therapeutic applications [2,3], as reflected by the high number of clinical trials rapidly developed in recent years [4] as well as by the approved siRNA medicines on the market of the USA and Europe [5,6]. CDs are cyclic oligosaccharides composed of α-(1 → 4)-linked glucopyranose units, most commonly naturally existing as α-,β-, and γ-CDs containing six, seven, and eight glucose units, respectively. Due to their unique toroidal structure with a hydrophilic outer surface and a hydrophobic inner cavity, CDs can form host–guest inclusion complexes

Academic Editor: Gabriele Grassi

Received: 13 January 2026
Revised: 17 February 2026
Accepted: 18 February 2026
Published: 21 February 2026

with a wide variety of molecules, ranging from small organic compounds to macromolecular assemblies. This supramolecular capability has made CDs valuable tools in fields such as drug delivery, catalysis, food technology, and environmental remediation [7]. CDs are EMA- and FDA-approved excipients with low toxicity and immunogenicity, but concerning the cationic derivatives, still, most of the information about their toxicity derives from in vitro studies, and there is a lack of knowledge on their interaction within the body, as well as on the mechanism of elimination of these carriers. Indeed, studies on the molecular mechanism of interaction between cationic CDs and biological components are still in their infancy [8,9]. The in vitro models, including specific cell lines or bacterial strains, greatly limit their translation to humans or animals [10]. Only in vivo studies can provide insights concerning their safety profiles, biocompatibility, and biodistribution [11]. β-CDs are the most frequently employed derivatives in pharmaceutical research because they offer an optimal balance between cavity dimensions and stability, providing robust support for siRNA binding and versatile chemical derivatization. In pharmaceutical sciences, CDs have mainly been employed to enhance solubility, stability, and bioavailability of poorly soluble drugs and to control release profiles while reducing drug toxicity. Their high biocompatibility, low immunogenicity, and great chemical versatility have further expanded their application scope from small-molecule encapsulation to the design of advanced nanostructured materials for biomedical purposes. Chemical modification of hydroxyl groups on CD rims allows for the introduction of functional moieties (cationic, amphiphilic, targeting ligands, or stimuli-responsive groups), thereby tailoring their physicochemical and biological properties [12–14]. In recent years, these features have been exploited in the development of CD-based supramolecular systems for gene delivery, including DNA and siRNA vectors. CDs can serve as non-viral carriers that condense, protect, and deliver nucleic acids to target cells while minimizing cytotoxicity and immunogenic responses. A first review on the use of CDs for siRNA delivery was written by Chaturvedi et al. about 15 years ago [15]. More recently, the review by Mousazadeh et al. has evidenced the potential of cyclodextrins as effective non-viral siRNA delivery systems for cancer gene therapy [16], suggesting that modification of CDs can improve transfection and safety of delivery systems. In this framework, the review by Hu et al. (2023) further highlighted the dual diagnostic and therapeutic potential of CD-based systems [17]. Specifically, it discussed how functionalized CDs can serve not only as siRNA carriers but also as multifunctional platforms for imaging, controlled release, and targeted cancer therapy, bridging the gap between nanomedicine and theragnostics. Taken together, these studies underscore the versatility of CD architectures as robust and adaptable frameworks for next-generation gene delivery technologies. The primary objective of the present review is to provide an updated overview of the most recent advances in modified CD-based NVs for siRNA delivery, with a focus on structural design and functionalization strategies. The main thermodynamic/kinetic aspects that influence complex formation and intracellular release are also discussed. Accordingly, this review is structured into three main sections. The review firstly focuses on the structural design and chemical functionalization of cyclodextrin-based nanovectors, describing the most relevant strategies employed to obtain cationic, amphiphilic, and stimuli-responsive derivatives. Then, the physicochemical and biological performance of these systems, with particular emphasis on siRNA complexation, protection from enzymatic degradation, cellular uptake, and gene silencing efficiency, have been deeply discussed. Finally, the review addresses critical challenges and future perspectives, including structure–function relationships, intracellular release mechanisms, safety considerations, and translational limitations of cyclodextrin-based siRNA delivery systems

2. Challenge and Strategies in siRNA Delivery

Despite the ideally promising scenarios for siRNA therapeutic applications, several intracellular and extracellular barriers limit siRNA clinical use. These are mainly inadequate stability and a limited pharmacokinetic profile, together with the possible stimulation of unwanted side effects. Indeed, RNases and phosphatases can degrade the phosphodiester bond, while enzymes found in serum and tissues can prevent its accumulation in the target tissue. A major limitation of naked siRNA is its high susceptibility to enzymatic degradation by serum nucleases, which rapidly cleave the phosphodiester backbone and severely limit circulation half-life. Naked siRNA-based drugs can only represent an effective strategy for local delivery, as in the case of eye treatments. Additionally, the size of siRNAs (about 7–8 nm in length and 2–3 nm in diameter), their hydrophilicity, and their polyanionic nature present some difficulties in penetrating the membrane lipid bilayer. Therefore, siRNA can be easily cleared by glomeruli and excreted within a time lapse from several minutes to one hour [18]. A further intracellular difficult step is the endosomal escape, and innate immune activation can occur when naked siRNA is used. Naked siRNAs leaving the bloodstream are accumulated in the bladder and quickly (a few minutes to half an hour) excreted from the body, which prevents their accumulation in the target tissues or cells. Various chemical modifications have been proposed to obtain clinically efficient medicines, together with the use of cationic cell-penetrating peptides. Additionally, N-acetylgalactosamine-conjugated siRNA has been largely used to enhance metabolic stability, and nowadays many drugs such as givosiran, lumasiran, inclisiran, vutrisiran, and nedosiran have been approved by the FDA for this purpose. However, this strategy is very successful for liver targeting by the asialoglycoprotein receptor [19,20].

Encapsulation or complexation of siRNA within nanovectors is therefore essential [21,22]. The use of drug delivery systems, in particular NVs, is an exciting prospect to avoid quick renal clearance and, more importantly, to obtain selective targeting of cells and tissues. Due to many limitations of virus-based vectors, drug delivery systems using lipids and cationic polymers, which provide the electrostatic binding of negatively charged siRNA, are suitable vectors [23]. Lipid nanoparticle (LNP) transport of siRNA has become one of the most advanced approaches in the field of RNAi therapeutics [18]. The first approved drug employing this technology is patisiran (ONPATTRO®), recommended for the treatment of hereditary transthyretin amyloidosis (hATTR) [24]. Since then, several candidates have entered clinical development, including BMS-986263 (Bristol-Myers Squibb), an LNP formulation carrying siRNA targeting HSP47 for the treatment of hepatic fibrosis [25]. Another type of NVs is represented by polymeric nanoparticles (PLGA, PEG, chitosan, PEI, and other cationic or ionizable polymers). They have also been explored as versatile siRNA delivery systems, offering tunable design parameters, controlled release, and robust nucleic acid protection, despite challenges such as potential cytotoxicity of certain cationic polymers and generally lower clinical maturity compared to LNPs [26,27].

Cationic micelles have also been used for the transport of small oligonucleotides and, in particular, siRNA [28,29]. Due to the possibility of monomer exchange, micelles present relatively flexible structures that can be squeezed or loosened to allow cargo loading and delivery. Moreover, their simple architecture can be modeled by computational methods, and the obtained information can be transferred to more complex systems based on other soft matter aggregates.

CDs are natural cyclic oligosaccharides derived from starch, characterized by a ring structure with hydrophilic primary and secondary sides and a hydrophobic cavity [30]. Due to the presence of hydroxyl groups, CDs can be easily functionalized to impart a positive charge to the molecule [31]. More generally, chemical functionalization can produce an unlimited number and variety of CD derivatives, including cationic, amphiphilic, and

PEGylated compounds. In particular, the electrostatic interactions between nucleic acid and cationic CDs provide additional self-assembly mechanisms.

As recently reported by Nazli and coworkers [32], the positively charged vectors can strongly interact with negative charges, promoting robust cellular interactions, improving permeability and cell uptake of siRNA, and increasing its activity. In addition, the amine groups of cyclodextrins facilitate the so-called "proton sponge effect", causing an increased flux of water with possible endosomal rupture and consequent release of siRNA in the cytoplasm, improving the biological effects as well. Furthermore, these effects can lead to cell toxicity effects because the strong electrostatic interactions of nanovectors can lead to an alteration of the cell membrane with consequent cell damage. An optimal balance between maximizing effective siRNA delivery and minimizing toxicity is critical for a successful therapy. From the available studies, it is clear that these nanovectors guaranteed site-specific drug release, maintaining high cell viability as compared to commercially available vectors such as PEI25 kDa and lipofectamine 2000. As recently reported by Pirvu et al. [33], cationic CD derivatives form nanoparticles that protect siRNA, promote endosomal escape, and target delivery while presenting low immunogenicity. Concerning their behavior in aqueous solution, it has been clearly established [34,35] that, like all other amphiphilic molecules, CDs undergo cooperative self-assembly into equilibrium structures that are in dynamic exchange with the monomers, according to the classical pseudophase model [36,37]. The large number of OH groups in the sugar ring, by allowing strong hydrogen bonds and hydration forces, plays a key role in this process, though, especially for functionalized CDs, hydrophobic interactions should also be taken into account. Moreover, if ionic groups are present in the molecule, the electrostatic contribution brings a further term in the free energy of aggregation, thus making the whole process very complex to model in quantitative terms [38,39]. Such complexity is mirrored by the different names and attributes given to the spontaneous aggregates that CDs form in water solution (transient clusters, nanoparticles, microparticles) [40–44], though all the standard techniques for establishing the onset of aggregates, including scattering, microscopy, and spectroscopy [45–47], agree on the presence of entities other than the monomers above a critical concentration value.

Beyond protection, an effective siRNA delivery system must also balance binding strength and reversibility, in that excessive stabilization can hinder intracellular release and reduce the gene silencing efficiency. This trade-off represents a central design challenge for non-viral nanocarriers [48].

Taken together, CD-based non-viral platforms illustrate how a diverse range of nanocarriers can offer complementary solutions to the challenges of siRNA transport, protection, and cellular uptake. Each platform brings distinct structural features, mechanisms of interaction with nucleic acids, and opportunities for tissue targeting, while also presenting specific limitations related to stability, biocompatibility, manufacturing, or clinical translation. To provide a consolidated overview, Table 1 summarizes the key attributes discussed in this section, highlighting the main advantages, drawbacks, and references cited in this article.

CD NVs are particularly promising, and significant research activity is currently underway to refine their properties. Despite this progress, substantial work is still required to fully exploit their potential and translate these systems into clinically validated siRNA delivery platforms.

Table 1. Summary of the main non-viral nanovectors discussed in this review, highlighting advantages and limitations.

NVs Type	Advantages	Limitations	References
CD NVs	High structural tunability, good siRNA complexation, high stability, promising transfection, and silencing results.	Scalable manufacturing and in vivo biodistribution data are less mature; endosomal escape can be challenging.	[13,15,16,31,32,49,50]
LNPs	Clinically validated; high encapsulation efficiency; excellent endosomal release; scalable GMP manufacturing.	Can induce immune activation; PEGylation can cause accelerated blood clearance and immune issues; targeting beyond the liver remains challenging.	[20,21,23]
Polymeric NVs	Large chemical/design space, tunable release, and mechanical stability; good protection of siRNA.	Potential cytotoxicity (especially non-degradable cationic polymers); heterogeneous formulations; less clinical precedence than LNPs.	[26,27]
siRNA conjugates	Highly defined stoichiometry; excellent potency for accessible tissues; simplified formulation (no nanoparticle vehicle needed).	Tissue scope limited by target receptor expression and by endosomal escape; designing stable conjugates for non-hepatic targets is challenging.	[28,29]

Haley et al. (2020) have provided a comprehensive overview of CDs as modular carriers in drug and gene delivery systems [49]. Their review illustrated how the chemical versatility of CDs allows for the complexation and protection of DNA and RNA, reduction in immunogenicity, and facilitated interactions with cell membranes. It also highlighted the ability of CDs to serve as platforms for combined systems—including chemotherapeutics, RNAi, and peptides—with potential applications in personalized therapies. However, this analysis was focused on studies up to 2020, leaving room for an update that includes more recent evidence of self-assembling and targeted systems for siRNA delivery. Table 2 provides a concise overview of the CD-based NVs reported in the literature.

Table 2. Review of CDs for gene delivery cited in the literature.

Authors	Year	Title	References
Chaturvedi, K.	2011	Cyclodextrin-Based siRNA Delivery Nanocarriers: A State-of-the-Art Review.	[15]
Xu, C.	2019	Cyclodextrin-Based Sustained Gene Release Systems: A Supramolecular Solution towards Clinical Applications.	[13]
Haley, R.M.	2020	Cyclodextrins in Drug Delivery: Applications in Gene and Combination Therapy.	[49]
Mousazadeh, H.	2021	Cyclodextrin-Based Natural Nanostructured Carbohydrate Polymers as Effective Non-Viral siRNA Delivery Systems for Cancer Gene Therapy.	[16]
Castillo Cruz, B.	2022	A Fresh Look at the Potential of Cyclodextrins for Improving the Delivery of siRNA Encapsulated in Liposome Nanocarriers	[50]
Nazli, A.	2025	Cationic Cyclodextrin-Based Carriers for Drug and Nucleic Acid Delivery	[32]

3. NVs Based on Modified CD for siRNA Delivery

CD-based NVs have gained increasing attention due to their biocompatibility, their ability to form stable complexes with siRNA, and their potential for targeted functionalization. Moreover, it has been reported that the combination of CDs with cationic polymers can promote cell penetration [32]. Selective chemical functionalization of cyclodextrin rims further enables the fine-tuning of surface charge through the introduction of cationic moieties, such as polyethylenimine or amino acid residues, ensuring efficient siRNA condensation and protection. In addition, the conjugation of targeting ligands (e.g., folic acid or anisamide) can promote site-specific cellular uptake via receptor-mediated endocytosis, while subsequent endosomal escape is facilitated by proton sponge effects or by the inherent membrane-disruptive properties of the cyclodextrin-based nanovectors.

The main portions of CD that are modified are the hydroxyl groups at positions 2 and 3, and the CH_2OH group at position 6 (Figure 1).

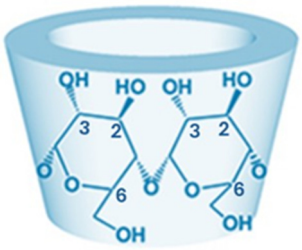

Figure 1. Modifiable groups of β-CDs.

Therefore, it appears that modification of the native CD structure is highly recommended for internalization. As an example, amphiphilic cationic CDs have been studied for siRNA release, showing success in mediating gene silencing both in vitro and in vivo. Malhotra et al. present the first example of CD-siRNA conjugates for gene silencing applications [51]. In this study, β-CD was covalently attached to the sense strand of siRNAs via both reducible (disulfide) and non-reducible (sulfanyl) linkers. The conjugates maintained gene silencing efficacy comparable to unconjugated siRNAs when delivered via polycationic lipids such as Lipofectamine 2000 [52] and amphiphilic cationic CDs (Figure 2).

CD NVs are also able to overcome physiological barriers such as the blood–brain barrier (BBB) and deliver siRNA to malignant or genetically affected tissues, underscoring their promise for the treatment of neurodegenerative diseases [53]. The system utilized amine-functionalized β-CDs, which facilitated electrostatic complexation with siRNA and promoted endosomal escape. These nanoparticles demonstrated efficient transcytosis across the BBB, along with significant gene -silencing effects in neuronal cells. Different approaches can be used to improve the interactions between CDs and siRNA, and in addition, targeting ligands can be added to improve siRNA transfection. Specifically, the PEGylation process can be used as passive targeting and as a means for prolonging systemic circulation time. Following this idea, adamantane–transferrin and adamantane—PEG derivatives of CDs have been produced, enhancing the performance of CD-based platforms by double functionalization with one targeting moiety [54]. In Figure 3, the main types of functionalization of CDs explored in this review are reported. Different structures of cationic CDs are obtained by conjugation with a cationic polymer, which can be linked to the smaller opening of the toroid (primary rim) corresponding to the C6-OH primary hydroxyls (type A) and the larger opening (secondary rim) to the C2-OH and/or C3-OH secondary hydroxyls (type B). Additionally, the modified cyclodextrins can be substituted with anionic or non-ionic polymers in the other rims (type C and type D).

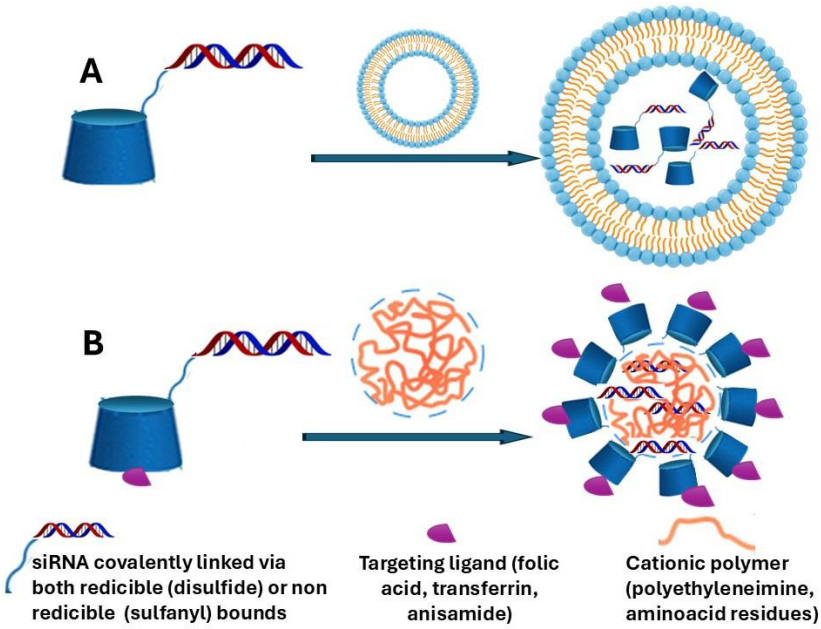

Figure 2. Conceptual representation of NVs developed by Malhotra et al. (2018) [51]. Panel (**A**) represents the lipofectamine-based system incorporating CD and siRNA, while Panel (**B**) illustrates the amphiphilic CD system complexed with siRNA.

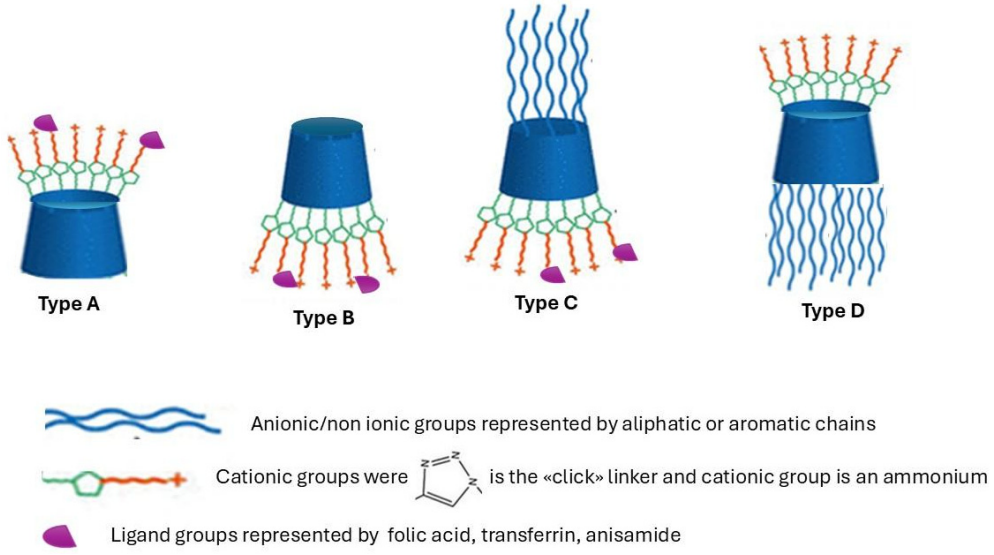

Figure 3. Functionalization of CD derivatives.

Moreover, amphiphilic CDs, which possess both hydrophilic and hydrophobic domains due to substitution with aliphatic or aromatic chains, can undergo hydrophobic-driven self-assembly into core–shell structures or micelle-like NVs. CD-based siRNA nanovectors are typically formed by self-assembly under mild aqueous conditions. This behavior is particularly advantageous for siRNA delivery, as it enables formulation under physiological conditions without harsh organic solvents or high-energy processes while allowing for size control, targeting moiety integration, and siRNA protection in a single-step process. In such configurations, siRNA is either electrostatically adsorbed to the particle surface or co-condensed within the hydrophilic shell. These amphiphilic assemblies improve NVs' stability at physiological conditions and promote membrane fusion or cellular endocytosis. This process may involve the complexation of cationic CDs with the anionic siRNA. In this case, the encapsulating CD superstructure can preserve the native siRNA conformation through a vast network of hydrogen bonds between the positively charged side arms of

the c-CD and the negatively charged siRNA skeleton. Additionally, CDs can participate in supramolecular self-assembly via host–guest interactions, such as the inclusion of hydrophobic guest molecules (e.g., adamantane and, cholesterol) within the CD cavity. This approach has been widely exploited to construct modular NVs by linking targeting ligands (e.g., transferrin, folic acid), PEG, or additional stabilizing elements via guest moieties, resulting in highly customizable delivery platforms [55]. In systems where CDs are functionalized with cationic side chains (e.g., amino, guanidinium, or polyethyleneimine-like moieties), electrostatic complexation with the negatively charged phosphate backbone of siRNA can drive spontaneous nano-condensation into stable nanoparticles. The resulting complexes can preserve the conformational integrity of siRNA, protecting it from serum nucleases and enhancing cellular uptake.

Seripracharat et al. (2022) describe the development of a supramolecular siRNA delivery system based on the host–guest assembly between cationic β CD derivatives (cCDs) and an adamantane-functionalized poly(vinyl alcohol)-poly(ethylene glycol) (Ad PVA PEG) polymer [56]. Three distinct amino-substituted cCDs—bearing putrescine, spermidine, or spermine moieties—were synthesized and confirmed via ^{1}H NMR and mass spectrometry. These cCDs spontaneously form spherical nanoparticles with Ad PVA PEG and siRNA, as shown by ^{1}H NMR and SEM, with particle sizes below 300 nm and a negative zeta potential at physiological pH. Gel electrophoresis demonstrated efficient siRNA loading (≈90%), while DLS analysis confirmed stable complexation. In vitro assays in A549 cells indicated effective GFP gene silencing, comparable to Lipofectamine™ 2000, with minimal cytotoxicity. Kont et al. 2022 report a novel strategy for siRNA delivery using co-formulated amphiphilic cationic and anionic β-CDs to treat acute myeloid leukemia (AML) [57]. A newly synthesized anionic amphiphilic CD was blended with a cationic CD complexed with siRNA targeting the epigenetic regulator KAT2a. The resulting nanoparticles displayed reduced surface charge (from +34 mV to +24 mV) and improved polydispersity, without compromising particle size or siRNA uptake (~60% in HL-60 AML cells). Despite a slightly slower endosomal escape for the co-formulated NVs, both formulations achieved comparable gene silencing (~21–29% KAT2a knockdown). These findings highlight the potential of charge-balanced CD nanocarriers to minimize toxicity while maintaining therapeutic efficacy for non-viral gene delivery in hematological malignancies. Sun et al. (2023) report the development of sialic acid-functionalized CD-based nanoparticles for targeted delivery of CSF-1R siRNA to tumor-associated macrophages (TAMs) in prostate cancer [58]. These findings demonstrate promising in vitro gene silencing efficacy with low cytotoxicity; however, further in vivo validation is required to assess biodistribution and therapeutic relevance [56–58]. The sialic acid ligand enables selective binding to Siglec-1 (CD169), highly expressed on M2-like TAMs, facilitating efficient uptake and significant CSF-1R gene silencing (42–58% knockdown vs. 19–39% for non-targeted controls; $p < 0.01$). The suppression of CSF-1R expression induces macrophage repolarization from the immunosuppressive M2 phenotype to pro-inflammatory M1, demonstrated by increased CD86+/CD68+ populations (~72%) and reduced CD206+/CD68+ (~25%). In co-culture models with prostate cancer cell lines (PC-3, TRAMP-C1), this macrophage reprogramming leads to enhanced cancer cell apoptosis (49–69% vs. 38–44%; $p < 0.01$). Hao et al. (2024) describe a hybrid nanoparticle system combining AS1411 aptamer–PD L1 siRNA chimera with glutamine-modified carboxymethyl-β-CD (Gln CM-β CD) and polyethylenimine/doxorubicin for combinatorial chemo-immunotherapy against lung squamous cell carcinoma [59]. Importantly, these results were further supported by in vivo studies, confirming therapeutic efficacy and immune modulation in relevant tumor models [59]. The AS1411 aptamer directs selective binding and internalization into NSCLC cells, achieving effective PD L1 silencing and stimulation of T cell and $CD8^{+}$ cytotoxic responses. SEM imaging revealed

conical nanoparticles (~250–500 nm), while glutamine modification enhanced doxorubicin uptake and apoptotic induction in tumor cells. In vivo studies demonstrated superior tumor inhibition (reduced volume and Ki 67 index, increased apoptosis) and elevated intra-tumoral T cell infiltration (1.34- to 1.41-fold increase in $CD8^+$ T cells), with reduced systemic toxicity compared to aptamer-only or chemotherapy-alone controls. Although no CD NV–based siRNA therapeutics have reached market approval so far, they represent an important area of preclinical research, with promising applications in oncology, neurology, and inflammatory diseases, underscoring their potential role in the future of non-viral gene therapy. Some formulations based on CD NVs are currently in clinical trials, such as, for example, CALAA-01, a self-assembling CD NV (CALANDO) functionalized with transferrin for tumor targeting. This system was designed for delivering siRNA against the RRM2 gene. The designed clinical trial product is a combination of siRNA (USP # 7427605, 23 September 2008) and RONDEL (United States Patent (USP) # 7807198, 5 October 2010). The Phase I clinical trial has provided the first evidence of siRNA-mediated gene silencing in human tissues following systemic administration and represents a significant milestone in RNAi therapeutics [60]. Another example is siG12D-LODER, a biodegradable intratumoral implant based on CD NVs that has advanced to Phase II for the treatment of pancreatic cancer, demonstrating sustained siRNA release directly within the tumor microenvironment [61].

Stimuli Responsive and Thermodynamics in CD-Mediated Gene Delivery

Following cellular internalization, siRNA-loaded nanovectors are typically entrapped within endosomal compartments, where insufficient release into the cytosol remains a major bottleneck. Efficient endosomal escape and controlled intracellular disassembly are therefore crucial to enable siRNA access to the RNA-induced silencing complex (RISC) [62,63].

NVs CDs can be formulated to selectively release siRNA in conditions where temperature, light, pH, and redox microenvironment [16] are modified. Recent advances in CD-based supramolecular systems have underscored the central role of both thermodynamic stability and kinetic accessibility in the design of effective gene-delivery platforms. The review of Zhang et al. (2020) highlights how host–guest interactions, threading or sliding of CD rings, and stimuli-responsive triggers (pH, redox, enzyme, and light) enable rapid morphological and functional transitions of CD nanocarriers, thereby influencing both the rate of assembly/disassembly and the release kinetics of the cargo under physiological conditions [64]. In parallel, the review of Mousazadeh H. et al. (2021) discusses how CD-based carbohydrate polymers (including CD-cationic polymers, CD-polyrotaxanes, CD-dendrimers, and CD-modified targeting ligands) can be finely tuned in terms of degree of functionalization, N/P ratio (that represents the molar ratio between the nitrogen atoms in the cationic components and the phosphate groups of the siRNA backbone [65]), ionic microenvironment, and presence of co-polymers to modulate both binding affinity and complex formation/release behavior of siRNA delivery systems [16]. Overall, these works suggest that the thermodynamics and kinetics of the self-assembly process in CD-based siRNA delivery systems are critically governed by multiple physicochemical parameters, including the CD substitution pattern and degree of functionalization, the ionic strength and pH of the surrounding medium, the N/P ratio (nitrogen in CD to phosphate in siRNA), and the presence of co-polymers or stabilizers such as PEG, hyaluronic acid, or chitosan. Isothermal titration calorimetry (ITC) has emerged as a powerful technique to quantify the binding thermodynamics of CD–siRNA interactions, providing access to parameters such as binding affinity (K_d), enthalpy (ΔH), entropy (ΔS), and Gibbs free energy (ΔG) [50,66]. Studies on self-assembled cationic β-CD nanostructures have demonstrated that the substitution degree of cationic groups markedly influences the electrostatic contribution to ΔH

and ΔS, with higher substitution leading to stronger exothermic interactions and reduced entropic penalties during complexation [5]. In particular, the entropic loss in the complexation of self-assembled cationic β-CDs mainly arises from a reduced conformational freedom of both CDs and guest molecules, as well as from the ordering of water molecules and counterions around the complexes. The enthalpic contribution is due to β-CDs stronger binding (ΔH < 0) to negatively charged molecules like siRNA when cationic groups are present in their structures. In this latter case, however, the entropic penalty is reduced because more water molecules and counterions are released during binding, which partially compensates for the loss of flexibility.

Recent molecular dynamics simulations and free energy studies have emphasized the critical role of solvent reorganization in the entropic term, showing that the release or rearrangement of water molecules and ions upon complex formation significantly contributes to ΔS and thus to the overall binding stability [67–69].

The ionic strength and pH of the medium are able to further modulate complex stability by altering electrostatic screening and protonation states, shifting the balance between enthalpic and entropic driving forces [7]. From a kinetic perspective, the dynamics of siRNA complexation and release strongly depends on the N/P ratio and the nature of co-stabilizing polymers. Elevating N/P ratios typically enhances complex compactness and reduces dissociation rates, whereas the inclusion of PEG, hyaluronic acid, or chitosan can modulate assembly kinetics and colloidal stability by steric or electrostatic contributions [70,71]. ITC combined with molecular dynamics simulations has revealed that self-assembled β-CD/siRNA complexes exhibit favorable binding kinetics driven primarily by electrostatic and dehydration effects [66]. Moreover, differential scanning calorimetry (DSC) and fast-scanning calorimetry (FSC) have been used to probe solid-state transitions and thermal stability, confirming that the substitution pattern and N/P ratio affect not only molecular affinity but also phase behavior and thermal robustness [7,72].

Overall, the interplay between thermodynamic stability (ΔG, ΔH, ΔS), solvent reorganization, and kinetic accessibility dictates the efficiency of siRNA complex formation, protection, and intracellular release.

4. Computational-Experimental Design of β-Self-Assembling CD

Singh et al. (2019) describe the design and characterization of self-assembled cationic β-CD (cCD) nanostructures for siRNA delivery, employing a combined computational and experimental approach [66]. Using extensive molecular dynamics simulations, they demonstrate that cCD molecules spontaneously assemble into supramolecular bilayer-like structures around siRNA, stabilizing its native conformation via extensive electrostatic interactions and hydrogen bonding. Unlike unmodified β-CDs, which form transient, non-specific complexes, cCD derivatives exhibit strong, specific binding to siRNA, mediated by their positively charged side arms and hydrophobic alkyl chains. These simulations reveal lipid-like interdigitated assemblies that encapsulate siRNA, mimicking natural biomembranes and potentially enhancing membrane permeability. Isothermal titration calorimetry experiments validate all these findings, confirming a spontaneous, enthalpy-driven complexation process with low dissociation constants.

5. Modified CD for Receptor-Mediated Targeted Delivery

Targeted formulations can achieve superior knockdown efficiency compared to non-targeted controls. Examples of this important issue have been described above in Section Stimuli Responsive and Thermodynamics in CD-Mediated Gene Delivery, since stimuli-responsive vectors are a first class of targeted systems. More specifically, CD can be modified to allow receptor-mediated delivery, particularly useful for cancer therapy. Malhotra

et al., 2018, prepared ligand-targeted nanoparticles by exploiting the inclusion complexation capabilities of CD and adamantyl-PEG-modified ligands combined with chitosan, obtaining a good internalization to glioblastoma (U87) and prostate cancer (DU145) cells [51]. This performance has been attributed to the formation of supramolecular structures through interdigitation of aliphatic tails for disulfide-linked conjugates, which demonstrated enhanced gene silencing, likely due to intracellular bioreduction [73]. Li et al. 2023 developed a folic acid-functionalized β-CD-grafted polyethylenimine (β-CD-PEI-FA) nanocarrier for the targeted delivery of miR-34a-5p against Kaposi's sarcoma-associated herpesvirus (KSHV) [74]. The β-CD-PEI-FA polymer formed stable nanocomplexes with miR-34a-5p via electrostatic interaction, effectively protecting the miRNA from nuclease and serum degradation. The nanocomplex exhibited suitable physicochemical properties (size ~203 nm, zeta potential ~27 mV) for cellular uptake and showed low cytotoxicity and hemolysis in vitro. Functional assays in KSHV-positive BCBL-1 and SK-RG cells demonstrated that β-CD-PEI-FA/miR-34a-5p complexes increased intracellular miR-34a-5p levels, inhibited cell proliferation by arresting cells in the G2 phase, and significantly downregulated KSHV genes (ORF26, LANA, and K8.1A). These results suggest that β-CD-PEI-FA represents a promising strategy for folate-receptor-targeted delivery of therapeutic miRNAs in antiviral applications. Table 3 provides an expanded qualitative comparison of cyclodextrin derivatives, functionalization strategies, and biological outcomes, together with the corresponding level of experimental validation.

Table 3. CD nanovectors for gene delivery from 2020 to 2025.

CD Derivative/Modification	Functionalization Strategy	siRNA/Target Gene	Biological Outcome	Level of Validation	References
TEPA-β-CD polyplexes	Cationic polymer functionalization	anti-GFP	Efficient siRNA complexation and gene silencing with low cytotoxicity	In vitro	[71]
β-CD derivatives/β-CD–Ad–PEG/anisamide ligand	Amphiphilic CD + PEGylation + targeting ligand	PLK1	Enhanced cellular uptake and receptor-mediated targeting in cancer cells	In vitro	[31]
Surface-modified β-CDs with RVG peptide	Cationic CD + peptide targeting	HTT mRNA	Effective BBB crossing and neuronal gene silencing	In vitro	[53]
Modified cationic β-CD–Ad–PVA–PEG	Host–guest self-assembly + cationic CD	anti-GFP	High siRNA loading, efficient silencing, low cytotoxicity	In vitro	[56]
Amphiphilic cationic CD/anionic CD co-formulation	Charge-balanced amphiphilic CDs	KAT2a	Reduced surface charge, preserved uptake, and effective gene knockdown	In vitro	[57]
Sialic-acid-functionalized CD nanoparticles	Targeting ligand (Siglec-1)	CSF-1R	Selective uptake by TAMs and macrophage repolarization	In vitro	[58]
AS1411 aptamer–PD-L1 siRNA + Gln–CM–β-CD/PEI–DOX	Targeting aptamer + CD–polymer hybrid	PD-L1	Tumor growth inhibition, immune activation, reduced toxicity	In vivo	[59]
CD–polymer–PEG with transferrin ligand (CALAA-01)	Targeted CD polymeric NV	RRM2	First evidence of RNAi-mediated gene silencing in humans	Clinical trial	[60]
Modified cationic β-CD nanostructures	Self-assembled cationic CD	PLK1	Stable complexation, efficient intracellular delivery	In vitro	[66]
Covalent β-CD–siRNA conjugates	Covalent conjugation	PLK1/GFP	Preserved silencing activity with improved stability	In vitro	[51]
FA–β-CD–PEI copolymer	Targeting ligand (folic acid) + cationic polymer	miR-34a-5p	Receptor-mediated uptake and antiviral gene regulation	In vitro	[70]

Most of the CD-based nanovectors reported to date have been primarily evaluated at the in vitro level, demonstrating efficient siRNA complexation, cellular uptake, and gene silencing in cancer and neuronal cell models, while in vivo validation remains limited to selected systems.

6. Translational Barriers

One of the principal challenges associated with cationic cyclodextrin derivatives is their complex and costly synthesis. These systems are generally produced on a small scale and often involve the use of environmentally hazardous reagents and organic solvents. Moreover, purification procedures frequently rely on techniques such as chromatographic separation, which are not easily scalable or economically sustainable for industrial production. Consequently, the development of green and scalable approaches for both synthesis and purification remains highly challenging [32,75].

Another important limitation concerns the selection of the most appropriate siRNA sequence for specific clinical applications. Careful patient stratification and target validation are required, which may delay patient enrollment in Phase I clinical trials; however, this strategy can significantly enhance the likelihood of accurately evaluating the therapeutic efficacy of siRNA in controlling the intended molecular target [16].

Furthermore, to improve selectivity and reduce potential off-target effects, nanovectors are often functionalized with targeting ligands capable of recognizing specific disease-associated cells or tissues. The field of targeted delivery has advanced rapidly in recent years, with significant progress in understanding biological barriers and in developing innovative strategies to functionalize nanocarriers with targeting moieties for accurate and selective delivery. Nevertheless, increasing structural complexity, such as the incorporation of multiple functional components, further complicates large-scale industrial production. Despite these challenges, emerging strategies, including multifunctional nanovector design and machine learning-assisted optimization, are expected to facilitate the development of safer, cell-specific, and more scalable nanoparticle delivery systems.

7. Conclusions

CD-based NVs are versatile and promising platforms for siRNA delivery, thanks to their structural adaptability, biocompatibility, and tunable host–guest interactions. The ability to modulate the physicochemical parameters of CDs, such as degree of substitution, cationic charge density, and functionalization with targeting or stimuli-responsive groups, allows fine control over complex stability, binding thermodynamics, and release kinetics under physiological conditions. Modified CD-based nanocarriers are capable of effectively condensing and protecting siRNA, facilitating its cellular uptake while minimizing cytotoxicity and immune responses. Self-assembled CD-based nanovectors rely on supramolecular host–guest interactions, offering greater formulation flexibility, adaptability, and translational potential.

Overall, the effectiveness of cyclodextrin-based nanovectors for siRNA delivery is strongly governed by structure–function relationships, since subtle variations in molecular architecture and supramolecular organization markedly influence biological performance. Key parameters such as degree of substitution, cationic charge density, nanovector architecture, and surface functionalization determine siRNA condensation, complex stability, intracellular trafficking, and cytotoxicity. Optimizing these features is essential to balance efficient cellular uptake and endosomal escape with serum stability and biocompatibility, underscoring the need for rational design strategies that integrate molecular structure, supramolecular dynamics, and biological response.

As yet, despite the significant progress reported, most CD-based siRNA systems remain supported predominantly by in vitro evidence, with a limited number validated in vivo and only a few reaching clinical trials. This highlight both the promise of cyclodextrin-based platforms and the need for further translational studies addressing biodistribution, long-term safety, and therapeutic efficacy.

8. Future Perspectives

Looking forward, a particularly promising direction is the development of multi-responsive CD architectures tailored to the tumor microenvironment (TME). In TME, conditions such as mildly acidic extracellular pH, low endosomal/lysosomal pH after uptake, and elevated intracellular reducing power represent exploitable triggers for controlled release [76,77]. By designing CD-based nanocarriers that respond to both pH and redox stimuli, it should be possible to achieve highly selective and efficient intracellular siRNA release upon tumor cell internalization. Dual pH/redox-responsive systems have already shown promise in non-CD nanocarriers for drug or siRNA delivery [78,79]. Moreover, incorporating targeting ligands (e.g., tumor-targeting peptides, hyaluronic acid, and antibodies) onto CD could enhance specificity and reduce off-target uptake.

To facilitate eventual clinical translation, future efforts should also focus on biodegradable and scalable CD-based polymers, as well as on detailed mechanistic studies to better understand how molecular structure, supramolecular dynamics, and environmental triggers (pH, redox, and ionic strength) influence siRNA complexation, release kinetics, intracellular trafficking, and gene silencing efficiency. The integration of dual-stimuli responsiveness, targeting functionality, and biocompatibility may offer a powerful route toward safe, efficient, and precise systemic siRNA delivery.

Furthermore, as reported for other nanovectors, the impact of carrier shape and size, surface charge, polydispersity index, and related physicochemical features on biocompatibility should be systematically investigated. In particular, long-term in vivo studies remain limited, hampering the translation of laboratory findings into clinical applications. Careful monitoring of renal and hepatic functions, as well as assessment of cumulative toxicity risk, will be essential before clinical implementation [80].

Off-target effects and non-specific gene silencing remain important limitations of siRNA therapeutics. These issues can be mitigated by optimizing siRNA size, primary sequence, and targeting location. The ideal nanovector should have a size between 50 and 200 nm to achieve effective delivery to target cells while minimizing off-target effects, increasing resistance to nuclease degradation, and preventing immune responses [81]. In this context, advanced protein array technologies are expected to play an increasingly relevant role, as they provide a more comprehensive picture of siRNA effects on the cellular protein expression profile. This approach is increasingly applied to evaluate protein interactions, expression profiling, and target discovery, helping to resolve undesired targeting. Protein microarrays are versatile tools for parallel, miniaturized screening of binding events involving large numbers of immobilized proteins in a time- and cost-effective manner [16,82].

In parallel, in silico studies are increasingly used for pre-development predictions to understand the nature and structure of active compounds, their interactions, and to identify potential toxicities through computational models such as molecular dynamics simulations, docking, and Quantitative Structure–Activity Relationship (QSAR) approaches. These methodologies are also employed to investigate complexation properties and to model NP–membrane interactions and cellular uptake based on minimal physicochemical data. More importantly, machine learning enables computational models to predict how specific modifications in nanovector physicochemical characteristics may improve functional

aspects such as drug retention and endocytosis efficiency. On a larger scale, these tools may also predict in vivo pharmacokinetics of the encapsulated drugs, including circulation half-life, toxicity, and biodistribution. However, the convergence of nanomedicine and computational approaches is still in its early stages and requires further validation to achieve reliable translational impact [83,84].

Author Contributions: Conceptualization, A.R.B. and I.C.; methodology, I.C., F.M., G.P. and S.R.; data curation, I.C. and G.P.; writing—original draft preparation, I.C. and G.P.; writing—review and editing, I.C., A.R.B., F.M. and S.R.; funding acquisition, A.R.B., F.M. and S.R. All authors have read and agreed to the published version of the manuscript.

Funding: The authors thank MIUR-Italy ("Progetto dipartimenti di eccellenza 2023–2027" allocated to the Department of Chemistry "Ugo Schiff", University of Florence, Italy). We acknowledge co-funding from Next Generation EU, in the context of the National Recovery and Resilience Plan, M4C2 Investment 1.4 CN_00000041 National Center for Gene Therapy and Drugs based on RNA Technology CUP B13C22001010001. This resource was co-financed by the Next Generation EU. The views and opinions expressed are only those of the authors and do not necessarily reflect those of the European Union or the European Commission. Neither the European Union nor the European Commission can be held responsible for them.

Data Availability Statement: No new data were created or analyzed in this study. Data sharing is not applicable to this article.

Conflicts of Interest: The authors declare no conflicts of interest.

Abbreviations

The following abbreviations are used in this manuscript:

siRNA	small interfering RNA
CD	cyclodextrin
NVs	nanovectors
RNAi	RNA interference
miRNA	microRNA
LNPs	lipid nanoparticles
hATTR	hereditary transthyretin amyloidosis
BBB	blood–brain barrier
cCD	cationic cyclodextrin
AML	acute myeloid leukemia
TAMs	tumor-associated macrophages

References

1. Fire, A.; Xu, S.; Montgomery, M.K.; Kostas, S.A.; Driver, S.E.; Mello, C.C. Potent and Specific Genetic Interference by Double-Stranded RNA in Caenorhabditis Elegans. *Nature* **1998**, *391*, 806–811. [CrossRef]
2. Friedrich, M.; Aigner, A. Therapeutic siRNA: State-of-the-Art and Future Perspectives. *BioDrugs* **2022**, *36*, 549–571. [CrossRef]
3. Ebenezer, O.; Oyebamiji, A.K.; Olanlokun, J.O.; Tuszynski, J.A.; Wong, G.K.-S. Recent Update on siRNA Therapeutics. *Int. J. Mol. Sci.* **2025**, *26*, 3456. [CrossRef] [PubMed]
4. Clinical Trials Clinicaltrials.Gov. Available online: https://clinicaltrials.gov/expert-search?term=siR (accessed on 17 February 2026).
5. Alabi, C.; Vegas, A.; Anderson, D. Attacking the Genome: Emerging siRNA Nanocarriers from Concept to Clinic. *Curr. Opin. Pharmacol.* **2012**, *12*, 427–433. [CrossRef]
6. Ahn, I.; Kang, C.S.; Han, J. Where Should siRNAs Go: Applicable Organs for siRNA Drugs. *Exp. Mol. Med.* **2023**, *55*, 1283–1292. [CrossRef]
7. Spiridon, I.; Anghel, N. Cyclodextrins as Multifunctional Platforms in Drug Delivery and Beyond: Structural Features, Functional Applications, and Future Trends. *Molecules* **2025**, *30*, 3044. [CrossRef] [PubMed]

8. Davis, M.E.; Brewster, M.E. Cyclodextrin-Based Pharmaceutics: Past, Present and Future. *Nat. Rev. Drug Discov.* **2004**, *3*, 1023–1035. [CrossRef]
9. Stella, V.J.; He, Q. Cyclodextrins. *Toxicol. Pathol.* **2008**, *36*, 30–42. [CrossRef]
10. Sehgal, V.; Pandey, S.P.; Singh, P.K. Prospects of Charged Cyclodextrins in Biomedical Applications. *Carbohydr. Polym.* **2024**, *323*, 121348. [CrossRef] [PubMed]
11. Li, J.; Loh, X.J. Cyclodextrin-Based Supramolecular Architectures: Syntheses, Structures, and Applications for Drug and Gene Delivery. *Adv. Drug Deliv. Rev.* **2008**, *60*, 1000–1017. [CrossRef]
12. Jansook, P.; Ogawa, N.; Loftsson, T. Cyclodextrins: Structure, Physicochemical Properties and Pharmaceutical Applications. *Int. J. Pharm.* **2018**, *535*, 272–284. [CrossRef]
13. Xu, C.; Wu, Y.-L.; Li, Z.; Loh, X.J. Cyclodextrin-Based Sustained Gene Release Systems: A Supramolecular Solution towards Clinical Applications. *Mater. Chem. Front.* **2019**, *3*, 181–192. [CrossRef]
14. Challa, R.; Ahuja, A.; Ali, J.; Khar, R.K. Cyclodextrins in Drug Delivery: An Updated Review. *AAPS PharmSciTech* **2005**, *6*, E329–E357. [CrossRef] [PubMed]
15. Chaturvedi, K.; Ganguly, K.; Kulkarni, A.R.; Kulkarni, V.H.; Nadagouda, M.N.; Rudzinski, W.E.; Aminabhavi, T.M. Cyclodextrin-Based siRNA Delivery Nanocarriers: A State-of-the-Art Review. *Expert Opin. Drug Deliv.* **2011**, *8*, 1455–1468. [CrossRef] [PubMed]
16. Mousazadeh, H.; Pilehvar-Soltanahmadi, Y.; Dadashpour, M.; Zarghami, N. Cyclodextrin Based Natural Nanostructured Carbohydrate Polymers as Effective Non-Viral siRNA Delivery Systems for Cancer Gene Therapy. *J. Control. Release* **2021**, *330*, 1046–1070. [CrossRef]
17. Hu, W.; Ye, B.; Yu, G.; Huang, F.; Mao, Z.; Ding, Y.; Wang, W. Recent Development of Supramolecular Cancer Theranostics Based on Cyclodextrins: A Review. *Molecules* **2023**, *28*, 3441. [CrossRef]
18. Paunovska, K.; Loughrey, D.; Dahlman, J.E. Drug Delivery Systems for RNA Therapeutics. *Nat. Rev. Genet.* **2022**, *23*, 265–280. [CrossRef]
19. Nair, J.K.; Willoughby, J.L.S.; Chan, A.; Charisse, K.; Alam, M.R.; Wang, Q.; Hoekstra, M.; Kandasamy, P.; Kel'in, A.V.; Milstein, S.; et al. Multivalent *N* -Acetylgalactosamine-Conjugated siRNA Localizes in Hepatocytes and Elicits Robust RNAi-Mediated Gene Silencing. *J. Am. Chem. Soc.* **2014**, *136*, 16958–16961. [CrossRef]
20. Springer, A.D.; Dowdy, S.F. GalNAc-siRNA Conjugates: Leading the Way for Delivery of RNAi Therapeutics. *Nucleic Acid Ther.* **2018**, *28*, 109–118. [CrossRef]
21. Setten, R.L.; Rossi, J.J.; Han, S. The Current State and Future Directions of RNAi-Based Therapeutics. *Nat. Rev. Drug Discov.* **2019**, *18*, 421–446. [CrossRef]
22. Hou, X.; Zaks, T.; Langer, R.; Dong, Y. Lipid Nanoparticles for mRNA Delivery. *Nat. Rev. Mater.* **2021**, *6*, 1078–1094. [CrossRef]
23. Moazzam, M.; Zhang, M.; Hussain, A.; Yu, X.; Huang, J.; Huang, Y. The Landscape of Nanoparticle-Based siRNA Delivery and Therapeutic Development. *Mol. Ther.* **2024**, *32*, 284–312. [CrossRef] [PubMed]
24. Hoy, S.M. Patisiran: First Global Approval. *Drugs* **2018**, *78*, 1625–1631. [CrossRef] [PubMed]
25. Qosa, H.; De Oliveira, C.H.M.C.; Cizza, G.; Lawitz, E.J.; Colletti, N.; Wetherington, J.; Charles, E.D.; Tirucherai, G.S. Pharmacokinetics, Safety, and Tolerability of BMS-986263, a Lipid Nanoparticle Containing HSP47 siRNA, in Participants with Hepatic Impairment. *Clin. Transl. Sci.* **2023**, *16*, 1791–1802. [CrossRef] [PubMed]
26. Cavallaro, G.; Sardo, C.; Craparo, E.F.; Porsio, B.; Giammona, G. Polymeric Nanoparticles for siRNA Delivery: Production and Applications. *Int. J. Pharm.* **2017**, *525*, 313–333. [CrossRef]
27. Ren, L.; Wang, S.; Li, B.-C.; Ding, G.-B. Research Progress on Polymer-Based Nanocarriers for Tumor-Targeted Delivery of Survivin siRNA. *Polymers* **2025**, *17*, 2279. [CrossRef]
28. Falsini, S.; Ristori, S.; Ciani, L.; Di Cola, E.; Supuran, C.T.; Arcangeli, A.; In, M. Time Resolved SAXS to Study the Complexation of siRNA with Cationic Micelles of Divalent Surfactants. *Soft Matter* **2013**, *10*, 2226–2233. [CrossRef]
29. Falsini, S.; Di Cola, E.; In, M.; Giordani, M.; Borocci, S.; Ristori, S. Complexation of Short Ds RNA/DNA Oligonucleotides with Gemini Micelles: A Time Resolved SAXS and Computational Study. *Phys. Chem. Chem. Phys.* **2017**, *19*, 3046–3055. [CrossRef]
30. Loftsson, T.; Duchene, D. Cyclodextrins and Their Pharmaceutical Applications. *Int. J. Pharm.* **2007**, *329*, 1–11. [CrossRef]
31. Fitzgerald, K.A.; Malhotra, M.; Gooding, M.; Sallas, F.; Evans, J.C.; Darcy, R.; O'Driscoll, C.M. A Novel, Anisamide-Targeted Cyclodextrin Nanoformulation for siRNA Delivery to Prostate Cancer Cells Expressing the Sigma-1 Receptor. *Int. J. Pharm.* **2016**, *499*, 131–145. [CrossRef]
32. Nazli, A.; Malanga, M.; Sohajda, T.; Béni, S. Cationic Cyclodextrin-Based Carriers for Drug and Nucleic Acid Delivery. *Pharmaceutics* **2025**, *17*, 81. [CrossRef]

33. Pirvu, A.S.; Varut, R.-M.; Trasca, D.-M.; Stoica, G.A.; Radivojevic, K.; Carmen, S.; Arsenie, C.C.; Popescu, C. Cyclodextrins as Active Therapeutic Agents: Beyond Their Role as Excipients. *Pharmaceuticals* **2025**, *18*, 1592. [CrossRef]
34. Ryzhakov, A.; Do Thi, T.; Stappaerts, J.; Bertoletti, L.; Kimpe, K.; Sá Couto, A.R.; Saokham, P.; Van Den Mooter, G.; Augustijns, P.; Somsen, G.W.; et al. Self-Assembly of Cyclodextrins and Their Complexes in Aqueous Solutions. *J. Pharm. Sci.* **2016**, *105*, 2556–2569. [CrossRef]
35. Muankaew, C.; Saokham, P.; Jansook, P.; Loftsson, T. Self-Assembly of Cyclodextrin Complexes: Detection, Obstacles and Benefits. *Pharmazie* **2020**, *75*, 307–312. [CrossRef]
36. Fendler, J.H. *Membrane Mimetic Chemistry*; Wiley: New York, NY, USA, 1982.
37. Romsted, L.S. *Surfactants in Solution*; Plenum Press: New York, NY, USA, 1984; Volume 2.
38. Do, T.T.; Van Hooghten, R.; Van Den Mooter, G. A Study of the Aggregation of Cyclodextrins: Determination of the Critical Aggregation Concentration, Size of Aggregates and Thermodynamics Using Isodesmic and K2–K Models. *Int. J. Pharm.* **2017**, *521*, 318–326. [CrossRef] [PubMed]
39. Guo, T.; Kong, L.; Xu, J.; Geng, Y.; Zhang, R.; Pan, Y.; Xiao, H. Intermolecular Interactions between β-Cyclodextrin and Water. *RSC Adv.* **2021**, *11*, 24807–24815. [CrossRef]
40. Szente, L.; Szejtli, J.; Kis, G.L. Spontaneous Opalescence of Aqueous γ-Cyclodextrin Solutions: Complex Formation or Self-Aggregation? *J. Pharm. Sci.* **1998**, *87*, 778–781. [CrossRef]
41. Valente, A.J.M.; Carvalho, R.A.; Söderman, O. Do Cyclodextrins Aggregate in Water? Insights from NMR Experiments. *Langmuir* **2015**, *31*, 6314–6320. [CrossRef] [PubMed]
42. Gadade, D.D.; Pekamwar, S.S. Cyclodextrin Based Nanoparticles for Drug Delivery and Theranostics. *Adv. Pharm. Bull.* **2020**, *10*, 166–183. [CrossRef] [PubMed]
43. Ciesielski, W.; Kulawik, D.; Girek, B.; Kozieł-Trąbska, K.; Zawierucha, I.; Girek, T. Poly-Amino-β-Cyclodextrin Microparticles for the Reduction of Xenobiotics and Emerging Contaminants, Including Pharmaceuticals, from the Natural Environment. *Materials* **2024**, *17*, 5424. [CrossRef]
44. Pyrak, B.; Rogacka-Pyrak, K.; Gubica, T.; Szeleszczuk, Ł. Exploring Cyclodextrin-Based Nanosponges as Drug Delivery Systems: Understanding the Physicochemical Factors Influencing Drug Loading and Release Kinetics. *Int. J. Mol. Sci.* **2024**, *25*, 3527. [CrossRef]
45. Bonini, M.; Rossi, S.; Karlsson, G.; Almgren, M.; Lo Nostro, P.; Baglioni, P. Self-Assembly of β-Cyclodextrin in Water. Part 1: Cryo-TEM and Dynamic and Static Light Scattering. *Langmuir* **2006**, *22*, 1478–1484. [CrossRef]
46. Rossi, S.; Bonini, M.; Lo Nostro, P.; Baglioni, P. Self-Assembly of β-Cyclodextrin in Water. 2. Electron Spin Resonance. *Langmuir* **2007**, *23*, 10959–10967. [CrossRef] [PubMed]
47. Messner, M.; Kurkov, S.V.; Jansook, P.; Loftsson, T. Self-Assembled Cyclodextrin Aggregates and Nanoparticles. *Int. J. Pharm.* **2010**, *387*, 199–208. [CrossRef] [PubMed]
48. Kulkarni, J.A.; Cullis, P.R.; Van Der Meel, R. Lipid Nanoparticles Enabling Gene Therapies: From Concepts to Clinical Utility. *Nucleic Acid Ther.* **2018**, *28*, 146–157. [CrossRef] [PubMed]
49. Haley, R.M.; Gottardi, R.; Langer, R.; Mitchell, M.J. Cyclodextrins in Drug Delivery: Applications in Gene and Combination Therapy. *Drug Deliv. Transl. Res.* **2020**, *10*, 661–677. [CrossRef]
50. Castillo Cruz, B.; Flores Colón, M.; Rabelo Fernandez, R.J.; Vivas-Mejia, P.E.; Barletta, G.L. A Fresh Look at the Potential of Cyclodextrins for Improving the Delivery of siRNA Encapsulated in Liposome Nanocarriers. *ACS Omega* **2022**, *7*, 3731–3737. [CrossRef]
51. Malhotra, M.; Gooding, M.; Evans, J.C.; O'Driscoll, D.; Darcy, R.; O'Driscoll, C.M. Cyclodextrin-siRNA Conjugates as Versatile Gene Silencing Agents. *Eur. J. Pharm. Sci.* **2018**, *114*, 30–37. [CrossRef]
52. Lipofectamine 2000. Available online: https://www.thermofisher.com/it/en/home/references/protocols/cell-culture/transfection-protocol/lipofectamine-2000 (accessed on 10 December 2025).
53. Mendonça, M.C.P.; Cronin, M.F.; Cryan, J.F.; O'Driscoll, C.M. Modified Cyclodextrin-Based Nanoparticles Mediated Delivery of siRNA for Huntingtin Gene Silencing across an in Vitro BBB Model. *Eur. J. Pharm. Biopharm.* **2021**, *169*, 309–318. [CrossRef]
54. Wang, J.-W.; Yu, K.-X.; Ji, X.-Y.; Bai, H.; Zhang, W.-H.; Hu, X.; Tang, G. Structural Insights into the Host–Guest Complexation between β-Cyclodextrin and Bio-Conjugatable Adamantane Derivatives. *Molecules* **2021**, *26*, 2412. [CrossRef]
55. Kulkarni, A.; DeFrees, K.; Schuldt, R.A.; Hyun, S.-H.; Wright, K.J.; Yerneni, C.K.; VerHeul, R.; Thompson, D.H. Cationic α-Cyclodextrin:Poly(Ethylene Glycol) Polyrotaxanes for siRNA Delivery. *Mol. Pharm.* **2013**, *10*, 1299–1305. [CrossRef]
56. Seripracharat, C.; Sinthuvanich, C.; Karpkird, T. Cationic Cyclodextrin-Adamantane Poly(Vinyl Alcohol)-Poly(Ethylene Glycol) Assembly for siRNA Delivery. *J. Drug Deliv. Sci. Technol.* **2022**, *68*, 103052. [CrossRef]
57. Kont, A.; Mendonça, M.C.P.; Cronin, M.F.; Cahill, M.R.; O'Driscoll, C.M. Co-Formulation of Amphiphilic Cationic and Anionic Cyclodextrins Forming Nanoparticles for siRNA Delivery in the Treatment of Acute Myeloid Leukaemia. *Int. J. Mol. Sci.* **2022**, *23*, 9791. [CrossRef] [PubMed]

58. Sun, Y.; Cronin, M.F.; Mendonça, M.C.P.; Guo, J.; O'Driscoll, C.M. Sialic Acid-Targeted Cyclodextrin-Based Nanoparticles Deliver CSF-1R siRNA and Reprogram Tumour-Associated Macrophages for Immunotherapy of Prostate Cancer. *Eur. J. Pharm. Sci.* **2023**, *185*, 106427. [CrossRef]
59. Hao, Y.; Yang, J.; Liu, D.; Zhang, H.; Ou, T.; Xiao, L.; Chen, W. Construction of Aptamer-siRNA Chimera and Glutamine Modified Carboxymethyl-β-Cyclodextrin Nanoparticles for the Combination Therapy against Lung Squamous Cell Carcinoma. *Biomed. Pharmacother.* **2024**, *174*, 116506. [CrossRef] [PubMed]
60. Zuckerman, J.E.; Gritli, I.; Tolcher, A.; Heidel, J.D.; Lim, D.; Morgan, R.; Chmielowski, B.; Ribas, A.; Davis, M.E.; Yen, Y. Correlating Animal and Human Phase Ia/Ib Clinical Data with CALAA-01, a Targeted, Polymer-Based Nanoparticle Containing siRNA. *Proc. Natl. Acad. Sci. USA* **2014**, *111*, 11449–11454. [CrossRef]
61. Varghese, A.M.; Ang, C.; Dimaio, C.J.; Javle, M.M.; Gutierrez, M.; Yarom, N.; Stemmer, S.M.; Golan, T.; Geva, R.; Semenisty, V.; et al. A Phase II Study of siG12D-LODER in Combination with Chemotherapy in Patients with Locally Advanced Pancreatic Cancer (PROTACT). *J. Clin. Oncol.* **2020**, *38*, TPS4672. [CrossRef]
62. Rekharsky, M.V.; Inoue, Y. Complexation Thermodynamics of Cyclodextrins. *Chem. Rev.* **1998**, *98*, 1875–1918. [CrossRef]
63. Wolff, J.A.; Rozema, D.B. Breaking the Bonds: Non-Viral Vectors Become Chemically Dynamic. *Mol. Ther.* **2008**, *16*, 8–15. [CrossRef] [PubMed]
64. Zhang, Y.; Liu, Y.; Liu, Y. Cyclodextrin-Based Multistimuli-Responsive Supramolecular Assemblies and Their Biological Functions. *Adv. Mater.* **2020**, *32*, 1806158. [CrossRef]
65. Godbey, W.T.; Wu, K.K.; Mikos, A.G. Poly(Ethylenimine) and Its Role in Gene Delivery. *J. Control. Release* **1999**, *60*, 149–160. [CrossRef]
66. Singh, R.P.; Hidalgo, T.; Cazade, P.-A.; Darcy, R.; Cronin, M.F.; Dorin, I.; O'Driscoll, C.M.; Thompson, D. Self-Assembled Cationic β-Cyclodextrin Nanostructures for siRNA Delivery. *Mol. Pharm.* **2019**, *16*, 1358–1366. [CrossRef]
67. Alvira, E. Molecular Simulation of the Complexes Formed by Hydroxypropyl-β-Cyclodextrin and Rifampicin with Different Solvents. *Macromol* **2024**, *4*, 843–855. [CrossRef]
68. Fereidounpour, P.; Steinmann, C.; Larsen, K.L. Prediction of the Free Energy of Binding for Cyclodextrin-Steroid Complexes: Phase Solubility and Molecular Dynamics Studies. *J. Incl. Phenom. Macrocycl. Chem.* **2024**, *104*, 535–546. [CrossRef]
69. Rivero-Barbarroja, G.; López-Fernández, J.; Juárez-Gonzálvez, I.; Fernández-Clavero, C.; Di Giorgio, C.; Vélaz, I.; Garrido, M.J.; Benito, J.M.; Ortiz Mellet, C.; Mendicuti, F.; et al. β-Cyclodextrin-Based Geometrically Frustrated Amphiphiles as One-Component, Cell-Specific and Organ-Specific Nucleic Acid Delivery Systems. *Carbohydr. Polym.* **2025**, *347*, 122776. [CrossRef]
70. Ping, Y.; Liu, C.; Zhang, Z.; Liu, K.L.; Chen, J.; Li, J. Chitosan-Graft-(PEI-β-Cyclodextrin) Copolymers and Their Supramolecular PEGylation for DNA and siRNA Delivery. *Biomaterials* **2011**, *32*, 8328–8341. [CrossRef] [PubMed]
71. Liu, C.-H.; Shih, P.-Y.; Lin, C.-H.; Chen, Y.-J.; Wu, W.-C.; Wang, C.-C. Tetraethylenepentamine-Coated β Cyclodextrin Nanoparticles for Dual DNA and siRNA Delivery. *Pharmaceutics* **2022**, *14*, 921. [CrossRef]
72. Gatiatulin, A.K.; Grishin, I.A.; Buzyurov, A.V.; Mukhametzyanov, T.A.; Ziganshin, M.A.; Gorbatchuk, V.V. Determination of Melting Parameters of Cyclodextrins Using Fast Scanning Calorimetry. *Int. J. Mol. Sci.* **2022**, *23*, 13120. [CrossRef] [PubMed]
73. Guo, F.; Li, Y.; Yu, W.; Fu, Y.; Zhang, J.; Cao, H. Recent Progress of Small Interfering RNA Delivery on the Market and Clinical Stage. *Mol. Pharm.* **2024**, *21*, 2081–2096. [CrossRef]
74. Li, F.; Cao, D.; Gu, W.; Cui, L.; Qiu, Z.; Liu, Z.; Li, D.; Guo, X. Delivery of miR-34a-5p by Folic Acid-Modified β-Cyclodextrin-Grafted Polyethylenimine Copolymer Nanocarriers to Resist KSHV. *ACS Appl. Nano Mater.* **2023**, *6*, 10826–10836. [CrossRef]
75. Kali, G.; Haddadzadegan, S.; Bernkop-Schnürch, A. Cyclodextrins and Derivatives in Drug Delivery: New Developments, Relevant Clinical Trials, and Advanced Products. *Carbohydr. Polym.* **2024**, *324*, 121500. [CrossRef]
76. Sun, Q.; Zhou, Z.; Qiu, N.; Shen, Y. Rational Design of Cancer Nanomedicine: Nanoproperty Integration and Synchronization. *Adv. Mater.* **2017**, *29*, 1606628. [CrossRef]
77. Mi, P. Stimuli-Responsive Nanocarriers for Drug Delivery, Tumor Imaging, Therapy and Theranostics. *Theranostics* **2020**, *10*, 4557–4588. [CrossRef]
78. Yao, Y.; Zhou, Y.; Liu, L.; Xu, Y.; Chen, Q.; Wang, Y.; Wu, S.; Deng, Y.; Zhang, J.; Shao, A. Nanoparticle-Based Drug Delivery in Cancer Therapy and Its Role in Overcoming Drug Resistance. *Front. Mol. Biosci.* **2020**, *7*, 193. [CrossRef]
79. Liu, J.; Liu, X.; Yuan, Y.; Li, Q.; Chang, B.; Xu, L.; Cai, B.; Qi, C.; Li, C.; Jiang, X.; et al. Supramolecular Modular Approach toward Conveniently Constructing and Multifunctioning a pH/Redox Dual-Responsive Drug Delivery Nanoplatform for Improved Cancer Chemotherapy. *ACS Appl. Mater. Interfaces* **2018**, *10*, 26473–26484. [CrossRef]
80. Bilia, A.R.; Piazzini, V.; Risaliti, L.; Vanti, G.; Casamonti, M.; Wang, M.; Bergonzi, M.C. Nanocarriers: A Successful Tool to Increase Solubility, Stability and Optimise Bioefficacy of Natural Constituents. *Curr. Med. Chem.* **2019**, *26*, 4631–4656. [CrossRef] [PubMed]
81. Jackson, A.L.; Linsley, P.S. Recognizing and Avoiding siRNA Off-Target Effects for Target Identification and Therapeutic Application. *Nat. Rev. Drug Discov.* **2010**, *9*, 57–67. [CrossRef] [PubMed]
82. Zhu, H.; Snyder, M. Protein Arrays and Microarrays. *Curr. Opin. Chem. Biol.* **2001**, *5*, 40–45. [CrossRef]

83. Jayasinghe, M.K.; Lee, C.Y.; Tran, T.T.T.; Tan, R.; Chew, S.M.; Yeo, B.Z.J.; Loh, W.X.; Pirisinu, M.; Le, M.T.N. The Role of in Silico Research in Developing Nanoparticle-Based Therapeutics. *Front. Digit. Health* **2022**, *4*, 838590. [CrossRef] [PubMed]
84. Yang, L.; Wang, H.; Leng, D.; Fang, S.; Yang, Y.; Du, Y. Machine Learning Applications in Nanomaterials: Recent Advances and Future Perspectives. *Chem. Eng. J.* **2024**, *500*, 156687. [CrossRef]

Journal Pre-proofs

Newly customized cationic ß-cyclodextrins as potential nanovectors for gene delivery

Ilaria Chiarugi, Francesca Maestrelli, Milo Malanga, Giulia Piomboni, Lorena Valverde Fraga, Sandra Ristori, Anna Rita Bilia, Alessio Gnerucci, Paola Faraoni, Francesco Ranaldi, Sara Falsini, Noemi Csaba

PII: S0378-5173(26)00269-3
DOI: https://doi.org/10.1016/j.ijpharm.2026.126821
Reference: IJP 126821

To appear in: *International Journal of Pharmaceutics*

Received Date: 4 December 2025
Revised Date: 25 March 2026
Accepted Date: 26 March 2026

Please cite this article as: I. Chiarugi, F. Maestrelli, M. Malanga, G. Piomboni, L.V. Fraga, S. Ristori, A.R. Bilia, A. Gnerucci, P. Faraoni, F. Ranaldi, S. Falsini, N. Csaba, Newly customized cationic ß-cyclodextrins as potential nanovectors for gene delivery, *International Journal of Pharmaceutics* (2026), doi: https://doi.org/10.1016/j.ijpharm.2026.126821

Newly customized cationic ß-Cyclodextrins as potential nanovectors for gene delivery

Ilaria Chiarugi [1], Francesca Maestrelli [1], Milo Malanga[6], Giulia Piomboni [1], Lorena Valverde Fraga[2], Sandra Ristori [1], Anna Rita Bilia* [1], Alessio Gnerucci [3], Paola Faraoni [4], Francesco Ranaldi [4], Sara Falsini[5], Noemi Csaba[2]

[1] Department of Chemistry "Ugo Schiff" (DICUS), University of Florence, Via Ugo Schiff 6, 50019Florence, FI, Italy; ilaria.chiarugi@unifi.it (I.C); francesca.maestrelli@unifi.it (F.M.); giulia.piomboni@edu.unifi.it (G.P.), sandra.ristori@unifi.it (S.R.); ar.bilia@unifi.it (A.R.B.)

[2] CIMUS (Centro Singular de Investigación en Medicina Molecular y Enfermedades Crónicas), Department of Pharmacology, Pharmacy and Pharmaceutical Technology, University of Santiago de Compostela, Avenida Barcelona, s/n, 15782, Santiago de Compostela (A Coruña), Spain; noemi.csaba@usc.es (N.C.); lorena.valverde@rai.usc.it (L.V.F.)

[3] Department of Physics and Astronomy, University of Florence, Via Sansone, 1, 50019 Sesto Fiorentino, FI, Italy; alessio.gnerucci@unifi.it (A.G.)

[4] Department of Experimental and Clinic Biomedical Sciences "Mario Serio", University of Florence, Viale Pieraccini 6, 50139 Florence, FI, Italy; paola.faraoni@unifi.it (P.F.), francesco.ranaldi@unifi.it (F.R.)

[5] Department of Biology, University of Florence, Via P.A. Micheli 3, 5012, Florence, FI, Italy; sara.falsini@unifi.it (S.F.)

[6] CarboHyde Zrt., Berlini str., 47-49, Budapest, Hungary; milo.malanga@carbohyde.com (M.M)

* Correspondence: ar.bilia@unifi.it

Keywords: New Cationic β-Cyclodextrins; Gene Delivery; Nanovectors; pGFP; siRNA

Abstract: Gene therapy represents a promising strategy for the treatment of severe diseases through delivery of genetic material into target cells. Its clinical translation, however, remains limited by the need for safe and efficient vectors. β-Cyclodextrins (β-CDs), owing to their biocompatibility and structural tunability, represent an attractive platform. In this study, three novel cationic β-CD derivatives (CD1, CD2, and CD3), functionalized with amino groups and different lipophilic chains, were evaluated. Preformulation studies were conducted to optimize the composition and preparation of β-CD-based nanovectors (NVs), which were subsequently complexed with a GFP-encoding plasmid (pGFP). Sodium hyaluronate (HA) and polysialic acid (PSA), were incorporated at 10% w/w, to enhance loading capacity and biocompatibility. Physico-chemical characterization included size, polydispersity index (PdI), and zeta potential. Further insights concerning the architecture of NVs were obtained by TEM, Cryo-EM, and synchrotron SAXS, which indicated a hierarchical arrangement in the structure of the complexes, while electrophoresis verified efficient nucleic acid binding. Stability was assessed at 4 °C for one week and in culture medium for 24 h. MTT test was performed in HeLa cells and transfection efficiency was analysed by flow cytometry and fluorescence microscopy. NVs were then complexed with GFP-targeting-siRNA (N/P = 10), and silencing efficiency was assessed in HeLa-GFP cells. All formulations displayed suitable size (<200 nm) and PdI (<0.3). CD1 showed the highest biopharmaceutical performance, achieving GFP expression and silencing efficiency comparable to commercial lipofectamine. Overall, CD1 emerged as the most promising candidate, supporting its potential as an effective and biocompatible NVs for gene delivery.

Introduction

Gene therapy has emerged as one of the most promising approaches for treating severe illnesses such as cancer, chronic diseases, and autoimmune disorders, which currently lack effective treatments (Aiuti et al., 2022; Morris and Schorge, 2022; Rosenblum et al., 2018). This therapeutic strategy involves the introduction of genetic material into the patient's cells to correct genetic defects or provide new instructions that can cure or improve a pathological condition. A significant challenge in this field is the safe and efficient delivery of genetic material to target cells, as well as its protection from degradation once administered *in vivo* (Tang and Khvorova, 2024). Thus, a key factor for the success of gene therapy is the use of nanovectors (NVs) able to properly transport DNA, RNA, or other genetic material into cells (Androsavich, 2024; Di Silvio et al., 2019; Sun, 2023).

Cyclodextrins (CDs) have found extensive use in pharmaceutical applications due to their ability to improve the solubility of poorly soluble drugs in water, as well as to improve bioavailability, and other key properties (Fiani et al., 2025; Haley et al., 2020). These cyclic oligosaccharides, particularly β-cyclodextrins (β-CDs), have been chemically modified to further expand their capabilities thanks to their facility of functionalization, and have been recognized for their biocompatibility.In recent years, the exploration of cationic modified CDs for gene delivery has gained attention and showed promising outcomes (Ceborska, 2017; Chiarugi et al. preprint.; Fitzgerald et al., 2016;Godinho et al., 2013; Malhotra et al., 2018;; Varan et al., 2017). However, these studies are still in its early stages and much remains to be understood about their potential as NVs in gene delivery. Certainly, their cationic nature has the potential to serve as effective candidates for creating drug delivery systems able to complex and deliver negatively charged genetic material, as well as to modify and control the release of genetic materials, potentially improving the safety and efficiency of gene delivery systems (Liu et al., 2022; Li et al., 2023 ;Mendonça et al., 2021, Singh et al., 2019).

Biocompatible anionic polymers, such as sodium hyaluronate (HA) and polysialic acid (PSA) can be added to NVs to improve colloidal stability by steric hindrance and decrease potential cytotoxicity by reducing the surface charge. Moreover, HA and PSA are known to enhance cellular interactions and biocompatibility (Krishnan et al., 2024; Matalqah et al., 2024; Negut and Grimezescu, 2021; Raval and Bhattacharya, 2025; Thwala et al., 2018).

In this study, we investigated three novel cationic β-CDs (Figure 1), designed and synthesized by CarboHyde Zrt, with the aim of assessing their suitability as gene delivery vectors. These will be hereinafter referred to as CD1, CD2, and CD3, respectively. All the CD derivatives share a common β-CD ring functionalized with a lipophilic alkyl chain of variable length and one or more ionizable amino groups. The presence of protonatable amino functionalities is crucial for establishing electrostatic interactions with the negatively charged genetic material, thereby facilitating complex formation, while also contributing to the self-assembly of nanocarriers. The hydrophobic alkyl chains, differing in length among the derivatives, play an essential role in modulating interactions with cellular membranes and biological environments, and can also serve as anchoring sites for further ligand conjugation or receptor-specific targeting. Moreover, the presence of sulfur-containing groups may enhance biological interactions, promoting more efficient intracellular trafficking and release (Kont et al., 2022; Nazli et al., 2025; Tian et al., 2020).Specifically, CD1 has a single amino group and an octyl (C8) hydrophobic chain linked to carbon 2 and 6 of CD moiety respectively ; CD2 contains two amino groups linked to carbon 2 and 3 of CD moiety and a longer C16 chain linked to carbon 6 of CD moiety; while CD3 possesses one amino group coupled with a C16 hydrophobic chain linked to carbon 2 and 6 of CD moiety respectively. These structural variations can influence the efficiency of nucleic acid complexation and the subsequent intracellular release of the genetic payload.

As a first step, since these CDs are newly developed, we conducted preformulation studies to identify the best method and optimal concentration to obtain NVs with suitable characteristics for gene delivery. Specifically, to assess their potential for gene delivery the β-CDs NVs were complexed with a GFP encoding model plasmid DNA (pGFP). In addition to these initial formulations, we also tested vectors by incorporating HA or PSA into the β-CDs. The rationale behind this choice is that the zeta potential of the NVs is relatively high, which may raise concerns about their toxicity profile. HA and PSA were not introduced as targeting ligands but as surface-modulating agents, with the aim of partially reducing surface charge and improving colloidal behavior, rather than actively promoting receptor-mediated uptake (Isert et al., 2025). These formulations were complexed with pGFP at the same N/P ratio. The vectors were further characterized using transmission electron microscopy (TEM) and synchrotron-SAXS to assess their structure and stability.

Stability studies were performed both under storage conditions at 4°C and in cell culture medium. The potential biological impact of the developed nanovectors was evaluated through in vitro cytotoxicity assays using the MTT

method. Transfection efficiency was assessed by flow cytometry, and representative images of transfected cells were acquired by fluorescence microscopy. The nanovectors were also complexed with GFP-targeting siRNA, characterized by dynamic light scattering and stability assays, and their gene silencing efficiency was subsequently evaluated. All formulations, both before and after nucleic acid complexation, were analyzed by dynamic light scattering to determine hydrodynamic diameter, polydispersity index (PdI), and zeta potential (ZP).

Most reported formulations rely on multicomponent architectures, polymeric conjugation, or other components, to achieve efficient nucleic acid delivery. This complexity may limit reproducibility, scalability, and translational potential. Moreover, relatively few studies directly compare plasmid DNA transfection and siRNA-mediated gene silencing within the same cyclodextrin-based platform.

The present study aims to address this gap by investigating a series of structurally related cationic β-cyclodextrin derivatives with systematic variations in hydrophobic chain length and cationic functionality, in order to elucidate structure–performance relationships in gene delivery. In addition, the effect of surface modulation using hyaluronic acid and polysialic acid is explored as a strategy to tune colloidal properties without increasing formulation complexity.

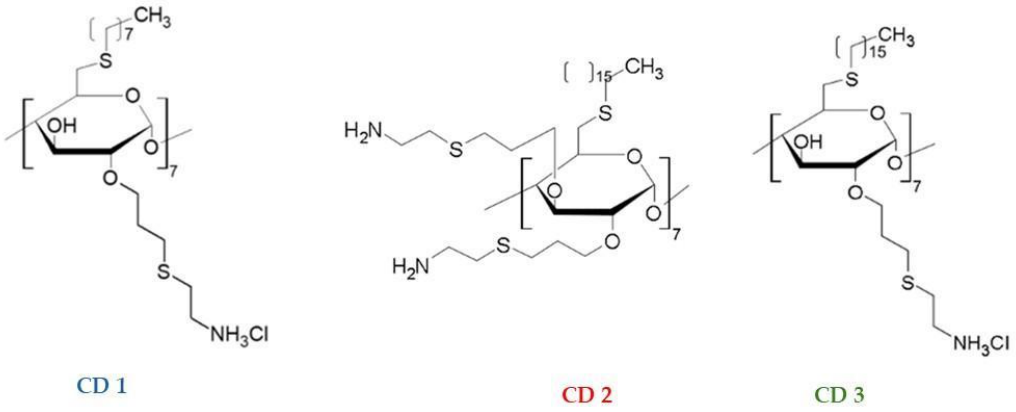

Figure 1. Chemical structure of new synthetised cationic β-CDs.

Materials and Methods

2.1. Materials

Hyaluronic acid (HA, sodium hyaluronate, 40 kDa) was purchased from LifeCore Biomedical (Minnesota, USA), polysialic acid (PSA, 30 kDa) was obtained from the Serum Institute of India (Maharashtra, India). Plasmid-GFP (pGFP) was kindly provided by the Biomaterials & Drug Delivery (BIDD) group from the University of Santiago de Compostela. HeLa and RAW cells were obtained from the American Type Culture Collection (ATCC, Manassas, VA, USA). GFP-targeting siRNA was purchased from Biospring (Frankfurt, Germany). RNase-free water, Syb-gold, Lipofectamine, Agarose, phosphotungstic acid and Opti-MEM were purchased from Thermo Fisher Scientific (USA). TBA buffer, Ethanol (EtOH), chloroform ($CHCl_3$), dimethyl sulfoxide (DMSO), HEPES buffer (10 mM, pH 6), and phosphate-buffered saline (PBS) were purchased from Merck (Darmstadt, Germany). Dulbecco's Modified Eagle Medium (DMEM), fetal bovine serum (FBS), and trypsin were obtained from VWR (Pennsylvania, USA). Beta cyclodextrin is a product of Wacker Chemie (Munich, Germany). Triphenylphosphine (99%), N-Bromosuccinimide (99%, ReagentPlus), sodium methoxide in methanol (25 wt%), anhydrous N,N-dimethylformamide (DMF, >99.8%), 1-octanethiol (98.5%), 1-

hexadecanethiol (99%), NaH (60% dispersion in mineral oil), allyl-bromide (ReagentPlus®, 99%,), cysteamine hydrochloride (≥98%), 2,2'-Azobis(2-methylpropionitrile) (AIBN, 98%) are product of Merck (Darmstadt, Germany). 1,4-Dioxane (puriss.), 25% ammonia solution (analytical grade), 1-propanol (lab. grade), methanol (lab. grade), n-hexane (lab. grade), ethyl acetate (lab. grade), toluene (lab. grade) were from Molar KFT (Halásztelek, Hungary).

2.2. Synthesis and characterisation of modified cationic β-CDs (CD1, CD2, CD3)

All the reagents were used without further purification. Solvents were dried by conventional methods and distilled immediately prior to use. Dialysis tube cellulose membrane molecular weight cut-off= 2.000 was from Sigma (Missouri, United States). Silica gel coated aluminum sheets were from Merck (Art. No.: 1.05554). Visualization was achieved under UV light at 254/366 nm by charring with a solution of EtOH (96%):H2SO4 (96%) = 9:1 charred by heating at 105-110 °C.

NMR spectra were recorded in deuterated pyridine-d5, chloroform-d, methanol-d4, or water-d2 on Varian VXR-600 at 400 or 600 MHz instrument at 295 K.

MALDI-TOF mass spectra were recorded on a Bruker Microflex LRF system. The microflex LRF operated in positive ion mode using the linear detector. Ion generation was achieved using a 60 Hz N2-Cartridge-Laser including variable power attenuator and UV optics. The laser operated at 337 nm, 2,5-dihydroxybenzoic acid (DHB) was used as the matrix.

2.3. Preformulation studies

A systematic screening was performed to evaluate ability to form NVs from the three cyclodextrins (CD1, CD2, and CD3) using various preparation methods, solvents, and concentrations. NVs formation was assessed in RNase-free water, EtOH, $CHCl_3$, DMSO, HEPES buffer (10 mM, pH 6), and PBS (10 mM pH 7,4), under different agitation conditions and heating up to 75 °C.

Since these cyclodextrins are novel derivatives, the primary objective was to identify suitable solvents for their dispersion and determine optimal concentrations. Only chloroform (at room temperature) and water (under agitation at 50 °C for 15 min, followed by 37 °C for 30 min) proved suitable for NV formation. Formulations containing CD2 were stable in water for up to 12 h, whereas CD1 rapidly precipitated. Based on these observations, NV formation for CD1 was further investigated using both chloroform (via thin-layer evaporation) and water, while for CD2, only aqueous formulations were pursued. For the aqueous formulations of the cyclodextrin derivatives, the critical micelle concentration (CMC) was determined by conductometric measurements in order to define the minimum concentration required for self-assembly. The CMC values for both cyclodextrins were found to be on the order of 10^{-5} M, with CD1 exhibiting a CMC of approximately 4.0×10^{-5} M and CD2 a CMC of 7.25×10^{-5} M. Based on these results, subsequent experiments were conducted to identify the optimal concentration range for nanovector (NV) formation.

2.4. NVs Preparation

NVs were prepared and loaded with pGFP using two methods for CD1 (in chloroform (A) and RNAse free water(B)) and one method for CD2 (in RNAse free water). For the chloroform preparations, sonication was applied to the empty NVs, whereas for the thin-layer evaporation method, the NVs were first rehydrated and then the plasmid was added. Detailed preparation parameters are reported in Table 1.

Parameter	**CD1 (A)**	**CD1 (B)-CD2**
Solvent	Chloroform	RNAse-free water
Dissolution conditions	2 mg/mL	2 mg/mL
Mixing conditions	/	450 rpm 50°C (15 min)-37°C(30min)

Film formation	(N2) evaporation	no
Rehydratation	RNAse-free water	/
Sonication	10% amp, 1/1 pulse, 1	/
Complexation pGFP/siRNA	After CD NV formation. 1h, 300 rpm, 25°C	After CD NV formation. 1h, 300 rpm, 25°C
HA/PSA addition	Simultaneously with nucleic acid	Simultaneously with nucleic acid

Table 1. Formulation parameter for NVs preparation

pGFP was incorporated at an N/P ratio of 10, where the N/P ratio was defined as the molar ratio between the protonatable amine groups of the cyclodextrin derivatives and the phosphate groups of the nucleic acid. The number of protonatable amines per cyclodextrin derivative was determined based on their chemical structures: one protonatable group per monomer for CD1 and CD3, and two per monomer for CD2, using the molecular weight of the cyclodextrins for calculations. The same methodology and molecular weights were applied for both pGFP and siRNA GFP (Bienvenu et al.,2012).

The N/P ratio of 10 was selected after preliminary evaluation with different N/P ratios (in the range 1-20) , as it enabled >90% complexation of the genetic material. Due to the high cost of the plasmid and siRNA, an initial screening was performed to identify the optimal N/P ratio, which was then used for subsequent studies in triplicate. Additionally, an N/P ratio of 10 has been widely reported and applied in previous studies (Singh et al., 2019; Sun et al., 2023; Wu et al., 2014; Xu et al., 2009).

2.5. Dynamic Light Scattering (DLS) and Electrophoretic Light Scattering (ELS)

DLS and ELS analyses were carried out with all empty and pGFP loaded CD NVs, as well as with or out the addition of HA or PSA.Size and PdI were measured using DLS, while zeta potential (Z) was determined using ELS. All measurements were performed using a Zetasizer Pro Red Label (Malvern Instruments, Malvern, UK). The instrument was equipped with 10 mW He-Ne laser operating at 632.8 nm, an avalanche photodiode detector, a digital correlator, and a temperature controller set at 25 °C, using water dispersant viscosity used for the analyses. Time correlation functions were analyzed using the software Zetasizer, version 7.02, provided by Malvern. For size and PdI measurements, polystyrene cuvettes (12 × 12 × 45 mm; minimum volume: 40 µL) were used, and 100 µL of the prepared solution was directly loaded into the cuvette. Z measurements were performed using capillary cells with a minimum volume of 0.7 mL; for this, 10 µL of the NVs solution was diluted to a final volume of 700 µL with RNase free water.

In both cases, the cuvette or capillary cell was placed into the instrument sample holder for analysis. All measurements were carried out in triplicate at a constant temperature of 25 °C with a detection angle of 173°.

All experiments were performed in triplicate, and results are reported as mean ± standard deviation (SD).

2.6. Transmission Electron Microscopy (TEM) Analyses

TEM analyses were performed on CD NVs empty, complexed with pGFP, and CD combined with HA or PSA and P. 10 µl of the sample was mixed with 10 µl of 2% phosphotungstic acid. Then, 1 µl of this solution was placed on the bright copper-colored area of the round grid and left until dry. After that, washing with water, and the grid was left to dry in

a desiccator chamber for at least 24 h and then the analysis was performed. The images were obtained using the FESEM Ultra Plus, (ZEISS, Jena, Germany) at the CACTUS facility, University of Santiago de Compostela.

2.7. Cryo-Electron Microscopy Analyses (Cryo-EM)

Cryo-EM was performed on CD1 and CD2 NVs with pGFP using a JEOL JEM-1230 microscope (JEOL Ltd., Tokyo, Japan) at the CIC Biogune (Bilbao, Spain). Samples were prepared on carbon-coated grids and vitrified by rapid freezing prior to imaging.

2.8. Synchrotron-SAXS

SAXS measurements of NVs, both empty and complexed with pGFP, were performed at the ID02 beamline of the European Synchrotron Radiation Facility (ESRF-Grenoble, France). The wavelength and energy of the incoming beam were 0.995 Å and 12.46 keV, respectively. The sample holder was a flow- through capillary with 2 mm diameter, maintained at 37°C to reproduce the physiological cellular condition. The scattering vector q covered a range of 0.11 to 9.70 nm-1 with sample-detector distance of 0.8 m. The 2D SAXS patterns were first circularly averaged and normalized to the absolute scale to obtain 1D patterns from the different configurations merged, then the contribution of the solvent filled capillary (background) was subtracted. The resulting SAXS curves were fitted using the SasView 6.0.0 package (Doucet et al., 2024).

2.9. Stability assessment

The stability of NVs complexed with pGFP was assessed under two conditions: storage at 4 °C and incubation in cell culture medium (at 37°C).

For storage stability NV–pGFP formulations were stored at 4 °C (±1 °C) and analyzed after 1, 4, and 7 days using DLS, as described in Section 2.4.

For stability in cell culture medium, the studies were conducted at 37°C and NV–pGFP stability was also evaluated at 0, 2, 4, and 24 h after dilution in cell culture medium. For each time point, 10 µL of NV dispersion was mixed with 90 µL of either non-supplemented DMEM or DMEM supplemented with 10% FBS. Samples were analyzed by DLS with the attenuator set to 7, using 10 runs per measurement, and each condition measured in triplicate.

Stability studies were designed as preliminary physicochemical assessments under storage conditions at 4°C and in cell culture medium, as commonly reported for cyclodextrin-based and non-viral gene delivery systems (Cifani et al.,2014; Trotta et al., 2012; Varan et al., 2017). Although these assays do not fully reproduce the complexity of the intracellular environment, they provide a standardized first-level evaluation of formulation robustness. Importantly, nanovector stability under biologically relevant conditions was further supported by successful cellular uptake, transfection, and siRNA-mediated gene silencing, indicating preservation of nanovector integrity in the cellular context.

2.10. Complexation efficacy of NVs

The complexation efficiency was evaluated using standard horizontal electrophoresis, a 2% (w/v) agarose gel prepared in a TBA buffer (Csaba et al., 2009; Mansouri et al., 2006, Kim et al.,2012).

For each sample, a total of 20 µL was loaded into each well. Each sample was mixed with 2 µL of SYBR™ Gold nucleic acid stain (Thermo Fisher Scientific, Waltham, MA, USA) and 1 µL of loading buffer (Thermo Fisher Scientific, Waltham, MA, USA). Free pGFP was loaded as a reference control to assess the extent of complexation.

To evaluate pGFP release from the NVs, samples were incubated with heparin at a 25-fold excess (w/w) relative to the CD content. The mixtures were incubated for 3 h at 37 °C under shaking at 420 rpm using a Titramax 1000 orbital shaker integrated with an Inkubator 1000 temperature-controlled incubator (Heidolph Instruments, Schwabach, Germany)). All samples were prepared and incubated in Eppendorf tubes prior to electrophoresis Gels were imaged using a GelDoc XR+ system (Bio-Rad, Hercules, CA, USA) (Maiorano et al., 2022). All experiments were performed in triplicate, a simple estimation of the siRNA complexation percentages was obtained by analyzing the gel images by means of dedicated ImageJ macros (Schindelin et al., 2012).

2.11 *In vitro* toxicity, transfection and silencing efficiency

The Hela cells lines were grown in with 10 mL DMEM supplemented with 200 mM L-Glutamine and 10% (v/v) FBS medium, in a humidified incubator (MEMMERT INE 400, Memmert, Germany) with 5% CO2/95% atmospheric air at 37 °C. Cells used for comparative experiments were maintained in cell culture dishes 10 mm and used between passages 10 and 20.

The cytotoxicity of empty and pGFP -loaded NVs was evaluated using the MTT assay with HeLa Cells. The assay was performed on standard 96-well tissue-culture–treated plates, with concentrations ranging from 31 to 500 µg/mL for empty NVs, and from 15,5 to 125 µg/mL for pGFP -loaded NVs. Cells were seeded in 96-well plates at fixed densities of 1×10^5 cells/mL. Cells were cultured for 24 h in standard culture medium. After this initial incubation, the medium was replaced with 160 µL of fresh medium and 40 µL of the NVs solution diluted in Opti-MEM. The cells were then incubated with NVs for an additional 24 h at 37 °C in a humidified 5% CO_2 atmosphere (Valverde-Fraga et al., 2023).

After incubation, the medium was removed and replaced with an MTT salt solution diluted in DMEM to a final concentration of approximately 1 mM. Plates were incubated for 1–2 h at 37 °C to allow for formazan crystal formation.

Following incubation, the MTT-containing medium was carefully removed and formazane crystals were solubilized. The absorbance was measured at 570 nm using a microplate reader Infinite M200PRO (Tecan, Männedorf, Switzerland). Background absorbance at 630 nm was subtracted from the 570 nm readings to obtain normalized absorbance values representing cell viability.

Transfection and silencing assays were performed in HeLa and HeLa-GFP cells, respectively, and evaluated at 24 and 48 h post-treatment. Cells were seeded in 24-well plates at a density of 1×10^5 cells/mL and incubated for 24 h under standard culture conditions (37 °C, 5% CO_2). Following incubation, the culture medium was removed, and 50 µL of the formulation diluted in Opti-MEM was added to each well, followed by 450 µL of complete DMEM. Cells were then incubated for 24 or 48 h (transfection assay) and for 24, 48, or 72 h (silencing assay) before preparation for flow cytometry analysis. For the silencing assay, the culture medium was replaced after 48 h of incubation.

All reported concentrations refer to the concentration of the cyclodextrin derivative (CD) employed in the formulation of the nanovectors

All experiments were performed in triplicate, and results are reported as mean ± standard deviation. For samples including a control group, statistical significance relative to the control was assessed by calculating p-values using GraphPad Prism software 2023 (GraphPad Software, San Diego, CA, USA).

2.12. Fluorescence Microscopy

Fluorescence images were acquired for transfection efficiency (24- and 48-h) post-treatment using an inverted fluorescence microscope Olympus IX73 (Olympus Corporation, Tokyo, Japan). The microscope was equipped with a digital camera and a filter set appropriate for the fluorophore used (CY3 for internalization and FITC for transfection respectively).

Images were captured using a 20× objective lens. Exposure time, gain, and contrast were adjusted to avoid saturation and maintain comparability between samples. Image acquisition was performed using the CellSens Standard software (Olympus Corporation, Tokyo, Japan). No image manipulations that could affect data interpretation were applied.

2.13. Flow cytometry

Flow cytometry was performed for transfection efficiency (24 and 48 h) and silencing efficiency (24, 48 and 72h) using a CytoFLEX flow cytometer (Beckman Coulter, Brea, CA, USA), collecting 10,000 cells/sample. Data were analyzed using CytExpert software (Beckman Coulter, Brea, CA, USA).

At the designated time points, the medium was removed, and cells were washed with 300 µL of PBS. Then, 120 µL of trypsin was added to each well and cells were incubated for 3 min at 37 °C to allow detachment. Subsequently, 380 µL of complete culture medium was added to neutralize the trypsin, and the cell suspension was transferred to 2 mL Eppendorf tubes.

Samples were centrifuged for 5 min at 1000 rpm using an Eppendorf 5425 R centrifuge (Eppendorf, Hamburg, Germany). The supernatant was discarded, and the cell pellet was resuspended in 400 µL of PBS supplemented with 10% FBS. The samples were kept on ice until analysis.

Results

3.1. Synthesis and characterization of newly customized cationic ß-Cyclodextrins

The synthesis of cationic amphiphilic β-cyclodextrin (β-CD) derivatives (5a, 5b, and 6) was achieved through a four-step regioselective sequence, as delineated in Figure 2.

Regioselective Halogenation: The primary face of β-CD was brominated to yield heptakis(6-deoxy-6-bromo)-β-cyclodextrin (1), following a modified Defaye procedure (Defaye et al., 1991). Selective Halogenation at Primary Positions of Cyclomaltooligosaccharides and a Synthesis of Per-3, 6-anhydro Cyclomaltooligosaccharides (Gadelle and Defaye, 1991). This approach ensures selective substitution at the C-6 positions while leaving the secondary hydroxyl groups intact.

Exhaustive Thiolation: Nucleophilic displacement of the primary bromides in 1 was performed using long-chain alkanethiols (1-octanethiol or 1-hexadecanethiol) in DMF, facilitated by sodium methoxide. This transformation yielded the amphiphilic intermediates 2a and 2b. These derivatives exhibit a distinct facial polarity, featuring a lipophilic primary rim anchored by thioether-linked alkyl chains, while maintaining the hydrophilic nature of the secondary face through the unmodified C-2 and C-3 hydroxyl groups.

Secondary-Side Functionalization: Regioselective allylation of the secondary face (C-2 and C-2/C-3 positions) was conducted in DMF using sodium hydride as the base (Poly-6-cationic amphiphilic cyclodextrins designed for gene delivery (Byrne et al., 2009). This transformation produced the per-allylated scaffold 4 and the partially allylated derivative 3a and 3b, providing the necessary terminal alkenes for subsequent conjugation.

Thiol-ene Click Chemistry: The final architecture was realized through the AIBN-initiated radical addition of cysteamine hydrochloride to the terminal allyl groups on the secondary face. This thiol-ene "click" reaction proceeded with high efficiency and absolute anti-Markovnikov regioselectivity, appending seven or fourteen cationic amino groups depending on the scaffold. This step significantly enhances the hydrophilic-lipophilic balance of the system, transforming the intermediates into the target polycationic amphiphiles (5a, 5b, and 6). The resulting clusters combine a rigid hydrophobic base with a highly dense cationic corona, optimized for electrostatic interaction with anionic biomolecules.

All CD derivatives were fully characterized by Thin Layer Chromatography (TLC), Matrix-Assisted Laser Desorption/Ionization (MALDI-TOF) mass spectrometry, and a combination of 1D and 2D NMR spectroscopy. Comprehensive analytical data are provided in the Supporting Information.

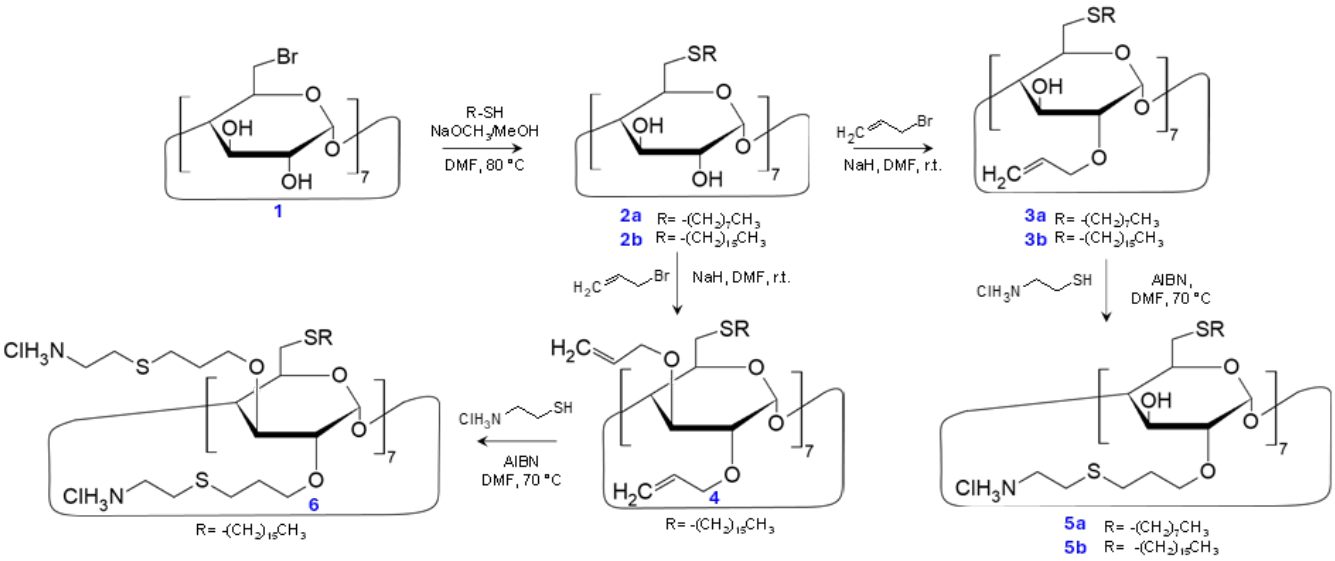

Figure 2. Synthetic route to cationic amphiphilic cyclodextrin derivatives.

3.2. Formulation and physico-chemical characterization

All three CDs were soluble in chloroform at room temperature, forming stable solutions for 2–3 days, while they showed variable stability in aqueous and hydroalcoholic media. In RNAse free water, the CDs solubilized after 15 min of agitation at 50 °C followed by 30 min mixing at 37°C. CD2 displayed the best aqueous dispersibility, remaining stable for approximately 12 hs, while CD1 and CD3 only for 1-2 h. CD1 and CD3 dissolved in ethanol after heating at 50 °C for 10 min; however, they undergo to precipitation upon returning to room temperature. CD2 could be dispersed in ethanol, DMSO, HEPES, and water after agitation at 50 °C for 10 to 40 minutes, but precipitation occurred upon cooling in all solvents.

Based on these findings, the optimal conditions for solubilizing the CDs were identified as follows: for CD1, either dissolution in chloroform or dispersion in water under agitation at about 50 °C for 40 min; for CD2, dispersion in water under the same conditions was selected as the preferred method.

As mentioned in section 2.3, NVs were prepared and loaded with pGFP using two methods for CD1 (in chloroform and RNAse free water) and one method for CD2 (in RNAse free water). This choice was driven by the variation in physicochemical features observed between the two CD derivatives: CD2 is stable when dispersed in aqueous medium, whereas CD1 tends to re-precipitate within a short time if it is not promptly complexed with genetic material. For this reason, it appeared relevant to investigate whether these distinct formulation strategies could influence the properties and performance of the resulting NVs. CD derivatives are amphiphilic and exhibit self-assembling behavior in aqueous environments. Upon dispersion, the molecules initially exist as monomers, which progressively aggregate until reaching the critical micellar concentration (CMC), where nanosized vesicular structures are formed. CMC data are reported in Supplementary materials S0.To identify the optimal formulation conditions, different CD concentrations were tested, and the resulting assemblies were characterized at DLS. A CD concentration of 2 mg/mL was selected as it yielded NVs with the desired size distribution and PdI (Auzély-Velty et al., 2000; Brettner et al., 2024; Trotta et al., 2012).

Successful nanovector formation was defined based on the ability to obtain reproducible dispersions with mean size below 300 nm, PdI ≤ 0.3, and no visible precipitation within the experimental timeframe.

Based on these criteria, CD1 and CD2 were selected for further investigation, while CD3 was excluded due to the formation of large, highly polydisperse aggregates (>700 nm), which were deemed unsuitable for gene delivery applications.

3.2.1. DLS and ELS Analyses

Tables 2 and 3 report the Size, PdI, and ZP values of the NVs before and after complexation with pGFP, for both CD1 and CD2. The CDs exhibit greater heterogeneity (with a PdI around 0.4–0.5) prior to complexation with pGFP. After complex formation, the PdI decreases ranging from 0.2 and 0.3, supporting the hypothesis of an underlying electrostatic interaction. ZP remained relatively high, which prompted the introduction of an anionic polymer into the formulation, as described in Section 2.3. A decrease in PdI was observed for the HA-containing formulation, while both HA and PSA led to a reduction in ZP potential compared to unmodified CD NVs.

Empty NVs	**Size (nm)**	**PdI**	**Zeta potential (mV)**
CD1(A)	231 ± 13	0.2	+41 ± 3
CD1 (B)	128 ± 63	0.4	+38 ± 6
CD2	54 ± 12	0.5	+41 ± 3
CD1+HA	195 ± 11	0.2	+28 ± 3
CD2+HA	160 ± 13	0.2	+30 ± 3
CD1+PSA	188±16	0.3	+31±4
CD2+PSA	172± 15	0.3	+23±6

Table 2. DLS and ELS analyses of empty CD-NVs. n=3 mean ± S.D.

NVs with pGFP	**Size (nm)**	**PdI**	**Zeta potential (mV)**
CD1(A)	178 ± 19	0.2	+39 ± 2
CD1(B)	163 ± 23	0.2	+44 ± 2
CD2	158 ± 18	0.3	+38 ± 4
CD1+HA	166 ± 18	0.2	+31 ± 3
CD2+HA	155 ± 18	0.2	+30 ± 3
CD1+PSA	180±13	0.3	+29±5
CD2+PSA	164±22	0.3	+20±5

Table 3. DLS and ELS analyses of CD-NVs loaded with pGFP. n=3 mean ± S.D.

.

3.2.2. Morphological analysis

TEM analysis of CD–pGFP complexes revealed heterogeneous and irregularly shaped nanostructures (provided in the Supplementary Materials (S1)) a morphological feature that is fully consistent with the cryo-EM findings (Figure 3). The overall size of polyplexes is well in line with DLS results, though these images evidence a more complex internal architecture, which cannot be accounted for by DLS data analysis, which models the scattering objects as equivalent spheres tumbling in solution. More details can be captured by SAXS (vide infra).

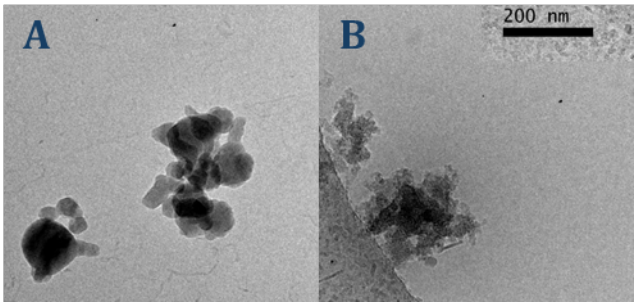

Figure 3. Cryo-em Images of CD1+pGFP (A) and CD2+pGFP (B).

3.1.3. Syncrotron SAXs Figure 4 reports the SAXS intensity diagrams of empty and complexed CDs and the corresponding best fits.

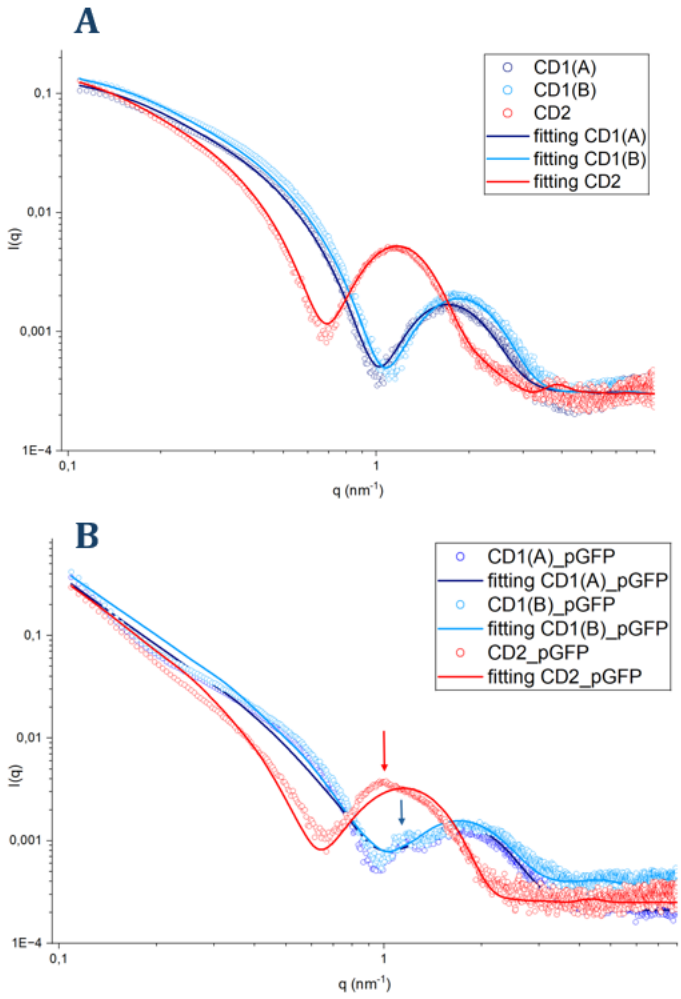

Figure 4. SAXS diagrams of the experimental (open circles) and fitted (continuous lines) empty CDs (A) and CD complexed with pGFP (B). The meaning of arrows reported in Fig 3B are explained in the text.

All these curves were fitted by using the "core-shell bicelle elliptical belt rough" model, suggesting that structural basic units in the structure of these CD NVs were elongated elliptical aggregates.

In particular, the x_core parameter of the model, which defines ellipticity, i.e. the axial ratio of the bicelle. took values between 0.1 and 0.2, consistently with an elongated shape in the length scale of few nanometers, i.e. below the values probed by cryo-TEM. A similar shape had also been reported in other modified β-cyclodextrins which tend to assume an ellipsoid configuration upon aggregation (Zerkoune et al., 2014). The SAXS diagrams of CD1(A) and CD1(B) show the same general pattern despite the different preparation methods. On the contrary, CD2 exhibits distinct features in the q range between 0.5 and 2 nm-1 with intensity minima shifted toward lower q values indicating the presence of objects with larger size (the obtained radius was 1,8 and 1.5 nm, respectively).

Figure 3 B shows the SAXS curves of CD NVs after complexation with pGFP. The main characteristics of the SAXS diagrams of these systems were fitted using the same model as for their unloaded counterparts, showing that the shape of flattened objects was substantially retained after interaction with pGFP.

In particular, for CD1 complexes a small increase in thickness and radius was observed while the x-core parameter and eccentricity remain unchanged. On the other hand, the scattering profile of NVs with CD2 showed increased asymmetry, and this effect was reproduced by assuming larger eccentricity of NVs, while the q-position of the minima

and peaks remained unchanged. It is worth noting that a secondary peak (evidenced by arrows in Fig 3B), positioned around 1 nm^{-1} emerged in the SAXS diagrams of CDs loaded with pGFP. Following the interpretation given by Safinya and coworkers who have reported the same small peak in multilamellar liposomes with DNA sandwiched between cationic bilayers (Rädler et al., 1997), we attributed this feature to the pGFP correlation. Therefore, in the CD-pGFP system the DNA strands were intercalated among layers of CD NVs. The best-fit parameters and diagram of a single CD of the SAXS diagrams shown in figure 3A and 3B are reported in the Supplementary Materials (S2-S3-S4).

3.2.4 NVs Stability

Figure 5 shows the variation in size and ZP for CD loaded with pGFP NVs stored at 4°C (± 1°C) (B) after 1, 4, and 7 days. A slight increase in size and a decrease in ZP was observed over time; however, the formulations remained stable throughout the observation period.

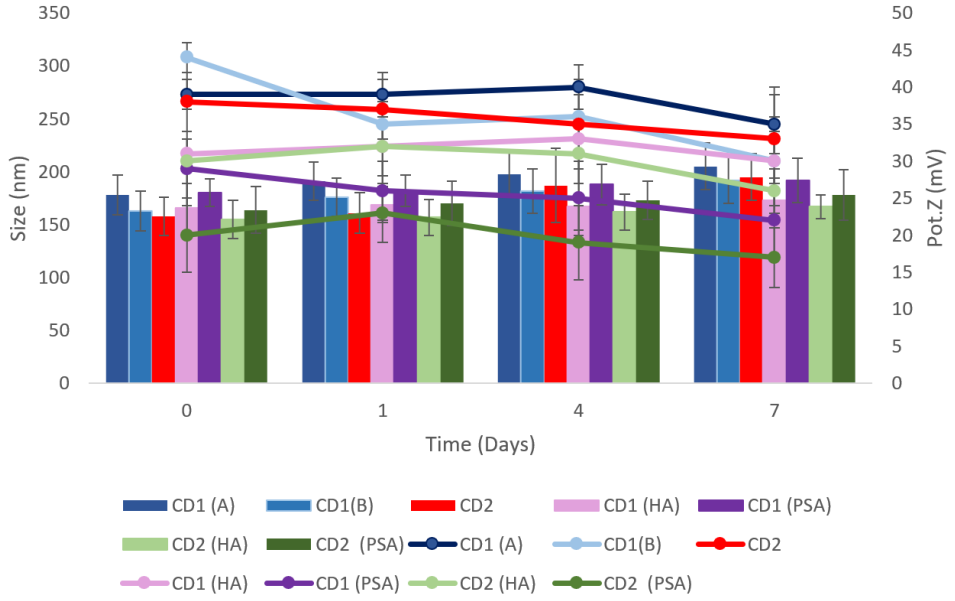

Figure 5. Stability of CD NVs with pGFP at 4°C (± 1°C). CD1(A) (blue), CD1(B) (sky blue), CD2 (Red), CD1 (HA) (pink), CD1 (PSA) (violet), CD2 (HA) (Light green), CD2 (PSA) (Dark Green). n=3 mean ± S.D.

The stability of NVs with pGFP was also evaluated in cell culture medium (DMEM), both with and without FBS supplementation. Figure 6 shows the evolution of particle size and derived count rate (Kcps) over time for NVs in supplemented medium.

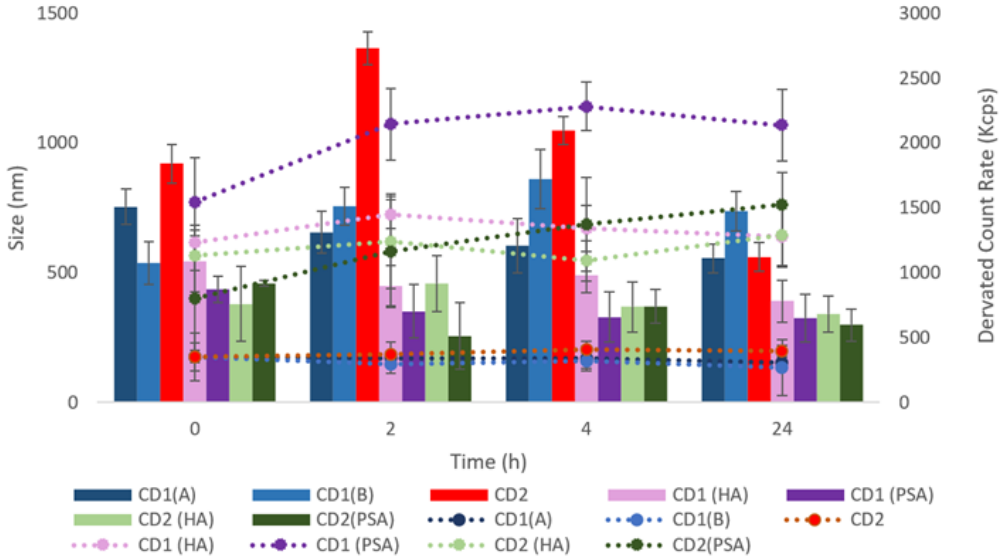

Figure 6. Stability of CD NVs with pGFP In DMEM with FBS. CD1(A) (blue), CD1(B) (sky blue), CD2 (Red), CD1 (HA) (pink), CD1 (PSA) (violet), CD2 (HA) (Light green), CD2 (PSA) (Dark Green). n=3 mean ± S.D.

The NVs showed an initial size increase followed by stabilization over time. Since cells are routinely cultured in DMEM supplemented with FBS and considering that this environment does not perfectly mimic physiological conditions, we consider it appropriate to proceed with further cellular studies under these supplemented conditions. The graph of CD NVs in DMEM is reported in supplementary materials (S5).

3.2.5 Complexation efficacy

Complexation efficiency was verified by horizontal agarose gel electrophoresis performed as described in Section 2.09. The resulting images were analyzed according to paragraph 2.9, confirming an encapsulation efficiency greater than 90% for all tested formulations. In contrast, samples treated with heparin exhibited a release of pGFP, showing a band intensity comparable to that of free pGFP. The corresponding figures and graphs illustrating these results are provided in the Supplementary Materials (S6-S7).

3.3 In *vitro* studies

3.3.1 MTT Assays

MTT assays were performed on HeLa cell lines to evaluate the cytotoxicity of the tested nanocarriers. As a first step, blank CD NVs were tested to screen for non-toxic concentration ranges. The results of this preliminary assessment are shown in Figure 7A. Contrary to expectations, the incorporation of HA and PSA did not reduce cytotoxicity. A possible explanation, consistent with previous studies (Thwala et al., 2018), is that although HA is generally regarded as biocompatible, its inclusion may alter NVs uptake mechanisms or extracellular stability, leading to increased intracellular accumulation or aggregation. In addition, HA–NVs interactions could elicit distinct cellular responses depending on receptor expression patterns. For all the empty formulation, the concentration of 31 µg/mL showed no significant difference compared to the control.

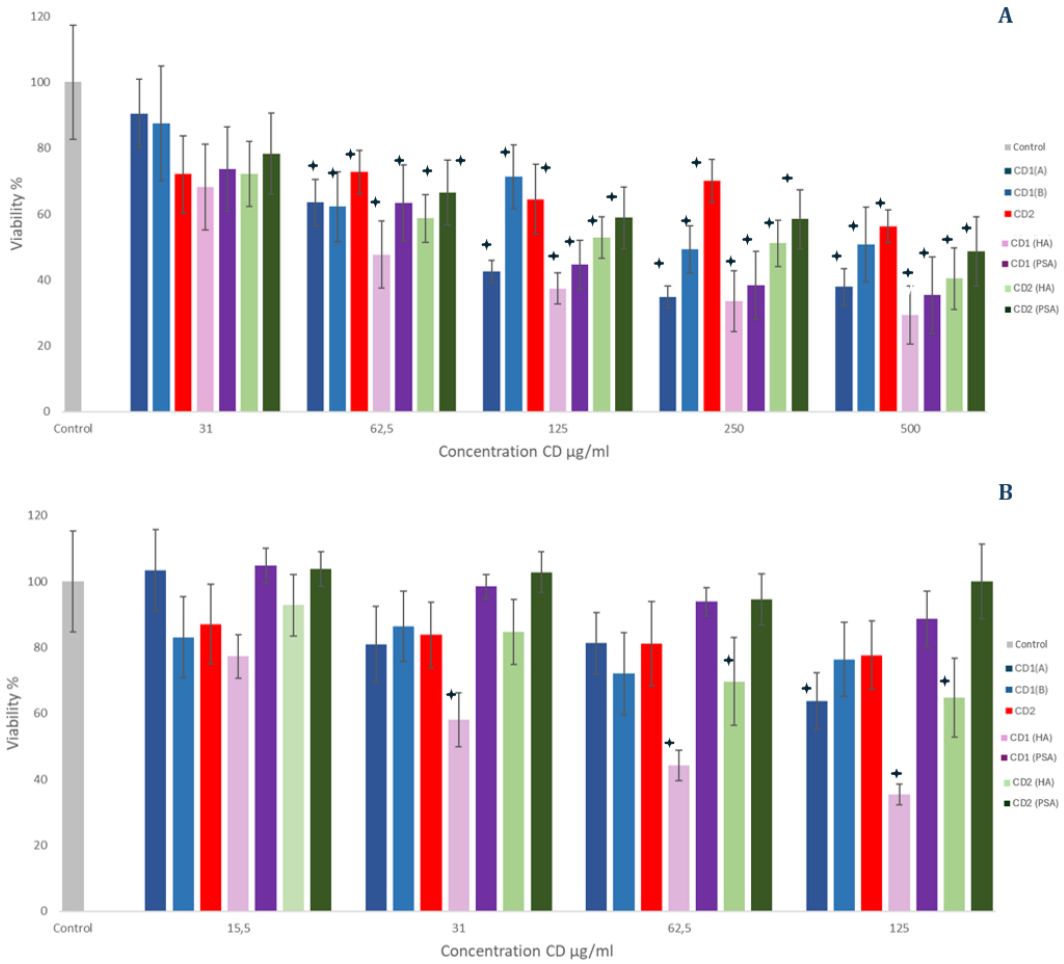

Figure 7. MTT Assays of empty (A) and pGFP loaded (B) CD NVs in HeLa Cells. CD1(A) (Blue) CD1(B) (light Blue), CD2 (Red), CD1 (HA) (pink), CD1 (PSA) (violet), CD2 (HA) (Light green), CD2 (PSA) (Dark Green). n=3 mean ± S.D. Statistical significance relative to the control was evaluated by calculating the p-value using a two-factor t-test. Data showing statistically significant differences compared to the control are indicated with an asterisk.

Based on these results, the concentrations were reduced for the evaluation of CD NVs with pGFP, as shown in Figure 7B. The data indicate an increased "safe" concentration range for CD- pGFP complexes compared to blank NVs. This effect is likely attributable to the reduction in surface potential following plasmid complexation, which may decrease interactions with the cell membrane and thereby reduce cytotoxicity. No significant cytotoxic effects were observed at the tested concentrations, except for CD1(A) and CD2 (HA), which exhibited cytotoxicity at 125 µg/mL, defining 62.5 µg/mL as the safe dose and CD1(HA) which showed a safe dose at 15,5 µg/mL.

Given the comparable results of the two CD1 production methods (A and B) in terms of size, PdI, and Z, and the demonstrated stability of both formulations, subsequent studies were focused on CD1(B) and CD2. CD1(B) was selected due to slightly improved complexation with P and a higher cell-safe dose, while CD1(A) was excluded.

MTT assays were also performed on RAW 264.7 cells for CD1 and CD2, both with and without pGFP, showing the same trend and indicating a higher safe dose compared to HeLa cells. The corresponding data are provided in the Supplementary Materials (S8).

3.3.2. Cellular uptake and transfection efficiency

Before assessing transfection, internalization efficiency was evaluated for CD1 and CD2 in both HeLa and RAW cells after 24 h of incubation. For RAW 264.7 cells, experiments were conducted at 37 °C and 4 °C to distinguish actual internalization from surface binding. The results demonstrated internalization levels exceeding 85% for all tested concentrations in both cell lines. The corresponding data are reported in the Supplementary Materials (S9-S10).

Transfection efficiency was carried out as described in Section 2.10. Cytofluorimetry analysis was performed after 24 and 48 h for NVs formulated with CD1, CD2, and with the addition of HA or PSA, the results are reported in figure 8.

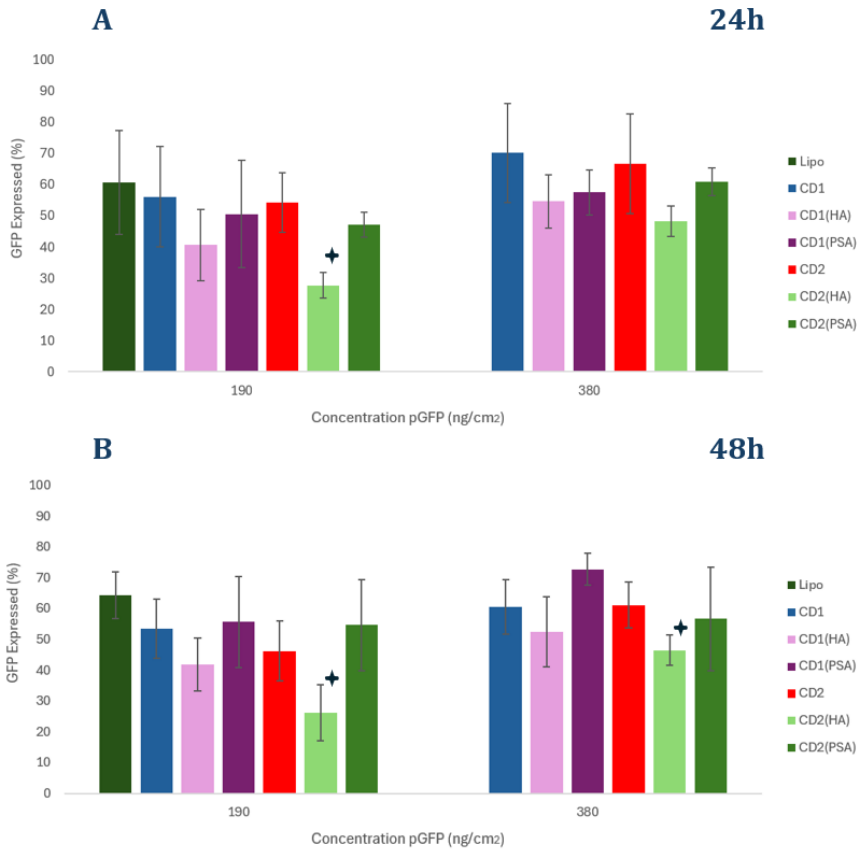

Figure 8. Cytofluorimetric Data of Transfection Efficiency of NVs loaded with pGFP (HA/PSA coated) on HeLa cells after 24h (A) and 48h (B). Lipofectamine (Green), CD1(B) (light blue), CD2 (Red), CD1 (HA) (pink), CD1 PSAP) (violet), CD2 (HA) (Light green), CD2 (PSA) (Dark Green). n=3 mean ± S.D. Statistical significance relative to the control was evaluated by calculating the p-value using a two-factor t-test. Data showing statistically significant differences compared to the control are indicated with an asterisk.

A substantial level of transfection was already achieved at 24 h, and at 48 h transfection increased slightly, with reduced variability as indicated by smaller error bars. Among the two pGFP concentrations tested (190 and 380 ng/cm^2), both resulted in similarly high transfection levels, with no substantial differences between them. Therefore, 190 ng/cm^2 can be considered optimal, as it provides comparable transfection efficiency while using a lower amount of material, thereby representing a safer option. After 24 h, transfection efficiency was relatively high for all tested formulations, above 55%, comparable to those obtained with Lipofectamine, which was used as the reference gold standard (Bramato et al., 2019; Bulkescher et al., 2017; Shi et al., 2018). Similar results were observed after 48 h. Statistical analysis revealed a significant difference in transfection percentage only for the CD2 (HA) formulation when compared to the control. However, analysis of GFP fluorescence intensity, reported in Supplementary Materials (S11), showed that CD2-based formulations exhibited lower GFP expression intensity, particularly after 48 h, indicating reduced levels of transgene expression despite comparable transfection efficiencies.

In Figure 9, the transfection images acquired by fluorescence microscopy are reported. Consistent with the quantitative data, these images confirm that transfection is higher in cells treated with CD1-based NVs compared to those treated with CD2.

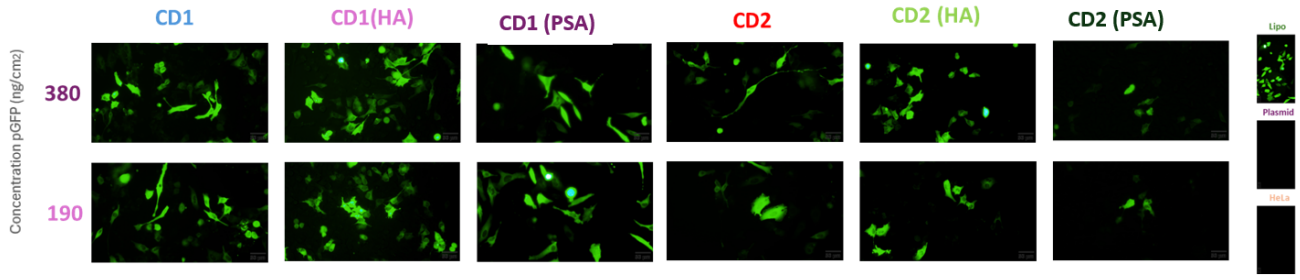

Figure 9. Representative fluorescence microscopy images of HeLa cells after 48h of transfection.

We can conclude that the CD1-based formulations exhibit the best transfection performance, achieving a percentage of transfected cells comparable to that obtained with Lipofectamine.

3.4 siRNA complexation

NVs of CD1 and CD2, with or without HA or PSA, were additionally complexed with GFP-targeting-siRNA at an N/P ratio of 10, following the methodology outlined in Section 2.3. Due to the high cost of siRNA, only preliminary experiments were conducted. DLS and ELS data, reported in table 4, showed an increase in size and PdI for all the formulations, except for those containing HA, that showed sizes around 150-180 nm and PdI= 0.3.

Formulation	**Size (nm)**	**PdI**	**Zeta potential (mV)**
CD1	255 ± 45	0.5	+ 33 ± 5
CD2	156± 38	0.4	+25 ± 8
CD1 (HA)	187 ± 24	0.3	+25 ± 5
CD2 (HA)	158 ± 20	.,3	+23 ± 6
CD1 (PSA)	230 ± 65	0.4	+25 ± 8
CD2 (PSA)	178 ± 48	.,4	+26 ± 6

Table 4. DLS and ELS analyses of CD-NPs loaded with siRNA (N/P=10). n=3 mean ± S.D.

Complexation efficacy was good for all the formulations (around 98%), data are reported in supplementary materials (S12-13).

3.4.1 Silencing efficiency

Silencing efficiency of all NVs was evaluated in GFP-expressing HeLa cells and quantified by flow cytometry after 24, 48, and 72 h. GFP-targeting siRNA requires a longer time compared with pDNA transfection onset to achieve gene silencing. After 24 h, all formulations, including Lipofectamine, exhibited less than 15% silencing activity. Flow cytometry data at 48 and 72 h are shown in Figure 10. A clear increase in silencing efficiency was observed at 48 h, particularly for CD1-based formulation. Statistically significant differences compared to Lipofectamine were observed for all CD2 formulations at 190 ng/cm^2 and for the CD2/HA formulation at 380 ng/cm^2. A similar trend was observed after 72 h. Since no statistically significant differences were detected between the two tested concentrations, the lower concentration was considered preferable, as it provides comparable silencing efficiency while potentially reducing side effects. In addition, lower variability, as indicated by smaller standard deviations, was observed for CD1-based samples, suggesting greater reproducibility of these formulations.

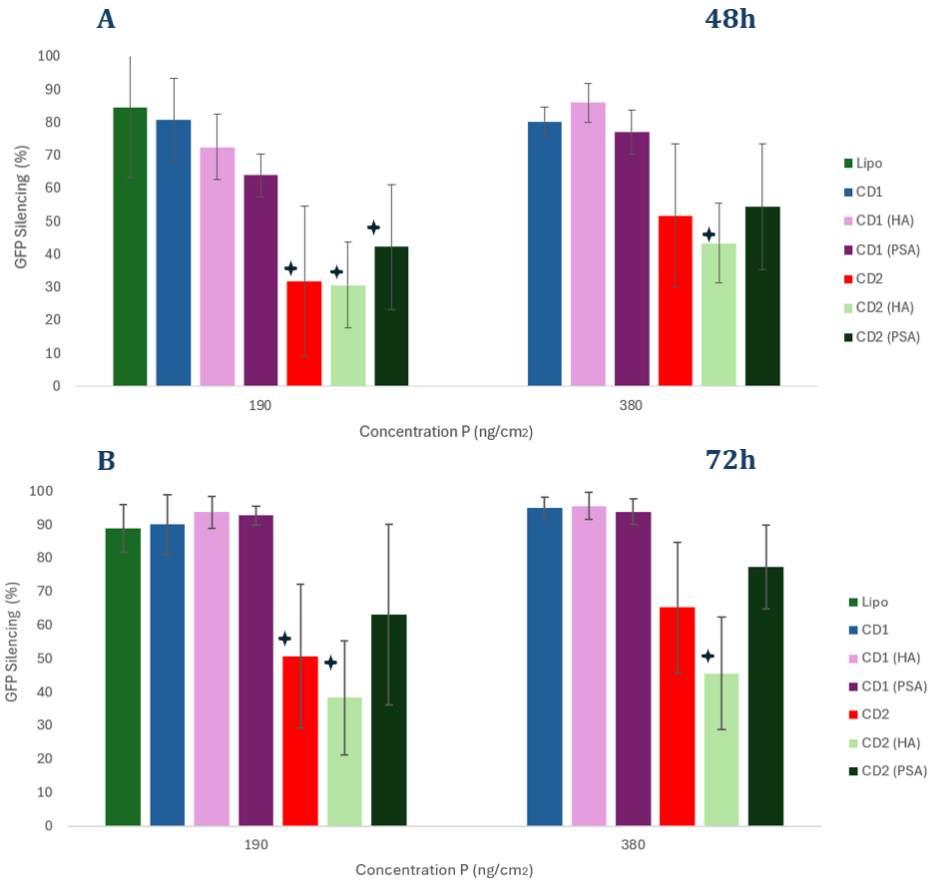

Figure 10. Cytofluorimetric Data of Silencing Efficiency of NVs with siRNA (HA/PSA) on HeLa GFP cells after 48h (A) and 72h (B) . Lipofectamine (Green), CD1(B) (light blue), CD2 (Red), CD1 (HA) (pink), CD1 (PSA) (violet), CD2 (HA) (Light green), CD2 (PSA) (Dark Green). n=3 mean ± S.D. Statistical significance relative to the control was evaluated by calculating the p-value using a two-factor t-test. Data showing statistically significant differences compared to the control are indicated with an asterisk.

Figure 11 reports the GFP fluorescence intensity data, which further confirm that CD1-based NVs achieve higher silencing efficiency compared with CD2-containing formulations. The GFP intensity of CD1 NVs was comparable to that obtained with Lipofectamine. The lowest fluorescence levels were detected at 72 h, highlighting the maximal silencing efficacy at this time point.

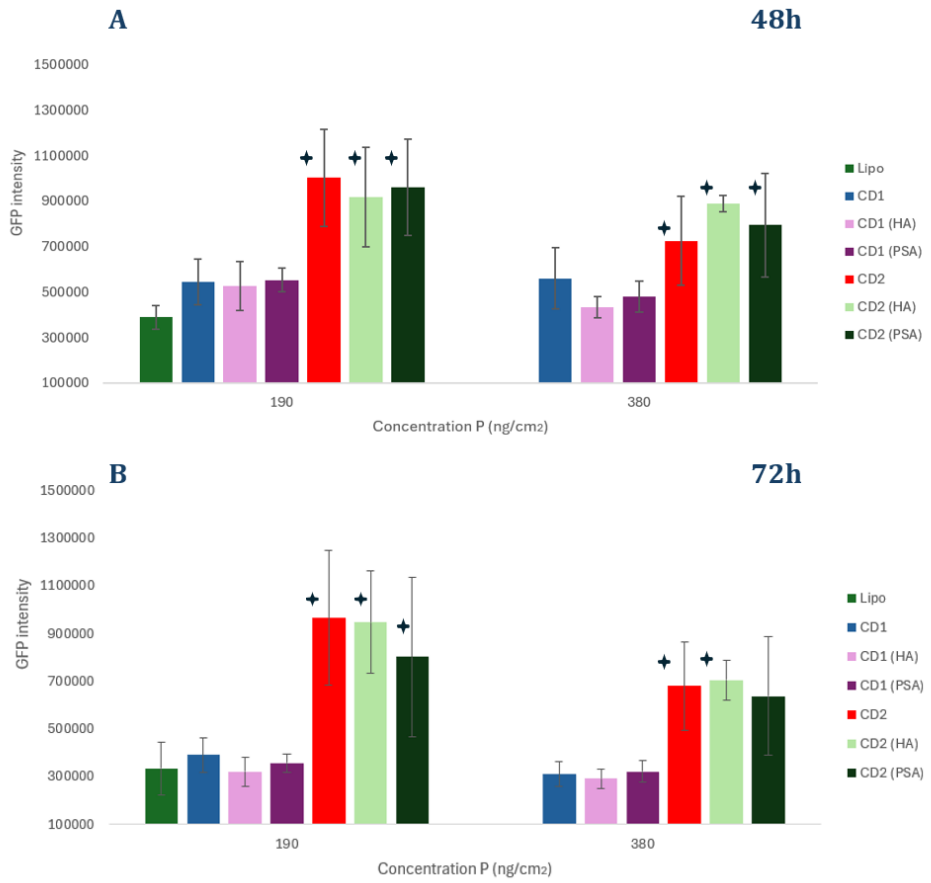

Figure 11. Cytofluorimetric *Data of GFP Fluorescence intensity of NVs with siRNA (HA/PSA) on HeLa cells after 48h (A) and 72h (B). Lipofectamine (green), CD1*(B) (light blue), CD2 (Red), CD1 (HA) (pink), CD1 (PSA) (violet), CD2 (HA) (Light green), CD2 (PSA) (Dark Green). n=3 mean ± S.D. Statistical significance relative to the control was evaluated by calculating the p-value using a two-factor t-test. Data showing statistically significant differences compared to the control are indicated with an asterisk.

We can conclude that the CD1-based NVs shows great potential, achieving a percentage of silenced cells and GFP intensity comparable to that obtained with Lipofectamine.

Discussions

Cationic and amphiphilic β-cyclodextrin derivatives have been widely explored as non-viral vectors for nucleic acid delivery, owing to their biocompatibility and modular chemical structure. Several studies have reported efficient DNA or siRNA delivery using β-CDs functionalized with multiple cationic groups, targeting ligands, or polymeric segments to enhance complexation and cellular uptake. For instance, Godinho et al. described self-assembling cationic β-cyclodextrin nanoparticles for neuronal siRNA delivery, achieving approximately 40–60% gene silencing depending on formulation and dose, albeit with a narrow therapeutic window due to dose-dependent cytotoxicity (Godinho et al., 2013). Similarly, Fitzgerald et al. reported anisamide-targeted cyclodextrin nanocomplexes for siRNA delivery in prostate cancer cells, reaching silencing efficiencies around 60–70%, but requiring receptor-specific targeting moieties and multicomponent architectures to achieve optimal performance (Fitzgerald et al., 2016).

Other approaches have relied on polymer–cyclodextrin hybrids or CD–polyethyleneimine conjugates to improve transfection efficiency. Liu et al. demonstrated tetraethylenepentamine-coated β-cyclodextrin nanoparticles capable of delivering both DNA and siRNA, achieving transfection and silencing levels comparable to commercial reagents;

however, these systems exhibited relatively high surface charge and required careful optimization to limit cytotoxicity (Liu et al., 2022). Comparable results were reported for folate-modified β-cyclodextrin–PEI copolymers, which showed enhanced uptake and silencing but at the expense of increased structural complexity and potential safety concerns (Li et al., 2023).

In this context, the CD1-based NVs developed in the present study offer several distinctive advantages. CD1 NVs achieves transfection efficiencies above 55% and siRNA-mediated silencing exceeding 90%, values that are fully comparable to Lipofectamine, without the need for polymer conjugation or targeting ligands. Notably, these performances are obtained using a single-component cyclodextrin derivative, formulated through a straightforward self-assembly process.

While many reported CD-based systems prioritize either DNA transfection or siRNA silencing, CD1 demonstrates dual functionality, effectively delivering both plasmid DNA and siRNA within the same formulation framework. This versatility compares favorably with previously published cyclodextrin systems that require different chemical designs for pDNA versus siRNA delivery (Malhotra et al., 2018; Mendonça et al., 2021).

Despite exhibiting a relatively high positive ZP, CD1 NVs display an acceptable cytotoxicity profile at biologically effective doses, in line with or better than several multicationic CD formulations reported in the literature (Ceborska, 2017; Kont et al., 2022). Importantly, the addition of HA or PSA allows partial modulation of surface charge without compromising transfection or silencing efficiency, a feature not consistently observed in other CD-based nanocarriers.

Finally, the superior biological performance of CD1 compared with CD2 highlights the relevance of fine structural tuning in cyclodextrin design. The presence of a shorter hydrophobic chain (C8) combined with a single protonable amine appears to provide a more favorable balance between membrane interaction, intracellular trafficking, and endosomal escape, as opposed to longer alkyl chains and higher charge density, which have been associated with reduced expression levels or increased toxicity in other CD-based systems (Nazli et al., 2025).

Conclusions

In this study we obtained favorable aggregation properties forming NVs for two of the three cationic modified β-CDs tested (CD1 and CD2) upon complexation with pGFP. Although these complexes displayed somewhat irregular morphology, ZP, TEM imaging and SAXS analyses indicated that the genetic material was successfully encapsulated within the NVs. The architecture of the developed NVs, emerging from in depth physico-chemical investigation, can be described as follows: small ellipsoids of 1.5-2 nm are joined together in clusters with 10-50 nm mean size, which are in turn super-assembled to form the scattering objects with 150-200 nm diameter, as revealed by DLS. *In vitro* tests showed that CD1 NVs achieved a transfection efficiency of approximately 55%, outperforming CD2 NVs. The incorporation of anionic polymers HA and PSA did not induce substantial changes, aside from a reduction in ZP, and the modified NVs exhibited behavior comparable to their unmodified counterparts. NVs complexed with siRNA demonstrated promising performance, particularly CD1 NVs, which produced greater gene silencing than CD2 NVs, achieving knockdown efficiencies above 90%, comparable to those obtained with Lipofectamine. Notably, NVs containing HA showed improved size and PdI. The differences observed between CD1 and CD2 NVs may be attributable to their distinct structural features. CD1 contains a shorter lipophilic chain (C8) compared with CD2 (C16) and carries only one protonable amine group, whereas CD2 possesses two protonable amine groups. These variations are likely to influence their interactions with cellular membranes and their behavior during endosomal trafficking. In particular, the combination of a shorter hydrophobic tail and a single amine group in CD1 may facilitate a more efficient membrane interaction and promote endosomal uptake or escape. Overall, these vectors still require further optimization and evaluation using nucleic acid encoding disease-relevant genes, both in appropriate cellular models and *in vivo*, to fully assess their targeted therapeutic potential. Conversely, the presence of sulfur-containing lipid chains offers a robust platform for ligand conjugation, providing a versatile strategy for future NV functionalization.

Acknowledgements

The authors would like to acknowledge the CIMUS research center at the University of Santiago de Compostela for hosting part of this work and providing access to its facilities and instrumentation. We are also grateful to Milo Malanga and CarboHyde Z.r.t. for their support and valuable input in the design and development of the modified cyclodextrins used in this study. The ID02 beamline of the ESRF (Grenoble, France) is acknowledged for providing beamtime. We acknowledge co-funding from Next Generation EU, in the context of the National Recovery and Resilience Plan, M4C2 Investment 1.4 CN_00000041 National Center for Gene Therapy and Drugs based on RNA Technology CUP B13C22001010001. The authors thank MIUR-Italy ("Progetto dipartimenti di eccellenza 2023–2027" allocated to the Department of Chemistry "Ugo Schiff", University of Florence, Italy).

Author contributions

Conceptualization, I.C., M.M. and F.M. ; methodology, I.C., F.M., S.R., L.V.F., M.M and N.C. ; investigation, I.C. , G.P., L.V.F. ; data analysis, I.C., G.P. A.G., P.F., S.F. and L.V.F.; Interpretation, I.C., G.P., S.F., A.G. and L.V.F.; writing—original draft preparation, I.C., M.M.; writing—review and editing, I.C., A.R.B, F.M., S.R and N.C.; project administration, F.M., A.R.B., S.R., F.R. and N.C funding acquisition, A.R.B., F.M., S.R. and N.C. All authors have read and agreed to the submitted version of the manuscript.

Funding

Funded by the European Union - Next Generation EU. National Recovery and Resilience Plan, Mission 4 Component 2 - Investment 1.4 - CN00000041 - 'Centro Nazionale' National Centre for Gene Therapy and Drugs based on RNA Technology (CN3, PNRR, Spoke 5: Inflammatory and infectious diseases). CUP B13C22001010001. Views and opinions expressed are, however, those of the author(s) only and do not necessarily reflect those of the European Union or the European Commission. Neither the European Union nor the European Commission can be held responsible for them.

Funded by Competitive Reference Groups (ED431C 2021/17-FEDER) and Ministerio de Ciencia e Innovación, Gobierno de España (PID2022-142689OB-I00).

Declaration of Competing Interest

The authors declare that they have no known competing financial interests or personal relationships that could have appeared to influence the work reported in this paper.

Appendix A

Supplementary data associated with this article can be found in the online version.

References

Aiuti, A., Pasinelli, F., Naldini, L., 2022. Ensuring a future for gene therapy for rare diseases. Nature Medicine 28, 1985–1988. https://doi.org/10.1038/s41591-022-01934-9

Androsavich, J.R., 2024. Frameworks for transformational breakthroughs in RNA-based medicines. Nature reviews Drug Discovery 6, 421–444. https://doi.org/10.1038/s41573-024-00943-2

Auzély-Velty, R., Djedaini-Pilard, F., Perly, B., Zhemb, Th., 2000. Micellization of hydrophobically modified cyclodextrins. Langmuir 16, 3727–3734. https://doi.org/10.1021/la991361z

Bienvenu, C., Martínez, Á., Jiménez Blanco, J.L., Di Giorgio, C., Vierling, P., Ortiz Mellet, C., Defaye, J., García Fernández, J.G., 2012. Polycationic amphiphilic cyclodextrins as gene vectors: effect of the macrocyclic ring size on the DNA complexing and delivery properties. Organic & Biomolecular Chemistry 10, 3056–3063. https://doi.org/10.1039/c2ob25786f

Bramato, R., Garzanelli, V., Romano, A., 2019. Comparison of DNA-transfection efficiency in HeLa cells using K4 Transfection System and Lipofectamine 3000.

Brettner, F.E.B., Schreiner, J., Vogel-Kindgen, S., Windbergs, M., 2024. Engineered Self-Assembly of Amphiphilic Cyclodextrin Conjugates for Drug Encapsulation. ACS Biomaterials Science & Engineering 10, 115–128. https://doi.org/10.1021/acsbiomaterials.2c01023

Byrne, C., Sallas, F., Rai, D.K., Ogier, J., Darcy, R., 2009. *Organic & Biomolecular Chemistry* 7, 3763–3771. https://doi.org/10.1039/B906234A

Bulkescher, R., Starkuviene, V., Erfle, H., 2017. Solid-phase reverse transfection for intracellular delivery of functionally active proteins. Genome Research 27, 1752–1758. https://doi.org/10.1101/gr.215103.116

Ceborska, M., 2017. Folate appended cyclodextrins for drug, DNA, and siRNA delivery. European Journal of Pharmaceutics and Biopharmaceutics 120, 133–145. https://doi.org/10.1016/j.ejpb.2017.09.005

Cifani, N., Chronopoulou, L., Pompili, B., Di Martino, A., Bordi, F., Sennato, S., Di Domenico, E. G., Palocci, C., Ascenzioni, F., 2015. Improved stability and efficacy of chitosan/pDNA complexes for gene delivery. Biotechnology Letters 37(3), 557–565. https://doi.org/10.1007/s10529-014-1727-7

Chiarugi, I., Maestrelli, F., Piomboni, G., Ristori, S., Bilia, A.R., n.d. Non-Viral Nanovectors based on Cyclodextrins for siRNA delivery: an update to current technologies. Preprint. https://doi.org/10.20944/preprints202511.1747.v1

Csaba, N., Köping-Höggård, M., Alonso, M.J., 2009. Ionically crosslinked chitosan/tripolyphosphate nanoparticles for oligonucleotide and plasmid DNA delivery. International Journal of Pharmaceutics 382(1-2), 205–214. https://doi.org/10.1016/j.ijpharm.2009.07.028

Defaye, J., Gadelle, A., Pedersen, C., 1991. Hydrogen fluoride-mediated synthesis of 1-thiotrehaloses involving reaction of D-glucose with hydrogen sulfide. *Carbohydrate Research* 217, 51–58. https://doi.org/10.1016/0008-6215(91)84116-V

Di Silvio, D., Martínez-Moro, M., Salvador, C., De Los Angeles Ramirez, M., Caceres-Velez, P.R., Ortore, M.G., Dupin, D., Andreozzi, P., Moya, S.E., 2019. Self-assembly of poly(allylamine)/siRNA nanoparticles, their intracellular fate and siRNA delivery. Journal of Colloid and Interface Science 557, 757–766. https://doi.org/10.1016/j.jcis.2019.09.082

Doucet, M., Adams, M., Agouzal, N., Alina, G., Attala, Z., Bakker, J., Beaucage, P., Berger, J., Bouwman, W., Bourne, R., Butler, P., Cho, J.H., Cadwallader-Jones, I., Campbell, K., Cooper-Benun, T., Crake-Merani, J., Drosos, G., Durniak, C., Farrow, C., Ferraz Leal, R., Ford, R., Forster, L., Gaudet, J., Gerina, M., Gilbert, P., Gonzalez, M., Heenan, R., Hewins, E., Jackson, A., Jensen, G., Juhas, P., King, S., Karliczek, J., Kienzle, P., Krzywon, J., Lin, J., Liu, Y., Lopes, R., Lozano, D., Lytje, K., Mannicke, D.,

Maranville, B., Markvardsen, A., Martinez, N., McKerns, M., Miller, B., Mothander, K., Murphy, R., Nelson, A., Nielsen, T., O'Driscoll, L., Oakley, M., Park, H., Parker, P., Patrou, M., Peterson, P., Potrzebowski, W., Prescott, S., Rakitin, M., Richter, T., Rooks, J., Rozyczko, P., Shan, X., Snow, T., Stellhorn, A., Teixeira, S., Tumarkin, J., Washington, A., Weigandt, K., Whitley, R., Wilkins, L., Wolf, C., Cortes Hernandez, R., Zhang, A., Zheng, A., Fragneto, G., Fultz, B., Perring, T., Rod, T.H., Taylor, J., 2024. SasView version 6.0.0. https://doi.org/10.5281/ZENODO.11395968

Fiani, S., Maestrelli, F., Micheli, L., Cirri, M., Mennini, N., Mura, P., 2025. Curcumin's niosomes coated with chitosan for the treatment of osteoarthritis: effect of cyclodextrin complexation. International Journal of Pharmaceutics 682, 125933. https://doi.org/10.1016/j.ijpharm.2025.125933

Fitzgerald, K.A., Malhotra, M., Gooding, M., Sallas, F., Evans, J.C., Darcy, R., O'Driscoll, C.M., 2016. A novel, anisamide-targeted cyclodextrin nanoformulation for siRNA delivery to prostate cancer cells expressing the sigma-1 receptor. International Journal of Pharmaceutics 499, 131–145. https://doi.org/10.1016/j.ijpharm.2015.12.055

Gadelle, A., Defaye, J., 1991. Selective halogenation at primary positions of cyclomaltooligosaccharides and a synthesis of per-3,6-anhydro cyclomaltooligosaccharides. *Angewandte Chemie International Edition* 30, 78–80. https://doi.org/10.1002/anie.199100781

Godinho, B.M.D.C., Ogier, J.R., Darcy, R., O'Driscoll, C.M., Cryan, J.F., 2013. Self-assembling Modified β-Cyclodextrin Nanoparticles as Neuronal siRNA Delivery Vectors: Focus on Huntington's Disease. Molecular Pharmaceutics 10, 640–649. https://doi.org/10.1021/mp3003946

Haley, R.M., Gottardi, R., Langer, R., Mitchell, M.J., 2020. Cyclodextrins in drug delivery: applications in gene and combination therapy. Drug Deliv. and Transl. Res. 10, 661–677. https://doi.org/10.1007/s13346-020-00724-5

Isert, L., Gialdini, I., Ngo, T.M.H., Loiudice, G., Lamb, D.C., Merkel, O.M., 2025. Upholding hyaluronic acid's multi-functionality for nucleic acid drug delivery to target EMT in breast cancer. *Nanoscale* 17, 16256–16273. https://doi.org/10.1039/D5NR00808E

Kim, S. T., Chompoosor, A., Yeh, Y.-C., Agasti, S. S., Solfiell, D. J., Rotello, V. M., 2012. Dendronized gold nanoparticles for siRNA delivery. Small 8(21), 3253–3256. https://doi.org/10.1002/smll.201201141

Kont, A., Mendonça, M.C.P., Cronin, M.F., Cahill, M.R., O'Driscoll, C.M., 2022. Co-Formulation of Amphiphilic Cationic and Anionic Cyclodextrins Forming Nanoparticles for siRNA Delivery in the Treatment of Acute Myeloid Leukaemia. International Journal of Molecular Sciences 23, 9791. https://doi.org/10.3390/ijms23179791

Krishnan, A., Callanan, D.G., Sendra, V.G., Lad, A., Christian, S., Earla, R., Khanehzar, A., Tolentino, A.J., Vailoces, V.A.S., Greene, M.K., Scott, C.J., Kunimoto, D.Y., Hassan, T.S., Genead, M.A., Tolentino, M.J., 2024. Comprehensive Ocular and Systemic Safety Evaluation of Polysialic Acid-Decorated Immune Modulating Therapeutic Nanoparticles (PolySia-NPs) to Support Entry into First-in-Human Clinical Trials. Pharmaceuticals 17, 481. https://doi.org/10.3390/ph17040481

Li, F., Cao, D., Gu, W., Cui, L., Qiu, Z., Liu, Z., Li, D., Guo, X., 2023. Delivery of miR-34a-5p by Folic Acid-Modified β-Cyclodextrin-Grafted Polyethylenimine Copolymer Nanocarriers to Resist KSHV. ACS applied nanomaterials. https://doi.org/10.1021/acsanm.3c02162

Liu, C.-H., Shih, P.-Y., Lin, C.-H., Chen, Y.-J., Wu, W.-C., Wang, C.-C., 2022. Tetraethylenepentamine-Coated β Cyclodextrin Nanoparticles for Dual DNA and siRNA Delivery. Pharmaceutics. https://doi.org/10.3390/pharmaceutics14050921

Maiorano, G., Guido, C., Russo, A., Giglio, A., Rizzello, L., Testini, M., Cortese, B., D'Amone, S., Gigli, G., Palamà, I.E., 2022. Hybrid Polyelectrolyte Nanocomplexes for Non-Viral Gene Delivery with Favorable Efficacy and Safety Profile. Pharmaceutics 14, 1310. https://doi.org/10.3390/pharmaceutics14071310

Malhotra, M., Gooding, M., Evans, J.C., O'Driscoll, D., Darcy, R., O'Driscoll, C.M., 2018. Cyclodextrin-siRNA conjugates as versatile gene silencing agents. European Journal of Pharmaceutical Sciences 114, 30–37. https://doi.org/10.1016/j.ejps.2017.11.024

Mansouri, S., Cuie, Y., Winnik, F. M., Shi, Q., Lavigne, P. L., Benderdour, M., Beaumont, E., Fernandes, J. C., 2006. Characterization of folate-chitosan-DNA nanoparticles for gene therapy. Biomaterials 27(9), 2060–2065. https://doi.org/10.1016/J.BIOMATERIALS.2005.09.020

Matalqah, S., Lafi, Z., Asha, S.Y., 2024. Hyaluronic Acid in Nanopharmaceuticals: An Overview. Current Issues in Molecular Biology 46, 10444–10461. https://doi.org/10.3390/cimb46090621

Mendonça, M.C.P., Cronin, M.F., Cryan, J.F., O'Driscoll, C.M., 2021. Modified cyclodextrin-based nanoparticles mediated delivery of siRNA for huntingtin gene silencing across an in vitro BBB model. European Journal of Pharmaceutics and Biopharmaceutics 169, 309–318. https://doi.org/10.1016/j.ejpb.2021.11.003

Morris, G., Schorge, S., 2022. Gene Therapy for Neurological Disease: State of the Art and Opportunities for Next-generation Approaches. Neuroscience 490, 309–314. https://doi.org/10.1016/j.neuroscience.2022.03.010

Nazli, A., Malanga, M., Sohajda, T., Béni, S., 2025. Cationic Cyclodextrin-Based Carriers for Drug and Nucleic Acid Delivery. Pharmaceutics 17, 81. https://doi.org/10.3390/pharmaceutics17010081

Negut, I., Grimezescu, A.M., 2021. Hyaluronic acid nanoparticles, in: Biopolymeric Nanomaterials: Fundamentals and Applications. Elsevier, pp. 155–171.

Raval, H., Bhattacharya, S., 2025. Exploring the Potentials of Hyaluronic Acid-coated Polymeric Nanoparticles in Enhanced Cancer Treatment by Precision Drug Delivery, Tackling Drug Resistance, and Reshaping the Tumour Micro Environment. Current Medicinal Chemistry 32, 3960–3999. https://doi.org/10.2174/0109298673302510240328050115

Rosenblum, D., Joshi, N., Tao, W., Karp, J.M., Peer, D., 2018. Progress and challenges towards targeted delivery of cancer therapeutics. Nature Communications 9, 1410. https://doi.org/10.1038/s41467-018-03705-y

Schindelin, J., Arganda-Carreras, I., Frise, E., Kaynig, V., Longair, M., Pietzsch, T., Preibisch, S., Rueden, C., Saalfeld, S., Schmid, B., Tinevez, J.-Y., White, D.J., Hartenstein, V., Eliceiri, K., Tomancak, P., Cardona, A., 2012. Fiji: an open-source platform for biological-image analysis. Nature Methods 9, 676–682. https://doi.org/10.1038/nmeth.2019

Shi, B., Xue, M., Wang, Y., Li, D., Zhao, X., Li, X., 2018. An improved method for increasing the efficiency of gene transfection and transduction. International Journal of Physiology, Pathophysiology and Pharmacology 20, 95–104.

Singh, R.P., Hidalgo, T., Cazade, P.-A., Darcy, R., Cronin, M.F., Dorin, I., O'Driscoll, C.M., Thompson, D., 2019. Self-Assembled Cationic β-Cyclodextrin Nanostructures for siRNA Delivery. Mol. Pharmaceutics 16, 1358–1366. https://doi.org/10.1021/acs.molpharmaceut.8b01307

Sun, Y., 2023. Sialic acid-targeted cyclodextrin-based nanoparticles deliver CSF-1R siRNA and reprogram tumour-associated macrophages for immunotherapy of prostate cancer. European Journal of Pharmaceutical Sciences. https://doi.org/10.1016/j.ejps.2023.106427

Tang, Q., Khvorova, A., 2024. RNAi-based drug design: considerations and future directions. Nat Rev Drug Discov 23, 341–364. https://doi.org/10.1038/s41573-024-00912-9

Thwala, L., Delgado, D., Leone, K., Marigo, I., Bennetti, F., Chenlo Miranda, M.A., Alvarez, C., Tovar, S., Dieguez, C., Csaba, N., Alonso, M., 2018. Protamine nanocapsules as carriers for oral peptide delivery. Journal of Controlled Release 291. https://doi.org/10.1016/j.jconrel.2018.10.022

Tian, B., Hua, S., Liu, J., 2020. Cyclodextrin-based delivery systems for chemotherapeutic anticancer drugs: A review. Carbohydrate Polymers 232, 115805. https://doi.org/10.1016/j.carbpol.2019.115805

Trotta, F., Zanetti, M., Cavalli, R., 2012. Cyclodextrin-based nanosponges as drug carriers. Beilstein Journal of Organic Chemistry 8, 2091–2099. https://doi.org/10.3762/bjoc.8.235

Valverde-Fraga, L., Haddad, R., Alrabadi, N., Sánchez, S., Remuñán-López, C., Csaba, N., 2023. Design and in vitro assessment of chitosan nanocapsules for the pulmonary delivery of rifabutin. European Journal of Pharmaceutical Sciences 187, 106484. https://doi.org/10.1016/j.ejps.2023.106484

Varan, G., Varan, C., Erdoğar, N., Hıncal, A.A., Bilensoy, E., 2017. Amphiphilic cyclodextrin nanoparticles. International Journal of Pharmaceutics 531, 457–469. https://doi.org/10.1016/j.ijpharm.2017.06.010

Wu, Y., Yu, J., Liu, Y., Yuan, L., Yan, H., Jing, J., Xu, G., 2014. Delivery of EZH2-shRNA with mPEG-PEI nanoparticles for the treatment of prostate cancer in vitro. International Journal of Molecular Medicine 33(6), 1563–1569. https://doi.org/10.3892/ijmm.2014.1724

Xu, F.-J., Zhang, Z.-X., Ping, Y., Li, J., Kang, E.-T., Neoh, K.G., 2009. Star-shaped cationic polymers by atom transfer radical polymerization from β-cyclodextrin cores for nonviral gene delivery. Biomacromolecules 10, 285–293. https://doi.org/10.1021/bm8010165

La borsa di dottorato è stata finanziata con risorse dell'Unione europea *NextGeneration EU*
Piano Nazionale di Ripresa e Resilienza Missione 4 – Componente 2 – "Dalla ricerca all'impresa" –Investment 1.4 - CN00000041 – (CN3, PNRR, Spoke 5: Inflammatory and infectious diseases). CUP B13C22001010001.